

Biphenyl-Cyclophanes: The Molecular Control over the Conductivity of Single-Molecule Junctions

Inaugural Dissertation

zur

Erlangung der Würde eines Doktors der Philosophie

vorgelegt der

Philosophisch-Naturwissenschaftlichen Fakultät

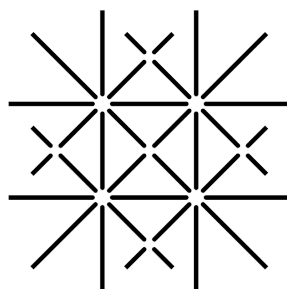
der Universität Basel

von

David Vonlanthen

aus Schmitten/Cordast (Switzerland)

Basel 2010



**U N I
B A S E L**

Genehmigt von der Philosophisch-Naturwissenschaftlichen Fakultät der
Universität Basel auf Antrag von

Prof. Dr. Marcel Mayor

Prof. Dr. Andreas Pfaltz

Basel, den 19.10.2010

Prof. Dr. Martin Spiess

Dekan

The work presented here was initiated and supervised by Prof. Dr. Marcel Mayor at the Department of Chemistry of the University of Basel. Excerpts from this work have been or will be published in:

D. Vonlanthen, A. Mishchenko, M. Elbing, M. Neuburger, T. Wandlowski, M. Mayor, Chemically Controlled Conductivity: Torsion-Angle Dependence in a Single-Molecule Biphenyldithiol Junction, *Angew. Chem. Int. Ed.* **2009**, 48, 8886-8890;
Chemisch kontrollierte Leitfähigkeit: Torsionswinkelabhängigkeit in Biphenyldithiol-Einzelmolekülbruchkontakten, *Angew. Chem.* **2009**, 121, 9048-9052

D. Vonlanthen, J. Rotzler, M. Neuburger, M. Mayor, Synthesis of Rotationally Restricted and Modular Biphenyl Building Blocks, *Eur. J. Org. Chem.* **2010**, 120-133

D. Vonlanthen, A. Rudnev, A. Mishchenko, A. Käslin, J. Rotzler, M. Neuburger, T. Wandlowski, M. Mayor, Conformationally-controlled electron delocalization in n-type rods: synthesis, structure, optical, electrochemical and spectro-electrochemical properties of dicyano-cyclophanes, *Phys. Chem. Chem. Phys.* **2010** (submitted)

A. Mishchenko, D. Vonlanthen, V. Meded, M. Bürkle, C. Li, I. V. Pobelov, A. Bagrets, J. K. Viljas, F. Pauly, F. Evers, M. Mayor, T. Wandlowski, Influence of Conformation on Conductance of Biphenyl-Dithiol Single-Molecule Contacts, *Nano Lett.* **2010**, 10, 156-163

J. Rotzler, D. Vonlanthen, A. Barsella, A. Boeglin, A. Fort, M. Mayor, Variation of the Backbone Conjugation in NLO Model Compounds: Torsion-Angle-Restricted Biphenyl-Based Push-Pull-Systems, *Eur. J. Org. Chem.* **2010**, 1096-1110

A. Mishchenko, L. Zotty, D. Vonlanthen, J. C. Cuevas, M. Bürkle, F. Pauly, M. Mayor, T. Wandlowski, Single molecule junctions based on nitrile-terminated biphenyls: A new promising anchoring group, *J. Am. Chem. Soc.* **2010** (accepted)

M. Bürkle, J. K. Viljas, V. Meded, A. Bagrets, A. Mishchenko, D. Vonlanthen, C. Li, I. V. Pobelov, G. Schön, M. Mayor, T. Wandlowski, F. Pauly, Density-functional study of transmission eigenchannels in dithiolated biphenyl-derived single-molecule junctions, *Phys.Rev.B.* **2010** (in preparation)

J. Rotzler, H. Gsellinger, M. Neuburger, D. Vonlanthen, D. Häussinger, M. Mayor, Racemisation Dynamics of Torsion Angle restricted Biphenyl Push-Pull Cyclophanes, *Org. Biomol. Chem.* **2010** (in press)

This work was supported by the Swiss National Science Foundation (SNSF)

Acknowledgements

It is a pleasure for me to express my gratitude to the many people who have made this work possible. Without their help and support this research would never have come so far.

My sincere thanks go to Prof. Dr. Marcel Mayor for confidence in my work and for giving me the opportunity to perform research in his group. I was highly motivated and inspired by the open-minded culture in his group enabling both my personal and scientific development.

Moreover, I thank Prof. Dr. Andreas Pfaltz and Prof. Dr. Uwe Bunz for taking the time to be co-referees of this work.

I am very grateful to Prof. Dr. Thomas Wandlowski for the successful collaboration and his excellent scientific contributions. It was a great honor to have the opportunity to collaborate with his research group. I want to especially thank Artem Mishchenko for his experimental work and all the stimulating and critical scientific discussions. I would also like to thank Alexander Rudnev for his contributions.

Moreover, I would like to thank my collaborators in Basel for the investigation of the “Ion-triggered-Conductance Switch” which unfortunately did not find place in this thesis. I thank Dr. Michele Calame, Prof. Dr. Christian Schöneberger, Andreas Wepf, Jan Brunner, Dr. Songmei Wu and Jon Agustsson. I also thank Dr. Emanuel Lörtscher and Dr. Heike Riel from the IBM Research Centre in Rüschlikon for the initial measurements on the biphenyl-dithiols.

I would like to thank the entire Mayor group for the warm environment and the great moments of humor that they provided.

Especially, I would like to thank Dr. Sandro Gabutti for being my lab mate. Moreover I thank Jürgen Rotzler and Markus Gantenbein for their help and discussions within my projects.

Efficient research would not be possible without a reliable support from the house staff. I would like to thank Markus Hauri giving me unlimited access to the department store. I also thank the “Werkstatt” team for their continuous

support of our labs. Many thanks to Brigitte Howald, Marina Mambelli and Beatrice Erismann for their administrative support.

Moreover, I am very grateful to Markus Neuburger for measuring so many X-ray solid state structures.

I thank Dr. Daniel Häusinger for the discussions concerning NMR spectroscopy, Dr. Heinz Nadig for FAB and EI mass spectroscopy and Werner Kirsch for elemental analysis. I thank Alexander Käslin and Anna-Caterina Senn for their contribution during the lab training.

I also want to acknowledge the students whose synthetic projects unfortunately did not find place in this thesis. Namely, Gabriel Schäfer (Mannosyl-C₆₀-Fullerenols as Radical Scavengers), Sebastian Ahles (Crownether-Conductance Switch) and Christian Ebner (Steroid Derivates for the Dissolution of Carbon Nanotubes).

Moreover, I want to thank Dr. Fabian Pauly from the Forschungszentrum Karlsruhe for teaching me computational chemistry. I also acknowledge all the fruitful scientific discussions.

Moreover, big thanks to Tom Eaton and Jürgen Rotzler for proof reading this thesis.

Especially I want to thank my parents for financing and supporting my education and for always believing in me. I am grateful to my brother for still sharing and enjoying the same world of music with me.

Finally, I want to thank all my friends who supported and motivated me during my PhD.

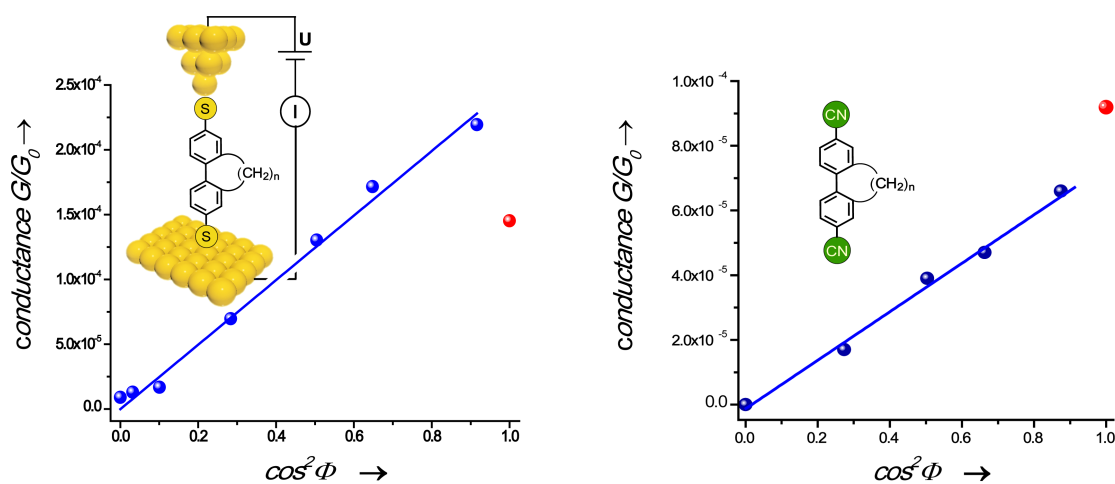
Summary

The ongoing miniaturization trend in the semiconductor industry will soon reach its technical and physical limit. Alternative concepts are required which allow a further reduction in size of the electronic active components. The idea to build cheap semiconductor devices with molecular-scale components is fueling the current interest in Molecular Electronics. However, our ultimate goal is to understand and master single-molecule devices. Organic molecules are very attractive because they can be engineered with high complexity, and their intrinsic physical properties can be tuned by chemists. Electronic devices such as switches or rectifiers using molecular systems have already been demonstrated.¹ Scientists have yet to develop a profound understanding of charge transport through a single molecular wire. The ultimate goal of this thesis is to develop, design and synthesize model compounds in order to contribute to the comprehension of structure-transport relationships in single molecule junctions.

The idea was to design and synthesize new “test sets” of model compounds and to characterize their electrical, electronic, optical and electrochemical properties in a multidisciplinary cooperation with physicists. In contrast to ensemble experiments, the observation of a single molecule uncovers molecular characteristics which would otherwise be averaged out in the bulk. To corroborate the molecular nature of observed transport characteristics a series of molecules with a single well defined variation of their torsion angle was investigated.

In order to gain access to parallel series of model compounds as “test sets”, a synthetic strategy was developed allowing post-modification of the principal model structures with various chemical labels, namely anchoring groups. Biphenyl-cyclophanes, functionalized with acetyl-protected thiol groups in their terminal positions, as a series of molecules of similar length and substitution pattern and the π -backbone conformation as the only structural variable, were first proposed and synthesized.

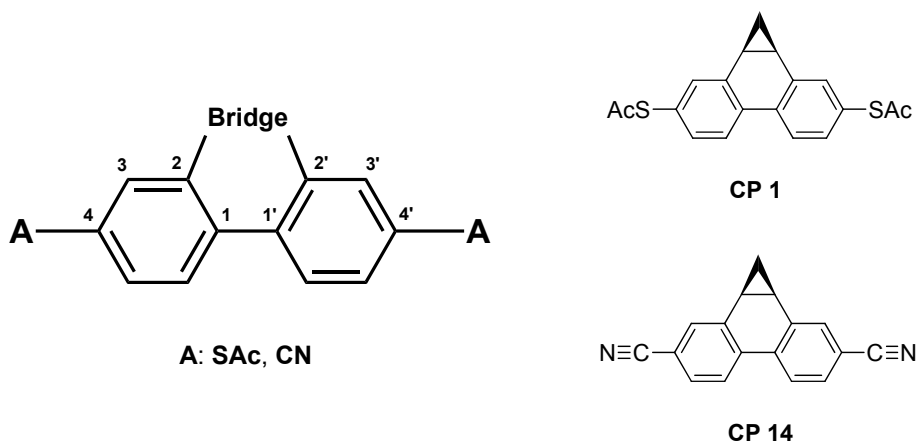
Charge transport investigations using a STM-based break junction technique revealed that electronic hole transport through the HOMO linearly depends on the $\cos^2\Phi$ of the torsion angle. In order to explore the extent to which these findings also apply to electrons delocalized in the structure's LUMO a series of dicyano-biphenyl-cyclophanes were synthesized and studied.



Transport investigation showed that the electron transport through the LUMO also follows the $\cos^2\Phi$ relation. Furthermore, a two step electrochemical reduction process was observed. Thereby, the potential gap between both reduction processes was found to follow the $\cos^2\Phi$ relation. Optical absorption spectroscopy of both series showed that the vertical excitation energy of the conjugation band correlates with the $\cos^2\Phi$ of the torsion angle. These correlations demonstrate that the angle measured in the solid state structure is a good proxy for the molecular conformation in solution. Furthermore, spectroelectrochemical investigations and DFT calculations support these observations. X-ray structures of nearly all model compounds, provided the torsion angles used in these correlations.

The conductance values of the fully planar model structures did not follow the trend. To understand this unexpected behavior of the fluorene derivatives within the respective series several fully planar biphenyl structures were synthesized. While the axial length within the series remains similar, the type of chemical bridge in 2,2'-position of the biphenyl scaffold varies.

Interesting candidates for charge transport investigation were the two dibenzonorcaradiene derivatives **CP 1** and **CP 14** which represent an unbent biphenyl system.



Furthermore, thiol and cyano groups were installed in the terminal position to investigate hole and electron transport. Optical absorption measurements showed that the π -systems are highly sensitive to the chemical nature of the second bridge in these planar biphenyl structures.

To conclude, this thesis discusses the relationship between molecular structure and electronic and electrical properties of several series of biphenyl systems with an emphasis on the spatial molecular conformation and the single-molecule conductance in solution. Due to the large number of related structures within a series the measured transport signatures could be assigned to their molecular origin.

Table of Contents

1	Introduction	1
1.1	Molecular Electronics	5
1.2	Testbed Structures to Probe Electrical Current	7
1.2.1	Monomolecular Film Devices	7
1.2.1.1	Mercury Drop Electrodes.....	8
1.2.1.2	Crossed-Wire Tunnel Junction	9
1.2.1.3	Electromigration.....	10
1.2.2	Single Molecule Devices	11
1.2.2.1	STM Based Break Junction (STM-BJ).....	12
1.2.2.2	Mechanically Controllable Break Junction (MCBJ).....	14
1.3	Anchoring Groups and Molecular Junctions	16
1.4	Molecular Conformation and Physical Properties	21
1.4.1	Biphenyl – A Preliminary Model Compound – Short Overview.....	21
1.4.1.1	Correlation between the Conformation and Physical Property: The Cosine Square Relation	26
1.4.2	The Rotation Barrier of <i>ortho</i> -Substituted Biphenyls.....	30
1.5	Aim of the work.....	31
2	Sulfur-Functionalized Cyclophanes (S)	33
2.1	Molecular Design.....	34
2.1.1	Synthetic Strategy	35
2.2	Synthesis of the BPDTs and their Modular Building Blocks.....	37
2.2.1	Propyl-Bridged Cyclophanes	38
2.2.2	Butyl-Bridged Cyclophanes	40
2.2.3	Pentyl-Bridged Cyclophanes	41
2.2.4	Fully Separated π -Systems	44
2.3	X-ray Solid State Structural Analysis.....	48
2.4	Electronic Spectra	52
2.5	Single Molecule Conductance	56
2.6	Conclusion.....	61

3	Exploring π-Electron-Delocalization in the Structure's LUMO:	
	Dicyano-Cyclophanes (CN).....	62
3.1	Introduction.....	62
3.2	Synthesis and Chemical Characterization	66
3.3	Physical Properties.....	75
3.3.1	Dipolar Interactions of the Cyano Group	75
3.3.2	The Weak Hydrogen Bonding of the Cyano Group	76
3.3.3	Solid state structure analysis.....	78
3.3.4	NMR Observations in Solution: The Aromatic Solvent-Induced Shift Effect.....	83
3.3.5	Computational Studies	89
3.3.6	Electronic Spectra	92
3.3.7	Electrochemical Properties.....	96
3.3.8	Spectroelectrochemistry	104
3.4	Single Molecule Conductance	108
3.5	Conclusion.....	111
4	Complementation of the Series:	
	Planar Biphenyl Model Structures (CP)	112
4.1	Introduction.....	112
4.2	Planar Biphenyl Structures under Investigation.....	114
4.3	Synthesis and Characterization	117
4.3.1	Dibenzonorcaradiene – Conjugation at its Best?.....	117
4.3.2	Phenanthrenes	125
4.3.3	9,9-Dipropyl-Fluorenes	126
4.3.4	Silafluorenes - Silicon-Bridged Biphenyls.....	128
4.4	UV Absorption Measurements.....	130
4.4.1	Probing the Conjugation in Cyclopropane	130
4.4.2	Planar Acetylsulfanyl-Terminated Compounds.....	134
4.4.3	Planar Cyano-Terminated Compounds	136

5	Experimental Section	138
5.1	Materials and Methods	138
5.2	Synthetic Procedures	140
5.2.1	Chapter 2: Sulfur-Functionalized Cyclophanes (S).....	140
5.2.2	Chapter 3: Exploring π -Electron-Delocalization in the Structure's LUMO: Dicyano-Biphenyls (CN).....	172
5.2.3	Chapter 4 - Complementation of the Series: Planar Biphenyl Model Structures (CP)	190
6	Abbreviations	216
7	Bibliography	218
8	Appendix	233
8.1	Contributions	233
8.2	Complete Paper List.....	235

Outline

The thesis is organized in the following way:

- The **first chapter** covers an introduction to Molecular Electronics and presents a selection of experimental tools in this field currently employed. Furthermore various Metal-Molecule-Metal contacts and their properties are discussed. A short review about the relationship between the conformation of biphenyl and the physical properties is shown.
- In the **second chapter** a new approach to control the conformation of biphenyl units, and thus the degree of π -delocalization in biphenyl is presented. The Synthesis is shown resulting in a series of sulfur-functionalized cyclophanes with stepwise adjusted torsion angles. The conductivity of the series is measured and correlated to torsion angles obtained from the X-ray structural analysis. In addition, the optical absorption spectra are discussed.
- In the **third chapter** a series of dicyano-cyclophanes with various π -backbone conformations is synthesized. Furthermore, the geometries and packing motifs in the solid state are analyzed. Electrochemistry, spectroelectrochemistry, UV absorption spectroscopy and concentration dependent NMR spectroscopy is performed. Additionally, electron transport at the single molecule level is studied. The physical properties are correlated with the torsion angles obtained from the X-ray structural analysis. These results are subsequently compared with the result obtained from DFT calculations.
- As a consequence of the gathered results, a series of fully planar biphenyl compounds with similar length is synthesized in the **fourth chapter**. The UV spectra are recorded and compared.

1 Introduction

Faster, smaller, and cheaper. This catchy phrase might describe the unbroken desire for the ongoing miniaturization in the communication and entertainment technology. Economical competition has been driving the semiconductor industry to double the number of transistors per integrated circuit every two years. This progress in technology is commonly referred to as *Moore's law*¹ and the exponentially increasing rate of circuit densification has been continued into the present. In 2000, Intel introduced the Pentium 4, containing 42 million transistors. However, increasing the packing density of the circuit and shrinking feature sizes cannot continue as we reach the fundamental physical limitations related to the materials of construction of the solid-state based devices.

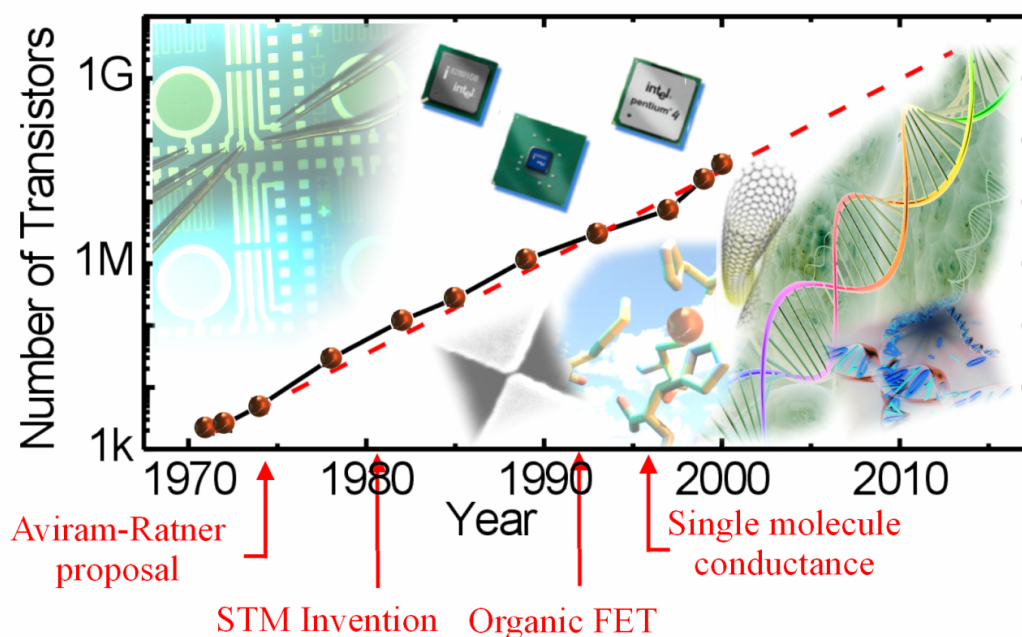


Figure 1. Moore's law, number of transistors as a function of time.² Points refer to the various processors introduced by Intel (the Pentium IV was released in 2000). Reproduced with the permission of Giuseppe Maruccio.²

Technology roadmaps to continuously increasing circuit density have been proposed.³ Extremely sophisticated tools would be required in order to assemble the tiny functional units of the devices due to a decreasing tolerance of defects and contaminations. As an example the use of expensive lithography, ultra-pure chemicals, massive water consumption and a longer manufacturing time for silicon wafers steadily increases the cost of a production plant.^{4,5} Today, the costs for a new semiconductor plant are grown-up to more than five billion US dollars which is the same order of magnitude as the net income of Intel in 2009 (figure 2). Both, the decrease in size of top-down fabricated silicon-based circuits and the increase in expenses will reach a limit where it is no longer possible to fabricate smaller devices.^{6,7}

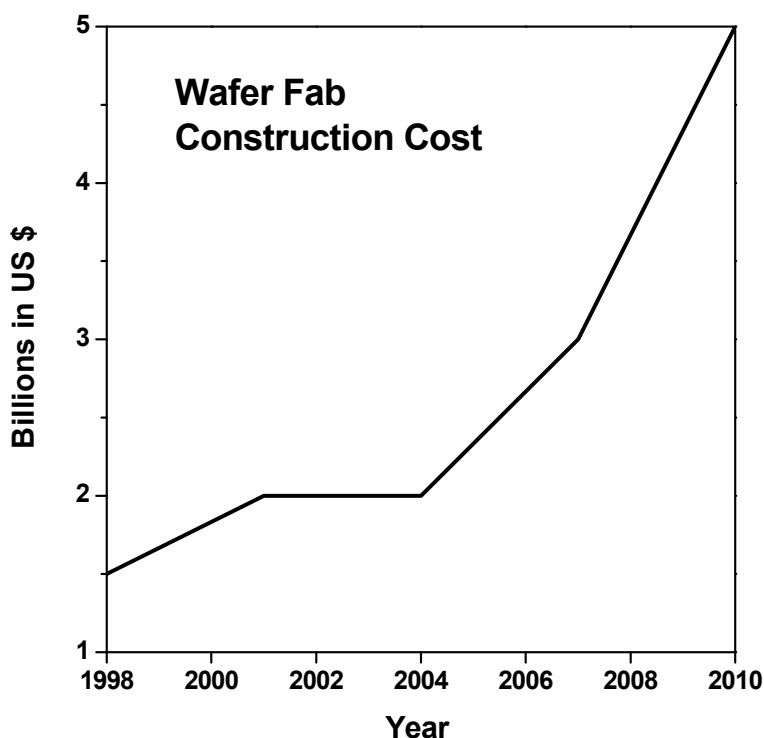


Figure 2. Exponential increase of production facility costs. The limitation on silicon chip technology might not be the laws of physics but those of economics. For comparison: Total financial turnover of Intel 2009: \$ 35.1 billion, net income: \$ 6.6 billion. Source: Intel Corporations.

However, the ultimate limit of scaling lies on the order of a few molecules or atoms. The semiconductor industry roadmap (ITRS) calls for new approaches in computing and integration of emerging technologies in devices at dimension

less than 20 nm.³ Novel concepts are required for future nano-devices tailored to the single molecular or atomic level.⁸

One of the fascinating concepts in nanotechnology is the vision of Molecular Electronics where tomorrow's engineers might use individual molecules to perform the functions in an electronic circuit that are performed by semiconductor devices today. Molecular Engineering as a visionary idea was introduced in the late 1970s by *Hans Kuhn*.⁹ His vision was to integrate designed molecular structures into electronic circuits performing electronic and logic operations. At about the same time *Aviram* and *Ratner* discussed potential rectification emerging from a single molecular structure based on a theoretical model (Gedankenexperiment).¹⁰ Since then, the application of molecular building blocks for the fabrication of electronic components is referred to as "Molecular Electronics".

The use of molecules as the smallest functional feature unit has a potential advantages over conventional semiconductor materials. Chemistry allows correlating function with structure in small assemblies of molecules or even on a single molecule level. The knowledge of synthetic chemists gathered over generations from various research areas including natural product synthesis, dyes and supramolecular chemistry has improved the skills to design and synthesize molecular structures with atomic precision. Furthermore the production of organic molecules is unique in low-cost. A tremendous improvement of physical device or experimental set-up's enabling the integration of monomolecular films¹¹⁻¹⁶ or small assemblies¹⁷ of molecules has already been achieved.

While the concept of "Single Molecular Electronics" excites many researchers in a highly multidisciplinary field it possesses a significant challenge. How can a single molecule be contacted? Individual molecules can be assembled between two electrodes in break junctions based on scanning tunneling microscopy (STM)¹⁸⁻²² or mechanically controlled break junctions (MCBJ).²³⁻³⁰

While these tools provide a good test geometry to probe the electrical properties of individual functional molecules they are too large for the massive parallel integration of molecules. Thus, the dimensional mismatch at the interface between the top-down fabricated electronic circuits with micrometer sizes and the bottom-up synthesized nanometer-scaled molecules is rather a scientific challenge than a particular appealing feature of the functional molecular unit. New concepts which allow a technical integration of individual molecules are required. Thereby, the nature of the molecule-electrode interface, namely the chemical bonding to the electrical leads is a major area of current research. Furthermore, the development of electronic devices at the single-molecule scale requires detailed understanding of charge transport through individual molecular wires.

Clear structure–property relationships are needed which form the basis for a successful application of new concepts of Molecular Electronics in tomorrow’s nano-scale devices.

1.1 Molecular Electronics

Today, Molecular Electronics can be divided into two distinct branches of research. **A)** “Bulk Materials” profit from molecular electronic properties in large assemblies of molecules at the macroscopic scale. Since the discovery in the 1970s (Nobel Prize in chemistry 2000) that plastic *can*, after certain modifications, be made electrically conductive,³¹ soon after conductive polymers have advanced rapidly in various directions.

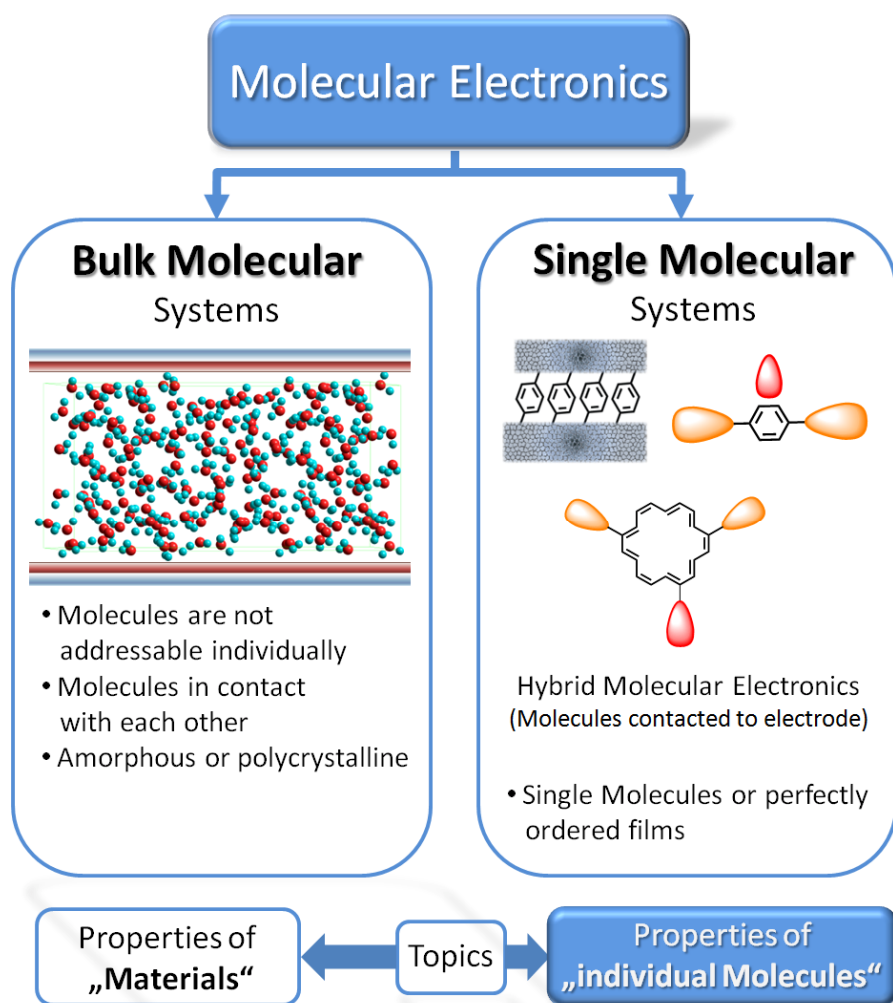


Figure 3. The two research topics in Molecular Electronics. A) Bulk Molecular System (Material Science), B) Single Molecular Systems.

With advances in manipulation techniques organic bulk materials in light-emitting field-effect transistors (OLET),³² light-emitting diodes (LED)³³ or liquid crystal displays (LCD)³⁴ have come onto the market. These are large

assemblies of molecules and are still orders of magnitudes larger than the dimensions of an individual molecule. Furthermore, the molecules are not directly and individually connected to external electrodes.

The dream is thus to realize electronic functions within a single molecule. In this context, Molecular Electronics is **B**) dealing with small assemblies of molecules or “single molecular systems”. In this approach the single molecule becomes the smallest unit in a nano-device profiting from its intrinsic molecular property and functionality. The comprehension of electric current through single molecules using “test devices” (see section 1.2) is a crucial requirement for a knowledge base in order to design future molecules comprising electronic functions.

“This thesis is mainly concerned with Single Molecular Electronics and therefore the design and synthesis of novel test compounds”.

1.2 Testbed Structures to Probe Electrical Current

The ultimate goal of Molecular Electronics is to use assemblies of molecules or even single molecules as functional building blocks and to integrate them into electric circuits. To contact ensembles of molecules is more practical, in terms of device fabrication. Thus, the first transport studies employed multi- and mono-layers using the *Langmuir-Blodgett*³⁵ and self-assembled monolayer³⁶ techniques and vapor deposition techniques.^{37,38} In the following section some selected techniques will be briefly introduced.

1.2.1 Monomolecular Film Devices

The “*Langmuir-technique*”^{35,39} can be used for building up highly organized multilayers or monolayers. This is accomplished by successively dipping a solid substrate (glass, SiO₂ or metals) up and down through the monolayer of amphiphilic molecules on a water surface while simultaneously keeping the surface pressure constant. Consequently the floating monolayer is adsorbed onto the solid substrate. In this way multilayer structures of hundreds of layers can be produced. These multilayer structures are commonly called *Langmuir-Blodgett* or simply “LB films”. The deposition processes is schematically shown in Figure 4. This technique allows to transfer, well-ordered functional films to solid surfaces.

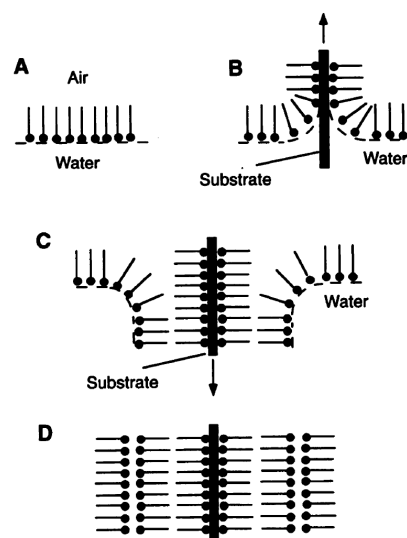


Figure 4. Conventional schematic of the LB technique. (A) An amphiphilic molecule (a molecule with a hydrophobic tail and a hydrophilic head) is spread at the air-water interface to allow formation of a *Langmuir* monolayer. With a barrier, the area of the trough can be altered to change the local density of the molecules. In order to deposit monolayers, a substrate (B) is slowly passed through the interface a given number of times, with each pass adding another monolayer to the LB film (C and D).³⁶

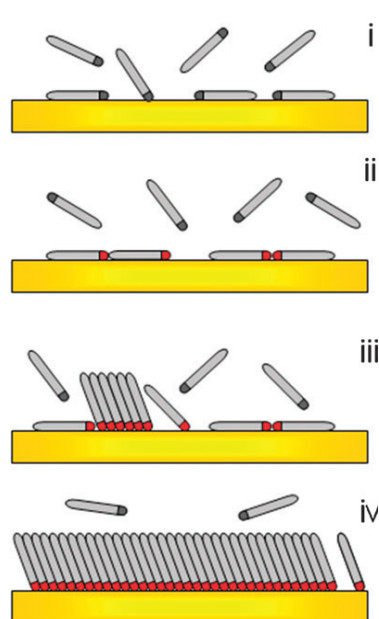


Figure 5. (L) Scheme of the different steps taking place during the self-assembly of alkanethiol on Au(111): (i) physisorption, (ii) lying down phase formation, (iii) nucleation of the standing up phase, (iv) completion of the standing up phase.^{35,36,40}

The spontaneous arrangement of organic molecules on a surface to almost defect-free structures is called self-assembly.³⁶ Formation of self-assembled monolayers (SAMs) is driven by the interplay of thermodynamics and kinetics. SAMs are obtained by dipping the substrate (e.g. one of the electrodes of a monomolecular film device) into a diluted solution of the desired molecule. In general, these molecules require a head-group that binds to the electrode, an organic chain and a terminal end-group installing chemical functionality. Compared to LB films, SAMs have higher chemical and mechanical stability, because they are chemisorbed on the substrate.⁴¹ The most widely studied system has been the gold-thiol-alkyl system, which forms very well ordered single monolayers with the very strong Au-S bond.⁴² Whitesides and other authors reviewed the principles of molecular self-assembly,^{40,43} including the possibility of using self-assembly to make semiconductor devices.

1.2.1.1 Mercury Drop Electrodes

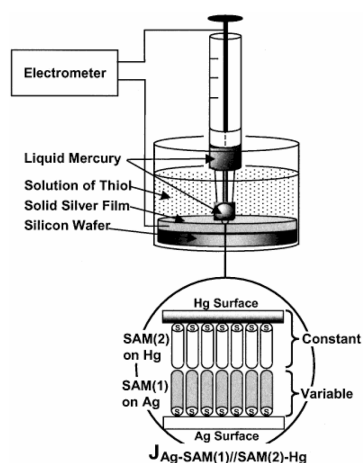


Figure 6. Schematic image of the mercury-junction-setup.⁶

A simple method to prepare a metal-molecule-metal junction was presented by Rampi and Whitesides.⁴⁴ These junctions are easy to assemble, mechanically stable and reproducible. The system takes advantage of the properties of mercury. In particular, i) mercury as a metal is highly conductive, ii) molecules with head groups at the liquid-mercury surface form

well-ordered SAMs in a few seconds, iii) the mercury surface, as a liquid, is free of structural features - edges, steps and terraces - that result in defects of adsorbed monolayers and iv) the mercury drop conforms to the topography of the solid surfaces, and forms a good conformal contact with the SAM-covered solid surface.^{45,46} Furthermore, no evaporation of the second electrode on top of the film is required and the nature of the second electrode can be gold or silver. Both electrodes are addressed to monomolecular films which can vary from each other forming a mixed M-SAM₁-SAM₂-M junction. Using transparent metal substrates allows irradiation of photoactive SAMs in the junction.^{5,44,47}

1.2.1.2 Crossed-Wire Tunnel Junction

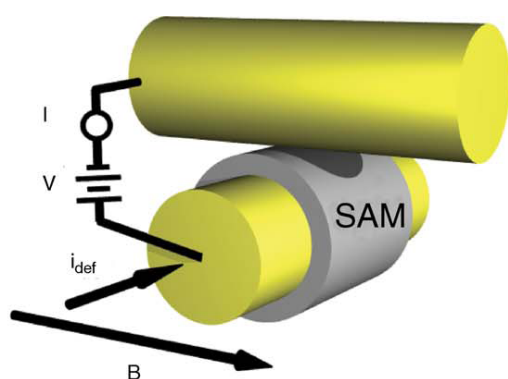


Figure 7. Crossed-wire tunnel junction.¹⁴

One metal wire is modified with a SAM of the molecule of interest. The covered layer is then topped perpendicular in a crossed geometry with a second metal wire. After forming the junction the current-voltage characteristics of the monomolecular assembly can be analyzed. Advantages of this method are that the junction formation is rather easy and the metal-molecule contact is made mechanically, so no metal evaporation is required that could decompose the molecules.^{13,48,49} Further advantage of this method is clearly the macroscopic separation of both electrodes which allows to control the electrode of SAM formation.

1.2.1.3 Electromigration

Electromigration (EM) is the electrical current-induced diffusion of atoms in a thin metal junction, and is a serious mode of failure in integrated circuit interconnects in the semiconductor industry.⁵⁰ The electric field and temperature controls the degree of EM. EM-induced nano-gaps have successfully been prepared to integrate single molecules, revealing various transport phenomena.⁵¹⁻⁵³ EM nano-gap starts with optical and e-beam lithography to fabricate designed metal structures on SiO₂ coated silicon wafers. In a typical EM experiment, the bias voltage across the metallic wire is ramped up to the point where it breaks due to the migration of metal atoms. A recent technique from *van der Zant*⁵⁴ allows the more controlled breaking of the junction by monitoring the resistance and adjusting the voltage applied during the breaking process. Finally, the samples are immersed in a solution of the molecules for several hours.

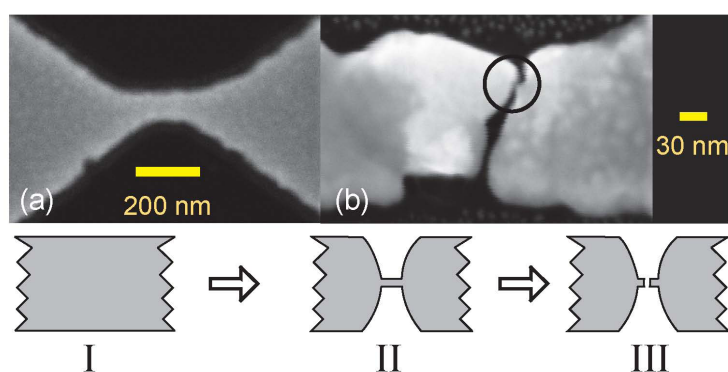


Figure 8. Scanning electron microscope (SEM) images of the nano gap formation by EM. (I) Metallic wire fabricated by lithography. (II) Junction formation due to EM. (III) Further voltage-ramping breaks the junction and molecules trapped within the gap.⁵⁵

Advantages of EM junctions are the compatibility to the standard silicon technology and that the gaps can be easily gated by an external electrode.⁵⁶ Thus, the electronic states of the junctions can be tuned. The gap size is typically 1-3 nm. While with EM many junctions can be formed in parallel, the control over the junction size is low.

1.2.2 Single Molecule Devices

The previously described methods contact small assemblies of molecules. While large numbers of contacted molecules increase the complexity of a junction, they also have certain advantages. The large number of molecules in these assemblies allows probing optical properties. Furthermore, lithographically fabricated molecular junctions are amenable for integration with conventional microelectronics.^{57,58} Beside these advantages in the “ensemble approach” comprises problems associated with defects, domain formation and interactions between molecules. To design future nano-devices comprising individual molecules it is essential to understand the “signature” of single molecule junctions.

In contrast to ensemble experiments (e.g. UV measurements absorption spectroscopy), the measurement of a single molecule uncovers molecular characteristics which would otherwise be averaged out in the bulk.

Current lithographic techniques (extreme ultraviolet lithography) allow the fabrication of structures in the order of 20 nm.⁵⁹ While the feasibility of the sub-10 nm lithography for industrial applications is still under debate, molecules are an order of magnitude smaller. Thus, other techniques are currently employed to establish a symmetric electrode pair that can be adjusted to the length of the molecule.²⁸ In the following section the two most frequently used techniques investigating the transport characteristics of individual molecules will be discussed. These techniques are typically performed under ultra high vacuum conditions or at the solid-liquid inter-phase.

1.2.2.1 STM Based Break Junction (STM-BJ)

In 1981 the scanning tunneling microscopy (STM) was invented by *Binnig et al.*⁶⁰ The STM was the first technique which allowed for the creation of atomic sized contacts. *Bumm* and *Tour* first demonstrated the integration of a molecular wire between an Au substrate and an Au tip using an STM setup.²²

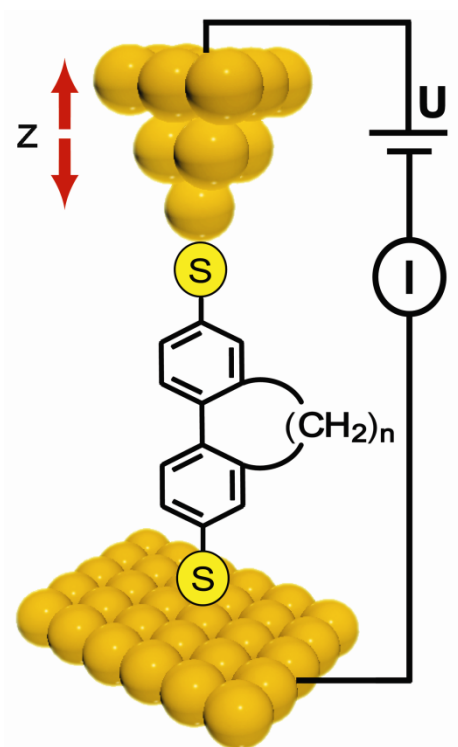


Figure 9. Schematic picture of an STM based break junction setup. A dithiol functionalized biphenyl is trapped between an Au tip and substrate. The STM tip is vertically moved up and down to form many thousands of single molecule junctions within a short period of time.^{18,19}

In 2003 *Tao* and co-workers reported an improved method that allowed the repeated formation of a molecular junction using an Au-STM tip on an Au substrate.^{20,21} They created individual molecular junctions by repeatedly (many 1000 times) moving a gold scanning tunneling microscope (STM) tip into and out of contact with an Au substrate in a solution containing 4,4'-bipyridine (only varying the vertical direction of the tip). During the initial stage of pulling the tip out of contact with the substrate, atomic sized Au chains were formed (figure 10, A) which leads to a stepwise decrease in

conductance. From these conductance curves histograms were created (figure 10, B).

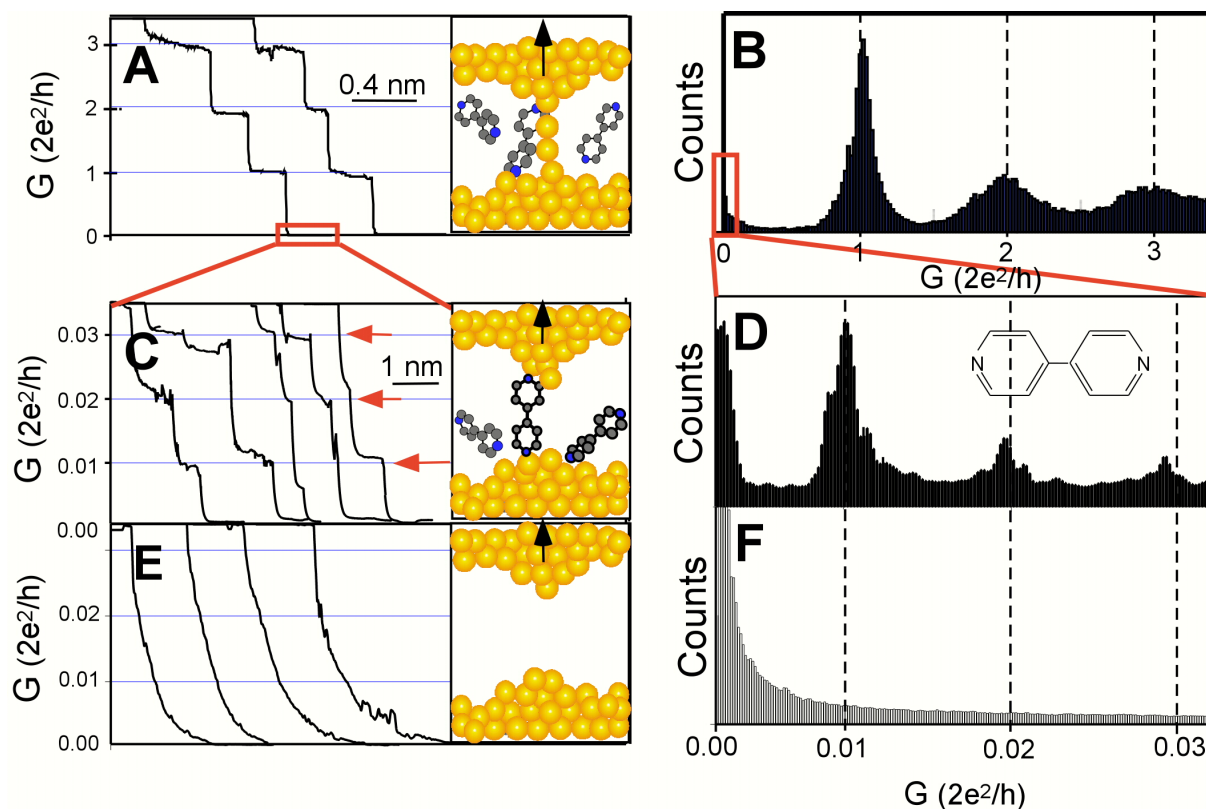


Figure 10. Steps of junction formation and construction of histograms.²⁰

The peaks in the histogram were assigned to integer multiples of Au chains present. The peak at one G_0 (conductance quantum $G_0 = 2e^2/h$) was assigned to the last atomic Au contact. By further opening the junction (figure 10, C) the last Au-Au contact broke and new pronounced peaks at a lower conductance regime were observed (figure 10, D). These peaks could be assigned to the trapped 4,4'-bipyridines binding to the Au contacts. The lowest observed histogram peak at $0.01 G_0$ with a resistance of two orders of magnitude higher than observed before was assigned to one single molecule in the junction. The peaks at integer multiples of $0.01 G_0$ were assigned to two and three molecules, respectively.

Further increase of the tip distance broke the molecule-Au contacts and no steps or peaks were observed within the same conductance range (figure 10, E/F). The width of the molecule-induced steps was determined to be ~ 1 nm, which is three to four times longer than that of the atomic Au steps

which additionally confirmed the presence of a single molecule. A control experiment with 2,2'-bipyridine evolved no such characteristic features which confirmed the dominant N-Au binding mode forming the junctions. The advantage of this method is its ability to construct histograms due to the automated movement of the tip recording thousands of opening and closing cycles. While performing statistics on the gap bridging cycle is a proper application of STMs in Molecular Electronics, performing I/V sweeps proves to be difficult due to the poor mechanical stability of the tip.²⁰

1.2.2.2 Mechanically Controllable Break Junction (MCBJ)

The break junction was first introduced by *Moreland* and *Ekin* in 1985 to study the tunneling characteristics of superconductors.⁶¹ Further development was

made by *Muller* and *Ruitenbeek* who introduced the term Mechanical Controllable Break Junction (MCBJ).²⁴ *Reed* and *Tour* pioneered this technique to contact 1,4-benzene-dithiole.²⁷

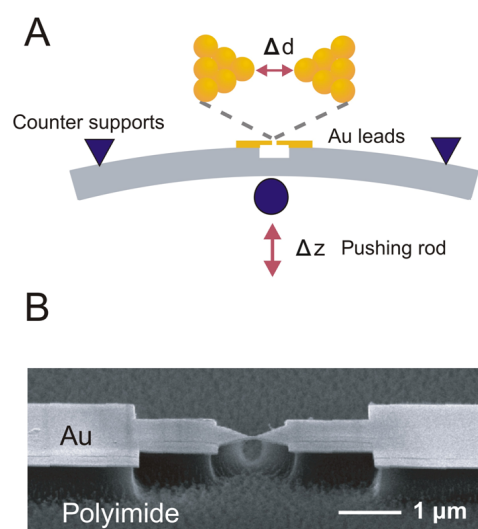


Figure 11. A) Schematic representation of the three-point bending mechanism. While the counter supports fix the sample, the Δz position can be varied by changing the position of the pushing rod, resulting in a tip to tip distance change (Δd) in a picometer regime. B) An SEM image showing a microfabricated gold structure.

The principle of a MCBJ is illustrated in figure 11 A. The sample is a thin freestanding metal bridge (figure 11 B) with a central lateral point of constriction fabricated on the top of a flexible substrate. The sample is then mounted in a three point bending system (figure 11 A). By pushing a rod versus the middle bottom of the substrate, the sample is bent up. This deformation exerts a lateral force on the sample and stretches the freestanding bridge. During the stretch, the gold is elongated and thinned until

it breaks to create two separate electrodes which can be controlled with picometer accuracy when both opening and closing the junction. Molecules can be trapped between these two atomic gold tips. The conductance can be measured during opening and closing of the junction evolving conductance plateaus. Due to the stability and symmetric geometry of the atomic sharp point-contacts current-voltage curves (I/V) can be recorded. The shape of I/V curves reveal intrinsic electrical characteristics of a molecule within the junction. *Reichert* and co-workers could, by measuring I/V curves, reproduce the spatial symmetry with respect to the direction of current flow.²⁸ The robust mechanical stability of the MCBJ system is a well established advantage over a STM based system.

1.3 Anchoring Groups and Molecular Junctions

The charge transport through single molecules or molecular arrays is controlled by many factors associated with electrodes, the molecular structure and the interfacial property.^{10,62-65}

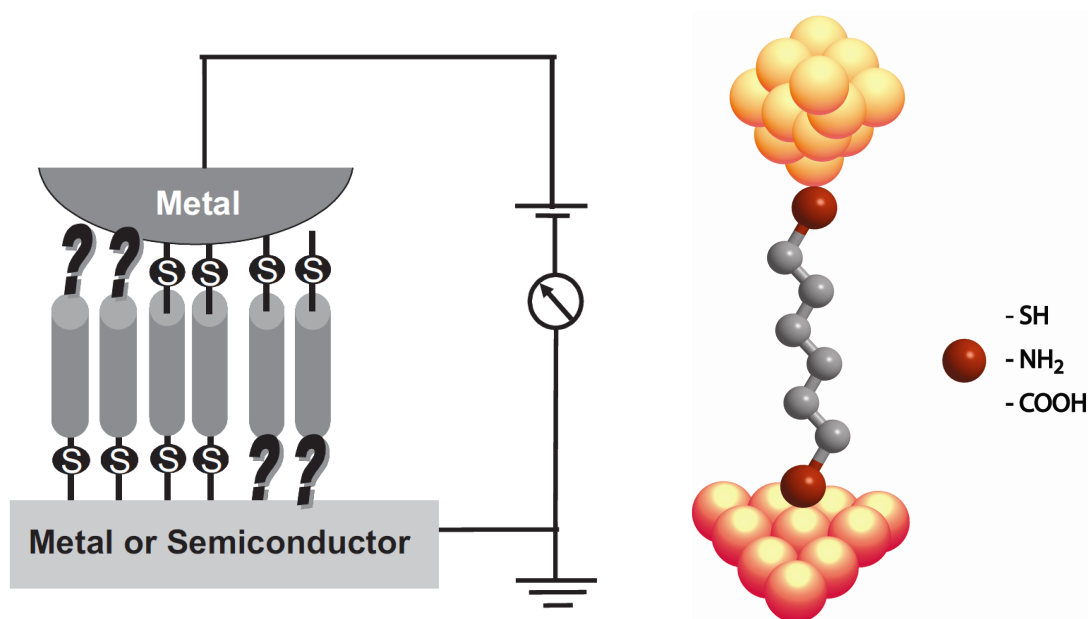


Figure 12. (Left side) Schematic of a measurement set-up and experimental configuration. While only sulfur-mediated bonds to the electrode are shown, this is for illustrative purposes only and other types of bonds can exist.⁶⁶ (Right side) Effect of anchoring groups on single-molecule conductance in a STM-based break junction device.⁶⁷

The search for a suitable anchoring group for metal-molecule-metal contacts has become one of the most important issues in Molecular Electronics.⁶⁸ The nature of the contact-molecule bond determines the degree of electronic coupling between the conductor and molecule. The transport of electrons from the contact onto the molecule can be controlled largely by the type of bond formed between them. If, for example the injection barrier between the molecule and contact is large, the overall device property may be “interface-dominated” and changes in the internal molecular structure no longer dominate the device characteristics.⁶⁹ *Seminario* and co-workers investigated various metal-molecule interfacing “alligator clips” including S, O, Se, Te, NC connections on a theoretical level. These investigations revealed thiols and

isocyanides (NC) as the best “alligator clips” binding molecules to metal contacts due to a strong metal-molecule coupling.⁷⁰⁻⁷²

Tao and co-workers have determined the effect of anchoring groups on the single molecule conductance of thiol-, amine-, and carboxylic-acid terminated alkanes using a STM-BJ (figure 12, right side). The conductance was found to be highly sensitive to the type of anchoring group, which varied in the order of Au-S > Au-NH₂ > Au-COOH. This large dependence was attributed to different electronic coupling efficiencies provided by the different anchoring groups.⁶⁷

Venkataraman studied the conductance of single molecules using alkane chains comprising phosphines, thioethers, and amines as anchoring groups. The conductance varied in the order of Au-P(Me₂) > Au-SMe > Au-NH₂. Additionally, very sharp conductance histograms were obtained for the phosphine anchoring group which was attributed to a specific bonding to the electrode.

*Kiguchi*⁷³ studied the conductance of a single 1,4-diisocyano-benzene, 1,4-dicyanobenzene, and 1,4-benzenedithiol molecules bridging two Au electrodes. The conductance of the molecular junction with the Au–CN (gold-isocyanide) bond was comparable to that of the molecular junction with the Au–S bond.⁷³

Tulevski proposed a ruthenium-carbon π -bond as an efficient conduit for charge carriers.⁷⁴ Other groups have used amines,^{67,75-78} pyridines,^{30,79,80} phosphines,⁸¹ thioethers^{81,82} selenides,⁸² carboxylic acids,⁶⁷ dithiocarbamates⁸³ and fullerenes^{77,84,85} as anchoring groups to study the conductance at the single-molecule level.

The ultimate goal would be to contact molecules without the use of any anchoring groups that create potential barriers in the junction (making directly a carbon-metal bond).^{68,74} *Kiguchi* and *van Ruitenbeek* demonstrated recently the single molecule conductance ($0.1-1 G_0$) of benzene forming a molecule-platinum junction.⁸⁶ Several types of bonding to conducting substrates which are used in single molecule or ensemble junctions are shown in figure 13.

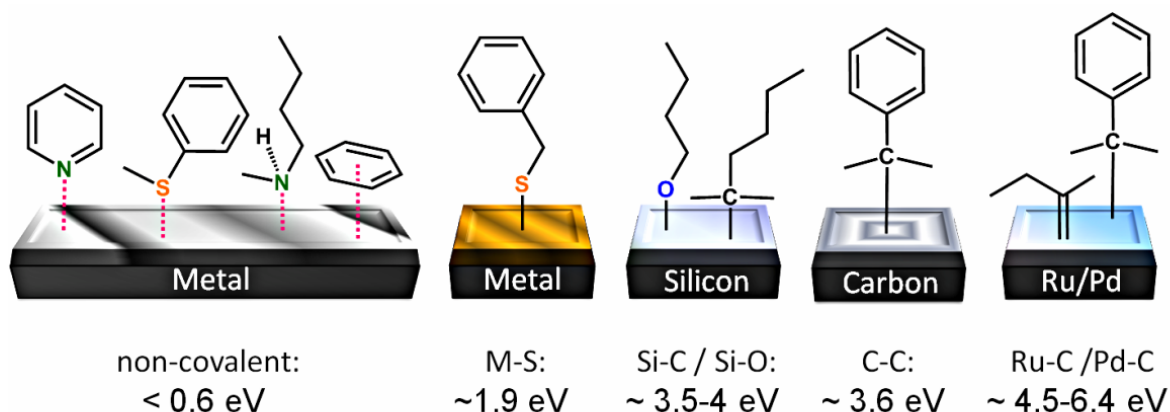


Figure 13. Bonding energies of various types of molecule-substrate interactions.^{42,69,74,87,88} The different anchoring groups determine the stability of layers or single contacted molecules which is important when considering making substrate-molecule-substrate contacts in molecular junctions.

The nature of the contact-molecule bond determines the degree of electronic coupling between the molecule and conductor. Strong coupling increases the orbital overlap of the contact group with the conductor. Covalent bonds which produce strong electronic coupling between contacts and molecules are the most likely candidates for realizing reproducible devices.⁶⁹

Furthermore, different anchoring groups induce different bond dipoles at the molecule-metal interface and internal polarization inside the molecules which is also effecting the transport through a molecule.⁸⁹

Another important aspect of the molecule-electrode interfaces is related to the binding geometry and symmetry of single molecules to metal clusters. Binding geometries of sulfur-gold linked molecules have been studied by various theoreticians.^{90,91} It was suggested that the symmetry of thiol-gold linkages changes currents by a factor of 1000 (figure 14, left side).

Bürkle and *Pauly* calculated bonding geometries of Au junctions comprising biphenyl-dithiols (figure 14, right side).⁹¹ The top-top (TT) and bridge-bridge (BB) geometries were found to be one order of magnitude more conducting than the hollow-hollow (HH) geometry. This was explained by the different degree of overlap of the sulfur lone pairs with the π -orbitals of the phenyl rings. The HH geometry shows clearly the increased local electron density due to the increased coupling to the gold.

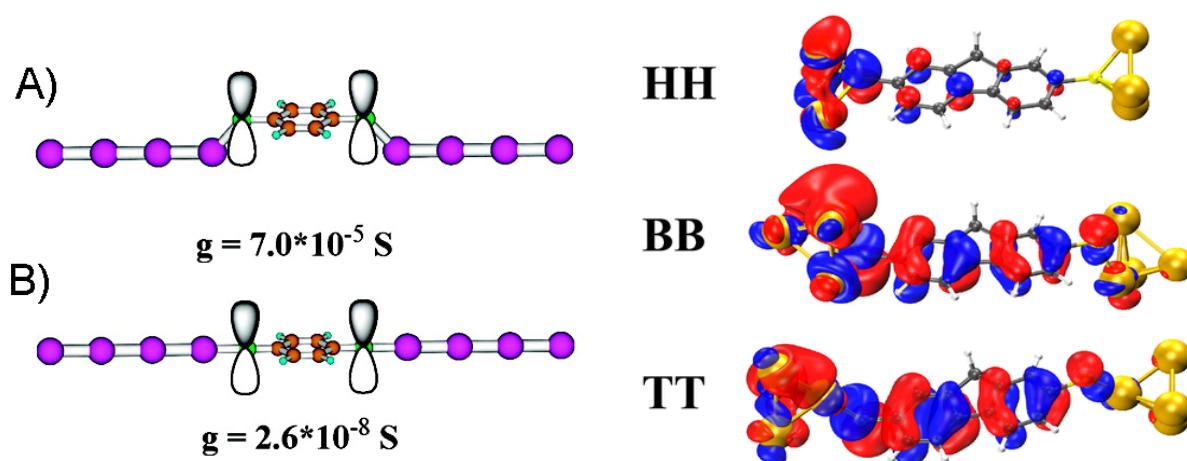


Figure 14. (Left side) Geometries in the model calculations of an Au-1,4-benzene-dithiol (BDT)-Au junction. (A) BDT is parallel to the electrode plane but elevated from it by 1.8 Å. (B) BDT is in the same plane of the gold electrode.⁹⁰ (Right side) Dominant transmission channel of fluorene-dithiol for hollow-hollow (HH), bridge-bridge (BB) and top-top (TT).⁹¹

A recent work of *Venkataraman* demonstrated the influence of conformation of the anchoring group electron lone pairs on the junction conductance.⁸² In this study the charge transport of the two model compounds **1** and **2** was (figure 15) investigated. The study revealed that the orientation of an Au-S bond relative to the aromatic π -system controls electron transport through conjugated molecules. In compound **1** the lone pair is oriented parallel to the π -orbital of the phenyl ring, hence has the better orbital overlap compared with compound **2**. Furthermore, narrower conductance histograms were obtained for structure **1** due to a reduced rotation of the sulfur electron lone pair away from the π -system.

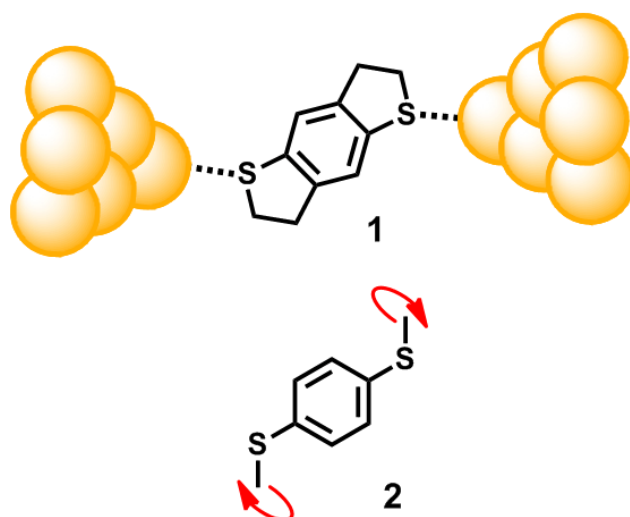


Figure 15. Tailor-made model compound to investigate the influence of orientation of the sulfur electron lone pairs on the charge transport. Compound **1** was found to be more conductive than **2** due to the restricted rotation of the sulfur electron lone pairs in **1**.⁸²

1.4 Molecular Conformation and Physical Properties

1.4.1 Biphenyl – A Preliminary Model Compound – Short Overview

The interdependence between the conformation and the chemical reactivity of biphenyl has been known to chemists for many years.⁹² In 1952 *Michael J. Dewar*, a theoretical chemist, discussed the resonance energy in π -conjugated systems that are twisted out of co-planarity.⁹³ A little later in 1959 *Hiroshi Suzuki* published a series of key papers on the relationship between electronic absorption spectra and spatial configurations of alkyl substituted biphenyls (figure 16). These studies revealed that the electronic bathochromic shift depends on the backbone configuration of biphenyl. This finding allowed further an interpretation of the spatial biphenyl conformation in solution.⁹⁴⁻⁹⁶

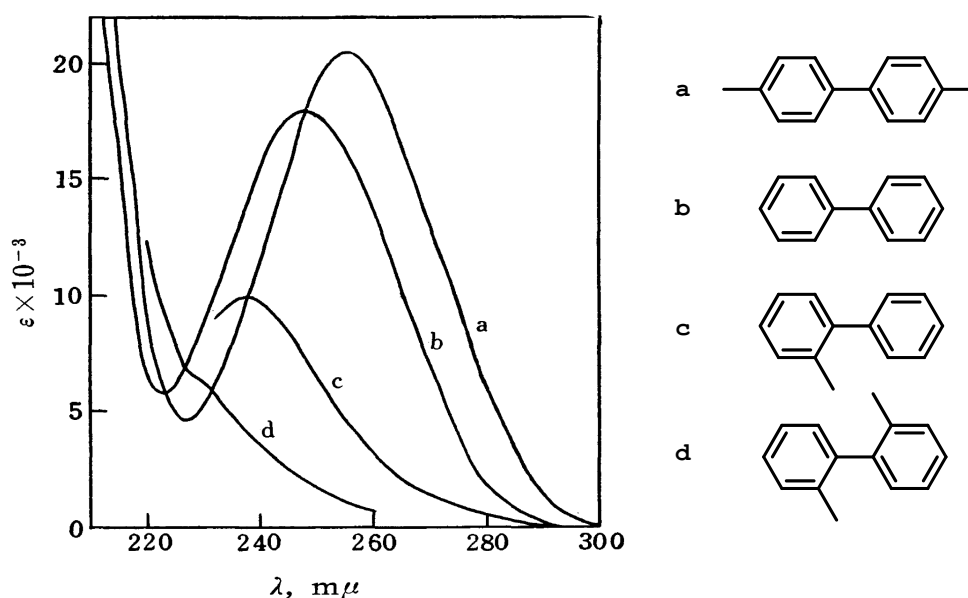


Figure 16. The UV absorption spectra of biphenyls: a) 4,4'-Dimethyl-biphenyl, b) biphenyl, c) 2-methyl-biphenyl, d) 2,2'-dimethyl-biphenyl.⁹⁶

Benniston and *Harriman*^{97,98} have studied the electron-transfer dynamics depending on molecular conformation in biphenyl-based dyads. Their work was based on an approach introduced by *McLendon*⁹⁹ whereby 4,4'-biphenyl was used as the bridge for two porphyrin units and the torsion angle between the phenyl rings was varied by substitution at the 2,2'-positions. It was

observed that the rate of through-bond electron transfer between the donor and acceptor was dependent on the angle around the central biphenyl linkage and reached a minimum at 45° . Unfortunately, the substitution pattern also led to changes in the electronic properties of the bridge, which affected the overall electronic system (figure 17, left side).

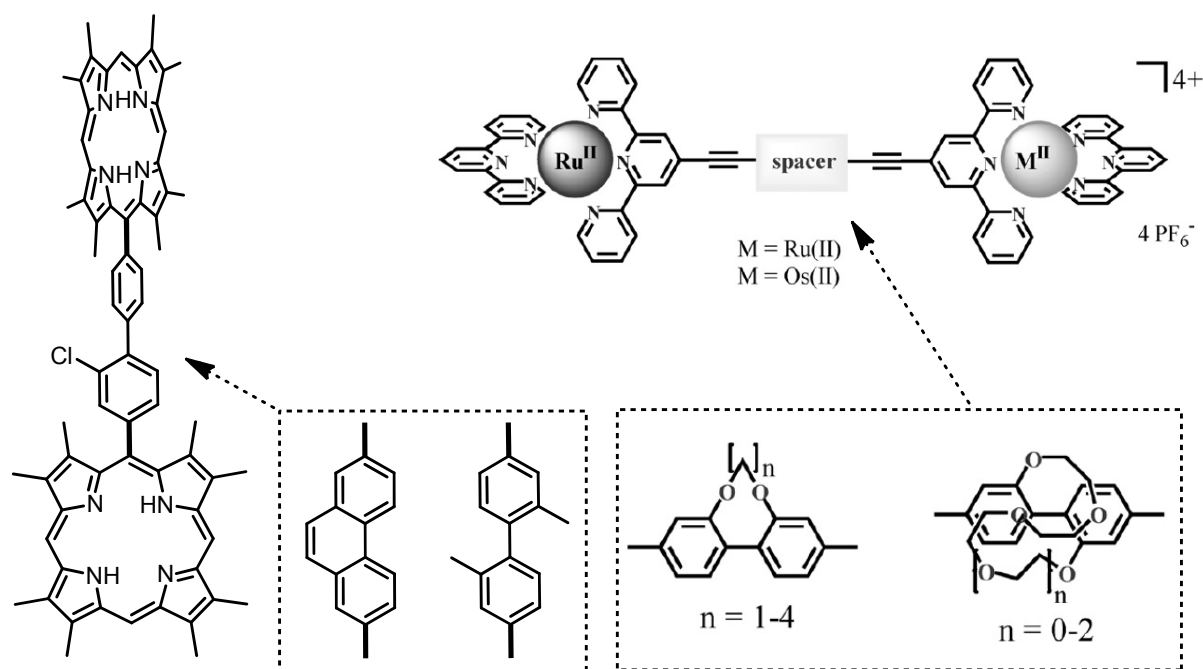


Figure 17. (Left side) Structure of the angle dependent dimer series.⁹⁹ (Right side) Model systems used to measure the effect of torsion angle on electron exchange, where the length of the strap controls size of the torsion angle.⁹⁸

The new approach of *Benniston* and co-workers was to attach a tethering strap across the 2,2'-positions, thereby keeping a constant substitution pattern, and using the strap length to control the central torsion angle (figure 17, right side). A range of torsion angles became possible according to the number of ether units in the strap, although conformational variability and thermal fluctuation had to be taken into account.^{97,98}

*Shaporenko*¹⁰⁰ and co-workers studied the self-assembled monolayers (SAMs) on Au(111) and Ag(111) of a few biphenyl-derived dithiol compounds with various conformations. *Lörtscher*¹⁰¹ and co-workers studied the influence of the reduced π -conjugation in *p*-(oligo)phenylenes (figure 18) on the electron charge transport at the single-molecule level. Maximum conductance peaks were found to vary between 50 nanosiemens (**2**) and 100 nanosiemens (**4**). They attributed the increase in conductance to a reduced conjugation rather than a full interruption of interring-conjugation. They finally concluded that the absolute conductance does not primarily depend on the number of phenyl units. Rather it is limited by the injection of charge carriers over the molecule-metal interfaces.

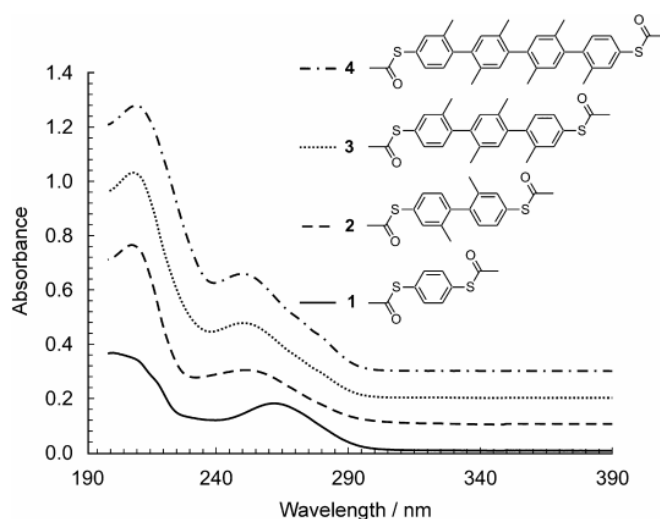


Figure 18. UV absorption spectra of **1-4**. Almost identical optical gaps were recorded for all compound in solution. The wavelength red shift of **1** was attributed to an extend conjugation due to the sulfur-electron lone pairs.¹⁰¹

In addition, UV absorption measurements revealed that the effective conjugation does not depend on the number of benzene units. This was attributed to the near orthogonal arrangement of the phenyl units separating each π -unit from its neighbors (the orthogonal arrangement of the phenyl rings in **2-4** emerges from the steric repulsion of the attached methyl groups).¹⁰¹

In another investigation it was found that the longest UV wavelength absorption band of *p*-(oligo)phenylenes¹⁰² which have no substituents on the phenyl rings (the π -conjugation along the molecular backbone is then

consequently increased due to the increased π -orbital overlap) bathochromically shift to longer wavelengths by increasing the number of benzene units approaching a limiting value, the so-called effective conjugation length.¹⁰²

The first comprehensive investigation on the interdependence between the single molecule conductance and molecular conformation was published by *Venkataraman* in 2006 (see next page).⁷⁵ By using a STM Break Junction, the single molecule conductance of a number of biphenyl compounds comprising various acceptor and donor substituents was measured (figure 19). It was suggested that the cosine square of the interplanar torsion angle correlates linearly with the single molecule conductance (figure 19, c). Amine groups were used to link the molecule to the electrode claiming to form single-molecule junctions with more reproducible current-voltage characteristics.¹⁰³

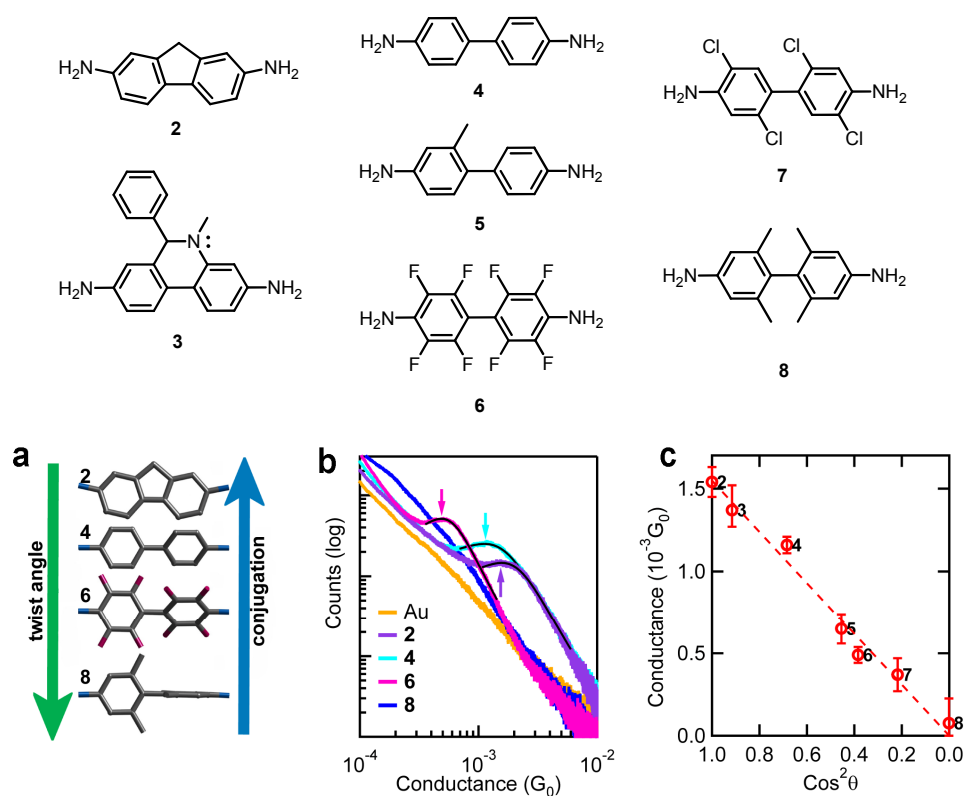


Figure 19. (Top) Model compound studied. (Bottom) **b**, Conductance histograms obtained from measurements using molecule **2** (scaled by 1/15), **4** (scaled by 1/7), **6** (scaled by 1/11) and **8** (1/5). All data were taken at a bias voltage of 25 mV. **c**, Position of the peaks for all the molecules studied plotted against $\cos^2 \Phi$, where Φ is the calculated interplanar torsion angle for each molecule.¹⁰³

While this study nicely demonstrated the correlation between the conductance and degree of π -conjugation in the biphenyl backbone some questions regarding the concept of the study remained. Do donor- and acceptor-substituents attached to these model compounds not influence the conductance? A study by the same author with the title "*Varying Single-Molecule Junction Conductance Using Chemical Substituents*" investigated this effect and concluded the conductance is tuned by using donor/acceptor substituents.¹⁰⁴ Furthermore, the conductance values extracted from the experimental histograms were correlated with calculated torsion angles obtained from theory.

1.4.1.1 Correlation between the Conformation and Physical Property: The Cosine Square Relation

Biphenyls as the smallest structures comprising two adjacent benzene rings as individual π -systems are ideal model compounds to investigate electronic transport properties.^{75,105,106} Particular appealing features are their rigidity resulting in a well defined spacing of their terminal units and their compactness provides detectable signals even for poorly conducting conformations. Usually, donor or acceptor subunits are interlinked by biphenyl structures to study electron transfer on a molecular level (see also previous section).^{99,107}

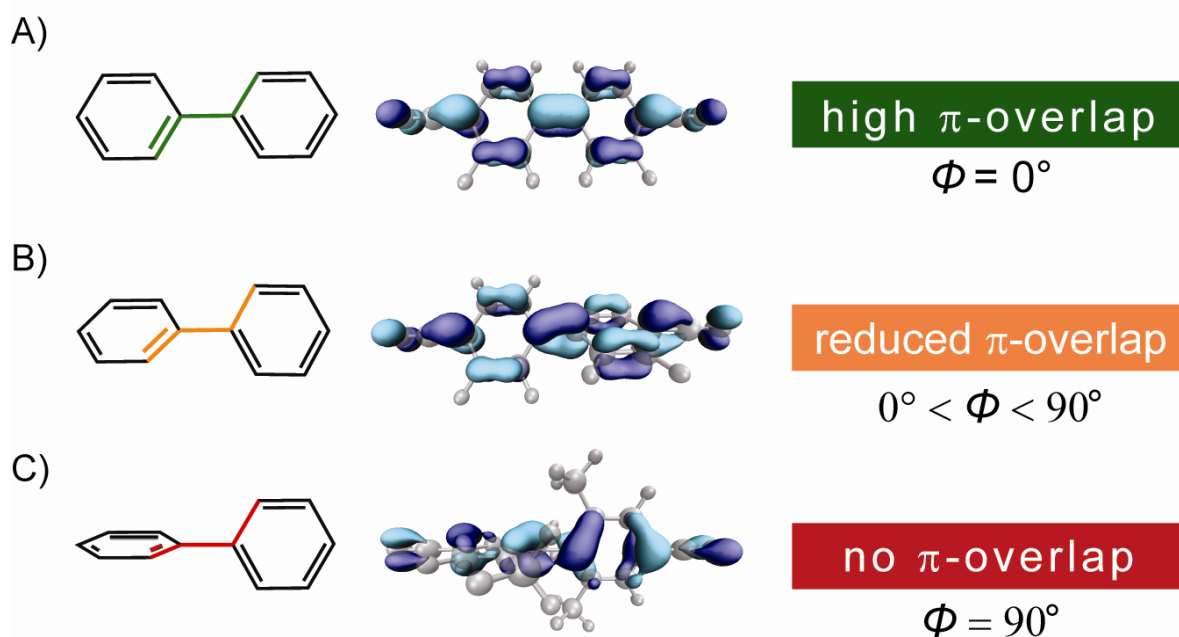


Figure 20. Schematic of the existing biphenyl conformations and the degree of π -conjugation. The LUMO orbitals of various 4,4'-dicyano-biphenyls are displayed as representative examples. A) The adjacent π -orbitals connecting the two phenyl rings overlap most efficiently. B) The overlap of the adjacent π -orbitals connecting the two phenyl rings is reduced. C) The adjacent π -orbitals are perpendicular to each other. The two π -systems are decoupled.

Thereby, the degree of π -electron delocalization between the two π -units in biphenyl is expected to vary with the torsion angle Φ between the planes. In other words, a high conducting state is expected for a biphenyl system with both phenyl rings in the same plane while considerably reduced conducting features are expected for systems with both rings perpendicular to each other (see figure 20).^{19,75,108-110}

*Jaffé and Orchin*¹¹¹ discussed the relationship between UV spectra and steric effects: The extent of interaction between two adjacent π -orbitals can be measured by the π -orbital overlap integral A_{RS} . This overlap integral is found to be approximately proportional to the resonance integral β_{RS} .

If R and S are the decoupled chromophores, the resonance energy of RS relative to the isolated chromophores $R + S$ is a measure of the interaction across the bond between R and S . Theoretical calculations revealed that the change of energy E_{RS} of the system, which is related to the resonance integral β_{RS} , varies approximately with $\cos^2\Phi$ (equation 1). (It should be mentioned that the $\cos\Phi$ function was also discussed as an approximation to describe E_{RS} . However, the simple $\cos\Phi$ dependence was reported to break down for appreciable torsion angles).

$$E_{RS} = \cos^2 \Phi \quad \text{(equation 1)}$$

This means that the π - π^* transition energy will increase upon increasing the torsion angle between two adjacent π -systems, since the resonance interactions between both π -systems are diminished. A similar $\cos^2\Phi$ law has been postulated for the relation between the extinction coefficient ϵ (oscillator strength) and the torsion angle Φ .¹¹¹⁻¹¹³

The shape of the $\cos^2\Phi$ function, shown in figure 21, implies that small angles have relatively little effect on the conjugation (a torsion angle of 15° reduces the resonance energy by only 7%, whereas a larger angle virtually decouples the two chromophores (an angle of 75° reduces the resonance energy by 93%).

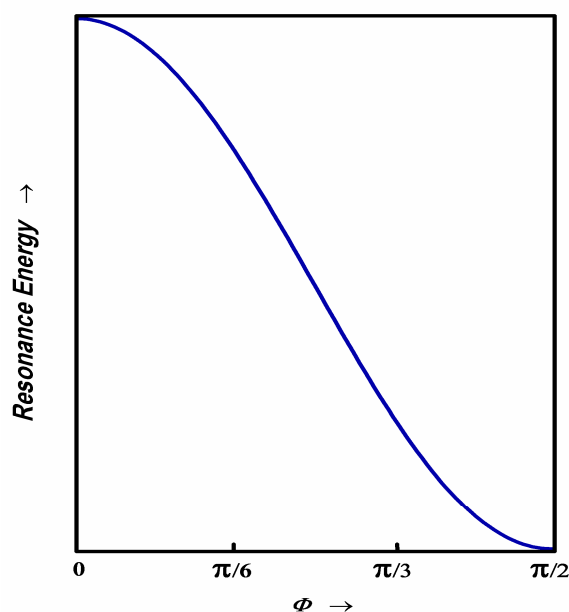


Figure 21. Variation of the resonance energy follows the cosine square function with the torsion angle ϕ between two conjugated chromophores.

It should be remarked that attributing the spectral changes entirely to the torsion angle of the central bond is only qualitatively correct. Additional structural features such as electron donating or withdrawing effects and distortion of interbond angles must also be considered. But it is convenient to concentrate attention on the largest single effect, namely, the twist in the biphenyl-connecting single bond.

*Venkataraman*⁷⁵ and co-workers suggested that the junction conductance of amino-functionalized biphenyls (figure 19) decreases with an increasing torsion angle according to the $\cos^2\phi$ relation. Thereby, they included the theoretical work of *Woitellier*¹¹⁴ and *Nitzan*.¹¹⁵

*Woitellier*¹¹⁴ considered the π - π -electronic coupling of adjacent pyridine rings finding an approximate relation of the cosine of the torsion angle ϕ between them. According to *Nitzan*¹¹⁵ the “electron transfer rate” is proportional to the square of the coupling between the two coupling elements (here two phenyl rings). Thus, the theory predicts a $\cos^2\phi$ relation.

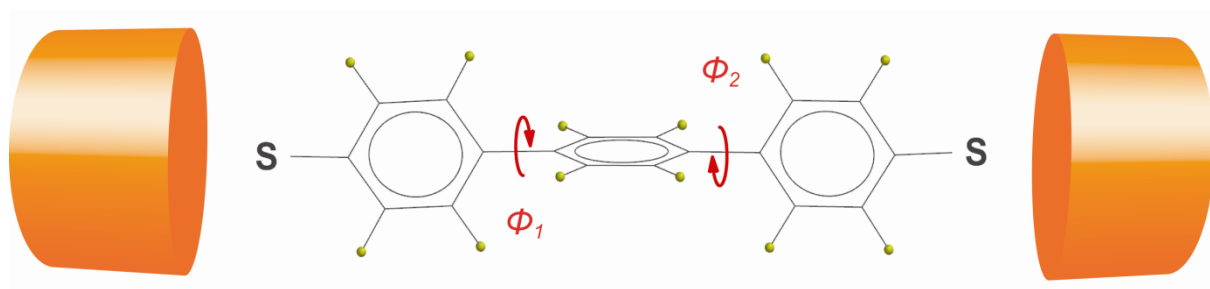


Figure 22. Schematic situation of an S-functionalized terphenyl immobilized between two metal contacts. The molecule comprises two equal torsion angles between three π -coupling elements, thus, both torsion angles are controlling the electronic communication through the wire.

Extension of the $\cos^2\Phi$ relation to more complicated π -systems was discussed by *Datta*.¹¹⁶ The electron transmission probability through a molecular wire consisting of three phenyl rings (thus, two assumingly equal torsion angles ($\Phi_1 = \Phi_2$) between three π -coupling elements) should be proportional to $\cos^4\Phi$ of the torsion angles. While these examples describe pure π - π orbital interactions other types of orbital interactions are considered to be involved in through bond electron transport.

Theoretical calculations revealed that σ - σ , and σ - π interactions are participating but the π - π coupling is by far the most important.¹¹⁴ If two chromophores are nearly perpendicular to each other, hence, the π - π coupling is very low, these other couplings become important and other transport channels will become dominant.^{114,117}

1.4.2 The Rotation Barrier of *ortho*-Substituted Biphenyls

The torsion angle between the two phenyl rings of biphenyl is markedly sensitive to its chemical¹¹⁸⁻¹²² and macroscopic¹²²⁻¹²⁷ environment. As an example the torsion angle of 4,4'-dicyanobiphenyl embedded in metal complexes is reported to vary between between 0° and 36° due to the low rotation barrier.

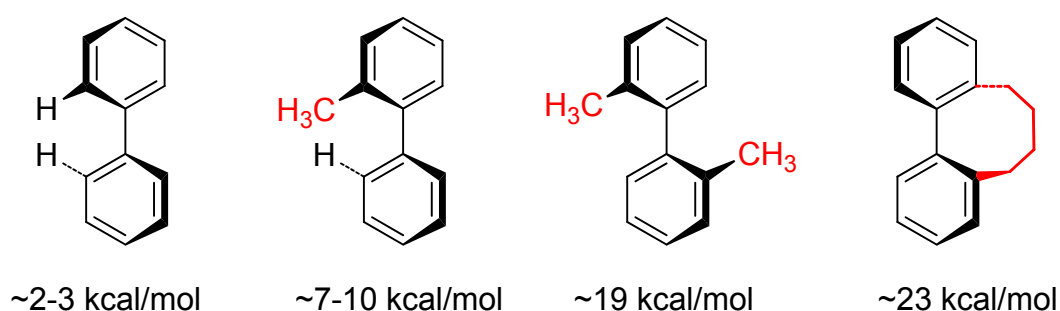


Figure 23. Rotational barriers of various biphenyl structures. These values were obtained by dynamic NMR spectroscopy.¹²⁸⁻¹³⁰

Attaching of methyl groups in the *ortho*-position of the biphenyl increases the rotational barrier to 7-10 kcal/mol and 19 kcal/mol respectively.^{128,129} Müllen reported a rotation barrier of 23 kcal/mol for the butyl-bridged biphenyl displayed in figure 23.¹³⁰

1.5 Aim of the work

The ongoing miniaturization trend in the semiconductor technology will soon reach its technical and physical limit. Alternative concepts that allow to further decrease the size of the electronic active components are required. One of the fascinating concepts in nanoscience is the vision of “Molecular Electronics” where individual molecules perform the functions in an electronic circuit that are performed by semiconductor devices today. For the successful development of Molecular Electronics several prerequisites have to be fulfilled. Techniques are required which allow to manipulate small assemblies of molecules or single molecules. Break junctions based on scanning tunneling microscopy (STM-BJ) and mechanically controlled break junctions (MCBJ) revealed to be good test geometry to probe the electrical properties of individual molecules. While these tools are too large for the massive parallel integration of molecules, they allow investigation of molecular structure-device property relationships. To correlate junction conductance with molecular structure is a challenging task as charge transport through single molecules is controlled by many factors associated with electrodes, intrinsic molecular properties and interfacial properties. Thereby, the investigation of tailor-made synthetic molecules with accurately defined electronic properties is an essential step toward a better understanding of charge transport through single molecule junctions.

The aim of this work was to design, synthesize and study various series of molecules with tailor-made electronic properties. The series of molecules have been designed in particular for the investigation of the charge transport behavior at the single molecule level using either a STM-BJ or a MCBJ.

These investigations were planned to be performed either in the group of Thomas Wandlowski at the Department of Chemistry (University of Bern), in the group of Hike Riel at the IBM Research Centre (Rüschlikon) or in the group of Michele Calame and Christian Schöneberger at the Department of Physics (University of Basel).

In particular the following investigations were planned and are included in this thesis:

- Influence of the degree of π -conjugation on the single molecule conductance: Biphenyl-cyclophanes as a series of molecules with similar length and substitution pattern and the inter-phenyl torsion angle as the only variable feature were designed. Thereby the lengths of the ring-interlinking alkyl chain, defines stepwise the degree of π -conjugation while overall electronic structure is maintained. Furthermore, thermal fluctuations around the equilibrium values of the torsion angle in these rather rigid cyclic structures were expected to be reduced compared to parent biphenyl model systems.
- The importance of the type of anchoring group, and thereby the influence of the coupling of the molecule to the electrode: For this purpose two series of biphenyl-cyclophanes series were synthesized and investigated. The first series was terminally functionalized with thiol groups to study the influence of the degree of π -conjugation on the charge transport through the HOMO. Another task was to introduce the new cyano-anchor group to link molecules to electrodes. Therefore a second series of biphenyl-cyclophanes, terminally functionalized with cyano groups, was synthesized. These model compounds were suitable to study the influence of the degree of π -conjugation on the charge transport through the LUMO.
- Based on the gathered results the influence on the electronic and transport properties of various chemical type of second intramolecular bridges in 2,2'-position of the biphenyl skeleton moved into the focus of interest. Several fully planar biphenyl model compounds were designed and synthesized.

2 Sulfur-Functionalized Cyclophanes

Theoretical studies about biphenyl-dithiols (BPDTs) have gained considerable attention^{108,110,117} and molecular junctions comprising biphenyl-dithiols have already been reported by *Haiss* and co-workers.¹⁰⁹

As mentioned in the previous section, the torsion angle between both phenyl rings in “biphenyl” model compounds is often not the only parameter which varies and thus, alterations in physical properties might be the result of several effects. In particular the electron density in the phenyl rings has been shown to be affected by various donor and acceptor substituents tuning the expected torsion angles.^{75,99} Furthermore, thermal motion leads to variation of the torsion angles for singly substituted biphenyl systems comprising a C-C single bond interlinking both phenyl rings.¹⁹ In spite of the large interest of the correlation between torsion angle and transport properties, suitable model compounds enabling the systematic variation of the torsion angle in biphenyl systems have not been realized so far.

Here, a new approach is introduced enabling the systematic variation of the torsion angle ϕ in biphenyl subunits with almost negligible alterations in electronic properties of the phenyl rings. This approach allows to create series of molecules of similar length and the π -backbone conformation as the only structural variable.

2.1 Molecular Design

The basic idea is to interlink both phenyl rings with an additional alkyl chain of various lengths bridging both *ortho*-positions (figure 24).

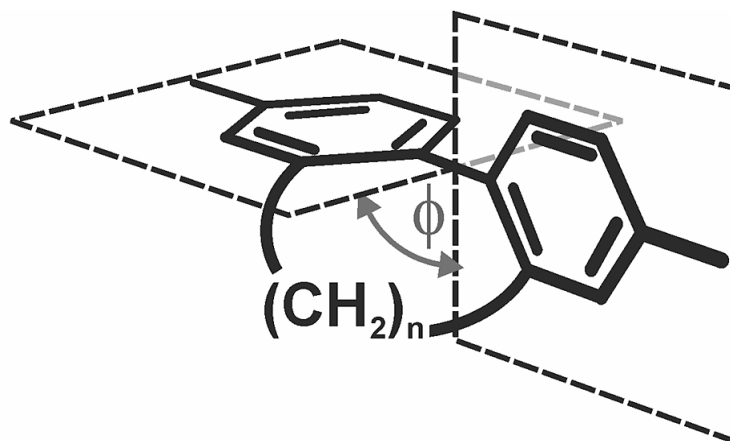
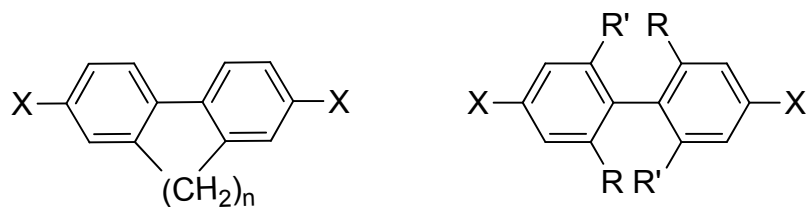


Figure 24. The interplanar torsion angle ϕ of the biphenyl backbone is adjusted by the length of the inter-ring alkyl chain.

- Thereby, the number of CH_2 units dictates the torsion angle ϕ and thus the degree of π -electron delocalization between the two π -systems, while the overall electronic structure and lengths of the molecule is maintained. As a result the biphenyl synthon becomes a subunit of a rather rigid cyclic structure and thermal fluctuations around the equilibrium values of the torsion angle are expected to be reduced compared to parent biphenyl model systems (figure 17, right side).^{19,131}
- Sulfur-functionalization in terminal position of the biphenyl synthons allows not only the immobilization between metal electrodes, but also provides considerably increased stabilities of the resulting single molecule junctions due to the covalent S-Au bonding compared to transiently immobilized biphenyl-diamines (see figure 19).¹³²
- Finally, single crystals suitable for the X-ray analysis of the members of the structural family can be grown providing insight into each inter-plane torsion angle ϕ .¹⁹

2.1.1 Synthetic Strategy



S1a: $n = 1$

S2a: $n = 2$

S3a-c: $n = 3$

S4a-c: $n = 4$

S5a, S5e: $n = 5$

S6a: $\text{R} = \text{R}' = \text{H}$

S7a: $\text{R} = \text{H}, \text{R}' = \text{CH}_3$

S8a, S8d: $\text{R} = \text{R}' = \text{CH}_3$

S9: $\text{R} = \text{CH}(\text{CH}_3)_2$

$\text{X} = \text{H}$

a: $\text{X} = \text{SAc}$

b: $\text{X} = \text{Cl}$

d: $\text{X} = \text{I}$

c: $\text{X} = \text{Br}$

e: $\text{X} = \text{OTf}$

Figure 25. Target Molecules and Modular Building Blocks. **S1a-S8a** are the dithioacetyl derivatives and **S2b-c**, **S3b-c**, **S4b-c**, **S5b** and **S8b** are the terminally chlorine-, bromine-, iodine- or triflate-functionalized building blocks.

To follow this strategy, the sulfur-functionalized biphenyls **S1a-S5a** (figure 25) with an increasing length of the inter-ring alkyl chain $n = 1-5$ and thus with increasing torsion angles were envisaged as target structures. The series of terminally acetylsulfanyl functionalized biphenyl systems was complemented by the compounds **S6a** and **S7a** and the derivative **S8a**. Within these three biphenyl systems variations of their inter-ring torsion angles were expected due to the different steric requirements of their substituents. The synthesis of the structures **S1a**, **S2a**, **S6a** and **S7a** was previously described by *Elbing*.¹⁰⁰

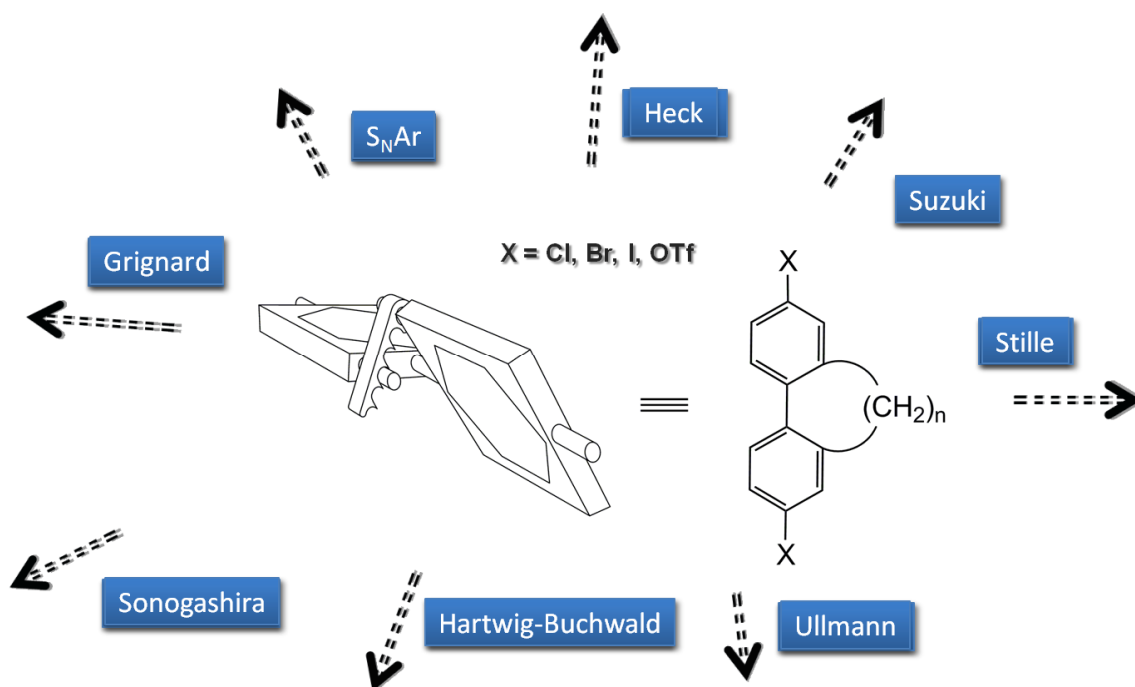


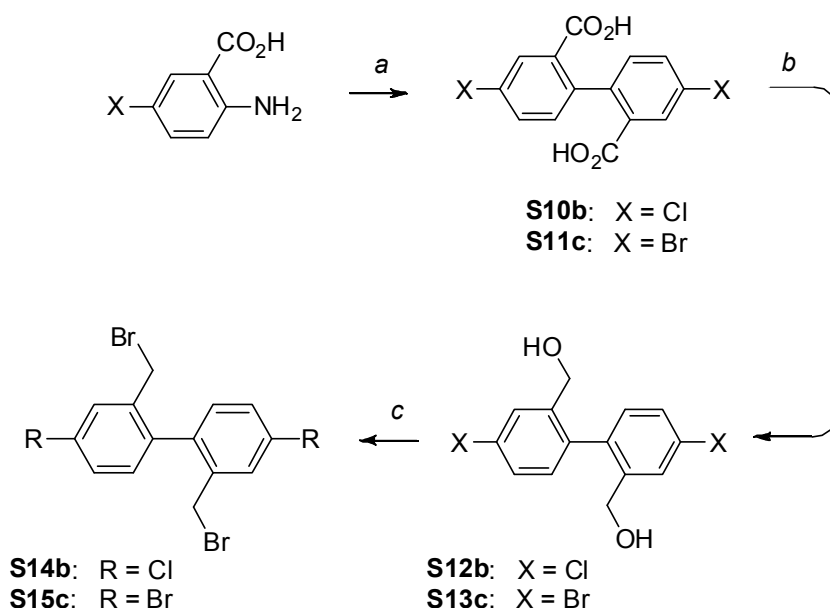
Figure 26. The concept of fixing the torsion angle by a clamping bridge of defined length is sketched. On the molecular level, an alkyl chain with $n \cdot (\text{CH}_2)$ -units is interlinking the two phenyl units, adjusting stepwise the interplanar torsion angle. The “*modular biphenyl building blocks*” are terminally functionalized with leaving groups X. The various leaving groups provide substrates for numerous reactions like e.g. *Hartwig-Buchwald*, *Heck*-, *Suzuki*-, *Stille*-, *Sonogashira*-, *Ullman*-, *Grignard*- or $\text{S}_{\text{N}}\text{Ar}$ -type of reactions.

As these biphenyl synthons **S1-S8** were envisaged as generally interesting and useful model structures the synthetic strategy was to perform the terminal functional groups modification in a very last step.

To enable functionalization and integration into molecular devices¹³³⁻¹³⁸ and materials,¹³⁹⁻¹⁴¹ the biphenyl synthons were functionalized in *para*-positions by typical leaving groups such as halogen atoms or triflate-groups. These bromine-, iodine- and triflate-functionalized building blocks are also suitable candidates for palladium-catalyzed cross coupling reactions. Namely, *Hartwig-Buchwald*-,¹⁴²⁻¹⁴⁴ *Heck*-,^{145,146} *Suzuki*-,^{147,148} *Stille*-¹⁴⁹ or *Sonogashira*-reactions.^{150,151} Furthermore, metal-mediated reactions such as *Ullman*-¹⁵² and *Grignard*¹⁵³-reactions or $\text{S}_{\text{N}}\text{Ar}$ -type reactions can be envisaged.^{19,154}

2.2 Synthesis of the BPDTs and their Modular Building Blocks

The synthetic concept of restricted rotation of biphenyl synthons was inspired by the “Geländer” molecules from *Fritz Vögtle* and coworkers.¹⁵⁵ By clamping the *para*-terphenyl backbone with an additional three atom bridges such as thiobis(methylene)- or ester-functionalized propyl-chains they synthesized *para*-terphenylophanes displaying chirality due to their screw type arrangement emerging from the fixed torsion angles of the biphenyl subunits.¹⁵⁵ Heteroatoms were avoided in the bridging structures in order to keep the electronic features of the substituents as comparable as possible within the series and to allow a broad range of reaction conditions in the subsequent functional group transformations.



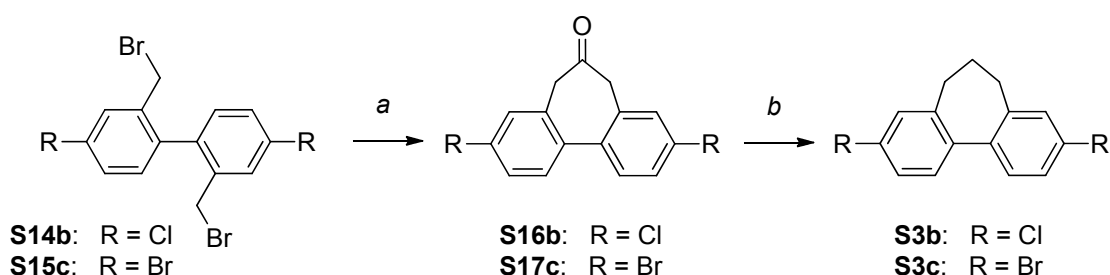
Scheme 1. (a) NaNO_2 , HCl, 0 °C, then CuSO_4 , HO-NH₂, NH₄OH, H₂O, 0 to 70 °C, 69% for **S10b**, 70% for **S11c**. (b) NaBH_4 , BF_3 -etherate, THF, 67% for **S13c**. (c) PBr_3 , CH_2Cl_2 , 0 °C, 48% for **S14b** (over 2 steps), 63% for **S15c**.

The synthetic strategy towards the propyl- and butyl-bridged building blocks **S3b-c** and **S4b-c** profiting from benzyl bromides is reminiscent of the approach of *Vögtle*. The key intermediates **S14b** and **S15c** (scheme 1) were synthesized on a large scale: 4,4'-dichlorodiphenic acid **S10b** was synthesized

from the bulk chemical 5-chloroanthranilic acid according to a previously described procedure by *Helms et al.*¹⁵⁶ Similarly, 4,4'-dibromodiphenic acid **S11c** was obtained in good yield (70%). The crude diphenic acids **S10b** and **S11c** were reduced to the diols **S12b** and **S13c** using sodium borohydride and $\text{BF}_3 \cdot \text{etherate}$ as the activating *Lewis* acid.¹⁵⁷ The crude diol **S12b** was subsequently transformed to the dibenzylic dibromide by an $\text{S}_{\text{N}}2$ reaction obtaining the key intermediate **S14b** in 48% (over two steps).¹⁵⁸ Similarly, we obtained the dibromo homologue **S15c** in 63%. An immediate purification of the crude diols by flash chromatography improved the yield considerably. Interestingly, attempts to repeat an already reported synthesis of **S14b** based on a radical bromination¹⁵⁹ were not successful and instead of the desired compound a tarry inseparable mixture was obtained.

2.2.1 Propyl-Bridged Cyclophanes

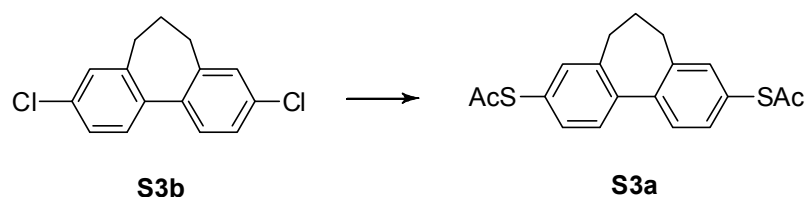
To achieve the keto-functionalized propyl bridge in **S16b** an additional carbon-atom was introduced by an intramolecular cyclization reaction of the dibromide **S14b** using the masked formaldehyde equivalent TosMic¹⁶⁰ to provide the dichloro-ketone **S16b** in a yield of 77% (scheme 2).



Scheme 2. (a) TosMic, NaOH, TBAB, $\text{CH}_2\text{Cl}_2/\text{H}_2\text{O}$, then HCl, *t*-BME/ H_2O , 77% for **S16b**, 44% for **S17c**. (b) PMHS, $(\text{C}_6\text{F}_5)_3\text{B}$, CH_2Cl_2 , rt, 61% for **S3b**, 78% for **S3c**.

In a similar way the dibromo-ketone **S17c** was obtained in 44%. A *Lewis* acid catalyzed reduction with polymethylhydrosiloxane (PMHS) of the keto group¹⁶¹ afforded the doubly chlorinated key building block **S3b** in 61%. Following the

same procedure the bromo-homologue **S3c** was obtained in 78%. The latter compound was purified by flash chromatography followed by recrystallization from hexane, to remove remaining impurities from the polymeric silane reagent. To obtain analytically pure material, again, repeated flash chromatography on silica with pure hexane as the eluent was necessary.



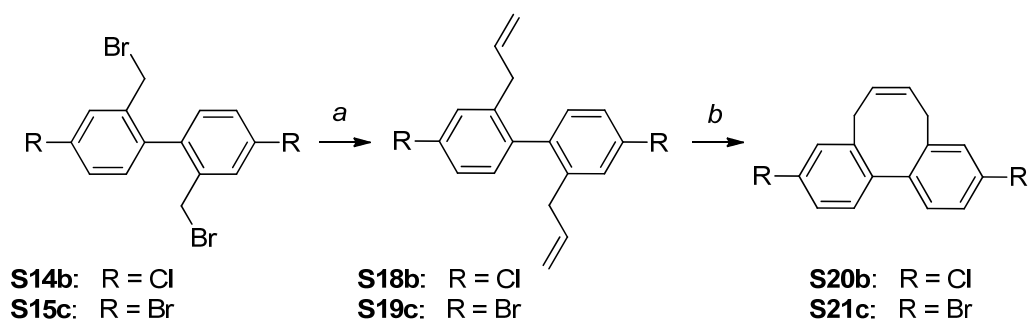
Scheme 3. NaSCH₃, DMI, 110 °C, then AcCl, 49%.

The aromatic nucleophilic substitution reaction of both chlorine atoms in **S3b** with methylthiolates and an *in situ* transprotection^{100,162,163} of the resulting methylsulfanyl groups provided the terminally acetylsulfanyl-functionalized and propyl bridged biphenyl **S3a** in 49% yield (scheme 3). Chlorine as the leaving group was first chosen as aryl chlorines provide ideal substrates (lower costs and less waste is produced than with iodides or bromides) in nucleophilic type of reactions as well as in metal-catalyzed reactions.¹⁵⁴ The reactivity of halogen substrates in palladium-catalyzed cross coupling reactions normally decreases in the order: I > Br > Cl > F where fluorine normally is not at all reactive. Interestingly, in nucleophilic aromatic substitution reactions the substrate reactivity is the opposite. Fluorine is reacting much faster than all others halogens. In this two-step addition-elimination reaction, fluorine accelerates the reaction speed of the first step by efficiently stabilizing the anionic reaction intermediate.¹⁶⁴

Due to difficulties in the conversion of the chlorinated building blocks to amines in our group using Pd-catalyzed cross-coupling conditions the building blocks comprising bromines as leaving groups turned out to be ideal substrates.¹⁶⁵

2.2.2 Butyl-Bridged Cyclophanes

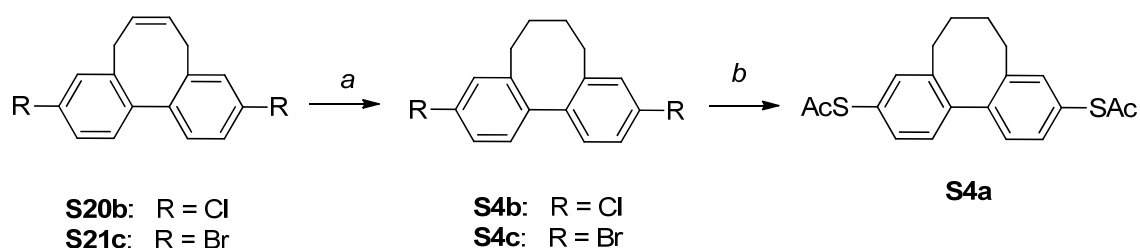
Starting again from the 4,4'-dihalogen benzylic dibromides **S14b** and **S15c**, a copper-mediated *Grignard* reaction¹⁶⁶ provided the diallylic biphenyl **S18b** in 58% and **S19c** in 77% as an odorous oil. In spite of the reported challenges faced during the formation of eight-membered rings¹⁶⁷ by ring closing metathesis (RCM), the cyclization proceeded smoothly in the case of **S18b** and **S19c**, probably due to the conformationally predisposed allyl chains.^{168,169} The metathesis reaction using first or second generation of the *Grubbs'* catalyst showed to be equally effective affording **S20b** and **S21c** in good yields of 88% and 94%, respectively as white solids (scheme 4).



Scheme 4. (a) CH_2CHMgBr , CuI , CH_2Cl_2 , $-40\text{ }^\circ\text{C}$ to rt, 58% for **S18b**, 79% for **S19c**. (b) *Grubbs'* catalyst, CH_2Cl_2 , reflux, 88% for **S20b**, 94% for **S21c**.

Subsequent hydrogenation with palladium on charcoal at atmospheric pressure yielded the doubly halogenated key building blocks **S4b** and **S4c** almost quantitatively (scheme 5).

Finally, a similar reaction sequence as described for **S3a** resulted in the transformation of the chlorines into acetylsulfanyl groups to provide the butyl-bridged derivative **S4a** in 32% yield (scheme 5).

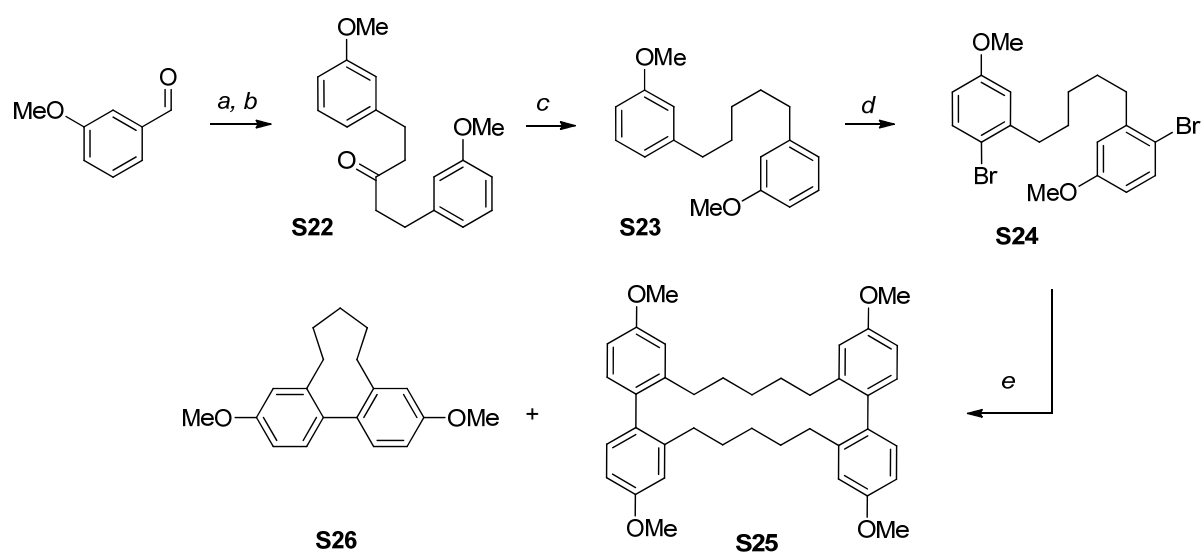


Scheme 5. (a) H₂, Pd/C 10%, rt, EtOAc, 95% for **S4b**, 98% for **S4c**. (b) NaSCH₃, DMI, 110 °C, then AcCl, 32%.

2.2.3 Pentyl-Bridged Cyclophanes

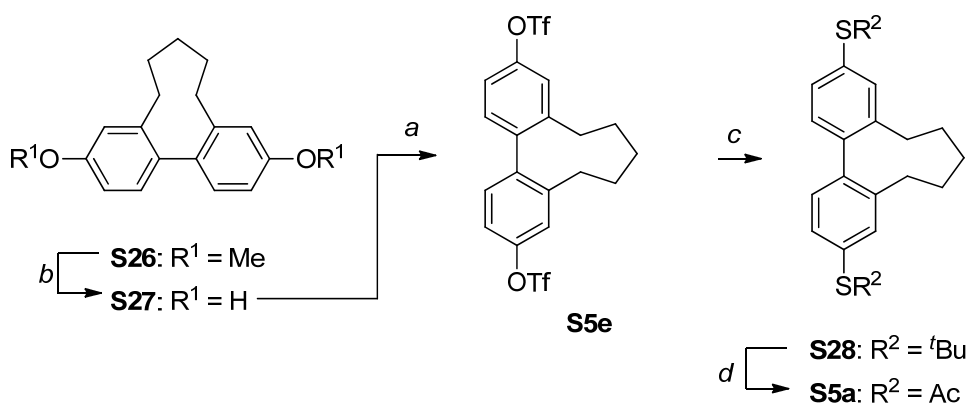
An alternative strategy was applied for the assembly of the cyclononane structure in the modular building block **S5e** (figure 25). As displayed in scheme 6, the inter-ring pentyl chain was established prior to the formation of the biphenyl backbone. The symmetric 1,5-bis(3-methoxyphenyl)-pentane **S23** has been synthesized according to a reported procedure.¹⁷⁰⁻¹⁷²

Thus, *meta*-anisaldehyde underwent a double aldol-condensation with acetone,^{170,171} followed by a hydrogenation¹⁷² which afforded **S22** in 46% over two steps. The reduction to **S23** was achieved by a classical *Wolf-Kishner* reaction in 72%.¹⁷² A subsequent bromination afforded regioselectively the dibromo key intermediate **S24** in 42% yield as a precursor of the subsequent cyclization reaction.¹⁷³ Repeated recrystallization was crucial to remove the formed regioisomeric side products at this stage. Similarly, the iodination¹⁷⁴ of **S23** with silver trifluoroacetate - iodine proceeded smoothly but separation of the formed side products by recrystallization was inefficient.



Scheme 6. (a) acetone, NaOH, EtOH.^{170,171} (b) H₂, Pd/C 10%, 1 EtOAc, 1 atm, 46% (over 2 steps).¹⁷² (c) Hydrazine 85%, KOH, triethylene glycol, 190-200°C, 72%.¹⁷² (d) Br₂, pyridine, -10 °C to rt, 42% (after recrystallization).¹⁷³ (e) *t*-BuLi, CuCN, LiBr, MeTHF, -60°C, then 1,3-dinitrobenzene, 23% for **S26** and 27% for **S25**.

The readily synthesized key substrate **S24** underwent a medium ring-forming reaction by a copper-mediated C-C biaryl bond formation. Whitesides¹⁷⁵ and more recently Lipshutz¹⁷⁶⁻¹⁷⁹ used oxidants on aryl cuprates to form biaryls intermolecularly. Adapting an experimental procedure of Schreiber¹⁸⁰, describing the synthesis of a series of asymmetric biaryl-containing macrocyclic rings, the cyclononane structure **S26** was synthesized successfully. Treatment of the dibromide **S24** with *tert*-butyllithium followed by CuCN formed a cyclic biaryl-cuprate as the intermediate. Upon exposure to 1,3-dinitrobenzene as oxidant two major products were isolated after purification by flash chromatography in about equal amount. Intermolecular dimerization of two molecules **S24** gave the undesired dimer **S25** which was formed in a yield of 27%, while the intramolecular reaction provided the desired macrocycle **S26** in a yield of 23%. Attempts to favor the intramolecular reaction by applying high dilution conditions did not improve the isolated yield of the monomeric product **S26**.



Scheme 7. (a) BBr₃, CH₂Cl₂, rt. (b) Tf₂O, pyridine, 4°C to rt. (c) *t*-BuSNa, Pd₂(dba)₃, xantphos, *p*-xylene, 140°C, 62% (over 3 steps). (d) BBr₃, AcCl, toluene, 61%.

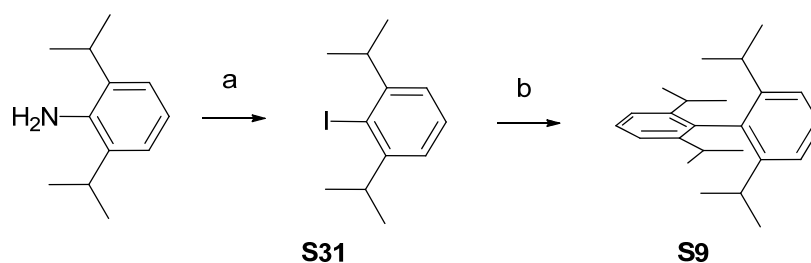
Subsequent functional group transformation allowed to transform the terminal methoxy groups of **S26** into the key building block **S5e** bearing triflate groups (scheme 7); The unfunctionalized pentyl bridge in **S26** allowed the electrophilic cleavage¹⁸¹ of the two methyl groups of the biaryl ether with boron tribromide at room temperature.

The crude biaryldiol **S27** was obtained as a fluffy material which was pure enough to use directly for the next step. The subsequent esterification of the diol **S27** with triflic anhydride in pyridine, acting as the base, gave the key building block **S5e** as colorless oil. Slight impurities, probably arising from the starting reagent, remained after purification by flash chromatography. However, these traces did not interfere with the subsequent reaction steps. The *tert*-butyl protected terminal sulfur groups in **S28** were obtained from the “modular biphenyl building block” **S5e** and sodium *tert*-butylthiolate by applying palladium-catalyzed cross coupling conditions. The conversion of triflates to thioarylethers displays a valuable reaction due to a wide range of phenol derivatives as pool chemicals. Though, few examples have been described. Researchers from the *Merck Laboratories*¹⁸² and *Mispelaere-Canivet*¹⁸³ have shown the cross-coupling of aliphatic and aromatic thiols with aryl triflates mediated by Pd/ligand catalytic systems, however bistriflate-functionalized aromatic system have never been investigated.

A catalytic amount of $\text{Pd}_2(\text{dba})_3$ and xantphos as the ligand in *p*-xylene were successfully applied to the cross-coupling of **S5e** with NaS^tBu to form **S28**. However, an elevated reaction temperature of 140°C turned out to be crucial for the formation of the doubly *tert*-butylsulfanyl functionalized **S28**. A yield of 62% was obtained in this three step reaction sequence. A final transprotection step of the *tert*-butylsulfanyl groups gave **S5a** as terminally acetylsulfanyl-functionalized macrocyclic biphenyl. Thus, **S28** was treated with an equimolar amount of boron tribromide removing the *tert*-butyl groups whereupon the formed free thiol groups were trapped *in situ* by acetyl chloride affording the thioester **S5a**.^{184,185}

2.2.4 Fully Separated π -Systems

To complement the series of cyclic biphenyls with restricted rotation along the biphenyl axes, systems with a close to perpendicular conformation moved into the centre of attention.



Scheme 8. (a) NaNO_2 , *p*-TSA, KI, *t*-BuOH, H_2O , 40% (b) *t*-BuLi, CuCN, LiBr, MeTHF, -60°C , then 1,3-dinitrobenzene, 20%.

To achieve a biphenyl structure with perpendicular conformation the new sterically demanding 2,2',6,6'-tetraisopropyl biphenyl synthon **S9** starting from the commercially available 2,6-diisopropylaniline was synthesized. Applying a *Sandmeyer* reaction the aryl iodide **S31**¹⁸⁶ was obtained in moderate yield which was subsequently converted to **S9** by a copper-mediated aryl-aryl coupling reaction similar to that used to prepare compound **S26**.¹⁸⁰

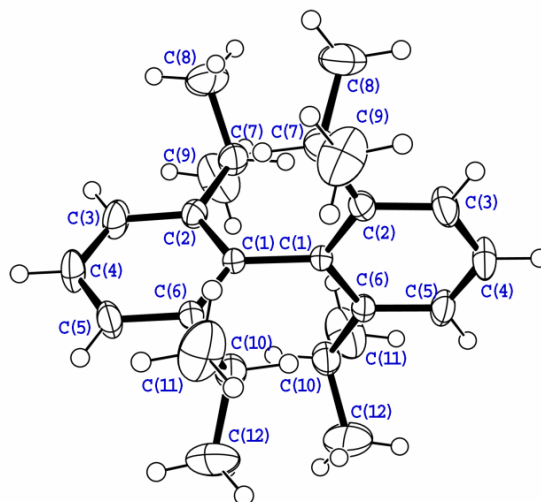
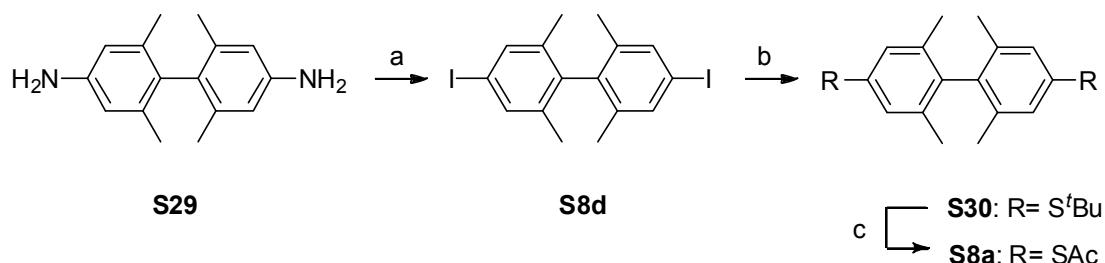


Figure 27. The X-ray structure of 2,2',6,6'-tetraisopropyl biphenyl **S9** displaying a torsion angle ϕ between both phenyl rings of 86.5° .

Single crystals of **S9** suitable for X-ray measurement were obtained from by slow evaporation of cold pentane. Interestingly, at first glance the even more sterically demanding four isopropyl groups in *ortho*-positions of **S9** cause a slightly reduced torsion angle ϕ of only 86.5° compared to **S8a** with 89.0° (section 2.3) bearing four methyl groups. The origin of this unexpected difference remains unclear. This difference in ϕ might either be a general trend in such *ortho* alkyl functionalized biphenyl compounds as well as simple packing effects in the solid state structures. All attempts to further functionalize the tetraisopropylbiphenyl synthon with leaving groups in *para*-position failed. While with mild reaction conditions such as bromine in trimethylphosphate no conversion of **S9** was observed, overbromination was observed for the *Lewis* acid (FeCl_3) catalyzed bromination with bromine in CH_2Cl_2 . Further attempts geared towards selective iodination with the hypervalent iodination reagent PIFA¹⁸⁷ resulted in complex mixtures of mono- and diiodinated derivatives of **S9**. Due to the challenging selective functionalization, **S9** was no longer considered as a potential modular biphenyl building block. Other attempted synthetic strategies to directly obtain *para* functionalized biphenyls with four *ortho*-isopropyl substituents did not lead to any satisfying results. These attempts included copper-mediated aryl-aryl coupling reactions with

preliminary and selective halogen/metal exchange of mixed halogen precursors. However, the series with restricted rotation along the biphenyl axes was completed by successfully synthesizing the tetramethyl compound **S8a**.



Scheme 9. (a) NaNO_2 , H_2SO_4 , H_2O , KI , I_2 , 51%. (b) $t\text{-BuSNa}$, $\text{Pd}_2(\text{dba})_3$, xantphos, $p\text{-xylene}$, 140°C , 74%. (c) BBr_3 , AcCl , toluene, 84%.

An interesting biphenyl building block with an almost perpendicular configuration of both phenyl rings and thus with a poor electronic coupling along its backbone is the known 4,4'-diiodo-2,2',6,6'-tetramethyl biphenyl **S8d** (scheme 9).

Starting from the benzidine[‡] precursor **S29**¹⁸⁸ bearing the four methyl groups in the desired position, the amine groups were diazotized with nitrous acid in aqueous media followed by the treatment of a iodide/iodine couple which gave the functionalized diiodo-building block in a four times higher yield compared to an earlier reported procedure.¹⁸⁹ Direct introduction of the sulfur-atom by the thioacetate anion using a palladium catalyzed procedure by *Lai*¹⁹⁰ was not successful. However, the key building block **S8d** underwent successfully a palladium catalyzed cross-coupling reaction according again to the protocol of *Mispelaere-Canivet*¹⁸³ to the thioether **S30** in 74%. The acetyl protected dithiol **S8a** was finally achieved by using a standard transprotection procedure as previously described in the synthesis of compound **S5a** in 84%. To separate the impurities emerging from the benzidine rearrangement (**S29**),[‡] a recrystallization from a mixture of hot hexane and cyclohexane was performed to yield highly pure **S8a** as single crystals.

‡ *The original procedure from 1945 to prepare benzidine **S29** includes a complex multi step purification procedure. Attempts to remove the isomeric impurity (2,2',4,6'-tetramethyl-6,4'-diaminobiphenyl) by repeated recrystallization in various solvents failed. This impurity was easily removed by recrystallization after introduction of the acetyl protected thiol groups.*

2.3 X-ray Solid State Structural Analysis

Of particular interest were X-ray solid state structure analysis of the new BPDT structures **S1a-S8a** not only to confirm the identity of the compounds, but also to investigate the correlation between the length of the bridging alkyl chain in **S1a-S5a** and the resulting torsion angles ϕ . While the attempts to crystallize the fluorene derivative **S1a** and the unsubstituted BPDT compound **S6a** failed (precipitated as powder), single crystals suitable for X-ray analysis were obtained for the bridged BPDTs **S2a-S4a** from hot cyclohexane and in the case of **S5a**, from hot pentane after storing at 4 °C. In addition, the solid state structure of **S7a** was already reported by *Elbing*¹⁰⁰ and co-workers and suitable single crystals from the tetramethyl substituted BPDT **S8a** were obtained again from hot cyclohexane.¹⁵⁴

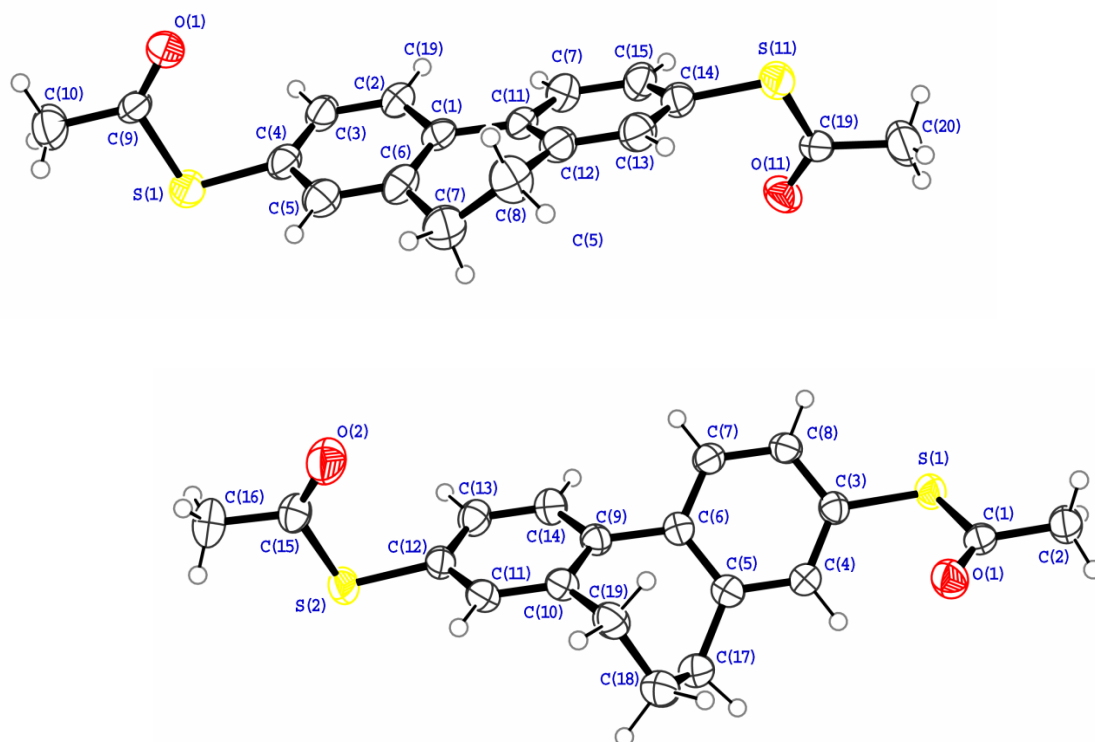


Figure 28. Ortep III view of the molecular structures of **S2a** (top) and **S3a** (bottom). Thermal ellipsoids are set at 50% probability. A torsion angle of 16.8° was measured for **S2a** and 44.7° for **S3a** respectively.¹⁵⁴

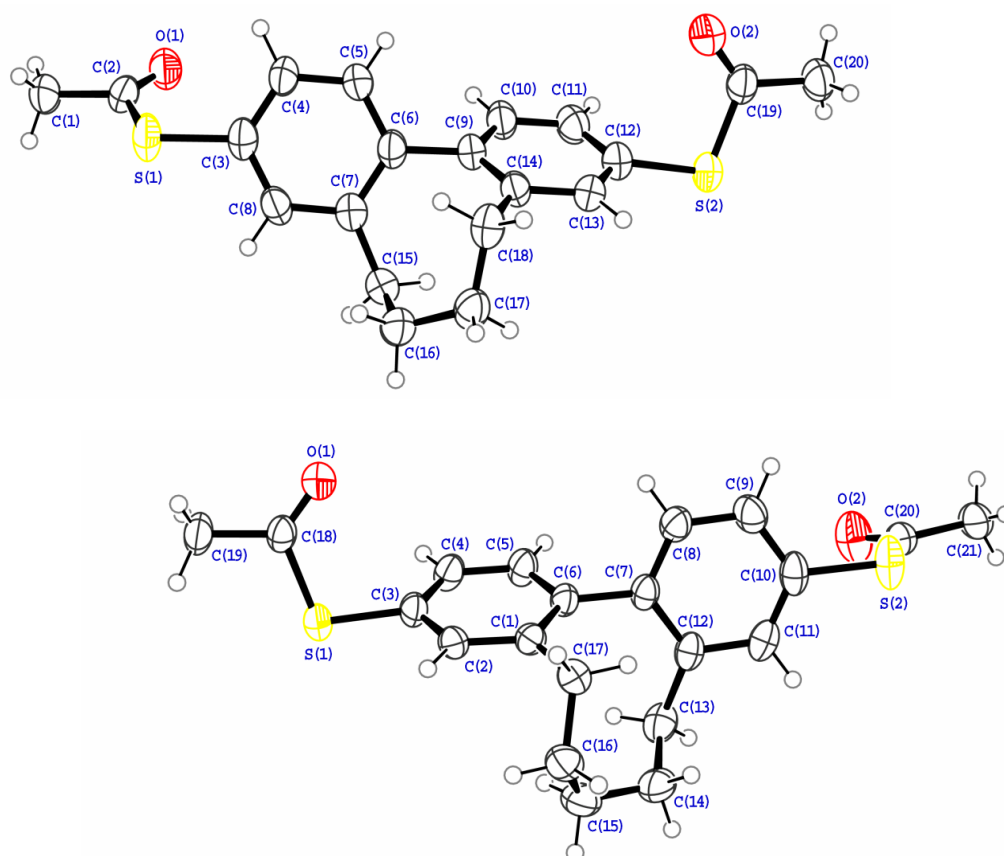


Figure 29. Ortep III view of target structures **S4a** (top), **S5a** (bottom). Thermal ellipsoids are set at 50% probability. A torsion angle of 57.8° was measured for **S4a**, 71.5° for **S5a**.¹⁹

Figure 28 and figure 29 display the solid state structures of the bridged BPDTs **S2a-S5a** as a series of increasing length of the bridging alkyl group. Furthermore, particular structural parameters including the intramolecular sulfur-sulfur distance as length axis of the molecule and the torsion angle ϕ are listed in table1. Very comparable intramolecular sulfur-sulfur distances within the series of X-ray analyzed derivatives with values between 1.059 nm for **S5a** and 1.062 nm for **S7a** (2,2'-dimethyl-BPDT)¹⁰⁰ point at hardly any effects of the various alkyl substituents on the linearity of the BPDT backbone. Obviously, steric repulsion emerging from various alkyl substituents seems to be intercepted by adjusting the inter-ring torsion angle ϕ .

This torsion angle was measured between the planes of both phenyl rings of the biphenyl system. These planes were obtained by considering all six carbon atom positions of the solid state structure for the least square minimization procedure.

Table 1. Molecular structures and measured properties.

#	torsion angle Φ /° from the solid state structure	S(1)-(2) distance (nm)
S1a	1.1 ^[a]	-
S2a	16.8	1.061(2)
S3a	44.7	1.060(9)
S4a	57.8	1.060(5)
S5a	71.5	1.059(4)
S6a	36.4 ^[b]	-
S7a	79.7 ^[c]	1.06(2) ¹⁰⁰
S8a	89.0	1.061(2)

[a] The value was taken from the solid state structure of fluorene.¹⁹¹ [b] The torsion angle was calculated at the DFT level.¹⁰⁸ [c] Taken from the solid state structure in ref.¹⁰⁰

The obtained torsion angles Φ are displayed in table 1 and display a continuous increase with elongation of the inter-ring alkyl bridge.

While the elongation by a CH₂ unit between the fluorene **S1a** and the dihydrophenanthrene **S2a** increases the torsion angle by 15.7°, the largest increase of the torsion angle Φ of almost 28° is observed between the dihydrophenanthrene **S2a** and the C₃-bridged BPDT system **S3a**. Further elongation to the C₄- and C₅-bridged derivatives **S4a** and **S5a** result in additional openings of the angle Φ by 13.1° and 13.7° respectively.¹⁹

The almost perpendicular arrangement of both phenyl rings were measured for the solid state structures of the dimethyl- and the tetramethyl-derivatives **S7a** and **S8a** with values of 79.7° and 89° respectively.

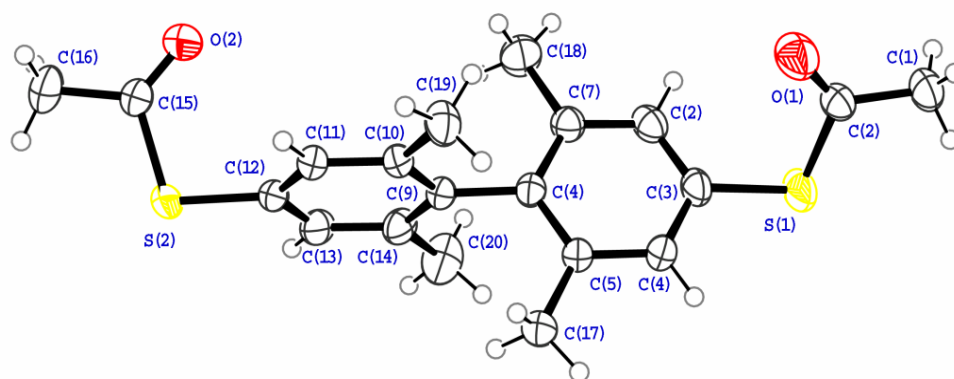


Figure 30. The X-ray structure of **S8a** with an interplane torsion angle ϕ of 89.0°. ¹⁵⁴

Compared to the parent BPDT **S6a** (2-3 kcal/mol⁻¹), the rotation barriers of the additionally methyl substituted compounds **S7a** and **S8a**, and in particular of the alkyl interlinked derivatives **S2a-S5a** are expected to be increased considerably (see section 1.4.2).¹⁹² Thus, in spite of the increased structural flexibility in solution, the values obtained by solid state structure analysis remain the best proxy for the value expected in solution.¹⁵⁴

2.4 Electronic Spectra

To investigate the correlation between electronic absorption properties and the interplane torsion angle ϕ , the entire series of biphenyl derivatives **S1a-S8a** comprising identical terminal groups was measured. The UV absorption spectra of the series **S1a-S8a** were measured in hexane with a concentration of $1.0 \cdot 10^{-5}$ M. The obtained absorption spectra are displayed in figure 31.

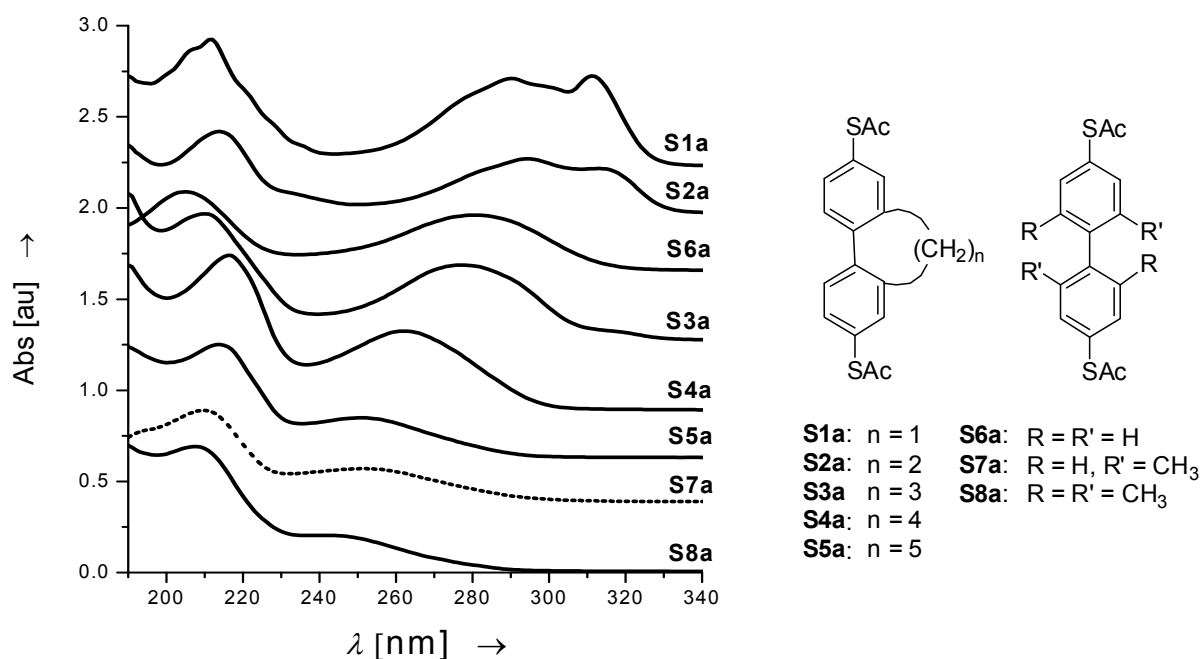


Figure 31. UV absorption spectra of the BPDTs in hexane with a concentration of $1 \cdot 10^{-5}$ M. The absorption spectra are displayed in a stacked mode.

The longest wavelength absorption bands of **S1a** and **S2a** are around 312 nm and, in analogy to their terminally unsubstituted counterparts, are assigned to the α -absorption band.¹⁹³ Similarly, the broad absorption bands of **S1a-S8a** between 240 and 300 nm can be assigned to the p -band of the biphenyl subunit.

This p -band is also called the conjugation band, as its position and intensity is reported to reflect the extent of conjugation in the biphenyl core.^{96,194,195}

Compared with the terminally unfunctionalized biphenyl, we observe for **S6a** a bathochromic shift of about 30 nm of the p -band (figure 31) which may be

attributed to the enlargement of the π -system due to the substitution with lone pairs containing S-acetyl groups.¹⁹⁵

Table 2. Torsion angles and UV-absorption properties of **S1a-S8a**.

#	torsion angle ϕ / ^o from the solid state structure	<i>p</i> -band λ_{\max} nm (eV)	Absorption onset nm (eV)	ε (L mol ⁻¹ cm ⁻¹)
S1a	1.1 ^[a]	291 (4.26)	327 (3.79)	28900
S2a	16.8	295 (4.20)	330 (3.76)	30500
S3a	44.7	278 (4.46)	309 (4.01)	24000
S4a	57.8	263 (4.71)	297 (4.17)	21700
S5a	71.8	250 (4.96)	290 (4.28)	17600
S6a	36.4 ^[b]	281 (4.41)	315 (3.94)	27000
S7a	79.7 ^[c]	251 (4.94)	294 (4.22)	17600
S8a	89.0	244 (5.08)	282 (4.40)	18300

[a] The value was taken from the solid state structure of fluorene.¹⁹¹

[b] The torsion angle was calculated at the DFT level.¹⁰⁸ [c] Taken from the solid state structure in ref.¹⁰⁰

In table 2 the onset and the λ_{\max} values of the *p*-band absorption of each absorption spectra is listed. According to theory, the π - π^* transition energy^{108,114} and the position of the λ_{\max} of the conjugation band should correlate with the conformation of the biphenyl core. The electron transfer properties between both π -systems is proportional to cosine square of their torsion angles.^{93,114,196}

Thus in figure 32 the longest wavelength onset of each spectrum reflecting the HOMO-LUMO band gap (adiabatic excitation energy) of the compound under investigation is plotted against $\cos^2\phi$. The values of the interplane torsion angles (ϕ) were determined from X-ray structural analysis. Within this series of compounds, the expected linear correlation between the HOMO-LUMO band gap and $\cos^2\phi$ was observed. The α -absorption band was only observed for fixed biphenyl systems with torsion angles ϕ below 45° like **S1a**, **S2a** and **S3a** (**S3a**: shoulder between 310 nm and 325 nm). Furthermore, a strong increase of this band with decreasing torsion angle was observed in this sub-series.

It is noteworthy that the unbridged biphenyl **S6a** with $\phi = 36.4^\circ$ does not exhibit this band.

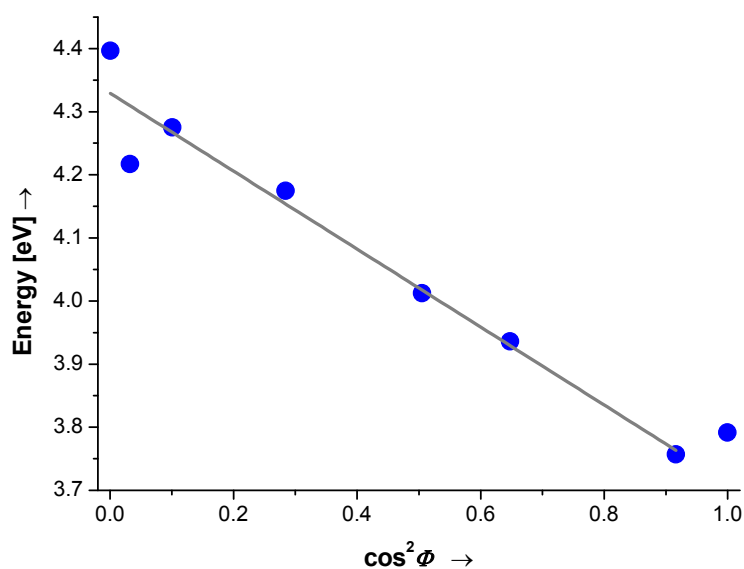


Figure 32. The onset of the UV absorption spectra of the molecules **S1a-S8a** is plotted against $\cos^2 \phi$. ϕ is the measured interplanar torsion angle obtained from the X-ray structure. The linear correlation coefficient R^2 is 0.943 (without **S1a**).

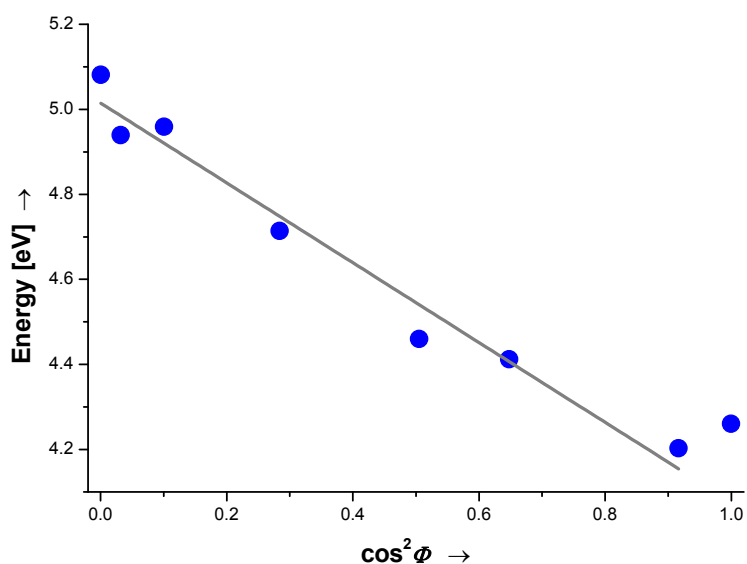


Figure 33. p -band absorption maxima of the molecules **S1a-S8a** plotted against $\cos^2 \phi$. ϕ is the measured interplanar torsion angle obtained from the X-ray structure. The linear correlation coefficient R^2 is 0.967 (without **S1a**).

The plot of the p -band absorption maxima (vertical excitation energy) against $\cos^2\phi$ is displayed in figure 33. Again the expected linear correlation between the λ_{\max} of the p -band and $\cos^2\phi$ was observed for the series. The only slightly exceptional behavior was observed for the fluorene derivative **S1a** displaying a p -band maximum a little bit below the expected value.

Interestingly, a similar trend was also observed in the single molecule transport investigations (see section 2.5).

2.5 Single Molecule Conductance

Of particular interest is the conductance through these BPDT structures mainly varying in the inter-ring torsion angle ϕ . The BPDT structures **S1a-S8a** were investigated between the gold tip and the gold substrate at the solid/liquid interface of a scanning tunneling microscope (STM) break junction set-up¹⁹⁷ protected by an argon gas atmosphere. A 250 μM solution in mesitylene/tetrahydrofuran 4/1 of the BPDT under investigation was treated with a 125 μM solution of tetrabutylammonium hydroxide to remove the acetyl protection groups, allowing the formation of covalent gold-sulfur bonds enabling the immobilization of the rod inside the junction.

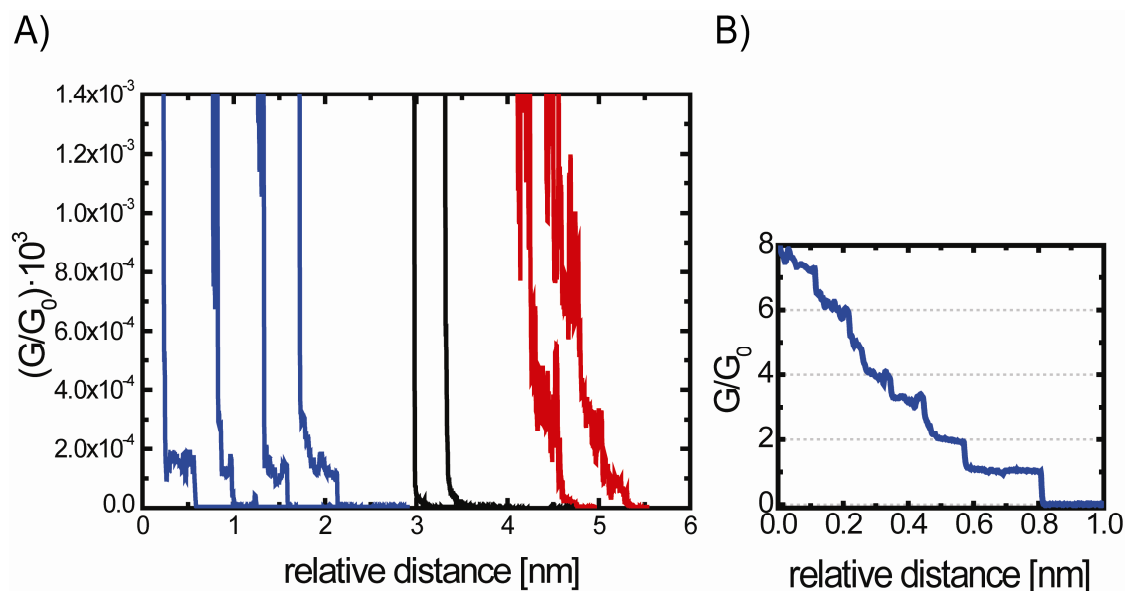


Figure 34. A) Examples of the three types of conductance–distance traces for **S6a'** at $V_{\text{bias}} = 0.1 \text{ V}$: type I (black), type I curves (60%) are exponential and represent direct electron tunneling between gold tip and substrate without molecular junctions being formed; type II (red), type II curves (10–20%) are non-monotonous with large fluctuations, which we attribute to mechanical instabilities or switching between single and multimolecular junctions; and type III (blue), type III curves (20–30%) are non-exponential, and exhibit well-defined steps separated by characteristic plateaus of 0.05–0.30 nm length. B) A typical trace for the breaking of gold nanocontacts in the presence of **S6a'** in a larger conductance range.

To distinguish the molecular junctions from the synthesized molecules **S1a-S8a**, they will be denoted as **S1a'-S8a'**. Three different voltages

(65, 100 and 180 mV) were applied between tip and substrate while the junction was repeatedly opened and closed to establish transient single molecule contacts. Several thousand junctions were created and their current vs. tip-distance traces (figure 34) were recorded. Only the current traces displaying typical single molecule current plateaus have been selected by an automated algorithm and were considered ($20 \pm 10\%$) for the conductance analysis. The extracted conductance histograms revealed characteristic peaks corresponding to the conductance of the single BPDT junction.

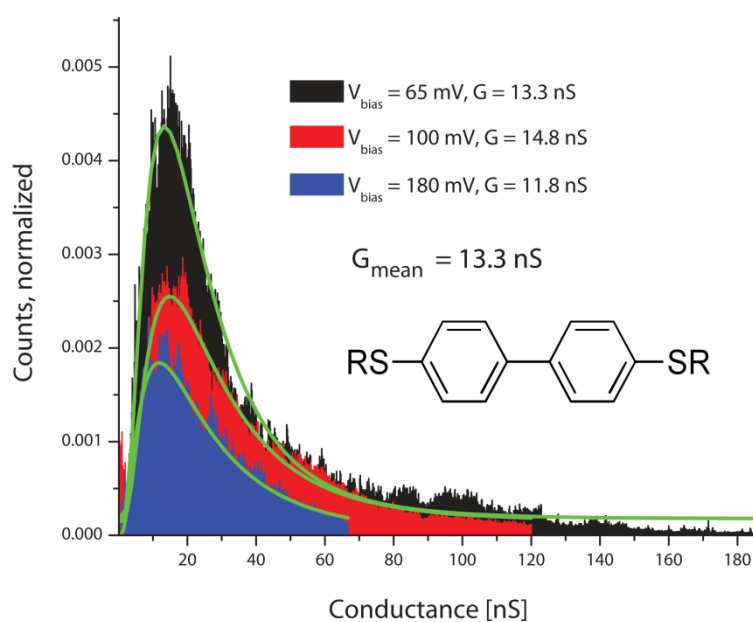
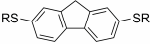
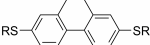
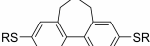
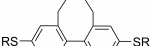

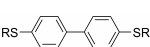
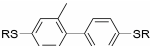
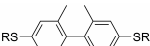


Figure 35. Representative plateau-point histogram for **S6a'**: (black) $V_{\text{bias}} = 65 \text{ mV}$, (red) $V_{\text{bias}} = 100 \text{ mV}$, and (blue) $V_{\text{bias}} = 180 \text{ mV}$.¹⁸

Figure 35 shows, as a representative example, the plateau data-point histogram of 0.25 mM acetyl-protected biphenyl-4,4'-dithiol (**S6a**) after deprotection at three bias voltages in a linear representation. Each histogram, constructed of about 1000 individual (type III) traces out of 3000 totally recorded, reveals a distinct maximum. Control experiments with bare THF/mesitylene, e.g. in the absence of **S6a**, did not show this feature, indicating clearly a **S6a'**-related junction response in figure 35. The position of the peak, which was taken as the most probable single junction conductance $G = (1.7 \pm 0.2) \times 10^{-4} G_0$ (table 3), was estimated by fitting a log-normal

distribution to the experimental data. It can be emphasized that the measurement time of a single conductance-distance trace (~ 50 ms) is long compared to the time scale for molecular rotations in solution (ps),¹⁹⁸ so that the conductance level of each step in a single trace is the thermal average over many dynamic fluctuations.

Table 3. Molecular structures and measured properties.¹⁹

#	Synthesized: R = Ac Immobilized: R = Au electrodes	Interpl. torsion angle Φ ($^\circ$)	Conductance G (G_0)
S1a		1.1	$1.45 \pm 0.1 \times 10^{-4}$
S2a		16.8	$2.19 \pm 0.2 \times 10^{-4}$
S3a		44.7	$1.30 \pm 0.2 \times 10^{-4}$
S4a		57.8	$6.97 \pm 1.7 \times 10^{-5}$
S5a		71.5	$1.68 \pm 0.3 \times 10^{-5}$
S6a		36.4	$1.72 \pm 0.2 \times 10^{-4}$
S7a		79.7	$1.29 \pm 0.2 \times 10^{-5}$
S8a		89.0	$9.03 \pm 1.7 \times 10^{-6}$

[a] The value was taken from the solid state structure of fluorene.¹⁹¹ [b] The torsion angle was calculated at the DFT level.¹⁰⁸ [c] Taken from the solid state structure in ref.¹⁰⁰

According to theory, the electron transmission is proportional to $\cos^2 \Phi$ of their torsion angles. Figure 36 displays the plot of the junction conductance (G/G_0) against $\cos^2 \Phi$ for each BPDT derivative investigated. The data represent averages of the three bias voltages applied as extracted from the corresponding conductance histograms.

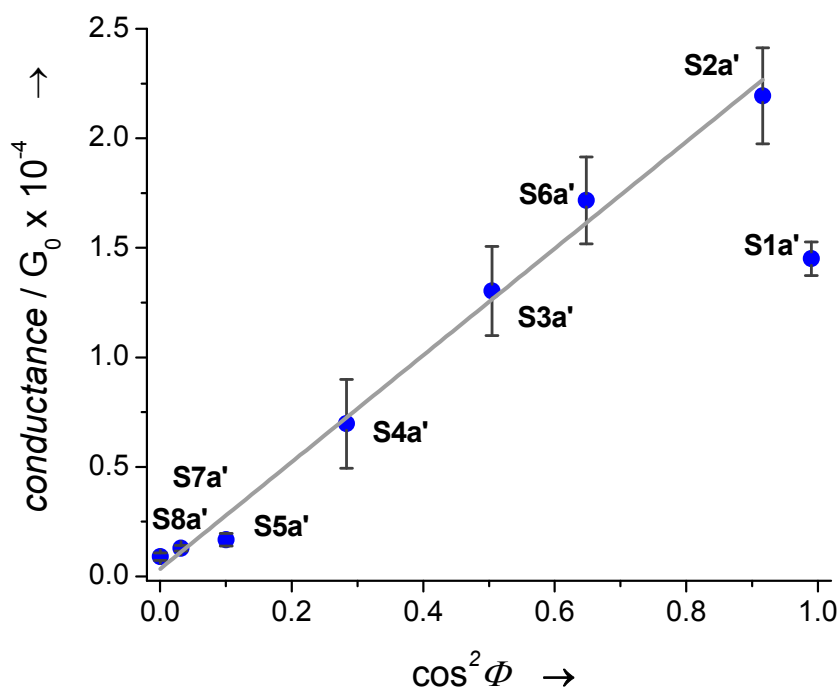


Figure 36. Conductance peaks of the molecular junctions **S1a'**-**S8a'** plotted against $\cos^2 \Phi$, with Φ as the measured interplanar torsion angle obtained from the X-ray structure.¹⁹

Using the linear equation $G = b + a \cos^2 \Phi$ from the data fit (excluding **S1a'**), the estimated slope and the intersection are $a = (2.44 \pm 0.097) \times 10^{-4} G_0$ and $b = (3.4 \pm 4.7) \times 10^{-6} G_0$, respectively. The residual conductance b_{ex} at $\Phi = 90^\circ$ can be probably attributed to σ - π couplings (see also end of 1.4.1.1).^{117,199} The much higher value of the slope suggests that the π - π overlap between the phenyl rings dominates the junction conductance.^{75,108,110}

With the exception of the fluorene structure **S1a**, the series of BPDTs display a linear correlation between the conductance of their single molecule junction and the $\cos^2 \Phi$ extracted from the X-ray data. Interestingly, the conductance values observed for **S1a** are considerably lower than expected.

From previous investigations of the electronic transport through benzene-dithiol, it can be assumed that hole transport is dominant for dithiol-biphenyls, where HOMO states are involved, since the LUMOs have a larger

energy gap to the *Fermi* level of the metal electrode.¹⁸ Surprisingly, semi empirical and DFT calculations do not show an additional stabilization of the HOMO level which could explain the reduced conductance of **S1a**.

Optical UV measurements also revealed an exceptional behavior for fluorene compound **S1a**. It was observed that both the value of the optical band gap as well as the position of the conjugation band do not follow the trend (see previous section). The exceptional optical behavior of fluorene has been mentioned by various authors^{96,113,195,200} and is rationalized by a hyperconjugative effect. When a bridging methylene unit is introduced in the 2 and 2' positions of biphenyl, the remaining hydrogen atoms of the methylene unit are forced into a strained eclipsed conformation. This not only induces torsional strain, destabilizing the π -system,^{201,202} but also allows the methylene unit to interact with the adjacent π -orbitals of the phenyl rings. This type of σ - π -orbital interaction is known as hyperconjugation.

However, DFT calculations of the ground state of the terminally thiol-functionalized fluorene derivatives **S1a** and **CN 1** (from chapter 2 and 3) do not show an σ - π -orbital interaction with the hydrogen atoms of the methylene unit with the adjacent π -orbitals of the phenyl rings.^{18,203} Thus, the origin of this unexpected behavior remains unclear but it is probably due to a subtle combination of factors.

2.6 Conclusion

In conclusion the synthesis and the structural analysis of a family of BPDTs with fixed torsion angles Φ due to an inter-ring alkyl chains was accomplished. The series was complemented by three derivatives with various numbers of methyl substituents in the 2,2',6,6'-position to vary Φ by steric repulsion. To determine the torsion angles Φ single crystals were grown for X-ray analysis. Furthermore, these novel biphenyl synthons were synthesized as modular building blocks comprising suitable leaving groups in the terminal position. This enabled selective functionalization with other functional (anchoring) groups in *para*-position or allows the integration of these building blocks in future molecular systems. Investigation of the single molecule conductance of the series displays a linear correlation with the $\cos^2\Phi$ of the inter-ring torsion angle Φ for BPDTs with a divided π -system.

Hence, the measured molecules-specific property obtained from this series comprising eight molecules varying in a single structural parameter can be assigned to the molecular origin.

A similar trend at increased conductance values has been reported for amine terminated biphenyls comprising various substituents.⁷⁵ In contrast to their findings, the planar fluorene derivative **S1a** displays a reduced conductivity, pointing at additional and equally important parameters governing the transport efficiency in addition to the planarity of the π -system.

These findings were confirmed by the linear correlation between the shift of the conjugation band and the $\cos^2\Phi$ of the torsion angle in solution. This spectroscopically reflects the degree of π - π coupling between both phenyl units and thus reflecting the separation of the HOMO-LUMO energy levels.

3 Exploring π -Electron-Delocalization in the Structure's LUMO: Dicyano-Cyclophanes (CN)

3.1 Introduction

Organic semiconductors can be divided into two classes: *p*-channel semiconductors (holes are injected into the material from the electrodes) and *n*-channel semiconductors (electrons can be injected into the material from the electrodes). The availability of both, efficient *n*- and *p*-channel semiconductor materials is one of the bottle necks currently limiting the development of electronic devices. For the development of efficient π -conjugated materials a profound understanding of the interplay between the π -electron delocalization and geometrical structural features is required. Structure/property relationships of π -conjugated polymers²⁰⁴⁻²⁰⁶ or molecular rods^{18,19,75} with *p*-type character (e.g. sulfur-functionalized biphenyls in chapter 2 and amine-functionalized biphenyls at the end of section 1.4.1) have been studied extensively. Most of these semiconductors are based on organic systems with electron-rich, oxidizable structures comprising thiophene,²⁰⁶ pyrrole or other nitrogen-donor containing systems.²⁰⁵

In contrast to that, structure/property correlations of *n*-channel materials are not well established due to the limited availability of stable and highly performing electron-accepting π -systems.^{204,207,208} Prototypical polymeric *n*-channel materials consist usually of rather rigid molecular subunits such as naphthalene or perylene tetracarboxylic diimides.^{209,210} Progress for the development of new types of *n*-channel semiconductors has been made over the past few years by chemical substitution of the aromatic subunits with electron-withdrawing groups.²¹¹

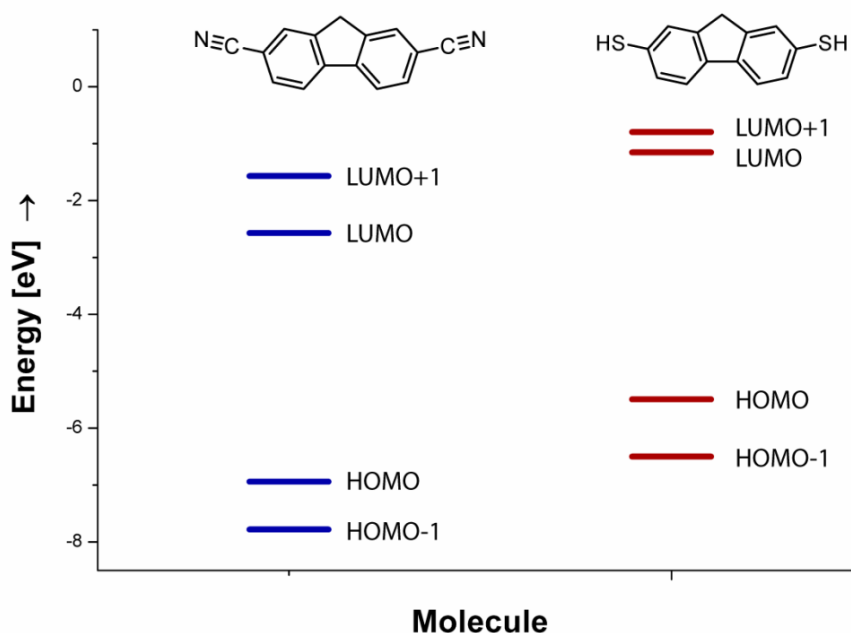


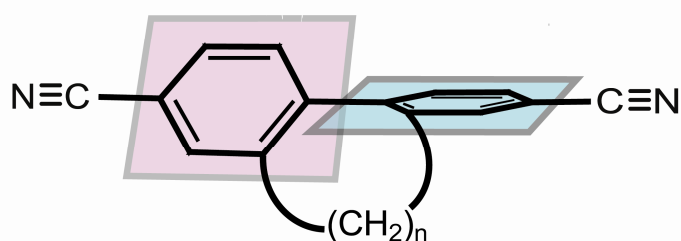
Figure 37. Comparison of the calculated energy levels of 2,7-dicyanofluorene **CN 1** and 2,7-dithiofluorene. The HOMO and LUMO energies of **CN 1** are considerably lowered compared to the fluorene derivative comprising thiol groups due to the electron withdrawing effect of the two cyano groups (DFT/B3LYP/TZVP).

Strong acceptor groups efficiently lower the frontier orbital levels (figure 37) and thereby are making the structures LUMO accessible for electrons at less negative potentials. In other words, acceptor groups are improving the reducibility of the system. However, a clear relationship between the spatial arrangement of neighboring π -systems and electronic properties is missing so far. Furthermore, charge transport in biphenyl model structures comprising donor substituents has been studied, showing that electronic hole transport through the HOMO linearly depends on $\cos^2\phi$ of the torsion angle between the two divided π -systems (see section 2.5).

To explore to which extent these findings also apply for electrons delocalized in the structure's LUMO was the motivation to investigate the physical properties of this series of model compounds.

In this chapter the synthesis of six dicyano-biphenyl model compounds (**CN 1-6**, figure 38) with *n*-channel semiconductor properties is presented. Subsequently the solid state molecular structure and packing properties are discussed, and these data are correlated with the electrochemical, spectroelectrochemical, optical and transport properties. In addition, the experimental data are compared with results obtained from DFT-calculations.

A)



B)

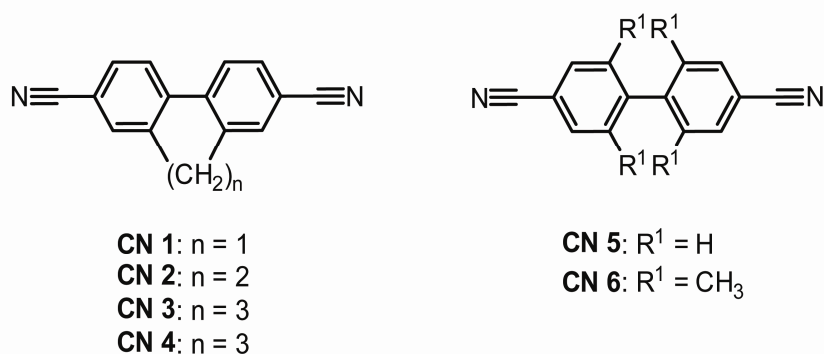


Figure 38. A) The interplanar torsion angle ϕ of the biphenyl backbone is adjusted by the length of the inter-ring alkyl chain. B) Synthesized model compounds: The series of dicyano-biphenyl cyclophanes **CN 1-4** and the dicyano-biphenyl derivatives **CN 5** and **CN 6**.

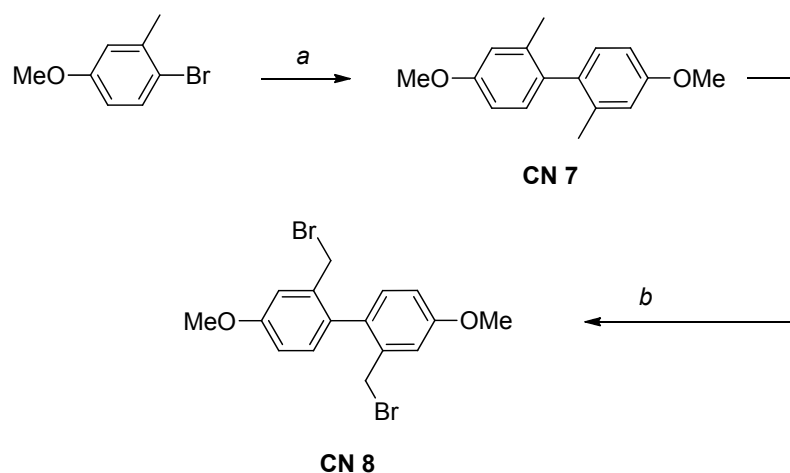
Substitution of the terminal positions of the biphenyl synthons with cyano groups improves the ease of electron injection into the π -system. As a consequence, the reduction potential of this subunit becomes an electrochemical label enabling the investigation of interring communication electrochemically.

Furthermore, with the terminal cyano groups as potential anchor groups for metal electrodes, these series of model compounds is ideally suited to study electron transport on a single molecule level. Thereby, the series enables a systematic investigation of the relationship between electron transport and the backbone conformation.

In addition, organic cyano derivatives are chemically highly stable compared to isocyanides (isocyanides undergo thermal²¹²⁻²¹⁴ and photoinduced^{215,216} isomerization yielding cyanides).²¹⁷ The high stability of the cyanide group can, thus, enhance considerably the lifetime of a molecular device.

3.2 Synthesis and Chemical Characterization

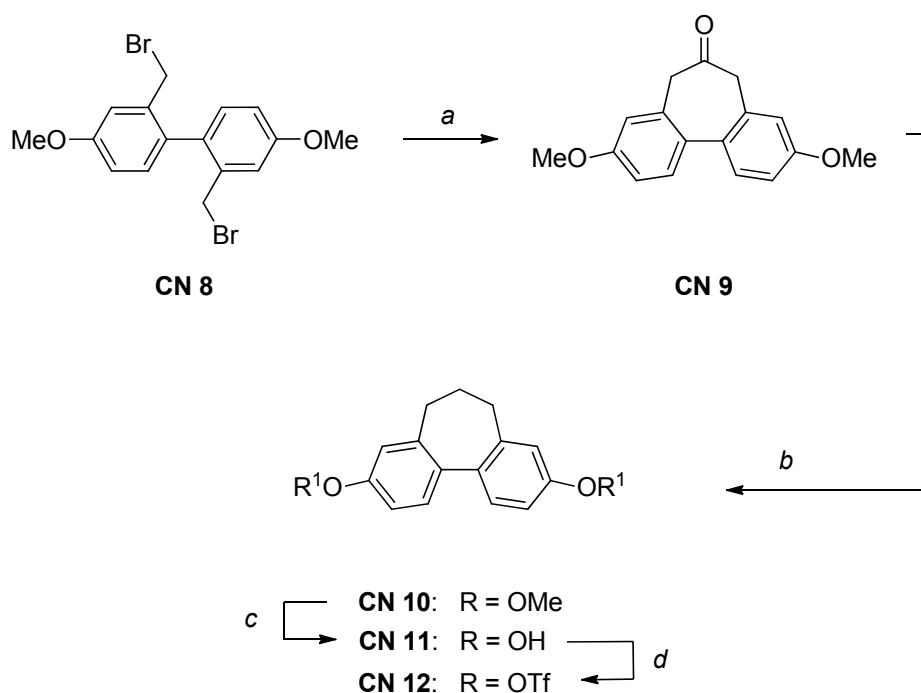
The synthetic strategy to build up the cyclophane synthons was based on the previously described synthetic work on angle-restricted biphenyl-dithiols (section 2.2).^{19,154} The cyclophanes **CN 1-4** (figure 38) with an increasing length of the inter-ring alkyl chain $n = 1-4$ and thus with increasing torsion angles were the initial synthetic target structures. The series of terminally cyano-functionalized biphenyl systems was complemented by the unsubstituted compounds **CN 5** and the 2,2',6,6'-tetramethyl derivate **CN 6** (figure 38). While the strategy to build up the cyclophane structures **CN 3** and **CN 4** is adapted (see section 2.2), the terminal halogen atoms are replaced by methoxy-groups. The new synthetic pathway can be easily scaled up to a few hundred grams and requires no longer difficult to handle polymethylhydro-siloxane and costly reagents. Furthermore, the overall yield of this new “methoxy” synthetic route is increased by almost a factor four compared to the previously described synthesis.¹⁵⁴ The synthetic pathway of the methoxy-functionalized key building block **CN 8** is shown in Scheme 10.



Scheme 10. Reagents and conditions: (a) Mg^0 (1.4 equiv), *methyl*-THF, FeCl_3 (7.1 mol%), 1,2-dichloroethane (1.7 equiv), reflux, 92%. (b) NBS (2.1 equiv), benzoyl peroxide (7.5 mol%), CCl_4 , reflux, 68%.

Starting from the bulk chemical 4-bromo-3-methylanisole, an oxidative iron-catalyzed homo-coupling reaction^{218,219} using stoichiometric amounts of

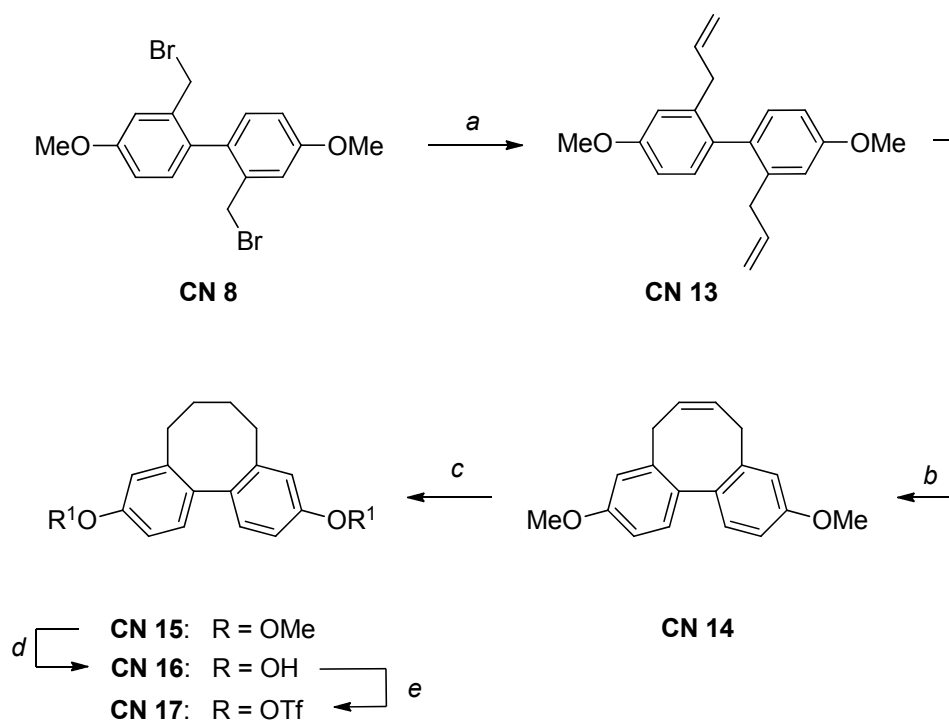
1,2-dichloroethane as the re-oxidation agent, afforded the building block **CN 7** in a yield of 92%. Subsequent double bromination with NBS afforded key intermediate **CN 8** in 68% yield. To achieve the oxo-functionalized propyl bridge in **CN 9**, an additional carbon atom was introduced by an intramolecular cyclization reaction of the dibromide **CN 8**, using the masked formaldehyde equivalent (tolylsulfonyl)methyl isocyanide (TosMic)¹⁶⁰ to provide the dimethoxy ketone **CN 9** as a white solid in a yield of 83% (scheme 11). The "methoxy" route allowed the reduction to **CN 10** by a *Wolff–Kishner* reaction¹⁷² in 86% yield. While the polymethylhydrosiloxane-B(C₆F₅)₃ reduction¹⁶¹ is completed within minutes, the produced polymeric residues lower the yield considerably due to the difficult purification procedure.



Scheme 11. Reagents and conditions: (a) TosMic (1.0 equiv), CH₂Cl₂, NaOH, tetrabutylammonium bromide (TBAB) (6.3 mol%), then HCl, *t*-BME/H₂O, 83%. (b). KOH (4.2 equiv), hydrazine monohydrate (2.3 equiv) diethylene glycol, 195 °C, 86%. (c) BBr₃ (5.5 equiv), CH₂Cl₂, 0 °C to rt. (d). Tf₂O (3.9 equiv), pyridine, rt, 84% over two steps.

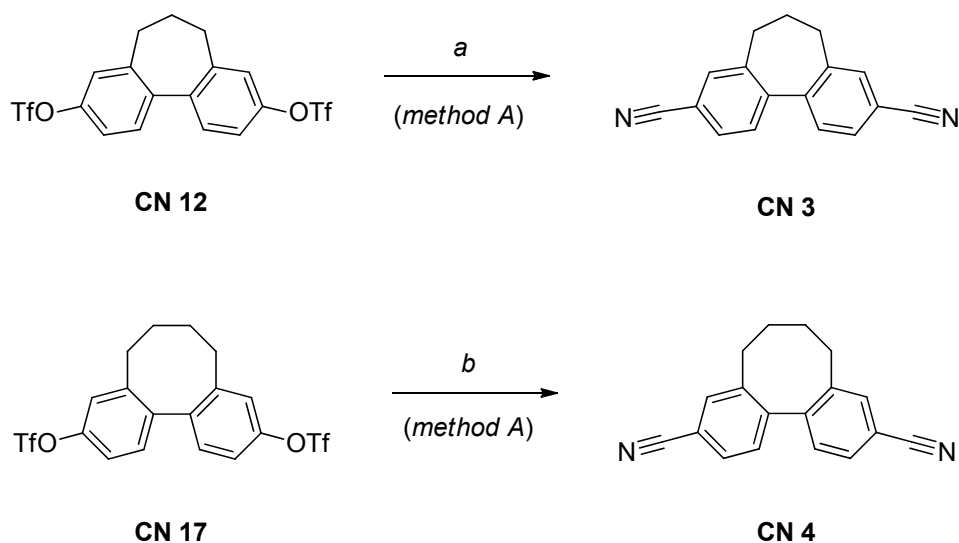
Subsequent functional-group transformations allowed **CN 10** with terminal methoxy groups to be transformed into **CN 12** bearing triflate groups. The unfunctionalized propyl bridge in **CN 10** allowed electrophilic cleavage of the two methyl groups of the biaryl diether with boron tribromide at room

temperature. Subsequent esterification of the diol **CN 11** with triflic anhydride in pyridine gave the triflate building block **CN 12** in a yield of 84% over two steps. An overall yield of 38% was obtained for this six-step reaction sequence.



Scheme 12. Reagents and conditions: (a) CH_2CHMgBr (6.0 equiv), CuI (1.0 eq), CH_2Cl_2 , -50°C to rt, 77%. (b) *Grubbs'* catalyst (5.0 mol%), CH_2Cl_2 , reflux, 79%. (c) H_2 , Pd/C 10%, rt, EtOAc , 98%. (d) BBr_3 , pyridine, rt. (e) Tf_2O (3.9 equiv), pyridine, rt, 83% over 2 steps.

Again, starting from the key intermediate **CN 8** (scheme 12), a copper-mediated alkylation, with the in situ generated *Normant* reagent, provided the diallylbiphenyl **CN 13** as a smelly oil in a yield of 77%. A ring-closing metathesis using *Grubbs'* catalyst afforded **CN 14** in high yield (79%). Subsequent hydrogenation with Pd/C at atmospheric pressure yielded the hydrogenated butyl-bridged biaryl ether **CN 15** almost quantitatively. Finally, a similar deprotection - re-protection reaction sequence as described for the synthesis of **CN 12** resulted in the transformation of the methoxy groups into triflate groups to provide the butyl-bridged key intermediate **CN 17** in 83% over 2 steps. An overall yield of 31% was obtained for this seven step reaction sequence.



Scheme 13. Reagents and conditions: (for a, b) $\text{Pd}_2(\text{dba})_3 \cdot \text{CHCl}_3$ (10.0 mol%), xantphos (10.0 mol%), tributyltin chloride (3.6 mol%), KCN (3.0 equiv), acetonitrile, reflux (*method A*). Yields: 82% for **CN 3** and 86% for **CN 4**.

Aromatic nitriles are of considerable interest in organic chemistry. The cyano functional group is valuable in installing functionalities such as aldehydes, amides, amines, tetrazoles, thioamides, carboxylic acid and their derivatives.^{220,221} Classical methods for the preparation of aryl nitriles involves the *Rosenmund-von Braun* reaction with aryl halides (I, Br, Cl) using stoichiometric amount of copper(I)cyanide.²²²⁻²²⁵ However, these methods require harsh conditions²²⁶ and more recent palladium catalyzed reactions have been developed using various CN^- sources to replace them such as Zn ^{227,228}-, Cu-salts²²⁹ or $\text{K}_4[\text{Fe}(\text{CN})_6]$.²²⁹ While these methods represented significant improvements over earlier procedures metal waste remains a problem and high reaction temperatures are still required.

The conversion of triflates to aryl nitriles is a valuable synthetic reaction due to the wide range of available environmental-friendly phenol derivatives. However, only a few examples on the conversion of triflate groups have been reported.²³⁰⁻²³² The synthesis of bis(triflate)-functionalized aromatic systems has not been investigated so far. The use of a catalytic amounts of Pd₂(dba)₃, tributyltin chloride and xantphos in refluxing acetonitrile (denoted as *method A*) was successful in the double cross-coupling reaction of **CN 12** with potassium cyanide to give the dicyano-cyclophane **CN 3** in 82% as white solid (scheme 13). Applying again cyanation *method A* to the ditriflate **CN 17** yielded the dicyano-cyclophane **CN 4** in 86% after purification by flash chromatography as white solid.

Single crystals of model compounds **CN 3** and **CN 4** suitable for the X-ray structural analysis were obtained by recrystallization from a mixture of hot dioxane and cyclohexane.

A reaction mechanism for the Pd-catalyzed cyanation reaction (*method A*) of triflates involving catalytic amounts of organotin reagents has been adapted from a proposal of Yang²³⁰ which is shown in figure 39. The catalytic cycle A shows the typical Pd-cycle with the oxidative addition step followed by the reductive elimination step yielding the cyano-aryl. The cycle C involving the organotin compound, delivers the catalytic cycle A by generating continuously small amounts of Bu_3SnCN by converting relatively small amounts of Bu_3SnOTf at the solid/liquid KCN-acetonitrile interface where cyanide is stored in stoichiometric amounts as solid KCN. Having only a small amount of cyanides in solution is assumed to prevent the side reaction in cycle B where the Pd catalyst would decompose with cyanides.²³⁰ There was further experimental evidence that Bu_3SnCl forms an tin ate complex²³³ in the presence of KCN. The presence of such an ate complex might favor the transport (dotted lines in cycle C) of the cyanide to the Pd(II) as required for the cyanation and the side reaction removing Pd might therefore be suppressed.²³⁰

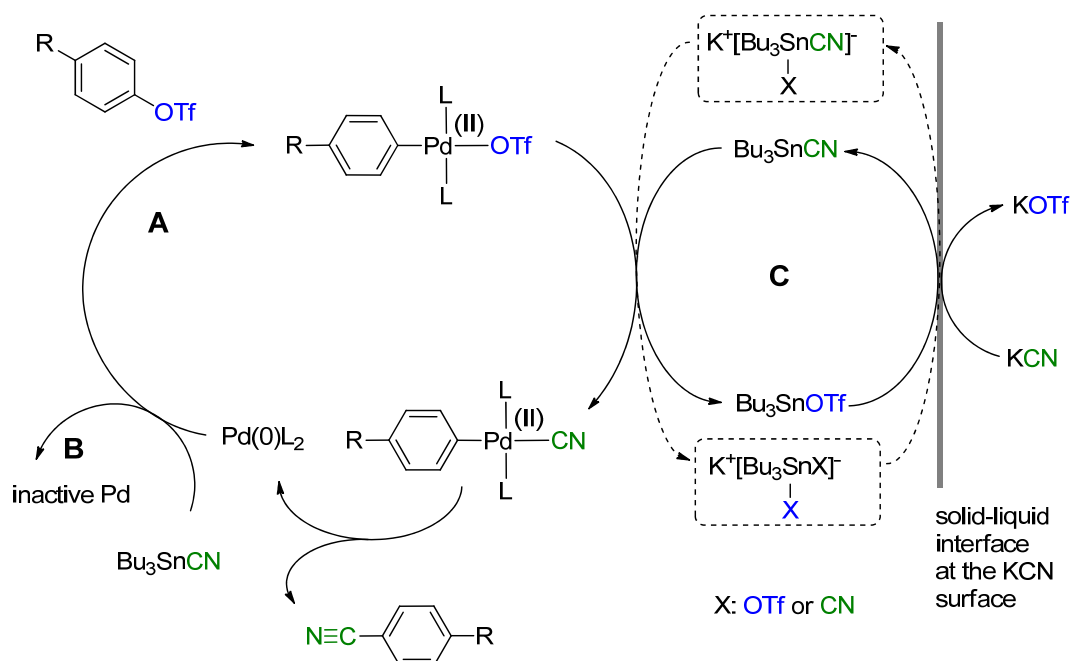
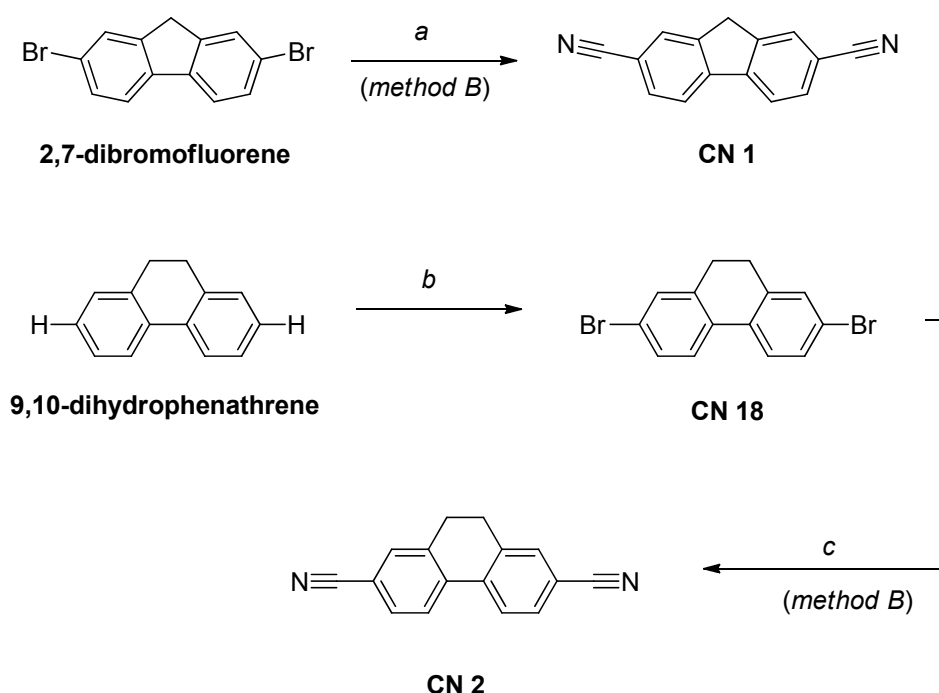


Figure 39. Catalytic cycle for a Pd-catalyzed cyanation (*method A*) of an aryl triflate adapted from Yang.²³⁰

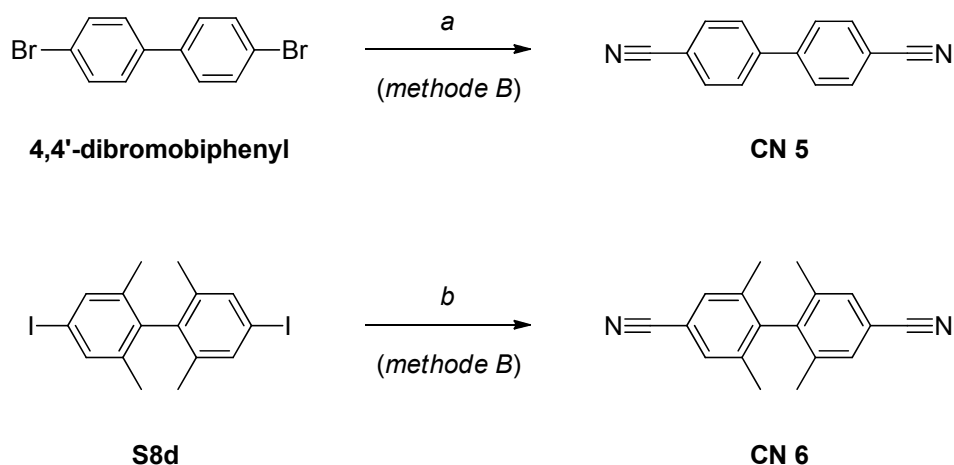
While the compounds **CN 3** and **CN 4** were assembled by the “*methoxy route*”, another strategy was applied to assemble the dicyano-cyclophanes **CN 1** and **CN 2**. Starting from 2,7-dibromofluorene,²³⁴ a *Rosenmund-Von Braun*²²² reaction using copper(I)cyanide was performed (denoted as *method B*) yielding the fully planar 2,7-dicyano-fluorene **CN 1** in a yield of 51% (scheme 14).



Scheme 14. (a) *Method B*: Cu(I)CN (2.6 equiv), DMF, 150-160 °C, 51%. (b) Bromine (2.1 equiv), trimethylphosphate, rt, 47%. (c) *Method B*: Cu(I)CN (2.6 equiv), DMF, 150-160 °C, 53%.

While other authors^{223,235-237} already reported the synthesis of 2,7-dicyanofluorene, a complete analytical characterization is still missing. Repeated attempts to purify **CN 1** were complicated due to the low solubility of the fluorene derivate. These attempts included repeated extraction of the product by ethyl acetate, filtration through silica, followed by repeated recrystallization from 1) acetonitrile, 2) ethanol and 3) 2-methoxyethanol yielding in crystalline samples of insufficient purity. A final chromatographic purification of **CN 1** was achieved by dissolving the compound in a large amount of chloroform and adsorbing it to the immobilized phase. This was

followed by a recrystallization from a hot mixture of dioxane and cyclohexane affording single crystals suitable for the X-ray analysis as the first sample satisfying all analytical criteria. 2,7-dicyano-dihydrophenanthrene **CN 2** containing an ethylene-bridge was assembled by a similar synthetic strategy (Scheme 14). 9,10-Dihydrophenanthrene was selectively brominated²³⁸ in the *para*-position of the biphenyl scaffold with elemental bromine under halogen-halide free conditions²³⁹ using trimethylphosphate as the solvent. Spontaneous crystallization afforded the **CN 18** in a reasonable yield of 47%. 2,7-Dibromo-9,10-dihydrophenanthrene **CN 18** underwent a cyanation reaction with copper(I)cyanide (*method B*) followed by recrystallization from hot toluene and subsequently from a boiling mixture of dioxane and cyclohexane to give single crystals of **CN 2** suitable for the X-ray analysis.



Scheme 15. (a) *Method B*: Cu(I)CN (3.0 equiv), DMF, 150-160 °C, 16 h, 73%. (b) *Method B*: Cu(I)CN (3.0 equiv), DMF, 140 °C, 8 h, 84%.

4,4'-Dicyano-biphenyl **CN 5** (scheme 15) was synthesized starting from the commercially available 4,4'-dibromobiphenyl. Again, a doubly copper mediated cyanation reaction (*method B*) afforded the target compound **CN 5** in a yield of 73%. Due to the low solubility of the core-unsubstituted biphenyl **CN 5**, similar purification problems were encountered as described before for the fluorene compound **CN 1**. An adapted purification procedure allowed separation of the

impurities in **CN 5**. The slow evaporation technique with dioxane/cyclohexane as the solvent mixture was crucial step to obtain single crystals suitable for the X-ray analysis

To complement the series biphenyl **CN 6** with two π -systems perpendicular to each other was synthesized. The already available diiodo building block **S8d** (section 2.2.4) with four methyl groups in *ortho*-position was successfully cyanated by applying *method B* except that the reaction was completed within a shorter reaction time and that the reaction proceeded at a slightly lower reaction temperature. This is pointing at the improved efficiency of iodine as leaving group compared to bromine. Purification by flash chromatography on silica followed by recrystallization from cyclohexane using the slow evaporation technique afforded the last member of the series **CN 6** as single crystals.

3.3 Physical Properties

3.3.1 Dipolar Interactions of the Cyano Group

Crystal design and engineering has received much attention in recent years.²⁴⁰⁻²⁴² One of the most important issues in this field is the rational design and structural control of molecular packing which affects and controls the macroscopic properties of a material including its electronic and optical properties. Furthermore, intermolecular interactions play an important role in the formation of supramolecular structures and can, most easily be explored in the solid state measuring the X-ray structure.²⁴³ Interactions such as hydrogen bonding, metal coordination, halogen bonding or aromatic non-covalent bonding have been widely studied over the years.²⁴⁴⁻²⁵³ However, weak noncovalent interactions of cyano groups exhibiting a local dipole moment have received much less attention.²⁵⁴ Recently, experimental evidence for dipolar $C\equiv N\cdots C\equiv N$ interactions have been systematically explored^{255,256} by analyzing the Cambridge Structural Database of non-disordered structures and comparing these with the well studied electrostatic interactions between carbonyl groups.²⁵⁷ Subsequent dipolar $C\equiv N\cdots C\equiv N$ interaction motifs have been found:

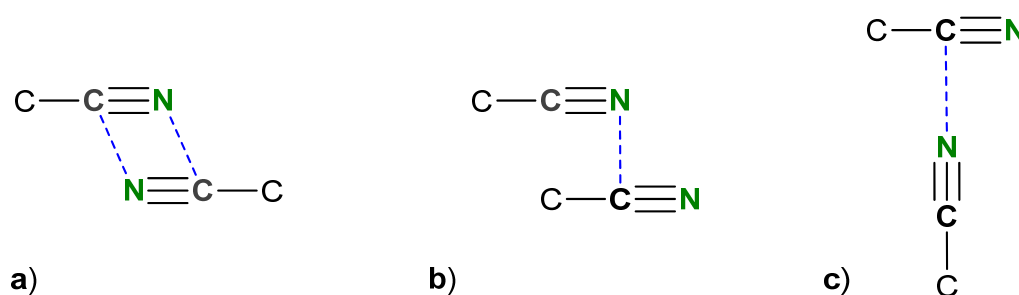


Figure 40. Observed motifs of dipolar $C\equiv N\cdots C\equiv N$ interactions.

a) The sheared antiparallel motive (predominant interaction), b) the sheared parallel motive, and c) the perpendicular motif. Despite of the increased steric bulk of the cyano group, compared to the carbonyl group,²⁵⁷ the calculated point charges of acetonitrile $C(+0.30e)\equiv N(-0.46e)$ are a bit less compared to acetone $C(+0.51e)\equiv O(-0.53e)$.²⁵⁵

3.3.2 The Weak Hydrogen Bonding of the Cyano Group

Beside the dipolar $C\equiv N\cdots C\equiv N$ interaction, examples of weak hydrogen bonding with cyano groups have been observed.²⁵⁸ Bonding modes of cyanides are either at the nitrogen non-bonding lone pair or perpendicular at the triple bond of the cyano group. Due to no-supporting charge at the triple bond one should expect gradual change in bonding energy between the two modes. As we shall see, the $H\cdots\pi$ bonding mode displays an often observed intramolecular interaction in the solid state.

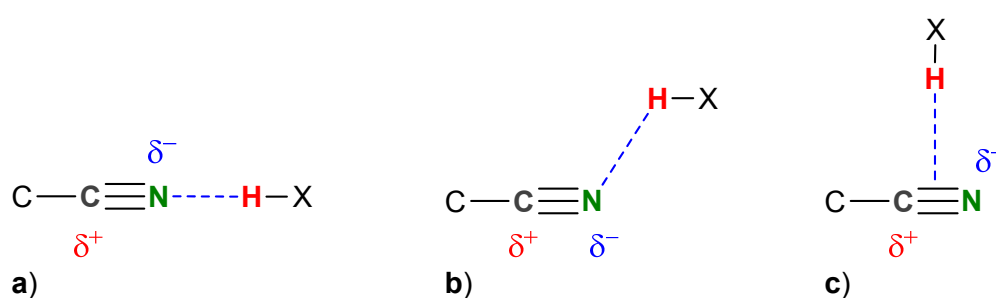


Figure 41. Modes of the weak hydrogen – CN bonding

An example with an alkynyl donor has been found by *Kumar et al.*²⁵⁹ forming a $C\equiv C-H\cdots N\equiv C$ hydrogen bond. The $H\cdots N\equiv C$ angle was found to be 93° indicating a perpendicular interaction where the hydrogen atom donates into the π -orbitals of the cyano group ($d(H\cdots N)$: 2.75 Å, $d(H\cdots C\equiv N)$: 3.05 Å). In a surface-based assembly of cyanophenyl substituted porphyrins using ultra-high vacuum deposition, it has been demonstrated that the molecular arrangement such as dimer, trimer, tetramer or linear chain can be induced by altering the position of the cyanophenyl group. Thereby a $H\cdots N\equiv C$ distance between 2.5 Å and 2.6 Å was found.²⁶⁰ A common method to assign hydrogen bond ($H\cdots A$) character is the *van der Waals* criterion. The *van der Waals* cut-off criterion requires that the distance of a hydrogen bond must be smaller than the sum of the covalent *van der Waals* of H-donor and A-acceptor together. This criterion does not stand on experimental or theoretical ground, but has been established for reasons of convenience. The criterion works well for strong hydrogen bonds which are almost always short enough to fulfill the

criterion. Weak hydrogen bonds are longer and application of the *van der Waals* cut-off criterion can have drastic consequences.²⁵⁴ For example the H $\cdots\pi$ interactions are much longer and would not pass the criterion. As a result the criterion can be useful but does not necessarily include all existing binding forces.

3.3.3 Solid state structure analysis

Figure 42 displays the solid state structures of the dicyano-biphenyls **CN 1-6** as a series of increasing torsion angle.

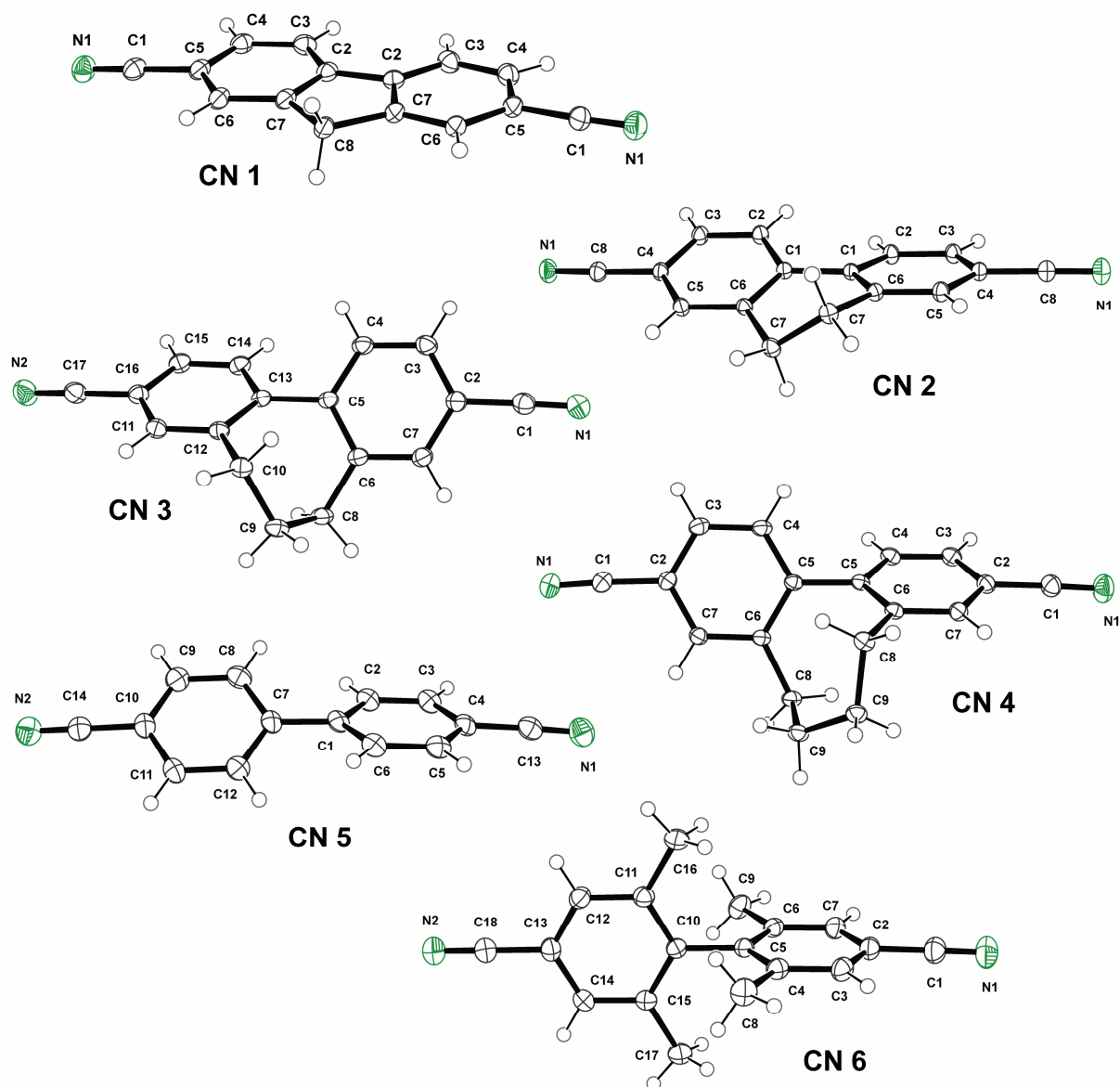


Figure 42. Solid state structures of the dicyano-biphenyl derivatives **CN 1-6**.

Furthermore, selected structural parameters like the intramolecular nitrogen-nitrogen distance as length axis of the molecule or the torsion angle ϕ are listed in table 4 and compared with the torsion angle obtained from the DFT

calculations. The torsion angles were measured between the planes of both phenyl rings of the biphenyl skeleton. These planes were obtained by considering all six carbon atom positions of the solid state structure for the least square minimization procedure. Very comparable intramolecular nitrogen-nitrogen distances within the series of X-ray analyzed derivatives with values between 11.96(9) Å for **CN 1** and 12.24(6) Å for **CN 6** point at hardly any effects of the various alkyl substituents on the length of the dicyano-cyclophane backbone.

Table 4. Molecular structures and measured properties.

#	crystal system	space group	Φ [°] solid state	Φ [°] DFT [a]	d (N-N) [Å]	type of interact.	d [Å] ^[b]
CN 1	<i>monoclinic</i>	P2/n	1.02	0.26	11.96(9)	CN...CN H _{Ar} ...NC Ar...Ar	3.44(4), 4.48(6) 2.53(5), 2.62(3) 3.44(9)
CN 2	<i>monoclinic</i>	C2/c	20.74	20.97	12.22(3)	CN...CN H _{Ar} ...NC Ar...Ar	3.87(7), 3.91(1) 2.53(5), 2.73(5) 3.74(6)
CN 3	<i>triclinic</i>	P-1	44.78	47.13	12.24(5)	CN...CN H _{Ar} ...NC Ar...Ar	3.65(3), 3.95(5) 2.63(3), 2.69(1) 4.16 (1)
CN 4	<i>monoclinic</i>	C2/c	58.47	59.94	12.24(6)	CN...CN H _{Ar} ...NC Ar...Ar	3.93(7), 4.41(2) 2.73(4), 3.07(7) 4.47(3)
CN 5	<i>monoclinic</i>	P21	31.77	36.96	12.20(2)	CN...CN H _{Ar} ...NC Ar...Ar	3.48(2), 3.57(0) 2.57(9), 2.63(5) 3.75(9)
CN 6	<i>monoclinic</i>	P21/c	89.26	90.00	12.21(4)	CN...CN H _{Ar} ...NC Ar...Ar	3.92(8), 4.48(6) 2.55(1), 2.73(6) 4.63(5)

[a] The interplanar torsion angles have been calculated at the DFT Level. [b] Shortest interaction distance. CN...CN: antiparallel dipolar interaction; H_{Ar}...NC: Aryl-hydrogen-N interaction; Ar...Ar: π - π interaction.

As expected a fully planar biphenyl backbone is observed in fluorene structure **CN 1**. Due to the bent backbone of **CN 1** the N-N distance of 11.96(9) Å is slightly decreased compared to all other derivatives. With elongation of the ring-interlinking alkyl chain a continuous increase of the torsion angle is

observed in the cyclophane structures **CN 2-4**. As shown in table 4, all measured torsion angles are in good agreement with the values obtained from the DFT calculation (see table 4 and section 3.3.5 for the calculations). Interestingly, the torsion angles of the dicyano-cyclophane series **CN 1-6** are very comparable with the one determined in an analogous series comprising terminal acetylsulfanyl donor-substituents (section 2.3).¹⁹ An exception displays the core-unsubstituted biphenyl compound **CN 5**. The torsion angle in the solid state was found to deviate from theoretically calculated value in the gas phase by 7.83°. However, the torsion angle of unsubstituted biphenyl is reported to be strongly dependent on state of aggregation.²⁶¹

Almost perpendicular arrangement of the two phenyl rings was measured for the solid state structures of the tetramethyl compound **CN 6** with a torsion angle ϕ of 89.26°. The rotation barriers of the methyl substituted^{128,129} model compound **CN 6**, and in particular of cyclophanes¹³⁰ **CN 1-4** are expected to be increased considerably compared to the solely in *para*-position cyano substituted derivative **CN 5** (see section 1.4.2). Thus, the ϕ values measured in solid state are considered to be a good proxy for the torsion angle expected in solution.

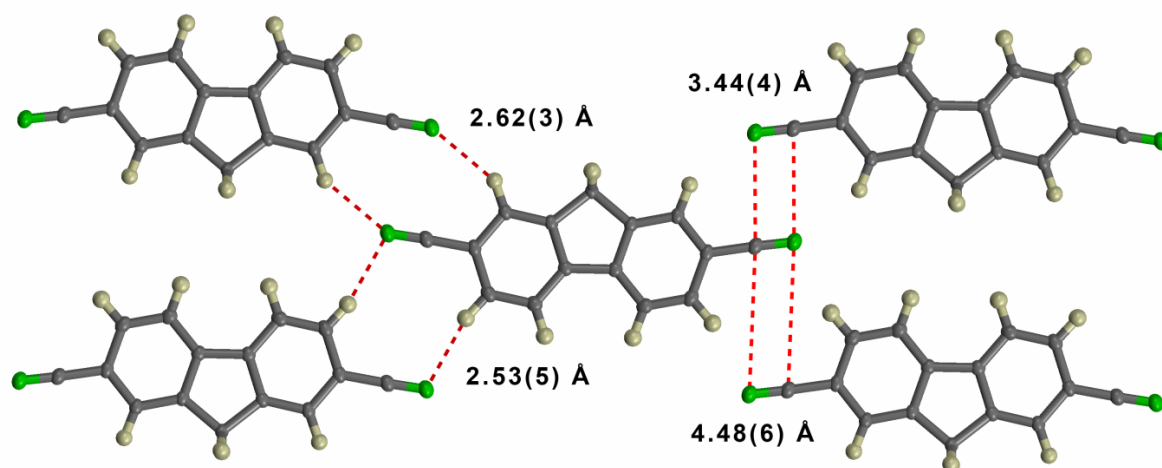


Figure 43. 1D-chains of **CN 1** in the solid state structure stabilized by intermolecular contacts. On the right side, the dipolar antiparallel CN...CN interactions are displayed and on the left side the weak hydrogen bond H_{Ar}...NC contacts are displayed.

In figure 43 the packing motif of the planar fluorene compound **CN 1** is shown as a representative example for the entire series of dicyano-cyclophanes. Figure 43 shows the top-view of the molecular network. The molecules form 1D-chains held together by dipolar antiparallel CN \cdots CN interactions (see section 3.3.1). Furthermore, there are short H_{Ar} \cdots NC contacts where the H \cdots N distance is below 2.8 Å. These contacts can be interpreted as weak hydrogen bonds (other similar contacts are omitted for clarity).

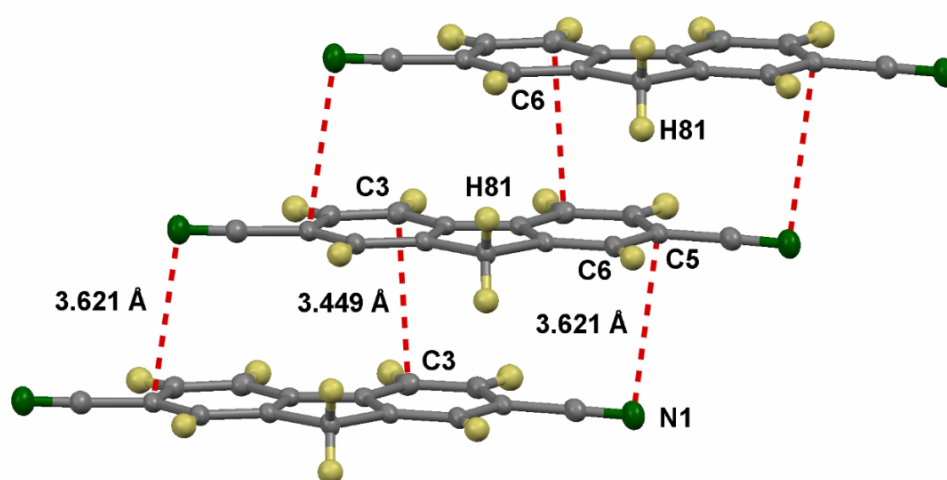


Figure 44. View along the *b*-axis of the unit cell of the solid state structure of **CN 1** to display the co-facial through-space interactions.

The side-view along the *b*-axis of the unit cell is displayed in figure 44. Half of the fluorene molecule is overlapping with the lower-lying and the upper-lying molecules in a parallel displaced manner forming columnar π -stacks. The closest plane-to-plane distance between the two neighboring planar 2,7-dicyano-fluorenes is found to be 3.44(9) Å between C3 and C3 of the parallel displaced rings. An additional stabilizing interaction may arise from the slightly positively polarized carbon atoms of the sp-hybridized cyano groups which are sandwiched between the phenyl rings' π -systems of the neighboring molecules supporting the intermolecular π - π -stacking.

In figure 45 the columnar π -stacks formed along the a -axis of the unit cell are shown. The red dotted lines show the $H_{Ar}\cdots NC$ contacts that probably contribute to the 2D-packing (the antiparallel $CN\cdots CN$ are omitted for clarity) structure while the π -stacking interactions form the 3D-motif.

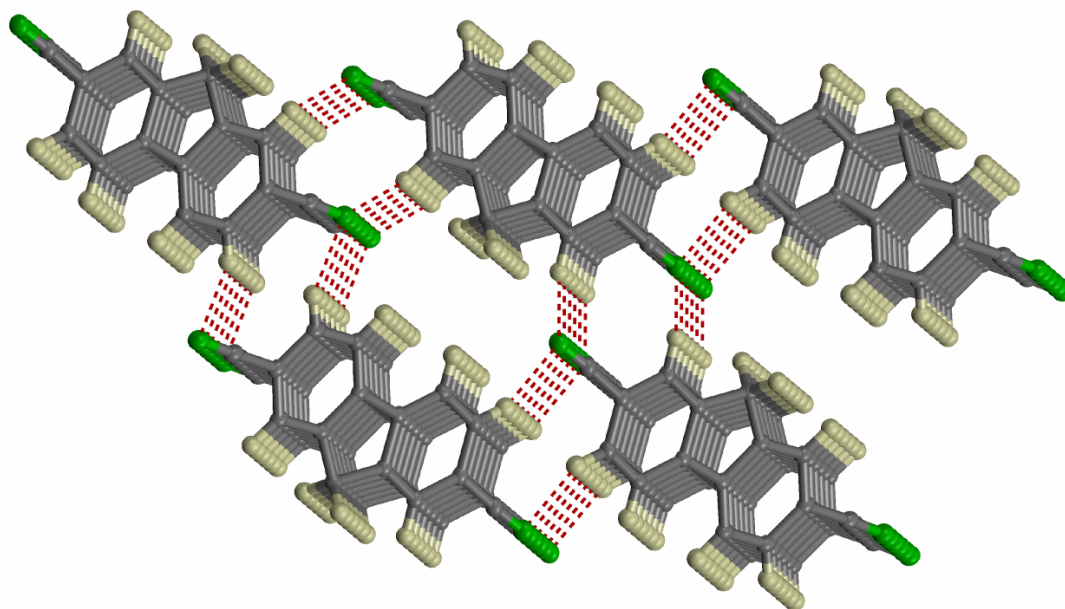


Figure 45. Packing structure of **CN 1**. View along the a -axis of the unit cell.

Comparable packing motifs with dipolar antiparallel $CN\cdots CN$ interactions and $H_{Ar}\cdots NC$ hydrogen bonds were observed in the packing structures of the model compound **CN 2-6**. Generally, it is found that the intermolecular distances of these aggregates stabilized by weak interactions gradually increase with the increasing steric requirements of alkyl chains and substituents attached to the phenyl rings. In particular the increasing length of ring-interlinking alkyl chain and attached methyl groups in *ortho*-position of the biphenyl bridge gradually enlarges the intermolecular distance between co-facial arranged phenyl planes. Absence of efficient π - π -overlap of phenyl planes is observed if the interplanar torsion angle has exceeded a value of 44.78° . Only dicyanocyclophanes **CN 1** (1.2°), **CN 2** (20.74°) and the un-substituted **CN 5** (31.77°) display intermolecular distances between the planes below 3.8 \AA .²⁶²

3.3.4 NMR Observations in Solution: The Aromatic Solvent-Induced Shift Effect

It is well known that a proton's chemical shift depends not only on the intrinsic shielding properties of the molecule, but also on the solvent in which these molecules are investigated. One of the most widely used solvent effect is known as "aromatic solvent-induced shift" (ASIS).²⁶³⁻²⁶⁵ In this technique the molecule is dissolved in two different solvents, usually chloroform and benzene, and its chemical shifts relative to an internal standard (TMS or the solvent peak) is measured. The ASIS is then simply the difference between these two chemical shifts).

$$ASIS = \Delta = \delta_x^{CDCl_3} - \delta_x^{C_6D_6} \quad (\text{equation 2})$$

To probe dimer π - π -interactions of the dicyano derivatives in solution, the planar fluorene **CN 1** was investigated first. Aromatic solvents are known to significantly reduce π - π stacking interactions because the solvent competes for the π - π interaction, while chloroform is less effective in preventing intermolecular stacking interactions.²⁶⁶

A solution of **CN 1** with a concentration of 1 mg/mL (4.5 μ M) was prepared. This solution was further diluted in a ratio of 1:10 and 1:100 with the corresponding solvent. All ^1H NMR spectra were recorded at 298 K. As displayed in figure 46, the proton chemical shifts of the aliphatic methylene unit and the aromatic core are independent of concentration. The absence of concentration dependent chemical shifts supports the notion that no π - π -driven association of the solute is present.

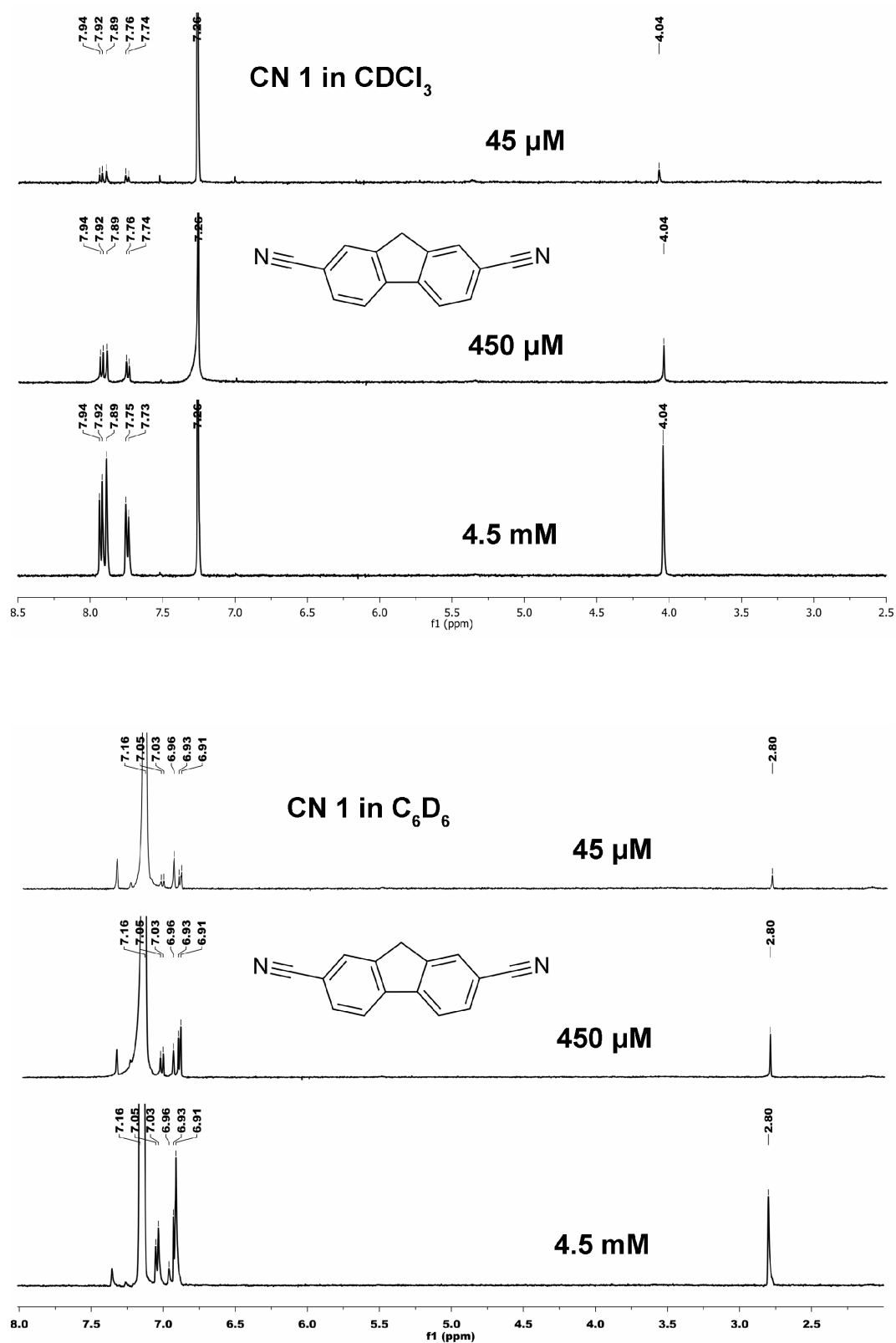


Figure 46. Concentration depended chemical shift experiment. Above, ¹H-NMR spectra of fluorene **CN 1** in CDCl₃ at various concentrations and (below) in C₆D₆.

While no concentration dependent chemical shift is observed, a strong solvent-induced shift is observed as shown in figure 47. The singlet at 4.04 ppm of the methylene unit remains almost unchanged in the polar aprotic DMSO, whereas the spacing between the doublets enlarges considerably in the more polar DMSO probably due to the enhanced dipolar coupling. A large up-field shift of 1.2 ppm of the benzylic protons is observed if benzene is used as the solvent. This effect is attributed to the influence of the ring current from the neighboring solvent molecules. Similarly, the aromatic core protons of the solute are shifted to higher field. With toluene a similar but less pronounced effect is observed.

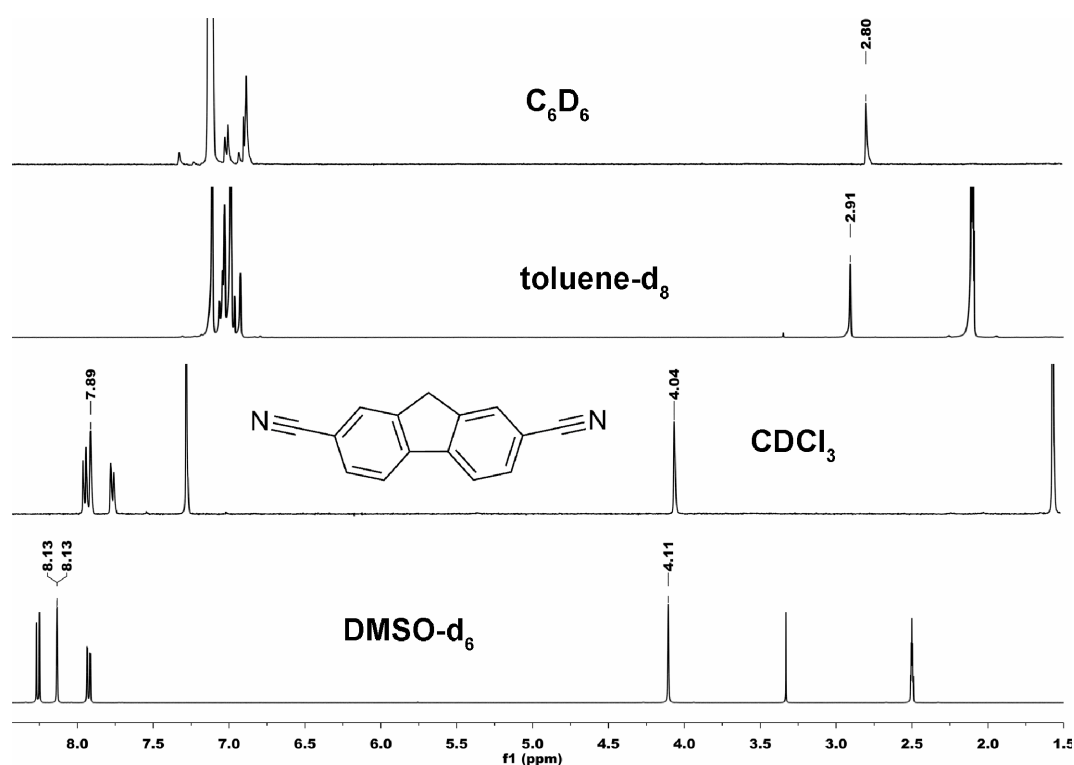


Figure 47. ^1H NMR of the compound **CN 1** in various solvents, measured at 298 K.

The slightly decreased aromatic solvent-induced shift effect of toluene can be attributed to the donor effect of the additional methyl group.

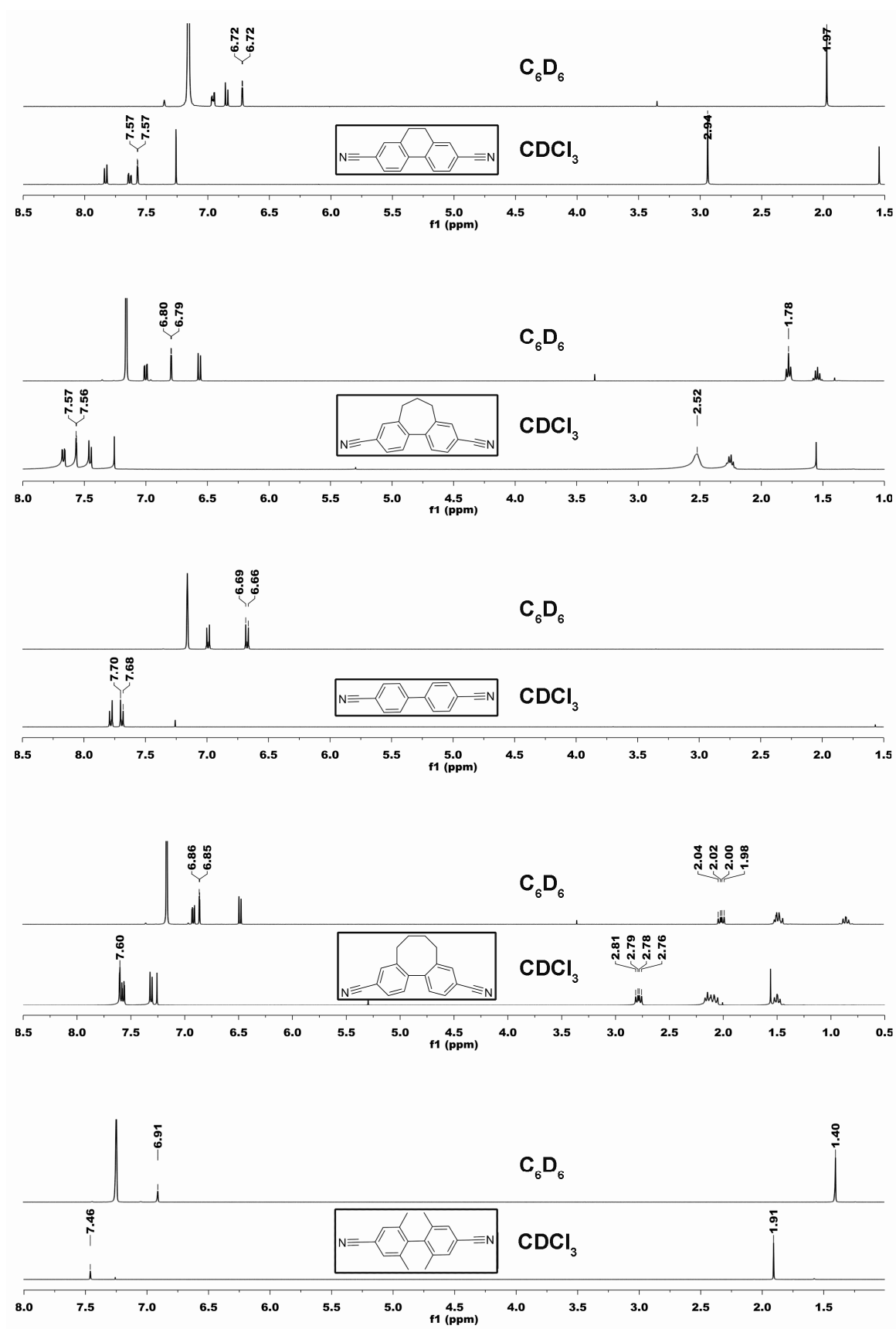


Figure 48. ^1H NMR of the compounds **CN 2-6** in CDCl_3 and C_6D_6 measured at 298 K.

As displayed in figure 48 a strong shift of all proton signals is observed measuring the solutes **CN 1-6** in benzene. For the alkyl bridged biphenyls **CN 1-4** a consistent 3d , $^4d^3d$, 4d splitting pattern (figure 49) is observed. These doublets shift their relative position and intersect with each other with changing of the torsion angle (figure 48). The proton H_A , adjacent to the cyano group and the alkyl bridge was selected to quantify the ASIS effect on the aromatic core.

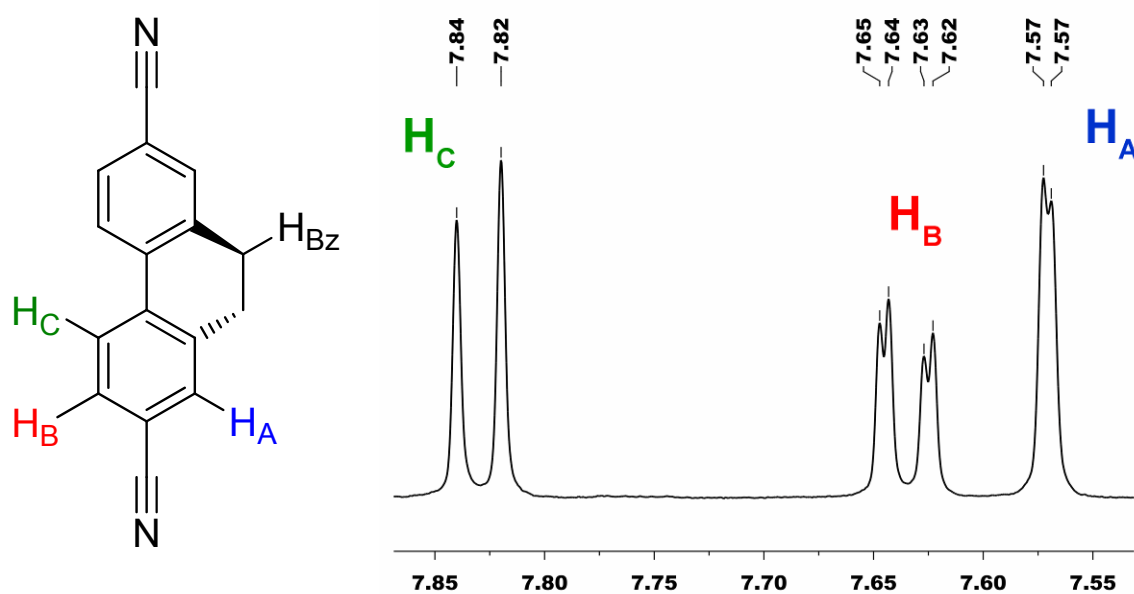


Figure 49. Assignment of the aromatic proton signals of dicyano-dihydrophenanthrene **CN 2** measured in $CDCl_3$ (400 MHz, 298K).

A clear trend of the ASIS was observed within the dicyano-biphenyl series. While fluorene **CN 1** exhibits the largest ASIS value in the series, no 4d signal arising from the aromatic proton coupling could be identified probably due to an overlapping benzene peak. The planar fluorene **CN 1**, with its benzylic protons oriented perpendicular to the planes are in a geometrically predisposed position to be effected by the neighboring solvent molecules.²⁶⁷⁻²⁶⁹

To conclude, the ASIS effect decreases with increasing torsion angle, in fact, beside the overall planarity of the biphenyl system, the increasing steric demands of the substituent decreases the ASIS probably due to a less pronounced solute-benzene interaction. While the ring-induced current effect on the benzylic protons results in an ASIS of 1.24 ppm for the planar fluorene **CN 1**, the ASIS effect is decreased to 0.78 ppm for **CN 6** with the two phenyl rings perpendicular to each other. Generally a less pronounced shift effect of the aromatic protons is observed due to solvent induced through space π - π interaction with the biphenyl backbone. The aromatic-core proton H_A is shifted by 0.8 ppm for fluorene **CN 1**, whereas a shift of 0.55 ppm is observed for **CN 6** bearing four methyl groups in the *ortho*-position of the biphenyl backbone. All values of the series are listed in table 5.

Table 5. Aromatic Solvent induced Shifts (ASIS) of the dicyanide series. All measurements were performed at 298 K.

	ϕ [°] ^[a]	CDCl₃		C₆D₆		ASIS	
		δH_{Bz}	δH_A	δH_{Bz}	δH_A	$\Delta \delta H_{Bz}$	$\Delta \delta H_A$
		[ppm]	[ppm]	[ppm]	[ppm]	($\delta_{CDCl_3} - \delta_{C_6D_6}$)	($\delta_{CDCl_3} - \delta_{C_6D_6}$)
CN 1	1.0	4.04	7.89	2.8	-	1.24	-
CN 2	20.7	2.94	7.57	1.97	6.72	0.97	0.85
CN 3	44.8	2.52	7.57	1.78	6.8	0.74	0.77
CN 4	58.5	2.79	7.6	2.01	6.86	0.78	0.74
CN 5	39.6 ^[b]	-	7.69	-	6.67	-	1.02
CN 6	89.3	1.91	7.46	1.4	6.91	0.51	0.55

[a] The interplanar torsion angles were obtained by the X-ray structural analysis.

[b] The interplanar torsion angle has been calculated at the DFT Level (B3LYP/TZVP).

3.3.5 Computational Studies

In order to explore geometries of the dicyano-biphenyls **CN 1-6**, in particular with respect to their conformation and molecular orbital energies, *ab initio* calculations of the molecules in vacuum were performed. The geometry of each molecule was optimized using the TURBOMOLE program package²⁷⁰⁻²⁷² version 5.9 and density functional theory (DFT) with the B3LYP hybrid exchange correlation functional²⁷³⁻²⁷⁵ in combination with the multiple accelerated resolution of identity in J (MARI-J) approximation²⁷⁶⁻²⁷⁸ and the TZVP basis²⁷⁹ set, as implemented in the TURBOMOLE program package.

In addition, the energy levels of the relaxed ground state of all structures of the series were calculated by DFT. All calculated torsion angles and the HOMO-LUMO energies are given in table 6. While the twisted form of the simple biphenyl comprising various substituents in the *para*-position is reported to be the dominant conformation in the gas phase and in solution,¹⁰⁸ planarization of the two phenyl rings occurs if e.g. molecule/surface^{123,124} interactions overrule the weak steric repulsion¹⁹² between the phenyl ring H-Atoms.

Table 6. Calculated torsion angles and energies of the dicyano-cyclophane series.

#	ϕ [°] DFT ^[a]	HOMO [eV]	LUMO [eV]	HOMO-LUMO separation [eV]
CN 1	0.00	-6.94	-2.57	4.37
CN 2	20.99	-6.92	-2.59	4.33
CN 3	47.13	-7.09	-2.38	4.71
CN 4	59.97	-7.14	-2.19	4.95
CN 5	39.60	-7.21	-2.54	4.67
CN 6	90.00	-7.39	-1.80	5.59

The torsion angle of **CN 5** turned out to be relatively sensitive to the used basis set. While the TZVP basis set gives a torsion angle of almost 40°, calculations with using the smaller basis set SVP gives a slightly reduced torsion angle of 36.96°.

Incorporation of an alkyl chain of variable length in 2,2'-position of the biphenyl skeleton controls the torsion angle between the two aromatic rings without changing the electronic environment of the π -system. As a result, the degree of electron π -delocalization is the only effect shifting the relative position of the HOMO and LUMO levels. The LUMO level is stabilized, while the HOMO is destabilized with decreasing torsion angle. As a consequence, the energy gap increases with increasing torsion angle (figure 50).

Compared to similar thiol-functionalized π -systems, the energy levels of the frontier orbitals of cyano-functionalized π -systems are down-shifted in energy by ~ 1.5 eV.^{7,280} *n*-Type semiconductor properties of cyano-functionalized π -systems are explained in particular by their lowered LUMO promoting efficiently electron transport.^{281,282}

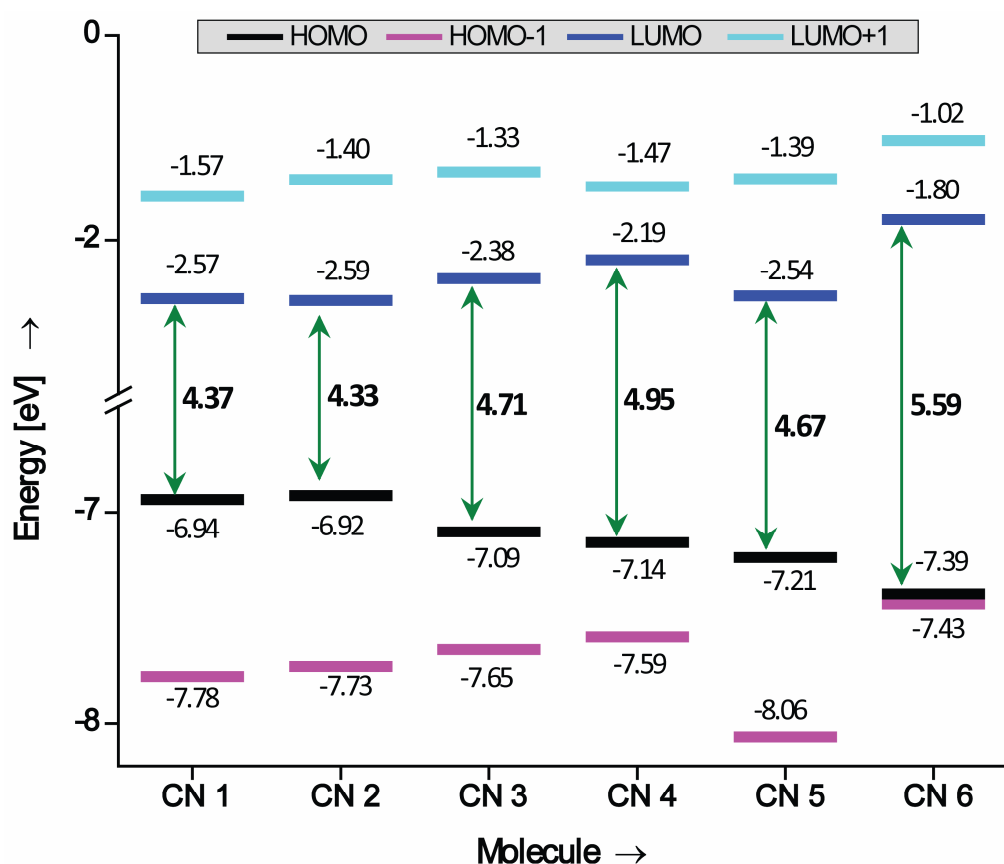


Figure 50. Energy diagram of the dicyano-biphenyl derivatives **CN 1-6**. The Energies are given in eV.

The energies of the HOMO, LUMO and their vicinal orbitals are visualized in figure 50. While DFT hybrid methods often underestimate ionization potential and electron affinities, the HOMO-LUMO separations obtained by the B3LYP functional is reported to agree well with the vertical excitation energy of the UV absorption spectra.²⁸³ Surprisingly, the calculation displays a slightly increased HOMO-LUMO separation for the fluorene structure **CN 1** compared to the cyclophane structure **CN 2** which is no longer planer.

3.3.6 Electronic Spectra

To investigate the correlation between electronic properties and the interplanar torsion angle ϕ of the dicyano-biphenyls **1-6** the absorption spectra of entire series were recorded in acetonitrile (CH_3CN) as 1×10^{-5} M solutions. All recorded spectra are displayed in figure 51 and a list of the most important UV absorption bands is given in table 7.

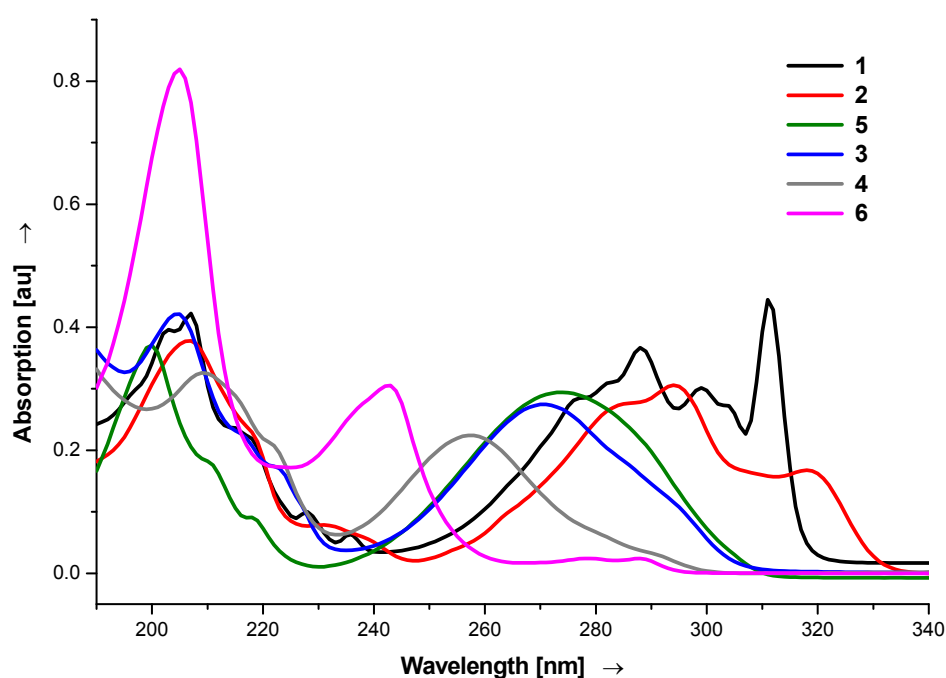


Figure 51. The overlaid UV absorption spectra of the dicyano-cyclophane series **CN 1-6** as 1×10^{-5} M solutions in CH_3CN .

The longest-wavelength absorption band of **CN 1** is at 311 nm and, in analogy to its terminally unsubstituted counterparts, is assigned to the α -absorption band (α -band, λ_{max} 300 nm).^{96,111,193,284-286} Similarly, the structured absorption band between 250 nm and 307 nm can probably be assigned to the p -band of the biphenyl subunit which exhibits a maximum absorption at 288 nm. The p -band of **CN 1** displays a vibrational fine structure, presumably because of its rigid, essentially planar geometry. The bathochromic shift of the absorption bands compared to fluorene can be attributed to an enlargement of the π -system arising from the substitution with two cyano groups.¹¹¹ Cyano

groups lead to an overall stabilization of the HOMO and LUMO levels,²⁸⁷ as expected from the acceptor nature of the substituent.

Table 7. UV adsorption properties of **CN 1-6** in acetonitrile at 298 K.

	Φ [°] ^[a]	λ_{\max} [nm (eV)] ^[b]	ϵ [Lmol ⁻¹ cm ⁻¹] ^[c]	λ_{on} [nm (eV)] ^[d]
CN 1	1.02	207 (5.99)	38600	322 (3.85)
		288 (4.31)	33500	
		299 (4.15)	27600	
		311 (3.99)	40800	
CN 2	20.74	207 (5.99)	37800	335 (3.70)
		294 (4.22)	30600	
		318 (3.90)	16800	
CN 3	44.78	204 (6.08)	42100	307 (4.04)
		271 (4.58)	27400	
CN 4	58.47	209 (5.93)	32600	298 (4.16)
		257 (4.82)	22400	
CN 5	39.60 ^[e]	199 (6.23)	60200	310 (4.00)
		274 (4.52)	38100	
CN 6	89.26	205 (6.05)	81900	294 (4.22)
		243 (5.10)	30500	

[a] Φ is the torsion angle between the planes of the phenyl rings as measured from the crystallographic data. [b] λ_{\max} is the wavelength at the maximum of each band. [c] ϵ is the extinction coefficient at λ_{\max} of each band. [d] λ_{on} is the absorption onset of the UV spectra. [e] The torsion value of was obtained from the DFT calculation.

The p -band is also called the conjugation band (π - π^* band)^{96,194} as its position is reported to reflect the extent of conjugation in the biphenyl core.^{96,194,195} Calculated HOMO/LUMO gaps of the series agree well with the vertical excitation energies of at the p -band absorption²⁸³ and do not deviate more than 0.15 eV for compounds **CN 1-5** and 0.49 eV for compound **CN 6**.

Surprisingly, we observe for the terminally cyano-functionalized cyclophane **CN 2** which is no longer planar, a bathochromic shift of 6-7 nm of the both the

ρ -(294 nm) and α -(318 nm) absorption band with respect to the fluorene derivative **CN 1**. Obviously, **CN 2** exhibits the smallest optical band gap as well as the lowest vertical excitation energy within the series which is consistent with the results from theory. In contrast to the terminally unsubstituted dihydrophenanthrene¹⁹⁴ (α -band, λ_{\max} 298 nm), the longest wavelength absorption of cyclophane **CN 2** shows a bathochromic shift of 20 nm. The onset of each absorption spectra and all λ_{\max} values are listed in table 7.

According to theory, the π - π^* transition energy^{96,111} which is observable as the λ_{\max} value of the conjugation band should correlate with the conformation of the biphenyl core. The orbital overlap of adjacent π -systems correlates linearly with the cosine Φ between their planes, and the electron-transfer properties between the two π -systems is proportional to $\cos^2\Phi$ of their torsion angles.^{93,114,196}

Thus, in figure 52 the vertical π - π^* excitation energy (ρ -band absorption maxima) of each compound under investigation is plotted against the $\cos^2\Phi$ of the torsion angle. All values of the interplanar torsion angles Φ were determined by the X-ray structural analysis. Within this series of compounds, the expected linear correlation between the vertical excitation energy and $\cos^2\Phi$ was observed.

While all structures of this series were determined by the solid state structural analysis, the interplanar torsion angle of the unsubstituted dicyano-biphenyl **CN 5** (39.60°) was taken from the DFT calculation. In this particular case the X-ray torsion angle is assumed to be dominated by packing effects and thus, the calculated angle represents a more realistic situation in solution.^{18,288-291}

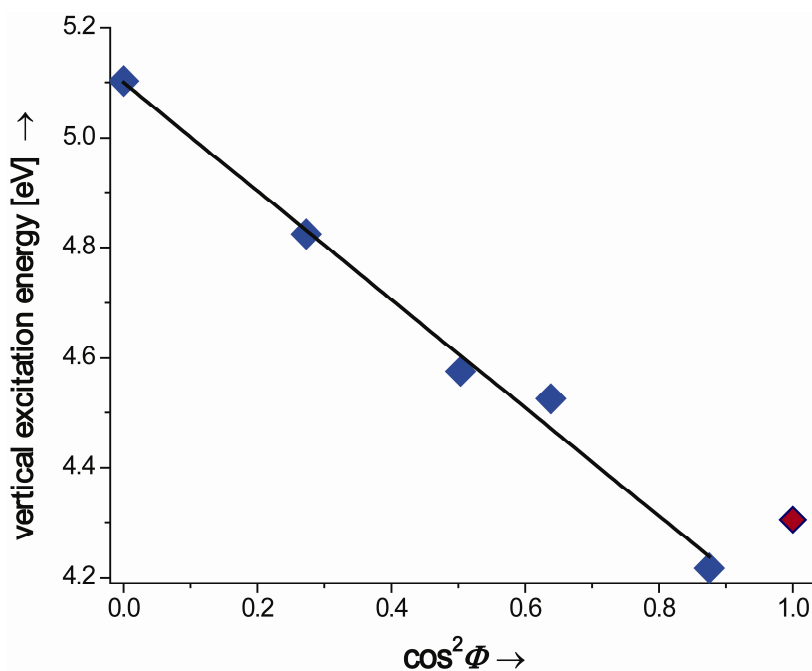


Figure 52. Vertical excitation energy from for the lowest valence π - π^* transition (ρ -band absorption maxima) of the molecules **CN 1-6** plotted against $\cos^2\phi$, where ϕ is the interplanar torsion angle obtained from the X-ray structures. The torsion value of **CN 5** was obtained from the DFT calculation. The linear correlation coefficient R^2 (with exclusion of **CN 1**) is 0.998.

The only exceptional behavior in the series was observed for the fluorene derivative **CN 1**, which displays a vertical excitation energy outside the linear fit. Though, the assignment of the structured UV bands of **CN 1** is speculative. Results from first principle calculations of the singlet excited states using TD-DFT and coupled cluster methods did not match with the experiment. DFT calculations (section 3.3.5) of the ground state revealed a slightly larger HOMO-LUMO gap for **CN 1** than for cyclophane **CN 2** which is no longer planar.

It is worth noting that the most resolved spectrum was obtained for compound **CN 1**. The broad band located at 250-307 nm has a set of sharp features for **CN 1** as opposed to other compounds studied. 2,7-Dicyanofluorene **CN 1** represents a rather hard (rigid) structure and it prevents any changes of the conformation of this molecule, while the molecules of other compounds have a certain degree of freedom resulting in a broadening of their absorption bands.

3.3.7 Electrochemical Properties

To characterize the electrochemical properties of the dicyano-biphenyls **CN 1-6**, cyclic voltammograms (CVs) were recorded using an Au net electrode in a three electrode all-glass electrochemical cell. 1,4-dicyanobenzene (**DCB**) consisting of only one benzene ring was also investigated for comparison. Two couples of reduction and oxidation peaks were observed for all molecules studied (figure 53).

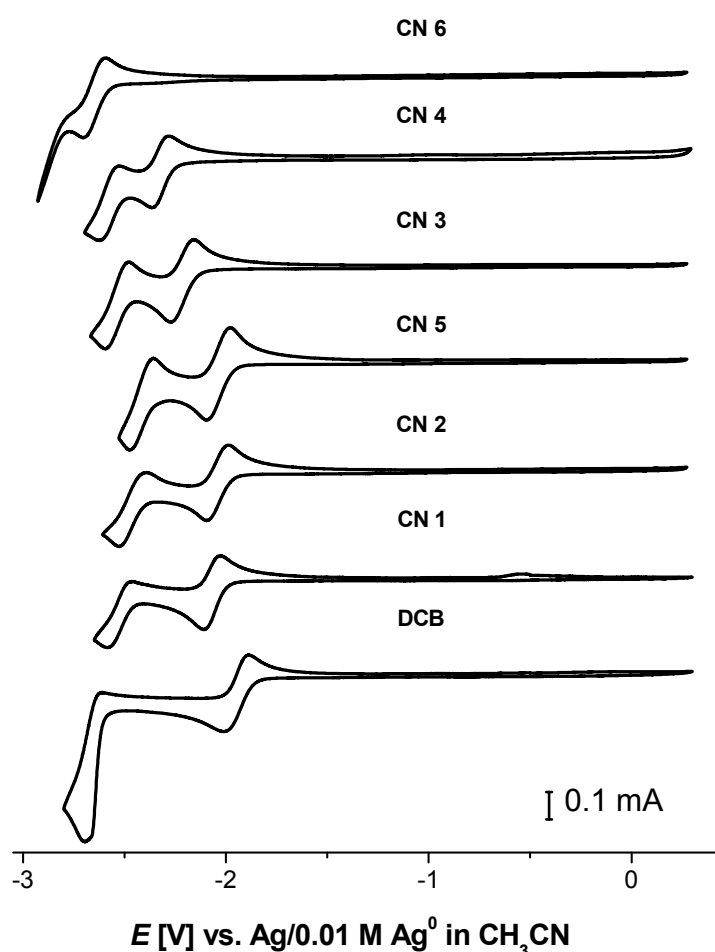


Figure 53. Cyclic voltammograms of the dicyano-biphenyls compounds **CN 1-6** recorded from 0.5 mM solutions in a 0.1 M TBAPF₆/CH₃CN electrolyte solution, scan rate 100 mV/s.

The second, i.e. the most negative reduction wave of **CN 6** could not be resolved due to electrolyte decomposition employing the gold working electrode. However, both reduction waves of **CN 6** were observed when using

a glassy carbon electrode (figure 54, left side). The redox potentials of the six dicyano-biphenyls **CN 1-6** are within $\Delta E_{\text{red}} < 10$ mV identical on Au and GC electrodes under the experimental conditions chosen.

Calibration experiments with ferrocene revealed that both redox peaks represent one-electron processes (see RDE experiment below).

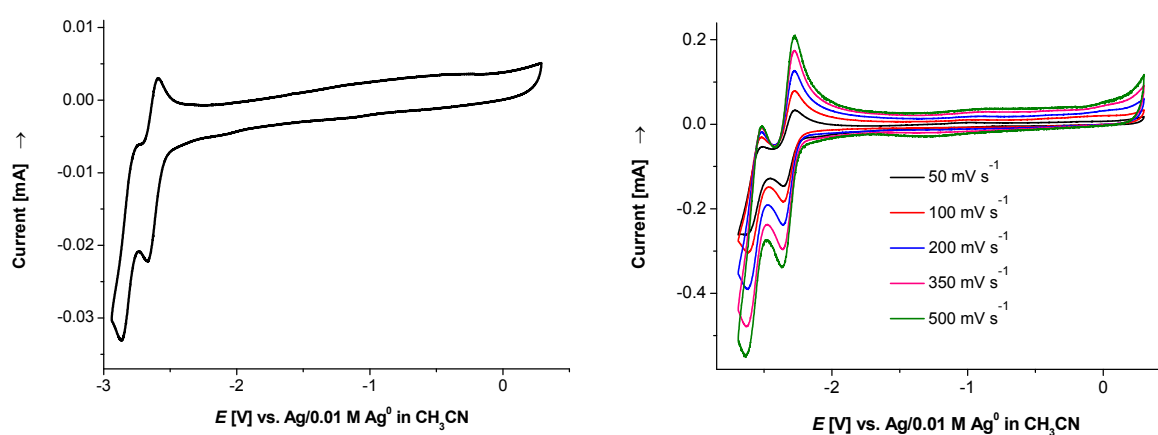
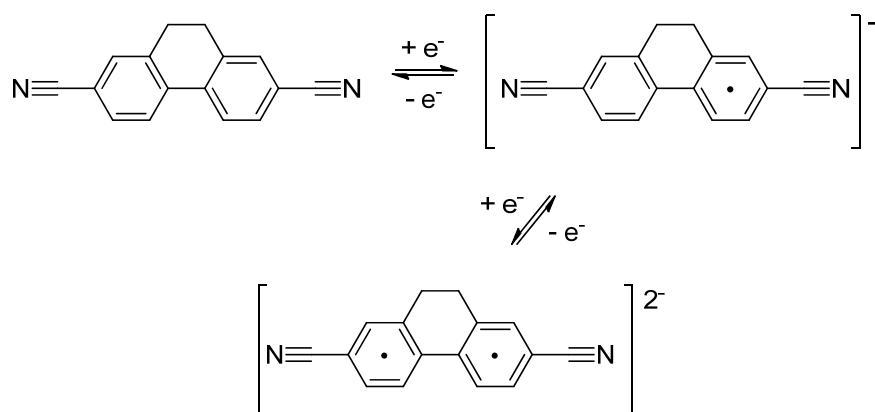


Figure 54. (Left side) CV of compound **CN 6** (0.5 mM) recorded at a GC electrode. The scan rate is 100 mV/s. (Right side) CVs of **CN 4** at different scan rates.

Experiments with different scan rates (ν) demonstrate that the peak-to-peak separation for each pair of redox peaks is larger than 59 mV, the expected value for an ideally reversible one-electron transfer process (figure 54, right side). On the basis of previous literature on aryl nitriles²⁹²⁻²⁹⁹ it can be suggested that the first reduction wave represents the formation of the anion radical and the second reduction wave is assigned to the formation of the dianion according to:



Scheme 16. Proposed two step reduction process of **CN 2** as representative example for the dicyano-cyclophane series. Injection of the first electron forms the radical anion. Injection of a second electron forms the dianion.

Experiments with the Rotating Disk Electrode (RDE) using ferrocene as an internal reference (representing a one electron process), further supports the proposed two electron transfer process. Due to the rotation of the electrode, mass transport of reactants and product is governed by convective-diffusional mechanism. The steady-state current is controlled by the solution flow rather than diffusion. As a consequence the current is proportional to the rotation speed of the electrode and also to the concentration of the species under investigation.³⁰⁰⁻³⁰² If the concentration of two analyzed species is known, the height of the current plateaus from the RDE voltammogram (at constant rotation speed) can be compared with each other.

In figure 55 the CV (black trace) and the RDE voltammogram (red trace) of **CN 2** is shown as a representative example for the entire series. Ferrocene is representing the reference system for a one electron transfer process (1.0 mM). The rotation speed is kept constant at 1000 rpm and the potential in scanned in positive direction.

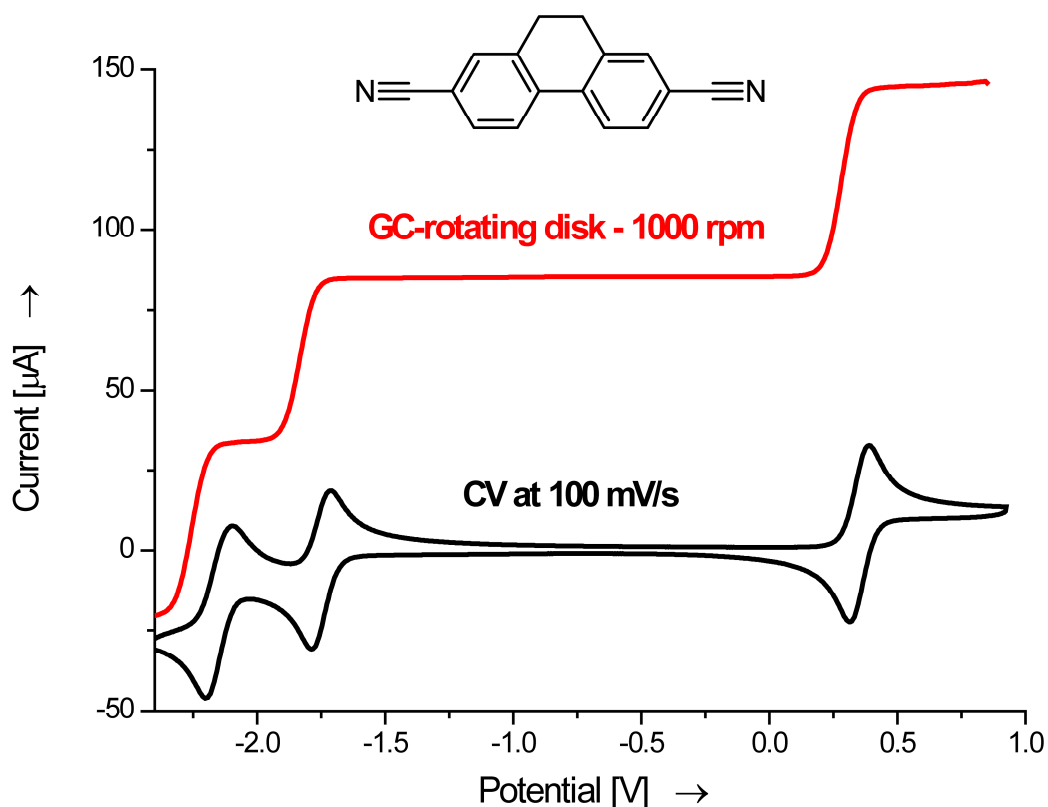


Figure 55. CV of **CN 6** using a GC working electrode (black trace). Voltammogram using a RDE electrode (GC), rotating speed: 1000 rpm (red trace). All measurements were performed in CH_3CN in a glass cell with TEABF_4 (0.1M). Sample concentration: 1.0 mM and the scan rate: 100 mV/s.

The first current plateau at around -2.2 V corresponds to back oxidation of the dianion and the second plateau at around -1.7 V to the back oxidation of the radical anion. The plateau at around +0.4 V corresponds to the oxidation wave of ferrocene ($\text{Fe}^{2+} \rightarrow \text{Fe}^{3+}$). Comparison of the plateau heights suggests a one electron transfer process during each redox event.

The values of the peak positions of the first and second reduction peaks and the ΔE_{red} of the CVs of **CN 1-6** (figure 53) are listed in table 8.

Table 8. Peak positions of the first and second reduction peaks and ΔE_{red} from the CVs of **CN 1-6**.

	ϕ [°] ^[a]	E_{red1} [V]	E_{red2} [V]	ΔE_{red} [V]
CN 1	1.02	-2.105	-2.569	0.464
CN 2	20.74	-2.098	-2.533	0.435
CN 3	44.78	-2.286	-2.619	0.333
CN 4	58.47	-2.363	-2.624	0.261
CN 5	39.60 ^[b]	-2.098	-2.478	0.380
CN 6	89.26	-2.671	-2.867	0.196

[a] ϕ is the torsion angle between the planes of the phenyl rings as measured from the crystallographic data. [b] The torsion value of was obtained from the DFT calculation.

It was attempted to correlate the energetic data obtained from cyclic voltammetry (table 8) and DFT (section 3.3.5) with the torsion angle ϕ . It is observed that the positions of the reduction peaks of both redox processes correlate linearly with the calculated LUMO energies (figure 50). With the planar fluorene **CN 1** as well as compounds **CN 2** and **CN 5** having the least negative reduction potentials (table 8), i.e. these are the best electron acceptors, and the tetramethyl compound **CN 6** as the most difficult molecule to be reduced.

Moreover, the first and the second reduction peaks of **CN 1**, **CN 2** and **CN 5** with torsion angles $\phi \leq 39.60^\circ$ appear at approximately the same potential. Interestingly, very similar LUMO energies have also been obtained for these structures in the DFT calculations.

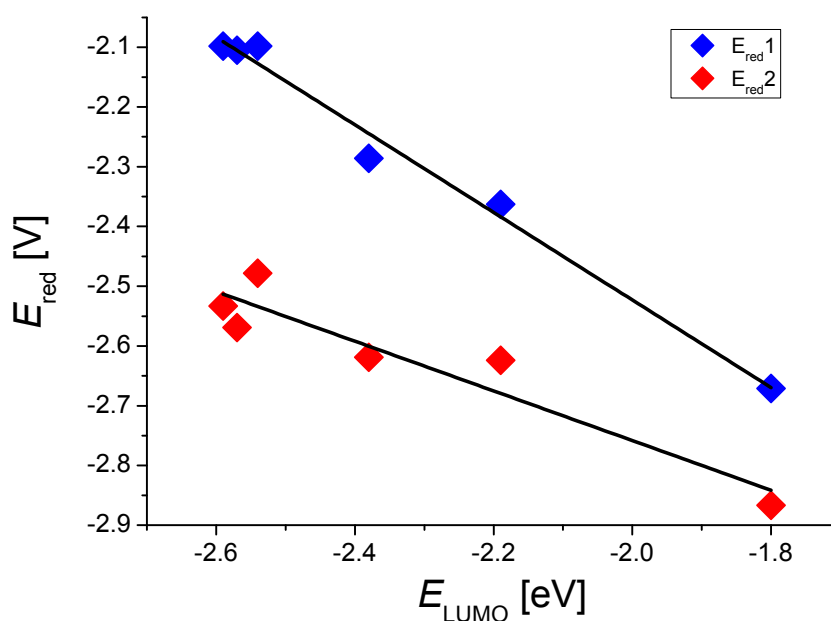


Figure 56. Peak positions of the first and second reduction peaks vs LUMO energies for **CN 1-6** compounds studied. The LUMO energies were obtained from DFT.

It is worth to note that the first reduction wave of the planar fluorene **CN 1** (1.02°) is slightly shifted to more negative potential as compared to the non-planar dihydrophenanthrene **2** (20.74°) and to compound **CN 5** (39.60° (DFT)). The reduction potentials of **CN 3**, **CN 4** and **CN 6** shift with increasing torsion angle ϕ ($\phi > 39.60^\circ$) significantly towards more negative values. This trend reflects directly the order of calculated LUMO energies.

The potential differences between the first and the second reduction peak (ΔE_{red} , table 8) exhibit a linear correlation with $\cos^2\phi$ (figure 57). While the extend of electronic communication between both benzonitrile subunits is expected to increase with decreasing torsion angle ϕ , the obvious preservation of these structural features even beyond the anion radical formation is surprising. This observation could be rationalized by the attached alkyl chains and substituents which limit rotation of the aryl rings around the central biphenyl C-C bond. Nevertheless, this is speculative in particular as the less restricted **CN 5** also prevent its structural features beyond the anion radical formation.

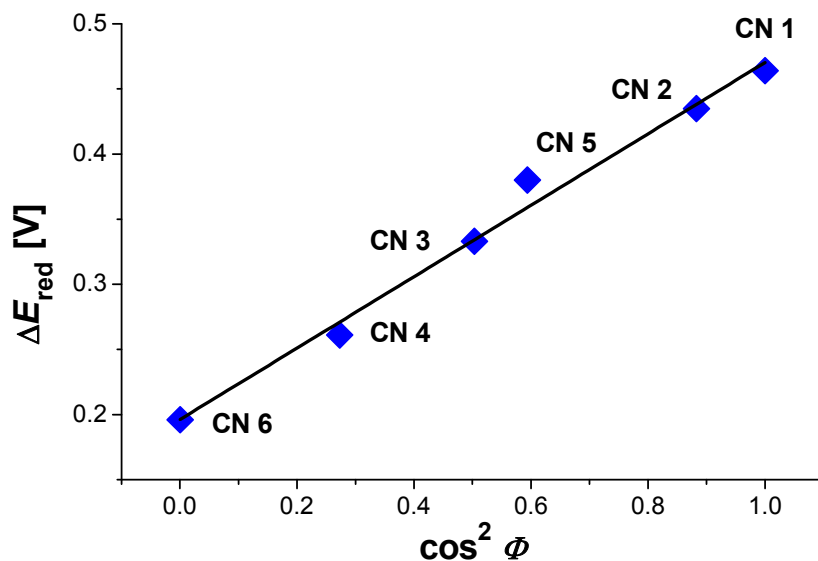


Figure 57. Linear correlation of the difference between the first and the second reduction peak ΔE_{red} with the cosine square of the torsion angle ϕ , where ϕ is the interplanar torsion angle obtained from the X-ray structures. The value for **CN 5** was obtained from DFT calculations. The linear correlation coefficient R^2 is 0.986.

The following scenario is suggested: The first $1e^-$ transfer process leads to the formation of the radical anion (see scheme 16), where the electric charge is partially delocalized on the π -system of one benzonitrile-unit (“donor”) whereas the adjacent second benzonitrile-unit remains uncharged (“acceptor”). The π - π -electronic coupling of the adjacent phenyl rings follows approximately with the cosine of the torsion angle ϕ between them.¹¹⁴ The “rate constant” of the “donor”-“acceptor” electron transfer is proportional to the square of the coupling between “donor” and “acceptor” rings.¹¹⁵ This back- and forth-electron donations lead to the delocalization of electrons over the entire biphenyl π -system. As a consequence, the extent of the π -electron delocalization (electron mobility) is linearly proportional to $\cos^2 \phi$.

The subsequent addition of a second electron (during the second $1e^-$ transfer process) onto the charged radical anion leads to a *Coulomb* repulsion between the two charges. Hence, the repulsion for the addition of the second e^- is larger the more the first e^- is already delocalized over both benzonitrile subunits.

Consequently, the potential difference between the first and the second reduction peaks (ΔE_{red}) increases linearly with $\cos^2\phi$ (figure 57).

The model compound **CN 6** (89.26°) with the two benzonitrile units perpendicular to each other displays a fully decoupled π -system. Only a slightly increased energy is required for the addition of a second electron as the first electron is localized on one benzonitrile subunit leaving the second one basically unaffected. In contrast to this situation, the planar fluorene compound **CN 1** (1.02°) has no longer a divided π -system, thus the addition a second electron induces strong *Coulomb* repulsion leading to a large value of ΔE_{red} . This hypothesis is further supported by large ΔE_{red} for **DCB**²⁹³⁻²⁹⁶ (figure 53) consisting, similar to fluorene, only of one fully delocalized π -system for the acceptance of two electrons.

3.3.8 Spectroelectrochemistry

All cyclic voltammograms (CV) were recorded in a spectroelectrochemical cell with a sample concentration of 0.1 mM dicyano-biphenyl. Figure 58a represent UV-visible spectra recorded before the first redox process ($E = -0.2$ V) and at the potentials of the first reduction peak (table 8) for a sample concentration of 0.1 mM. Spectra during the first reduction process were recorded while maintaining the potential at the first reduction peak constant. The limited cathodic stability of the Au/electrolyte system did not allow to record spectroelectrochemical data of **CN 6**.

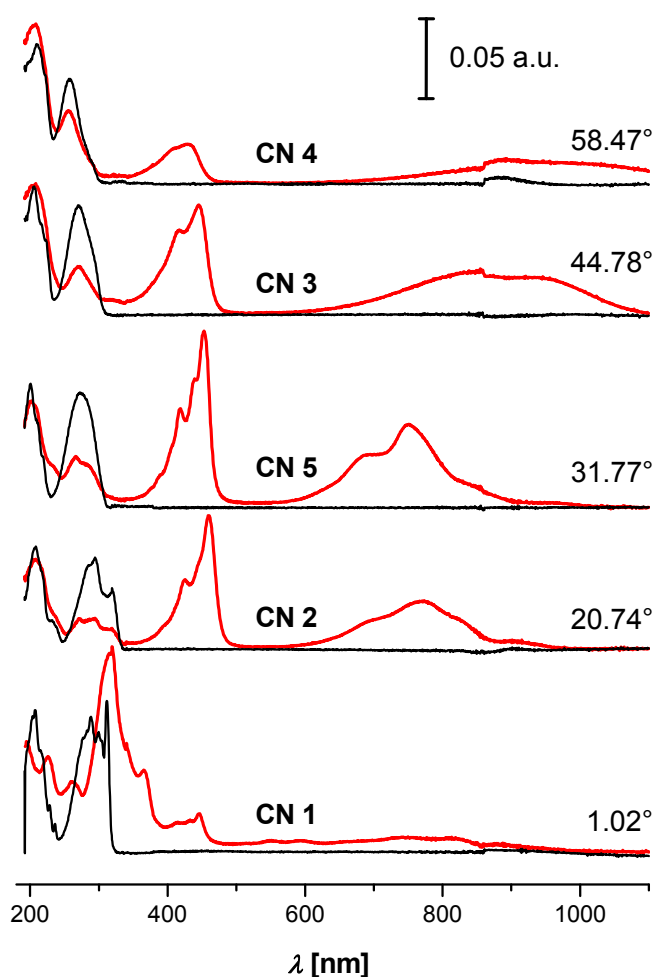


Figure 58a. Spectroelectrochemical investigation of the dicyano-biphenyls **CN 1-5**. UV-visible spectra with 0.1 mM sample concentrations in 0.1 M TBAPF₆/CH₃CN electrolyte solution at -0.2 V (black lines) and at the potential of the first reduction peak maximum (red lines).

The formation of the radical anion of the model compounds **CN 2** to **CN 5** is represented by the evolution of two new spectral features at ca. 450 nm and around 600-1100 nm (red curves). Simultaneously, the absorption band around 260-290 nm (black lines) decreases with time due to the reduction of

the uncharged species. The current observed during the electrode polarization remains rather high, which is attributed to the continuous formation of the radical anion, and its diffusion from the electrode surface into the electrolyte.

The radical anion is oxidized to the neutral species upon changing the potential back to positive direction (-0.2 V). This is reflected by the decrease of the absorption bands above 400 nm and by re-appearance of the initial spectra recorded at -0.2 V). Thus the anion radicals are reversibly and completely oxidized back at the electrode surface to the neutral compound. During the formation of the anion radical, an additional electron occupies the LUMO of the neutral molecule which becomes a SOMO (singly occupied MO).^{303,304} Thus, the smaller excitation energies in the case of radical anions as compared with the neutral molecules correspond to the transitions from the SOMO to the unoccupied orbitals (B_i type) and also from the filled orbitals to the SOMO (A_i type) (see figure 58b). It is interesting to note that the position of the peak at ca. 450 nm hypsochromically shifts with increasing torsion angle ϕ for compounds **CN 2-4** (red lines in figure 58a). This follows the trend observed for the absorption bands at 240-295 nm (black lines in figure 58a) of the neutral molecules. In contrast, with increasing torsion angle ϕ a bathochromic shift is observed for the band between 600-1100 nm.

The assignment of the energetic transitions observed is based on a recent work of Nelsen et. al.³⁰⁴ These authors investigated optical spectra of dinitro-aromatic anion radicals including 4,4'-dinitrobiphenyl ($4,4'\text{-BI}^-$), which has a strong structural similarity with compound **CN 5**. It consists of a biphenyl backbone with terminal nitro-groups as strong electron acceptors. The use of *Koopmans*-based calculations allowed the authors to assign the peak at ca. 455 nm in the UV/visible spectrum of the $4,4'\text{-BI}^-$ anion radical to the A_1 (HOMO-SOMO) transition and the peaks at $\lambda > 500$ nm to B_i -type transitions.

In analogy, for the anion radicals of the dicyano-biphenyls an A-type transition for peaks at around 450 nm and B-type transitions for peaks at longer wavelength can be proposed (figure 58b).³⁰⁴

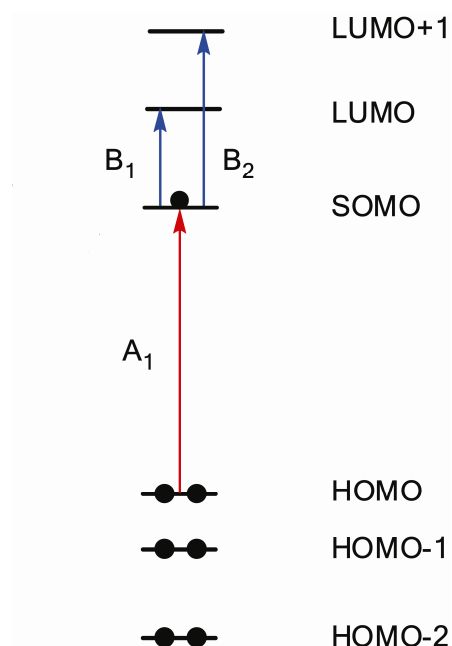


Figure 58b. Orbital energies in a restricted open-shell model showing the type A and type B transitions for a radical anion.³⁰⁴

The observed hypsochromic shift of the peaks at ca. 450 nm (red lines in figure 58a) can be rationalized as follows: The HOMO-SOMO gap (from the fully occupied orbital to the singly occupied orbital, A_i type transition) increases with increasing torsion angle due to the stabilizing HOMO and destabilizing SOMO. Similarly the HOMO-LUMO energy separations calculated by DFT for the ground state of the neutral molecules (figure 50) increases with increasing torsion angle. This increasing energy gap separation shifts both the absorption band at 240-295 nm (black lines in figure 58a) of the neutral molecules and the absorption band at 450 nm (red lines in figure 58a) hypsochromically to shorter wavelength.

The absorption bands at around 600-1100 nm can be assigned to type B_i transitions from the SOMO to the unoccupied molecular orbitals LUMO+i (to the LUMO: “B₁ transition” and to the LUMO+1: “B₂ transition”). A bathochromic shift of this band is observed and can be rationalized with the MO picture of the neutral molecules.

Figure 50 shows that the energy gap between the LUMO and the LUMO+1 decreases with increasing torsion angle due to the destabilizing LUMO. Similarly, the type B transition energies decrease due to the destabilizing SOMO (the former LUMO). Thus, the energy gaps between the SOMO and the populated LUMOs are decreasing with increasing torsion angle.

The spectrum for the radical anion of **CN 1** represents an exception with an intense band at 320 nm, a less intense band at 446 nm and very broad feature between 500-900 nm. UV/Vis spectra at the second reduction potential were not reproducible.

3.4 Single Molecule Conductance

To measure electron transport through a single molecule via binding a molecule to two metal electrodes one must use a suitable anchoring group because not only the metal–molecule interaction is modified but also the energy and charge distribution of the HOMO and LUMO orbitals are changed. Thus, search for the suitable anchoring groups for metal–molecule–metal contacts is an important research topic.⁶⁸

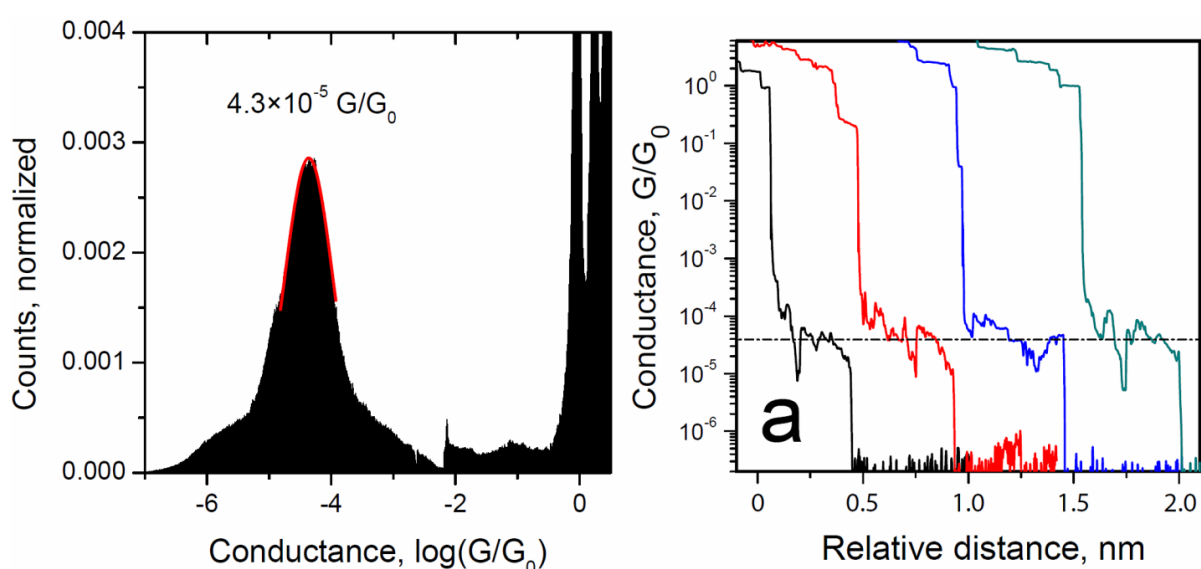
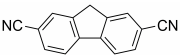
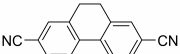
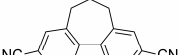
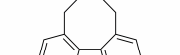
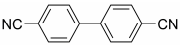
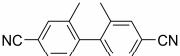


Figure 59. Conductance histogram of and conductance–distance traces for **CN 3** at $V_{\text{bias}} = 0.1$ V.

The conductance of single-molecule junctions was studied using an STM-break junction (STM-BJ) approach¹⁸ for measuring the current through dicyano-cyclophanes **CN 1-6** trapped between the STM tip and the sample substrate. These transport measurements were performed by Artem Mishchenko in the group of Thomas Wandlowski. The measurements were performed in a mixture of mesitylene/THF (4:1) at room temperature with a sample concentration of 1 mM. All investigated compounds were of single crystalline quality. Typical conductance histogram for **CN 3** is presented in figure 59. Several peaks around integer multiples of G_0 corresponded to the breaking of Au–Au bonds followed by prominent single peak around

$4 \times 10^{-5} G/G_0$ which can be attributed to the most probable conductance of single molecule **CN 3**. The small sharp feature around $5 \times 10^{-3} G/G_0$ is an artifact due to analog switch for the used dual channel preamplifier.

Table 9. Molecular structures and measured properties.

#	Structure	Interpl. torsion angle Φ ($^\circ$)	Conductance G (G_0)
CN 1		1.02 ^[a]	$(9.2 \pm 1.7) \times 10^{-5}$
CN 2		20.74 ^[a]	$(6.6 \pm 0.6) \times 10^{-5}$
CN 3		44.78 ^[a]	$(3.9 \pm 0.5) \times 10^{-5}$
CN 4		58.47 ^[a]	$(1.7 \pm 0.2) \times 10^{-5}$
CN 5		35.48 ^[b]	$(4.7 \pm 0.6) \times 10^{-5}$
CN 6		89.26 ^[a]	$< 10^{-6}$

[a] The value was taken from the solid state structures.

[b] The torsion angle was calculated at the DFT level.¹³¹

The conductance dependence on the torsion angle Φ between two phenyl rings, was further explored (Table 9). All dicyano-cyclophanes allowed to built conductance histograms without data selection in contrast to the thiol molecules where data selection is usually very important for building conductance histograms (see section 2.5). All histograms showed only one conductance value. Conductance of **CN 6** was below the measurable range. Each histogram was constructed of about 2000 individually recorded stretching traces. For each molecule the data were recorded at three different bias (65mV, 100mV and 170 mV). Surprisingly, a pronounced peak in the conductance histogram in the experiment appeared not before approximately three hours. An explanation of this observation is currently missing.

Figure 60 displays the plot of the junction conductance (G/G_0) against $\cos^2\phi$ for the series of dicyano-biphenyls investigated.

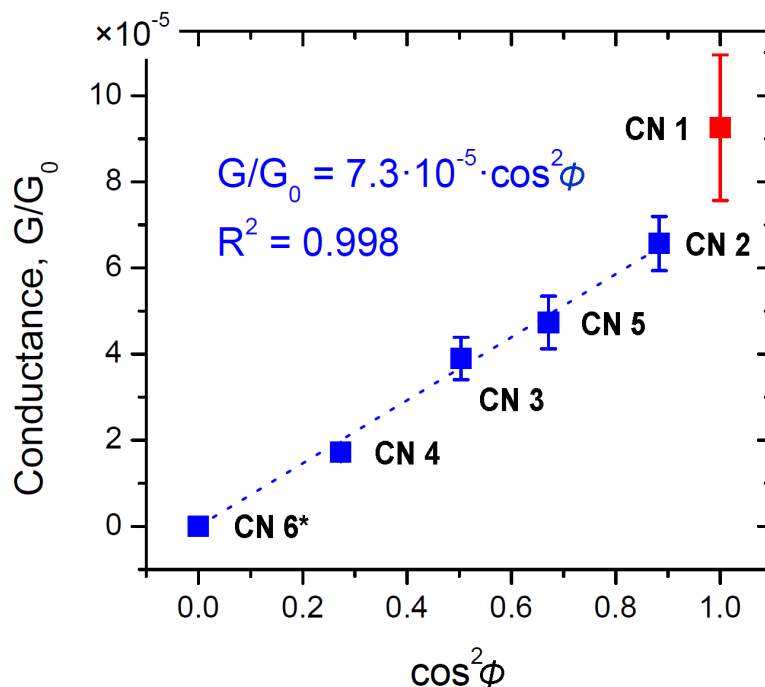


Figure 60. Experimentally measured conductance G/G_0 of dicyano-cyclophanes as function of the cosine square of torsion angle ϕ , for molecule **CN 6** the conductance was set to 0 (**CN 1** was excluded from the linear fitting).

Planar dicyano-fluorene (**CN 1**) deviates from $\cos^2\phi$ law: it exhibits a pronounced higher conductance than dihydrophenanthrene **CN 2** which is no longer planar. Surprisingly, exceptional conductance at the single molecule level was already observed for the sulfur-functionalized fluorene derivate **S1a**.

3.5 Conclusion

A series of dicyano-biphenyls **1-6** with various torsion angles ϕ between both phenyl rings were designed and synthesized as model compounds to investigate electron delocalization within gradually divided π -systems. The new structures were fully characterized and in particular X-ray crystal analysis documented the gradual increase of the torsion angle with increasing length of the alkyl chain interlinking the biphenyl system in 2 and 2' position. The extent of electron delocalization on the biphenyl backbone was investigated by UV/Vis spectroscopy, electrochemistry and spectroelectrochemistry. Particular spectral features like the conjugation band in the series of absorption spectra or the potential difference between both reduction peaks in the series of cyclic voltammograms correlate with the cosine square of the torsion angle. Interestingly, electrochemical investigations suggest that the separation of the π -systems within these biphenyls is even maintained beyond the radical anion. Furthermore, these correlations demonstrate that the fixed intramolecular torsion angle ϕ dominates the extent of electron delocalization in these model compounds and that the angle ϕ measured in the solid-state structure is a good proxy for the molecular conformation in solution. In addition, the results are supported by quantum mechanical investigations based on the density functional theory. Transport investigations at the single molecule level revealed a $\cos^2\phi$ relation with the torsion angle ϕ from the X-ray structures, similar found for sulfur-functionalized cyclophanes (chapter 2). The narrow conductance histograms could be constructed without any data selection. From the obtained results it can be concluded that the cyano-bound junctions show a strong structural selectivity and are more uniform as compared, for example, to thiol-based ones. Thus, the observed variation in conductance can be assigned to the molecular origin. The planar fluorene compound **CN 1** displays an enhanced conductivity.

4 Complementation of the Series: Planar Biphenyl Model Structures (CP)

4.1 Introduction

In the previous chapters the electron transport through various series of conformationally restricted biphenyl cyclophanes comprising thiol and cyano anchoring groups was studied. These Investigations revealed that the single molecule conductance linearly correlates with the $\cos^2\phi$ of the inter-ring torsion angle in biphenyls with a divided π -system.

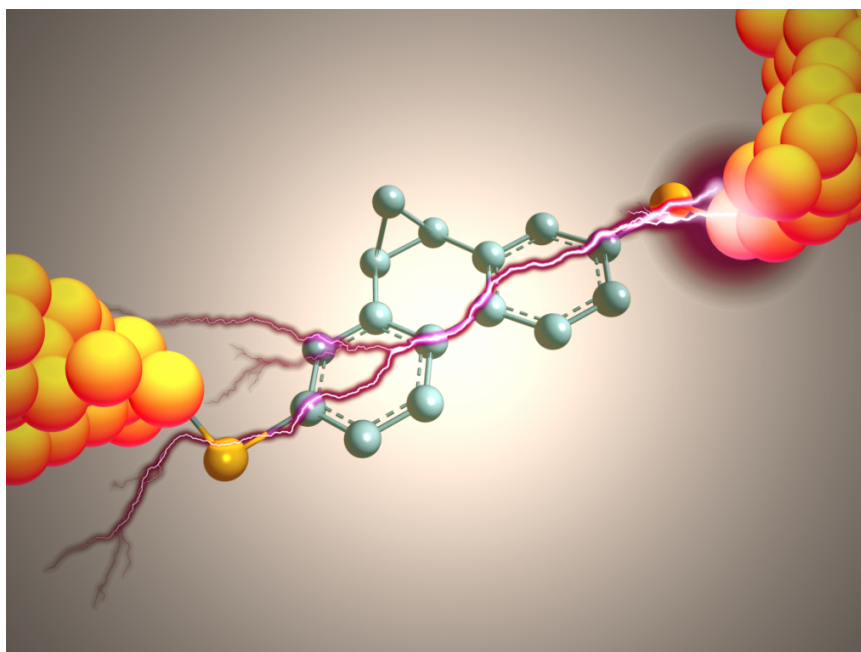


Figure 61. Artistic illustration of the thiol-functionalized dibenzonorcaradiene **CP 1** embedded between atomic sized gold contacts.

While the influence of the spatial conformation on the conductance has been demonstrated, other structural features revealed to be equally important. A recent study by *Venkataraman* reported the influence of various chemical substituents on single molecule conductance.¹⁰⁴ This investigation showed that the conductivity of molecules can be chemically gated by installing various donor and acceptor groups.

Furthermore, *Löhneysen* and co-workers have shown that I/V characteristics of molecules depend on the spatial symmetry of a molecule.³⁰⁵

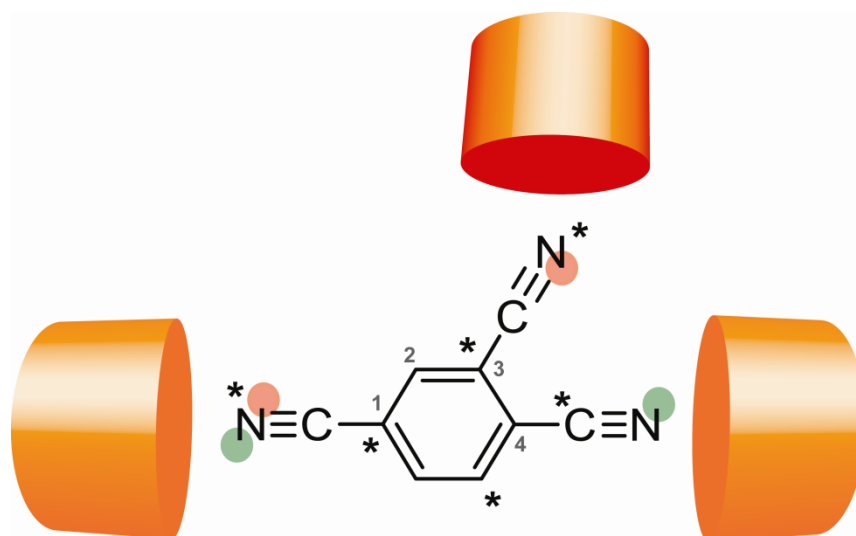


Figure 62. Illustration of Quantum-Interference-Controlled Molecular Electronics. If an electrode is contacting the cyano group at C1 (starred position) of the benzene ring and at the cyano group at C4 (unstarred position) strong electronic interaction occurs (green dots \rightarrow 1,4-*para* pathway). If the electrodes are contacting the cyano groups in the positions C1 and C3 (both starred positions, red dots \rightarrow 1,3-*meta* pathway) the electronic communication is suppressed.³⁰⁶ A similar device arrangement was proposed to function as a Quantum Interference Effect Transistor (QuiET). Thereby, a voltage applied to the one contact regulates the flow of current between the other two.³⁰⁷

Furthermore, quantum interference determines at which position molecules have to be connected to electrodes to be a good conductor.^{306,308,309} *Mayor* and co-workers have shown that the resistance of an electrode-molecule-electrode device strongly depends on the relative position of the anchoring group in a molecular wire.³¹⁰ Alternant molecules (often referred to as “alternant hydrocarbons”) are π -systems in which each neighboring conjugated carbon atom (or a heteroatom that contributes to the conjugation) can be marked with or without a star and no two starred or unstarred atoms are bonded to each other (most organic molecules are alternant).³¹¹ The strongest coupling occurs when the one electrode is connected at a starred position and the other at an unstarred position (figure 62).^{306,311,312}

4.2 Planar Biphenyl Structures under Investigation

Despite the reported insight into the structure/property relationship, we were interested to investigate the effect of various second bridges in the 2,2'-position on the π -backbone conjugation (figure 63).

This series of model compounds was proposed to understand the unexpected behavior of the fluorene derivatives within the respective series.

Furthermore, the structure/property relationship of these planar biphenyl structures is of interest as such structures are used as monomeric building blocks to build up charge-transporting polymers.

The installed bridges are varied in terms of their ability to conjugate with the neighboring π -systems. Thereby, the length of the bridge is chosen such that the two phenyl rings are constrained into one plane. Furthermore, acetyl protected thiol-anchoring groups are installed in 4,4'-position, not only to allow immobilization between two atomic-sized metal electrodes, but also to investigate HOMO-transport. Cyano-anchoring groups are installed to explore LUMO transport (see also section 3.1).

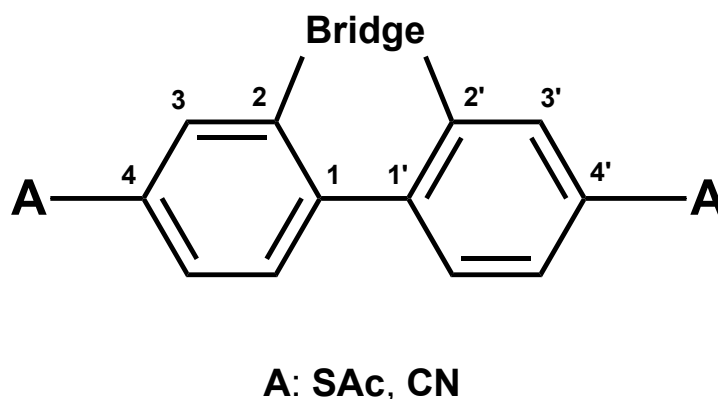


Figure 63. Schematic of the planar biphenyl scaffold. Second bridges are installed in 2,2'-position. Terminal anchoring groups in 4,4'-position are installed to contact metal electrodes.

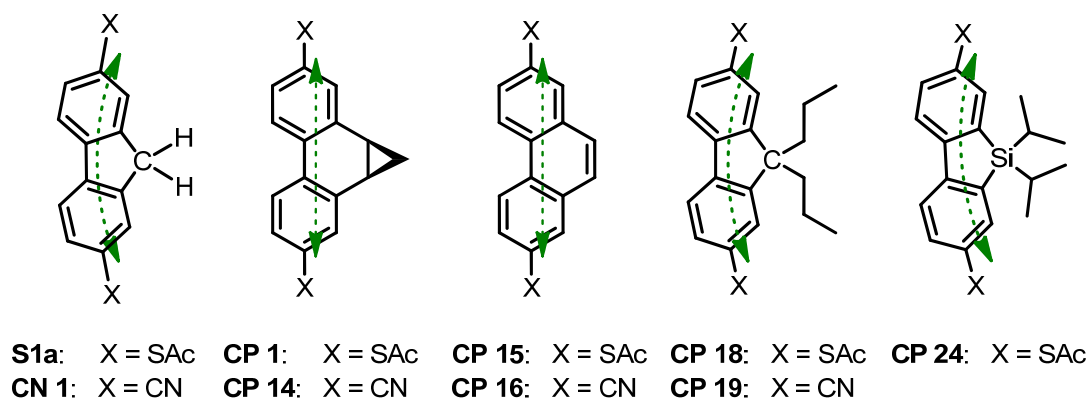


Figure 64. Target structures under investigation.

This investigation may reveal more insight into the structure/property relationship to understand the electron transport through larger π -systems such as graphene. UV absorption spectra of the parent structures indicate that the delocalization of π -electrons is considerably influenced by additional bridges in 2,2'-position. In figure 64 all target structures under investigation are displayed. The synthesis and properties of the fluorene compounds **S1s** and **CN 1** are discussed in the previous chapters 2 and 3. Furthermore, the conductivity of these two planar derivatives did not follow the trend. Motivated by these finding, the two novel dibenzonorcaradiene model structures **CP 1** and **CP 14** (all compounds in this chapter will be denoted as **CP**) were designed and envisaged as suitable structures to probe electron transport through a fully planar biphenyl geometry. The biphenyl backbone in dibenzonorcaradiene exhibits no distortion along the molecular axis, thus, it displays a mimic for a highly symmetric π -system. While the backbone geometry in dibenzonorcaradiene is linear the cyclopropyl-bridge in 2,2'-position may electronically interact with the biphenyl π -system.

Extension of the π -system is achieved in the two phenanthrenes derivatives **CP 15** and **CP 16**. Furthermore the series was extended by the doubly α -propylated fluorenes derivatives **CP 18** and **CP 19**. While the fluorene backbone in these compounds remains unchanged compared to the parent compounds **S1s** and **CN 1**, the acidic α -hydrogen atoms can no longer be abstracted. Furthermore, the perpendicular propyl-chains which are perpendicular to the fluorene-plane reduce the probability of intermolecular aggregation and increase also the solubility. The single methylene unit in fluorene is discussed to participate to the π -system of biphenyl via hyperconjugation (fluorene is then consequently assumed to be a non-alternant hydrocarbon).^{96,313,314}

While the effect of hyperconjugation in fluorene is not conclusive (see also end of section 2.5),³¹⁵ pronounced σ^* - π^* hyperconjugation is expected for the silafluorene derivate **CP 24** where the sp^3 hybridized carbon-atom is substituted by a sp^3 hybridized silicon-atom. The exocyclic Si-C σ^* -orbital effectively mixes with the π^* -orbital of the butadiene fragment to afford an exceptionally low-lying LUMO.³¹⁶⁻³¹⁹ Silafluorenes display an important class of monomers in the synthesis of polymeric materials with high electron accepting ability.³¹⁷⁻³²³

4.3 Synthesis and Characterization

4.3.1 Dibenzonorcaradiene – Conjugation at its Best?

The idea was to design a biphenyl model structure that exhibits no geometric distortion along the molecular axis. The phenyl rings in dihydrophenanthrene can be constrained into one plain by replacing the two “bridge” H-atoms and replacing them by one bridging carbon atom (figure 65). Thereby, the two phenyl rings adopt a fully planar and linear geometry. While the biphenyl axis is linear, the cyclopropane ring exhibits π -bond character and is reported to conjugate with neighboring double bonds.³²⁴⁻³²⁷

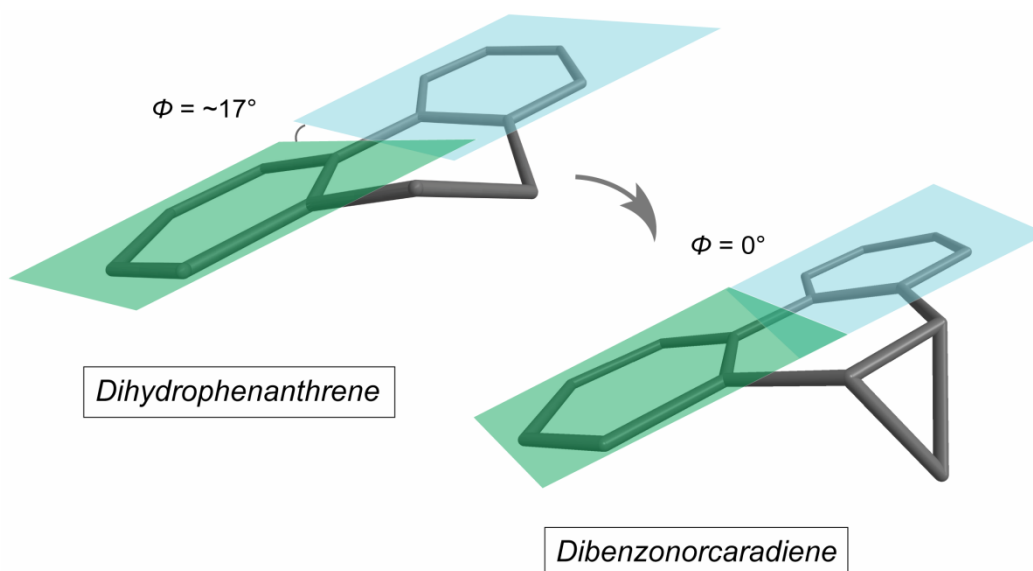
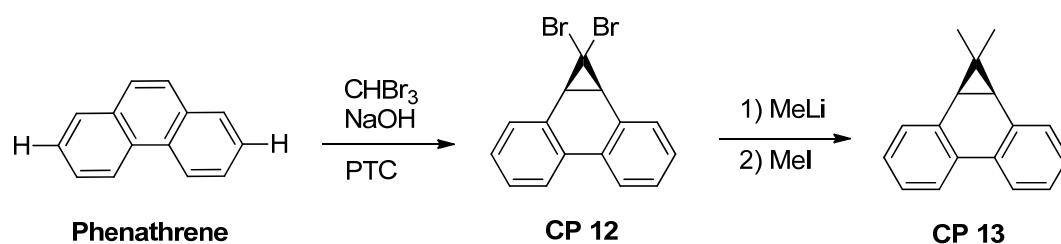


Figure 65. The phenyl rings in dihydrophenanthrene are constrained into one plain by replacing the two “bridge” H-atoms and replacing them by one bridging carbon atom.

Dibenzonorcaradiene (1a,9b-dihydro-1*H*-cyclopropa[*l*]phenanthrene) is a fairly stable compound due to the stabilizing effect of the benzene rings fused to the norcaradiene skeleton.³²⁸⁻³³⁰ The first attempts in this thesis to synthesize the dibenzonorcaradiene skeleton involved several carbene-addition reactions starting from the 2,7-functionalized phenanthrene derivatives **CP 10** and **CP 11** (see next page). The phenanthrene approach is simple and straightforward. As an example the dibromo-carbene addition³³¹ to phenanthrene (scheme 17) is a well established reaction and has been developed even on large scales.³³¹



Scheme 17. The first performed reaction sequence to afford the “all carbon” dibenzonorcaradiene structure **CP 13** is shown.

Subsequent removal of the halogen atoms in the bridge-head of **CP 12** by reduction³³² or substitution with alkyl groups³³³⁻³³⁵ was considered as the subsequent step. The additional methyl groups at the bridge-head were assumed to have no considerable effect on the overall electronic structure of the molecule. Following this strategy dibromide **CP 12** was successfully synthesized and subsequently methylated by sequential treatment of the dibromide **CP 12** with MeLi and MeI. Single crystals of **CP 13** were grown for X-ray measurement.

Figure 66 displays the crystal structure of co-crystalline **CP 13** and **CP 12** due to inclusions of the precursor.

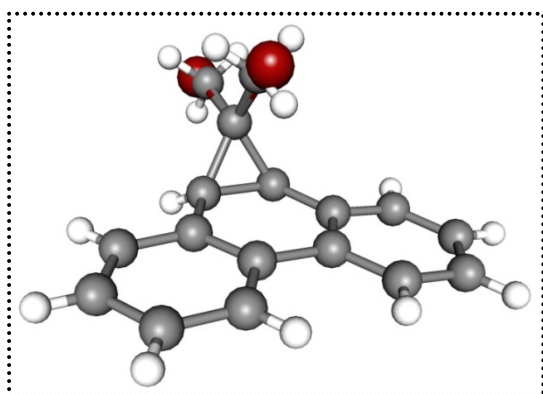
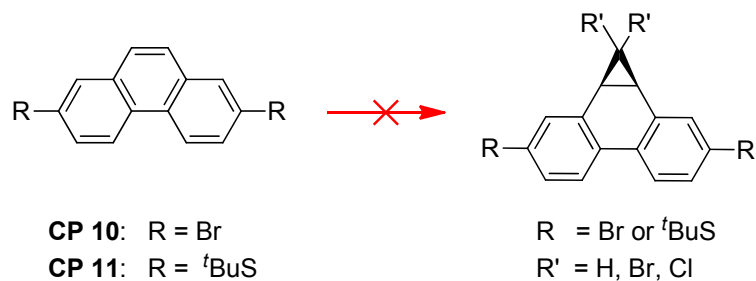


Figure 66. X-Ray structure of **CP 13** superimposed with structure **CP 12**. The red atoms are the bromine atoms of the structure **CP 12**.

Other reaction conditions were tested to achieve the dibenzonorcaradiene scaffold. These included the addition of CCl_2 carbene³³⁶ or the

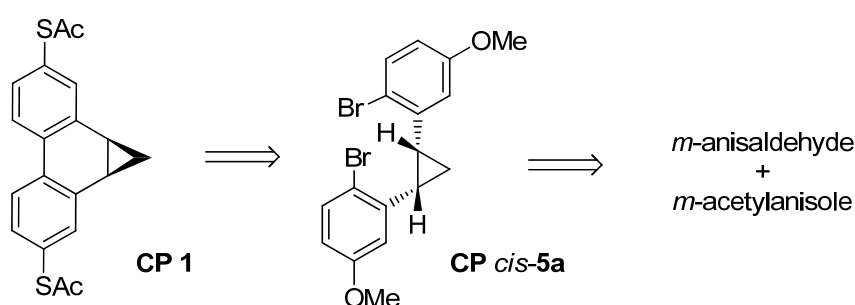
cyclopropanation with an iron-containing methylene-transfer reagent at elevated temperature.³³⁷⁻³³⁹



Scheme 18. Various cyclopropanation reactions starting from the 2,7-functionalized phenanthrene derivatives **CP 10**³⁴⁰ and **CP 11** failed (see experimental section for the synthesis of **CP 10** and **CP11**).

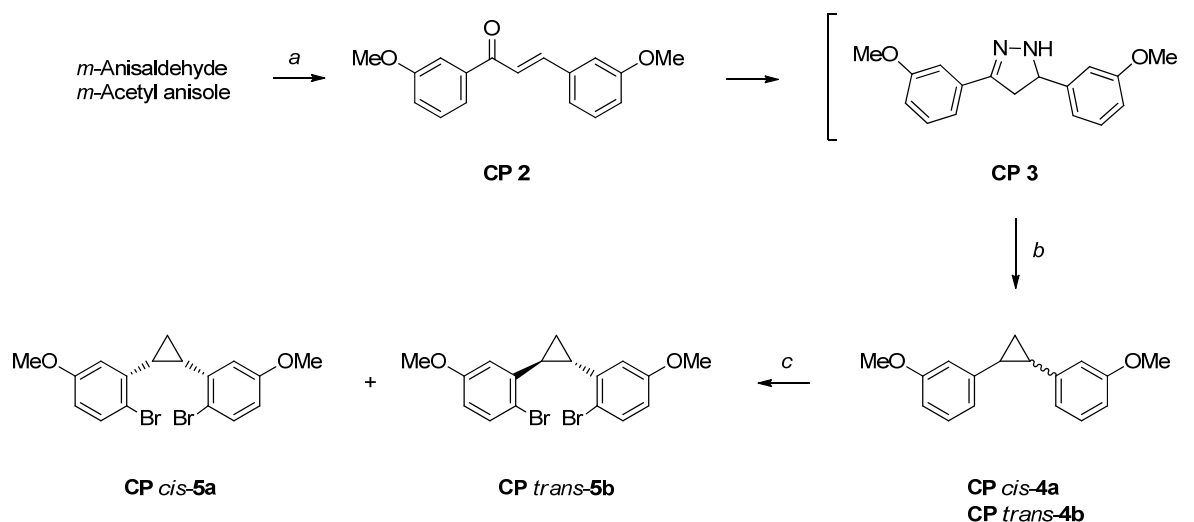
Unfortunately, none of these reactions did succeed (not even traces of new products could be detected by using various analytical techniques). Due to the low reactivity of the derivatives **CP 10**³⁴⁰ and **CP 11** another synthetic strategy was required to build up the dibenzonorcaradiene synthon.

In scheme 19 the retrosynthetic analysis of **CP 1** is shown. Dibenzonorcaradiene **CP 1** can be assembled in a last step by an intramolecular carbon-carbon bond formation. **CP cis-5a** is a suitable precursor as both aryl-halogen units are in a predisposed position to undergo an oxidative aryl-aryl coupling reaction via intramolecular Ar-Cu-Ar formation. 1,2-Diphenyl-cyclopropane **CP cis-5a** is obtained from a dimethoxy-chalcone³⁴¹ that is accessible from the two carbonyl compounds *m*-anisaldehyde and *m*-acetylanisole by an aldol condensation.



Scheme 19. Retrosynthetic analysis of dibenzonorcaradiene **CP 1** via **CP cis-5a** to *m*-anisaldehyde and *m*-acetylanisole.

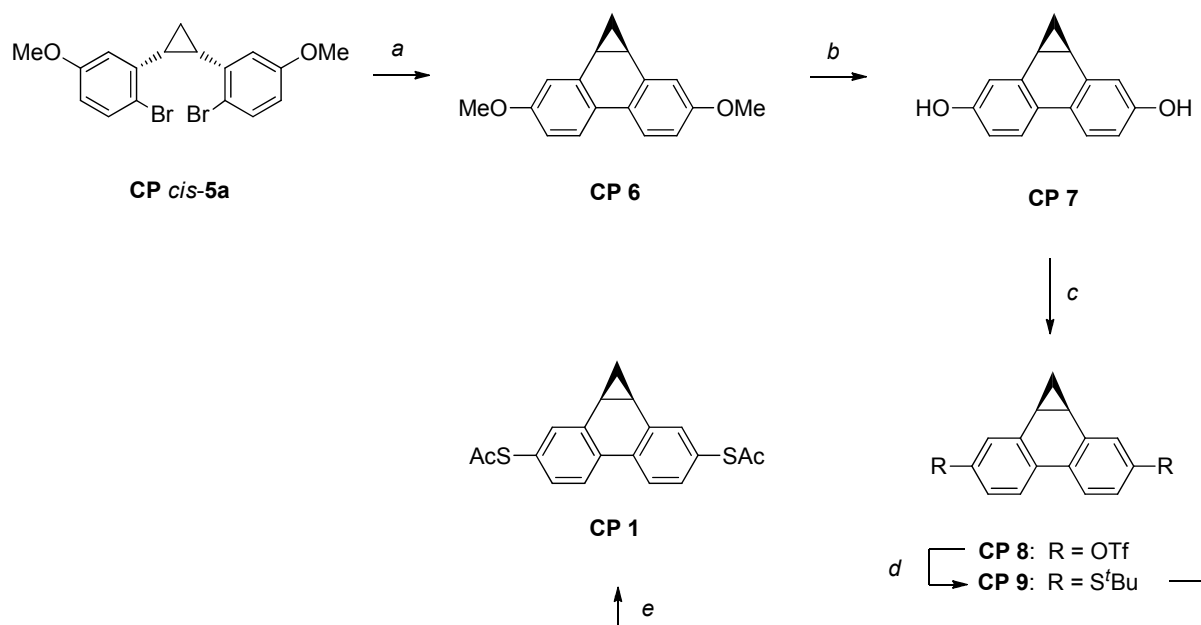
Following this strategy the doubly methoxy-functionalized chalcone **CP 2** was synthesized on a large scale starting from *m*-anisaldehyde and *m*-acetylanisole. The aldol-condensation reaction using NaOH as the base proceeded smoothly at room temperature yielding the α,β -unsaturated carbonyl compound **CP 2** as a yellow oil. A subsequent cycloaddition reaction of the crude **CP 2** with hydrazine gave the thermodynamically favored³⁴² 2-pyrazoline derivate **CP 3** as an intermediate. Subsequent thermal *in situ* decomposition yielded a mixture of the 1,2-diphenyl-cyclopropanes **CP cis-4a** and **CP trans-4b** as the only products.³⁴³



Scheme 20. (a) NaOH, MeOH, rt. (b) Hydrazine monohydrate, EtOH, reflux. Then, cat. KOH, diethylene glycol, 190-210 °C, 92% (over two steps). Ratio of **CP cis-5a**/**trans-5b** is 44:56. (c) Bromine, pyridine, CH₂Cl₂, -10 °C to rt, 45% (**CP cis-5a**) and 26% (**CP trans-5b**).

Integration by ¹H NMR revealed an almost equivalent *cis/trans* ratio of 44:56. While this type of cyclopropanation reaction is low in cost owing to cheap reagents no *cis/trans*-selectivity is achieved. Subsequent regioselective bromination of **CP cis-4a/trans-4b** mixture yielded the doubly brominated isomers **CP cis-5a** and **CP trans-5b**. Separation of the two isomers was achieved by flash chromatography on silica gel which gave **CP trans-5b** in 26% yield as a white solid. Another fraction of 45% mass yield was isolated as an oil containing **CP cis-5a** as the major component together with remaining amounts of **CP trans-5b**.

Further enrichment of the *cis*-isomer was achieved by dissolving the mixture in hot *n*-hexane and storing it at 4°C. Subsequent removal of crystallized *trans*-product gave the final *cis*-fraction **CP cis-5a** as an oil which was pure enough for the subsequent cyclization reaction.



Scheme 21. (a) *t*-BuLi, CuCN, LiBr, MeTHF, then 1,3-dinitrobenzene, -60° C to rt, 36%. (b) NaH, *n*-PrSH, DMF, 140 °C, 72%. (c) Tf₂O, pyridine, 0 °C to rt, 99% (d) *t*-BuSNa, Pd₂(dba)₃ (10.0 mol%), xantphos (12.0 mol%), *p*-xylene, 140°C, 68%. (e) BBr₃, AcCl, toluene, 0 °C to rt, 58%.

Trans-lithiation with *t*-BuLi of the dibromide **CP cis-5a** and subsequent intramolecular aryl-aryl coupling via cuprate formation similar to that reported in the preparation of torsion angle restricted cyclophanes¹⁹ yielded the methoxy-functionalized dibenzonorcaradiene key intermediate **CP 6** in 36% yield.

Subsequent deprotection of the methoxy group turned out to be challenging. Decomposition was observed when using boron tribromide as the deprotection reagent. In contrast nucleophilic cleavage of the methyl groups using *n*-propyl thiolate was successful, affording diol **CP 7** in 72% yield as an off-white solid. To our surprise the dibenzonorcaradiene system in **CP 7** was stable under these rather harsh nucleophilic deprotection conditions (140°C). Subsequent esterification with triflic anhydride in pyridine afforded the ditriflate **CP 8** in 99% yield which crystallized upon standing at room temperature. Introduction of the acetylsulfanyl groups was achieved by a three step reaction sequence.

A palladium catalyzed cross-coupling reaction¹⁵⁴ was performed in a first step to install two *tert*-butyl ether groups in *para*-position of **CP 9** in 86% yield. By applying a modified transprotection procedure^{19,184} the *tert*-butyl groups were removed with boron tribromide and the free thiol groups were *in situ* protected with acetyl chloride. A careful subsequent work up procedure was crucial. Sodium acetate was added to trap free acid evolved during the work up. Immediate purification by flash chromatography on silica gel afforded the acetyl protected dithiol **CP 1** in 58% over two steps.

To gain more insight about the dibenzonorcaradiene structure, single crystals of the methoxy functionalized **CP 6** were grown from cyclohexane using the slow evaporation technique.

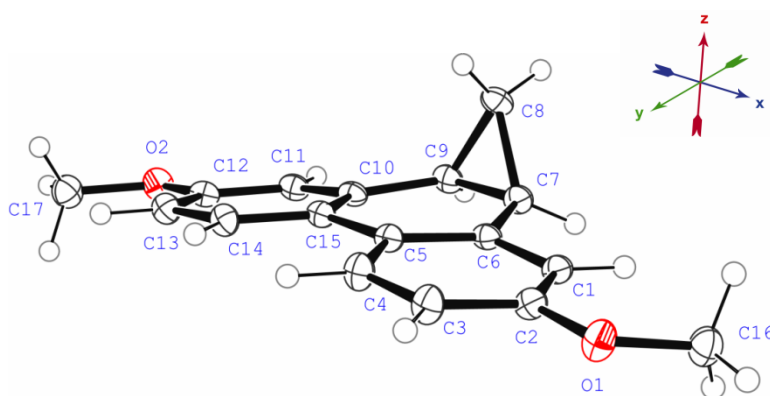
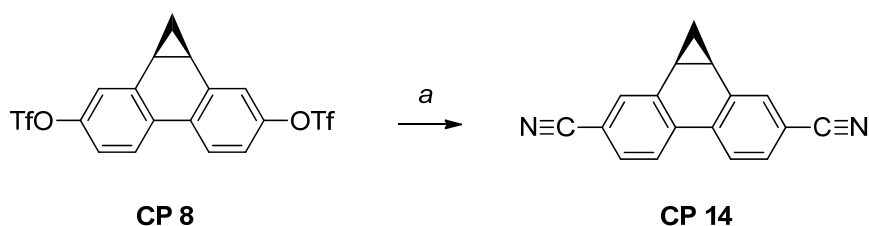


Figure 67. Solid state structure of **CP 6**.

The solid state structure of the dibenzonorcaradiene structure **CP 6** is displayed in figure 67. The C-C distance between C2-C12 is 7.18 Å. The dihedral angles C10-C15-C5 and C15-C5-C6 are 120.2° and 120.8°, respectively displaying a planar and unbent biphenyl π -system. In contrast to the parent planar fluorene structure, **CP 6** exhibits no bending along the molecular axis. A small deflection of the backbone along the z-axis is observed. The origin of the deflection remains unclear. It might be a simple packing effect in the solid state structure.



Scheme 22. (a) $\text{Pd}_2(\text{dba})_3 \cdot \text{CHCl}_3$, xantphos, tributyltin chloride, KCN, acetonitrile, reflux, 15%.

The triflate groups in *para*-position of the biphenyl backbone in compound **CP 8** allowed installation of two cyano groups. A palladium-catalyzed cyanation reaction promoted by low-level organotin chloride²³⁰ was successful to convert ditriflate **CP 8** to dibenzonorcaradiene **CP 14** bearing two cyano acceptor groups. Purification by silica gel chromatography afforded target compound **CP 14** in 15%. Single crystals were successfully grown by recrystallization from a mixture of cyclohexane and dioxane using the slow evaporation technique.

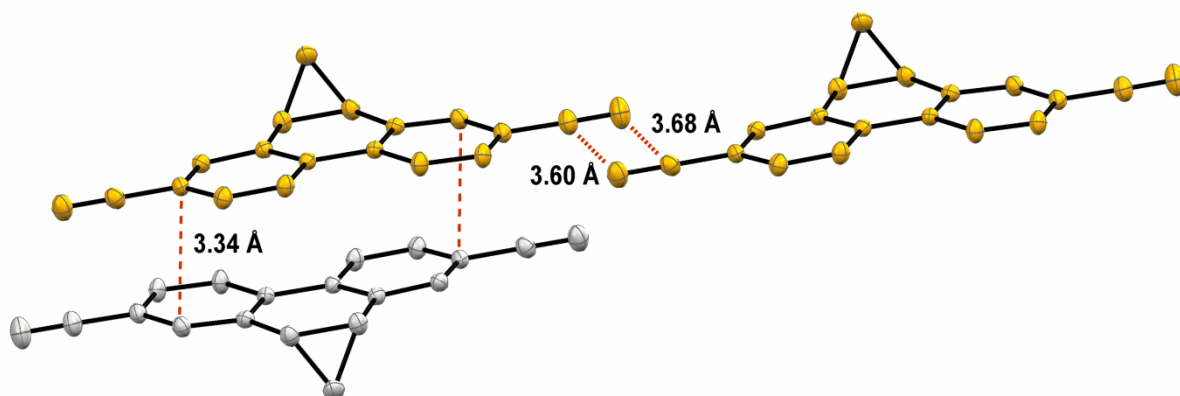


Figure 68. Crystal packing of **CP 14**.

Figure 68 shows the X-ray structure of **CP 14**. Compared to the methoxy functionalized **CP 6** which exhibits a deflection along the z-axis, a fully planar structure is observed in **CP 14**. This corroborates the idea that a simple packing effect causes deflection in dibenzonorcaradiene **CP 6**.

The molecules form 1D-chains held together by dipolar antiparallel CN...CN interactions. The molecules are stacked pair wise in a parallel, displaced manner. The intramolecular N-N distance is 12.26(4) Å which is comparable with the intramolecular N-N distances found in the dicyano biphenyl series **CN 1-6**. The smallest distance found between the overlaying phenyl rings is 3.34(2) Å which is similar to the shortest interplanar distance found in the crystal structure of the fluorene derivate **CN 1** (3.44(9) Å).

4.3.2 Phenanthrenes

2,7-Dibromo-phenanthrene³⁴⁰ (**CP 10**, see 5.2) was converted by a cyanation reaction using an excess of CuCN to yield 2,7-dicyano-phenanthrene **CP 16** in 27%. While attempts to obtain single crystals of **CP 16** failed, suitable single crystals of the acetylsulfanyl-functionalized **CP 15**¹⁰⁰ could be grown from a hot mixture of cyclohexane.

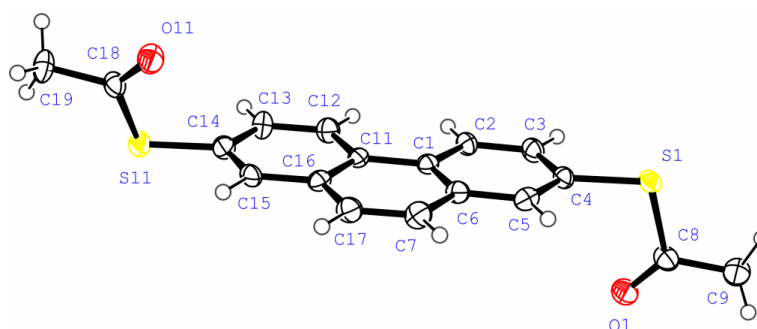


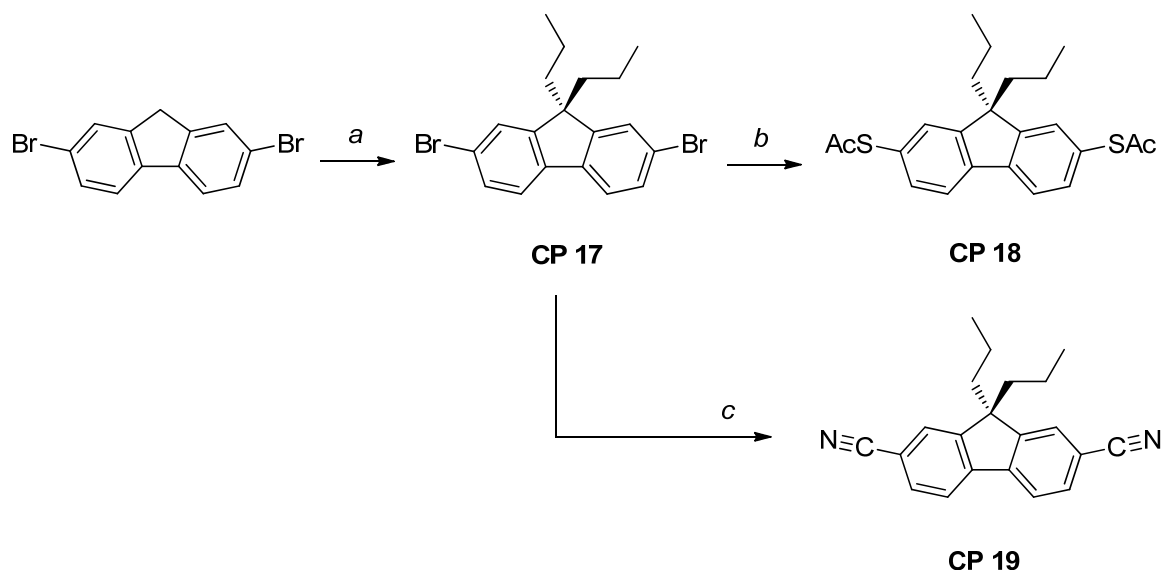
Figure 69. X-ray structure of the acetylsulfanyl functionalized phenanthrene **CP 15**.

The crystal structure of **CP 15** is displayed in figure 69. As expected a fully planar structure is observed for this fully aromatized compound with an intramolecular S-S distance of 10.63(8) Å which is comparable with the S-S distances found in the series **S1a-S8a** (chapter 2).

4.3.3 9,9-Dipropyl-Fluorenes

The motivation to include 9,9-dialkyl-fluorenes as model compounds was to remove the acidic hydrogen atoms in the benzylic position (C7 in figure 70) of the fluorene synthon. Furthermore, introduction of alkyl chains were expected to increase the solubility of the fluorene derivatives in solution.

The route which was followed to assemble the fluorenes **CP 18** and **CP 19** (scheme 23) started with masking the acidic protons of the commercially available 2,7-dibromofluorene by a dialkylation reaction.³⁴⁴ The resulting 2,7-dibromo-9,9-propylfluorene **CP 17** reacted with methylthiolates and the resulting methylsulfanyl functional groups were transprotected^{100,163} *in situ* to obtain the acetyl protected terminal sulfur anchor groups in **CP 18**. Single crystals of **CP 18** were grown from hot hexane.



Scheme 23. (a) *n*-PrBr, *t*-BuOK, THF, 5 °C, 65%. (b) NaSCH₃, DMI, 140 °C, then AcCl, 0 °C to rt, 22%. (c) CuCN, DMF, 67%.

Again starting from **CP 17**, a cyanation reaction with copper cyanide gave the dicyano compound **CP 19** in 67% yield after recrystallization from a hot mixture of ethanol and water. These crystals were already suitable for the X-ray measurement.

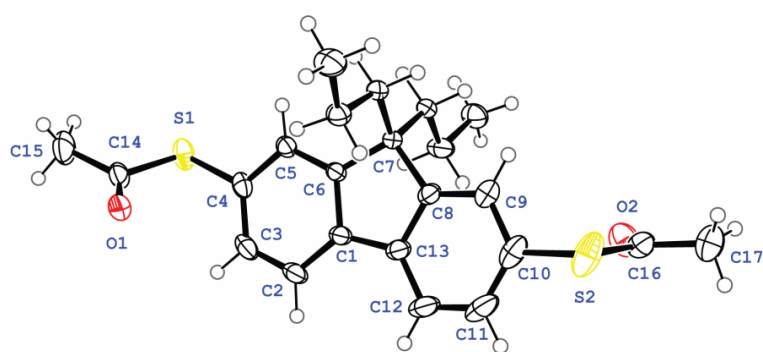


Figure 70. X-ray structure of target compound **CP 18**.

The propyl chains in **CP 18** are orthogonal with respect to the biphenyl plane. The length of the propyl chains are approximately 4.65 Å and are intended to reduce the probability of possible intermolecular aggregation in solution. Due to the bent backbone the intramolecular S-S distance (10.32(1) Å) in **CP 18** is shortened compared to the S-S distances in the B PDT series **S2a-S8a** (10.59(4)-10.61(2) Å).

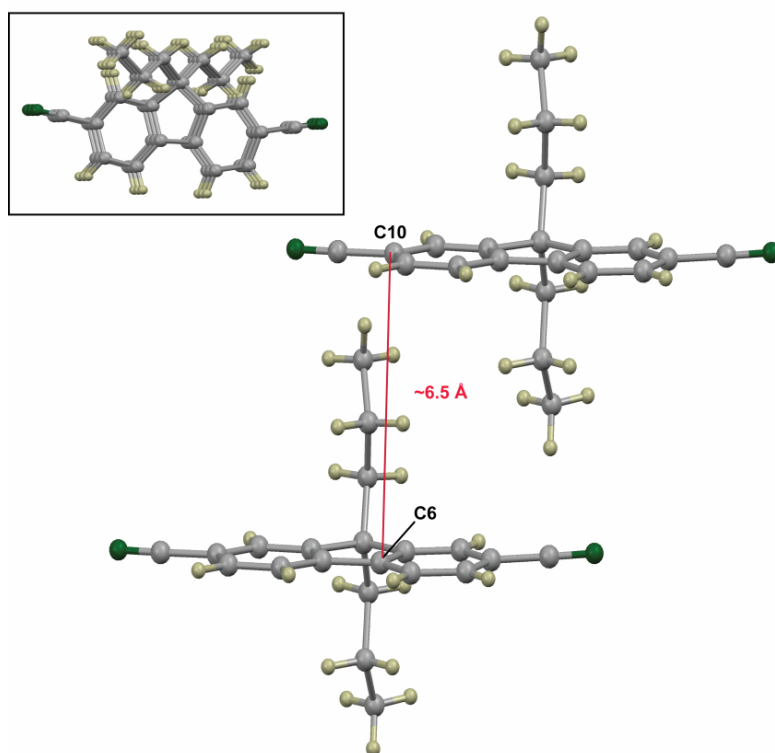
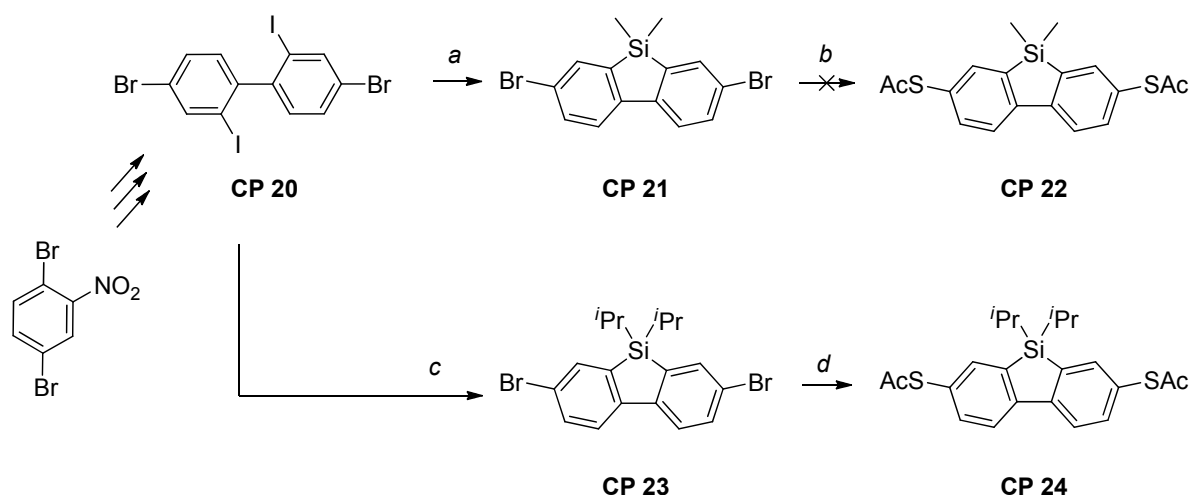


Figure 71. The inset shows the columnar arrangement of **CN 19** along the *a*-axis of the unit cell. Compared to parent fluorene compound **CN 1** (non-alkylated fluorene) the intermolecular distance is drastically increased to ~6.5 Å (C10-C6).

4.3.4 Silafluorenes - Silicon-Bridged Biphenyls

To assemble the silicon bridged model compound **CP 24** the building block 4,4'-dibromo-2,2'-diiodobiphenyl **CP 20** was envisaged as suitable starting structure. **CP 20** was synthesized over three steps according to a reported procedure.³¹⁹ The dimethyl-silicon moiety in **CP 21** (2,7-dibromo-9,9-dimethyl-dibenzosilole) was considered first as the bridging unit. According to a modified procedure³¹⁹ a selective trans-lithiation with *t*-BuLi in THF followed by subsequent intramolecular cyclization with dimethyldichlorosilane gave **CP 21** in 52%. To introduce the acetylsulfanyl groups in **CP 22** a known one-pot three step procedure was applied.³⁴⁵ This involved a halogen-metal exchange with *t*-BuLi, followed by quenching with elemental sulfur and an *in situ* protection using acetyl chloride.³⁴⁵ Unfortunately, no product could be isolated.



Scheme 24. (a) *t*-BuLi, THF, (CH₃)₂SiCl₂, -60 °C, 52%. (b) *t*-BuLi, THF, -60°C, S₈, then AcCl. (c) *t*-BuLi, THF, (*i*-Pr)₂SiCl₂, -60 °C, 56%. (d) KSAc, Pd₂(dba)₃·CHCl₃ (5.0 mol%), xantphos (1.0 mol%), Et(*i*-Pr)₂N, dioxane, MW 160°C, 22%.

The dimethyl silicon-bridge in intermediate **CP 21** was considered as rather unstable due to the small methyl groups. Enhanced stability was expected for the bulkier alkyl moiety in **CP 23** protecting the reactive silicon centre. Applying similar reaction conditions as before, the diiodide **CP 20** was cyclized to the silafluorene **CP 23** bearing two isopropyl groups on the silicon atom. Furthermore, these bulkier alkyl substituents were expected to prevent

decomposition of the immobilized silicon-containing synthon during STM conductance measurements.¹⁸

In a final step the dibromide **CP 23** was converted to the acetyl-protected dithiol **CP 24** using a palladium-mediated cross-coupling reaction with potassium acetate in 22% yield.¹⁹⁰ Single crystals suitable for the X-ray measurement were obtained from hexane using the slow evaporation technique.

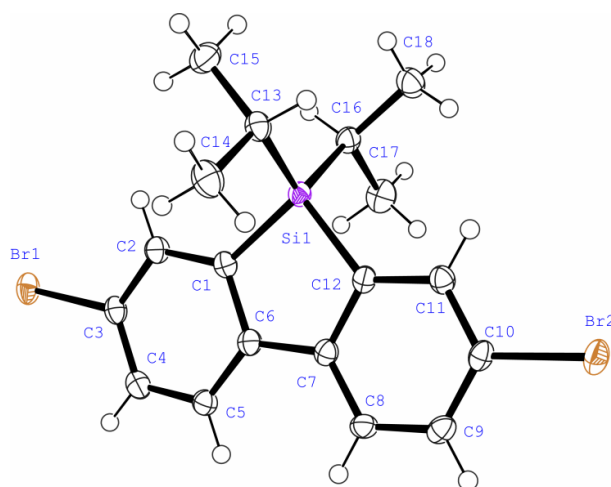


Figure 72. X-ray structure of **CP 23**.

Among the other new π -electron systems synthesized, the structures of compound **CP 23** has been determined by X-ray crystallography, as shown in figure 72. **CP 23** has highly coplanar π -conjugated frameworks due to the silicon bridge. The angles in the butadiene fragment are $114.8(3)^\circ$ (C1-C6-C7) and $114.7(7)^\circ$ (C6-C7-C12). These almost identical angles are slightly increased compared to corresponding angles in the fluorene skeleton ($\sim 108^\circ$) due to the increased size of the silicon atom. The intramolecular distance between the two terminal carbon atoms (C3-C10) is $7.01(5) \text{ \AA}$ which is slightly increased compared to the terminal C-C distance in the fluorene skeleton of **CN 1** ($6.84(9) \text{ \AA}$). Thus indicating a similar extent of bending of the biphenyl backbone along the molecular axis as in fluorene derivative **CN 1**.

4.4 UV Absorption Measurements

In a simple electron transport picture the Highest Occupied Molecular Orbital (HOMO) and the Lowest Unoccupied Molecular Orbital (LUMO) and the orbitals which are close to them are assumed to dominate the electron transport.³⁴⁶ UV/VIS spectra of molecules are associated with transitions between these electronic energy levels. Light can excite electrons from bonding σ -, π -orbitals or non-bonding n -orbitals (electron lone pairs) to antibonding σ^* -, π^* -orbitals. The type of transitions are designed as $\sigma \rightarrow \sigma^*$, $\pi \rightarrow \pi^*$, $n \rightarrow \sigma^*$ or $n \rightarrow \pi^*$ transitions. UV-spectroscopy gives, thus, insight about the electronic structure of molecules, and displays an indispensable tool to characterize the electronic properties of molecules.

4.4.1 Probing the Conjugation in Cyclopropane

The motivation of the following work was to probe optically the extent of double bond character of a cyclopropane ring when compared to an ethylene or acetylene bond. To explore the ability of a cyclopropane ring to conjugate with neighboring π -systems, three sulfur-functionalized model compounds (figure 73) were synthesized (see chapter 5, **CP 25-31**) and their optical UV spectra were compared. All compounds were measured in hexane at room temperature with a concentration of $1 \cdot 10^{-5}$ M.

The essentially planar **OPV (CP 31)** structure with a double bond connecting the two phenyl rings shows the longest wavelength absorption with $\lambda_{\max} = 326$ nm due to extensively delocalized π -electrons. Hypsochromic shift to $\lambda_{\max} = 303$ nm is observed for the **OPE** structure with a triple bond connecting the two phenyl rings. This conjugation is not particularly effective, as the distance of the triple bond is shortened, hence the π -electrons are quite tightly bound.¹¹¹ Hypsochromic shift is further increased if cyclopropane is connecting both phenyl rings. λ_{\max} of *trans*-**OPCP (CP 30)** is hypsochromically shifted to 254 nm.

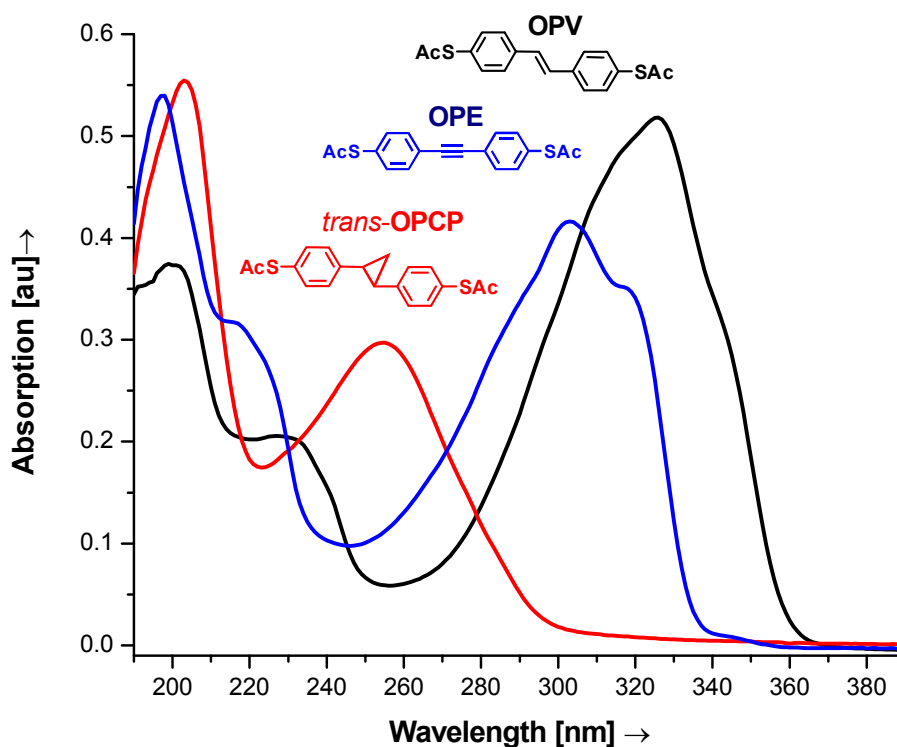


Figure 73. UV absorption of OPV, OPE and *trans*-OPCP in hexane at a concentration of $1 \cdot 10^{-5}$ M.

The two π -systems are nearly decoupled due to the low first-order conjugation. However, cyclopropane is well known to exert conjugative effects intermediate between the hyperconjugation of alkyl groups and first-order π -conjugation. This resonance effect has been attributed to two non-localized MO's (*Walsh* orbitals) of the cyclopropane ring. These orbitals lie in plane of the cyclopropane ring but have π -symmetry with respect to the non-ring bonds of cyclopropane and hence the correct symmetry for conjugation with the phenyl rings.³⁴⁷ The extent of conjugative effect of the cyclopropane ring to the adjacent benzene ring is dictated by the conformation.^{348,349}

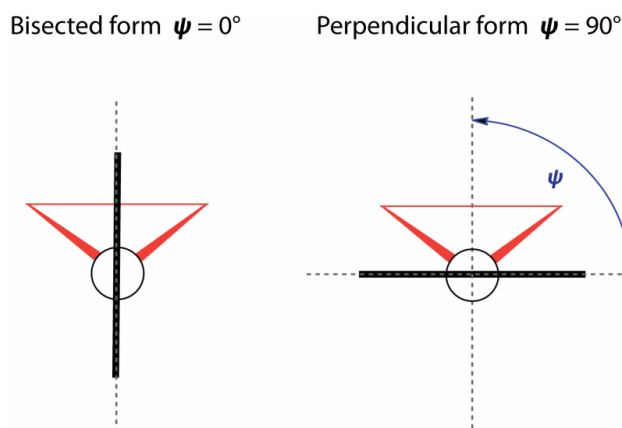


Figure 74. Molecular diagram of the bisected and perpendicular form of cyclopropyl-benzene. Cyclopropyl-benzene adopts the bisected conformation in the solid state.³⁴⁸

In the bisected conformation (figure 74), orbital alignment between the benzene π -system and the cyclopropyl HOMO is maximal and electron donation from the cyclopropyl to the arene is taking place. In the perpendicular conformation, the π -system of the arene is orthogonal to the cyclopropyl HOMO, but aligned with the LUMO of the cyclopropyl group. Consequently, the cyclopropyl group can only act as an electron acceptor. As cyclopropane is a weak π -acceptor no significant electronic interaction between the benzene and the cyclopropyl group is observed in the perpendicular conformation.³⁴⁹

Solid state structural analysis gave insight into the structure of the *trans*-**OPCP**. The plane of the phenyl ring is twisted by about 30° away from the bisected line (figure 75, A). In contrast the plane of the second phenyl ring lies almost on the bisected line of the cyclopropane ring (figure 75, B). Thus, the aromatic π -systems on both sides of the cyclopropane ring are in a good geometry for an electronic interaction.

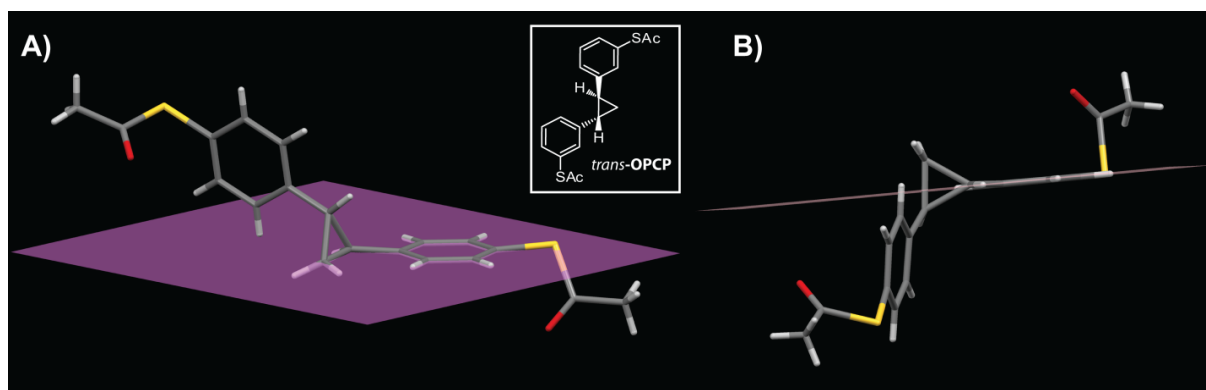


Figure 75. Visualization of the bisected configurations observed in the solid state structure of *trans*-OPCP.

To conclude, comparison of the UV spectra indicates that the π -systems of the two phenyl rings in *trans*-OPCP are rather decoupled by the cyclopropane unit compared to OPV and OPE.

These results can be summarized with the following statement:

“The cyclopropane ring can be regarded as an ideal non-conjugative spacer unit building future molecular device structures. There are no other rigid chemical units of this length available that conjugate so inefficiently”

4.4.2 Planar Acetylsulfanyl-Terminated Compounds

UV spectra of the planar diacetylsulfanyl-biphenyls have been recorded as $1 \cdot 10^{-5}$ M solutions in hexane at 25°C (figure 76). Almost identical absorption spectra are observed for the dialkylated fluorene compound **CP 18** and the parent compound **S1a**. The small bathochromic shift of the absorption bands can be attributed to the weak σ -donor-effect of the alkyl groups attached to the benzylic position of fluorene.¹⁹⁵

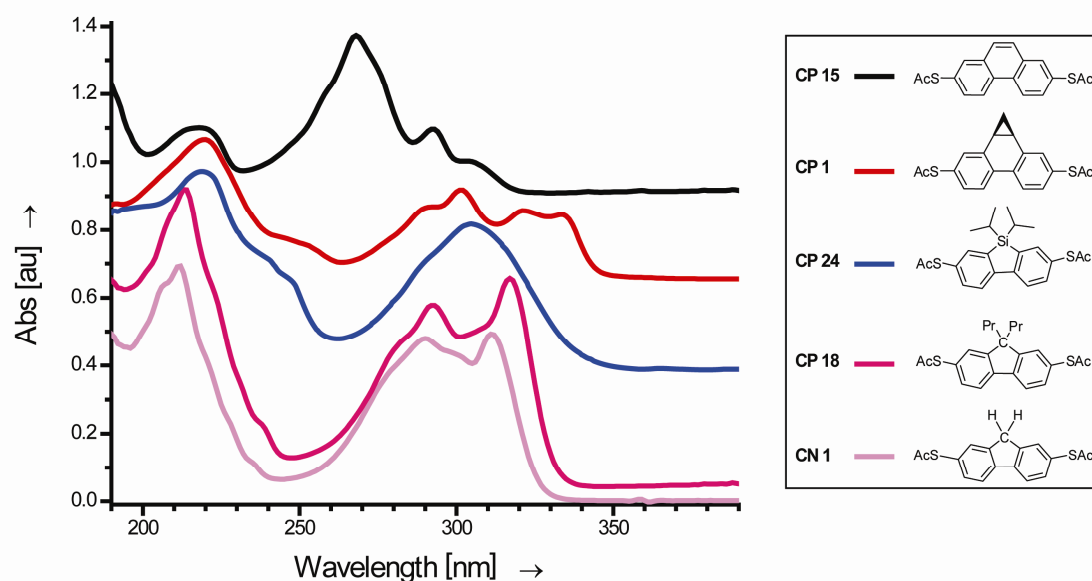


Figure 76. UV adsorption spectra of the planar diacetylsulfanyl-biphenyls in hexane at 25°C with a concentration of $1 \cdot 10^{-5}$ M. The absorption spectra are displayed in a stacked mode for clarity.

The onset of the spectra of **CP 18** is shifted to the red by 7 nm to 340 nm compared to **S1a**. The spectra of silafluorene **CP 24** exhibits two intense and broad absorption bands with λ_{max} at 221 nm and 303 nm. The substitution of the bridging methylene unit with a silicon-atom shifts the onset of the spectra to longer wavelength (355 nm) which can be rationalized by the stabilized LUMO.³¹⁷⁻³¹⁹

The onset of the dibenzonorcaradiene **CP 1** is bathochromically shifted to 353 nm and thus exhibits an increased optical band gap compared to fluorene **S1a**. The spectra exhibits three pronounced absorption bands. The longest wavelength absorption band exhibits two λ_{max} at 334 nm and 322 nm with

about equal intensity. Another intense and structured band is observed with λ_{max} at 302 nm. The third and most intense absorption band exhibits λ_{max} at 220 nm.

The last member of the sulfur-functionalized series is the fully aromatic phenanthrene derivate **CP 15**. According to parent compound phenanthrene¹⁹⁵ the three observed bands can be assigned as follows. The broad maximum at 219 nm can be assigned to the β -band, the most intense maximum at 268 nm and a weaker absorption at 293 nm can be assigned to the p -band (figure 76). In addition a vibrational fine-structured band with five maxima is observed between 326-359 nm which can be assigned to the α -band (not displayed).^{111,195} The bathochromic shift of the observed bands compared to phenanthrene can probably be attributed to the presence of the sulfur lone pair electrons. The onset of the UV spectra is at 323 nm (excluding the very weak α -bands). Interestingly, extending the biphenyl π -system by one double bond seems not to decrease the optical band gap. In contrast the onset of the **CP 1** is bathochromically shifted to longer wavelength. This demonstrates that the cyclopropane ring in 2,2'-position effects the π -biphenyl system essentially different. The bathochromic shift of **CP 1** can be rationalized by a hyperconjugative σ - π donating effect of the cyclopropyl-bridge similar as observed for dialkyl-fluorene **CP 18**.

4.4.3 Planar Cyano-Terminated Compounds

UV spectra of the planar biphenyl molecules with similar length have been recorded as $1 \cdot 10^{-5}$ M solutions in acetonitrile at 25°C (figure 77). Dipropylated fluorene compound **CP 19** shown similar absorption characteristics as **CN 1**. The maximum of the longest wavelength absorption is bathochromically shifted to 318 nm (α -band).¹⁹⁵ Similarly the maximum of the fine structured ρ -band is shifted to 293 nm due to the attached alkyl chains.¹⁹⁵

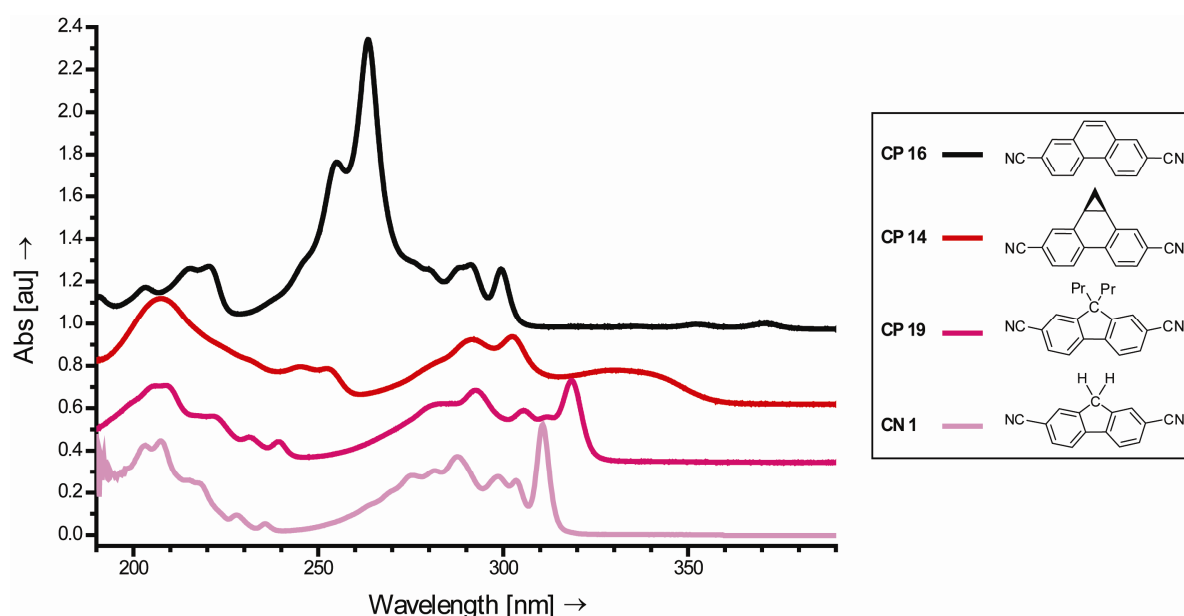
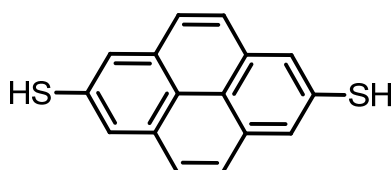


Figure 77. UV adsorption spectra of the planar dicyano-biphenyls in hexane at 25°C with a concentration of $1 \cdot 10^{-5}$ M. The absorption spectra are displayed in a stacked mode for clarity.

The onset of **CP14** is red shifted by 42 nm to 364 nm compared to fluorene **CN 1**. The last member of the series is the phenanthrene **CP 16**. Similar as observed for the sulfur-functionalized phenanthrene **CP 15** three absorption bands are observed for **CP 16** (figure 77). A fine-structured very weak absorption band with four sharp maxima were observed between 310-380 nm that can be probably assigned to α -band (not displayed).^{111,195} The most intense maxima at 261 nm is accompanied by a less intense fine-structured band between 284-309 nm.

4.5 Conclusion and Outlook

In conclusion a series of nine planar rod-like model structures with similar length have been synthesized and their structures have been determined by X-ray analysis. The model structures comprise both thiol and cyano anchoring groups to enable immobilization between metal electrodes. The second bridge in 2,2'-position is varying in terms of its chemical nature. Optical UV measurements show clearly that the π -system is sensitive to the type of bridge. The onset of UV spectra of the dibenzonorcaradiene structures **CP 1** and **CP 14** are bathochromically shifted to longer wavelength compared to the fluorene derivatives. Interestingly, the UV spectra of the dibenzonorcaradiene structures **CP 1** and **CP 14** comprising a cyclopropyl bridge exhibit considerably different absorption spectra than the phenanthrene compounds **CP 15** and **CP 16**. Introduction of a silicon bridge in **CP 24** shifts the onset of the UV spectra to longer wavelengths compared to fluorene.



Pyrene-2,7-dithiol

Furthermore, pyrene displays an interesting future model structure as its symmetry is increased compared to phenanthrene. One might expect that this structure conducts better as enlarged π -systems are expected to have smaller band gaps. *Cohen*³⁵⁰ and *Liu*³⁵¹ recently found reduced conductance based on theoretical calculations for 2,7-dithiol-pyrene compared to the unbridged planar biphenyl-dithiol. This indicates that not only the extent of π -conjugation (and the consequently lowered band gap) but also the spatial arrangement of the π -system influences the electron transport properties of a molecular wire. Charge transport investigations are currently ongoing.

5 Experimental Section

5.1 Materials and Methods

Solvents and Reagents

Reagents were used as received from *Fluka AG* (Buchs, Switzerland), *Acros AG* (Basel, Switzerland), *Merck* (Darmstadt, Germany) and *Aldrich* (Buchs, Switzerland) unless otherwise stated. Solvents for chromatography and extractions were of technical grade. Dry solvents used for reactions corresponded to the quality *puriss p. a., abs., over Molecular Sieves* from *Fluka AG*. For an inert atmosphere *Argon 4.8* from *PanGas AG* (Dagmersellen, Switzerland) was used.

UV/vis spectroscopy

UV/vis spectra were recorded on an *Agilent 8453* diode array detector spectrophotometer.

NMR spectroscopy

Nuclear magnetic resonance (NMR) spectra were recorded using a *Bruker DPX-NMR* (400 MHz for ^1H and 100 MHz for ^{13}C) or a *Bruker BZH-NMR* (250 MHz for ^1H) spectrometer at ambient temperature in the solvents indicated. Solvents for NMR were obtained from *Cambridge Isotope Laboratories* (Andover, MA, USA). Chemical shifts are given in ppm relative to tetramethylsilane (TMS). The spectra are referenced to the residual proton signal of the deuterated solvent (CDCl_3 : 7.26 ppm, DMSO-d_6 : 2.50 ppm, CD_3CN : 1.94 ppm) for ^1H spectra or the carbon signal of the solvent (CDCl_3 : 77.2 ppm, DMSO-d_6 : 40.5 ppm, CD_3CN : 118.3 ppm and 1.3 ppm) for ^{13}C spectra. The coupling constants (J) are given in Hertz (Hz), the multiplicities are denoted as: s (singlet), d (duplet), t (triplet), q (quartet), m (multiplet) and br (broad).

Mass spectrometry (MS)

Electron impact (EI) mass spectra and fast atom bombardment (FAB) mass spectra were recorded by *Dr. H. Nadig* on a *finnigan* MAT 95Q for EI-MS and on a *finnigan* MAT 8400 for FAB-MS in the mass spectrometry laboratory of the institute. As matrix for FAB-MS *m*-nitro-benzyl alcohol or glycine was used. Electron spray ionization (ESI) mass spectra were recorded on a *Bruker Esquire* 3000plus. Matrix-assisted laser desorption/ionization-time of flight (MALDI-TOF) mass spectra were performed on a *Applied Bio Systems Voyager-De™ Pro* mass spectrometer using 1,8,9-anthracenetriol or α -cyano-4-hydroxycinnamic acid as matrix. Important signals are given in mass units per charge (*m/z*), the fragments and intensities are given in brackets.

Elemental analysis (EA)

Elemental analyses were carried out by *W. Kirsch* on a *Perkin-Elmer Analysator 240*. The values are given in mass percent.

Melting points (MP)

Melting points (MP) were determined in °C using a *Stuart SMP3* apparatus and are uncorrected.

Column Chromatography

For preparative separations by column chromatography, silica gel 60 from *Fluka* (0.043-0.06 mm) was used.

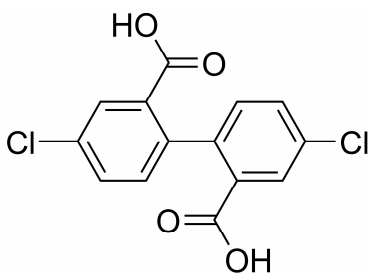
Thin layer chromatography (TLC)

Thin layer chromatography was performed on 0.25 mm pre-coated glass plates (silica gel 60 F₂₅₄, *Merck AG*, Darmstadt, Germany). Compounds were detected at 254 nm by fluorescence quenching or at 366 nm by self-fluorescence. If necessary, the plates were stained by dipping into a cerium(IV) reagent^[132] (molybdophosphoric acid and cerium(IV)sulfate dissolved in a mixture containing water and concentrated sulfuric acid) or Gibbs reagent^[132] (100 mg 2,6-dibromoquinone-4-chloroimide with sodium hydrogen carbonate in DMSO/chloroform).

5.2 Synthetic Procedures

5.2.1 Chapter 2: Sulfur-Functionalized Cyclophanes

4,4'-Dichlorobiphenyl-2,2'-dicarboxylic acid (**S10b**)



2-Amino-5-chlorobenzoic acid (23.90 g, 0.140 mol) was suspended in HCl (49.6 mL, 0.600 mol, 37%) and water (110 mL). At 0 °C the amine was diazotized by adding slowly a solution of NaNO₂ (11.50 g, 0.169 mol, 1.2 equiv) in water (40 mL). After stirring 1 h at 0 °C the solution was carefully induced via canula into a freshly prepared solution of CuSO₄ pentahydrate (69.30 g, 0.278 mol, 2.0 equiv), NH₄OH (148 mL, 0.96 mmol, 6.9 equiv 25 %), water (250 mL) and hydroxylamine·HCl (20.70 g, 0.30 mmol, 2.1 equiv) dissolved in a NaOH solution (49.5 mL, 0.300 mol, 2.1 equiv). Then stirring was continued from 25 °C to 70 °C for 1 h. The mixture was cooled to room temperature and acidified with HCl (37%). After filtering, washing with water and drying in the oven (70°C) 4,4'-dichlorobiphenyl-2,2'-dicarboxylic acid **S10b** was obtained as a beige powder (15.10 g, 48.53 mmol, 69%).

MF C₁₄H₈Cl₂O₄, **MW** 311.12 g/mol

M.p. 246-250 °C

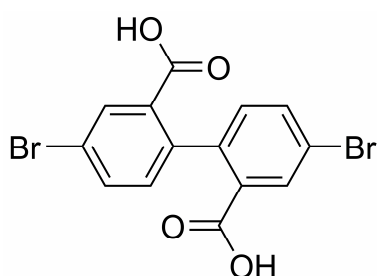
TLC *R_f* 0.06 (ethyl acetate)

¹H NMR (400 MHz, DMSO-d₆, δ/ppm) 7.18 (d, 2H, ³J = 7.6), 7.59 (d, 2H, ³J = 7.6), 7.85 (s, 2H), 13.0 (br s, 2H)

¹³C NMR (100 MHz, CD₃OD, δ/ppm) 130.0, 131.4, 132.0, 133.2, 141.7, 167.4

EI-MS *m/z* (%) = 310.0 (30) [M⁺], 292.0 (21) [M⁺-H₂O], 292.0 (21), 265.0 (100) [M⁺-CO₂], 248 (68), 186.0 (42), 150.1 (31)

4,4'-Dibromobiphenyl-2,2'-dicarboxylic acid (**S11c**)



By applying the same conditions as described for 4,4'-dichlorobiphenyl-2,2'-dicarboxylic acid **S10b**, the dibromo-derivate **S11c** was obtained as a deep red powder (70%).

MF C₁₄H₈Br₂O₄, **MW** 400.02 g/mol

M.p. 246-250 °C

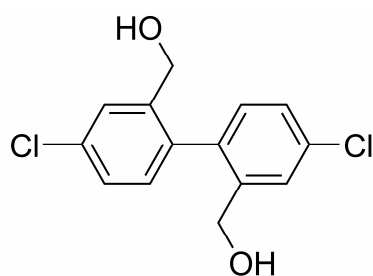
TLC *R_f* = 0.06 (ethyl acetate)

¹H NMR (400 MHz, DMSO-d₆, δ/ppm) 7.05-7.20 (m, 2H), 7.67-7.50 (m, 2H), 7.94 (br s, 2H), 13.1 (br s, 2H)

¹³C NMR (100 MHz, CD₃OD, δ/ppm) 121.4, 133.5, 134.7

EI-MS *m/z* (%) = 397.9, 399.9, 401.9 [M⁺]

(4,4'-Dichlorobiphenyl-2,2'-diyl)-dimethanol (**S12b**)



Under inert atmosphere 4,4'-dichlorobiphenyl-2,2'-dicarboxylic acid **S10b** (17.10 g, 54.96 mmol) was dissolved in dry THF (200 mL). NaBH₄ (6.24 g, 0.165 mol, 3.0 equiv) was added in portions keeping the temperature below 30 °C. After stirring at room temperature for 1 h, BF₃·Et₂O (31.1 mL, 0.253 mol, 4.6

equiv) was dropped to the reaction mixture keeping the temperature between 10 °C to 25 °C. The mixture was stirred overnight and quenched with HCl (5%), diluted with ethyl acetate (450 mL) and filtered through celite pad. The brown solution was washed with sat. Na₂CO₃, brine and dried over MgSO₄. After evaporation of the solvents (4,4'-dichlorobiphenyl-2,2'-diyl)-dimethanol **S12b** was obtained as a brown oily solid (16.40 g), which was used immediately without further purification for the next step. For analytical purposes a sample was purified by flash chromatography (silica gel, hexane/ethyl acetate, 7:3).

MF C₁₄H₁₂Cl₂O₂, **MW** 283.15 g/mol

M.p. 121 °C

TLC *R_f* 0.15 (hexane/ethyl acetate, 7:3)

¹H NMR (250 MHz, DMSO-d₆, δ/ppm) 4.08 (dd, 2H, ²J = 14.1, ³J = 5.4),

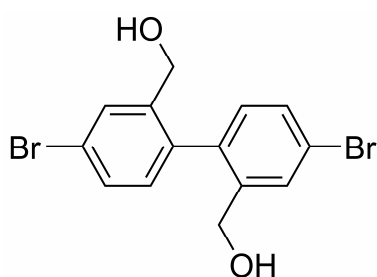
4.19 (dd, 2H, ²J = 14.1, ³J = 5.4), 5.26 (dd, 2H, ³J₁ = 5.4, ³J₂ = 5.4),

7.11 (d, 2H, ³J₁ = 8.1), 7.36 (dd, 2H, ³J = 8.1, ⁴J = 2.3), 7.58 (d, 2H, ⁴J = 2.3)

¹³C NMR (100 MHz, DMSO-d₆, δ/ppm) 61.04, 127.20, 127.46, 131.71, 133.41, 136.35, 143.28

EA Analysis calcd for C₁₄H₁₂Cl₂O₂: C 59.39, H 4.27; found: C 59.40, H 4.23

(4,4'-Dibromobiphenyl-2,2'-diyl)-dimethanol (**S13c**)



Target compound **S13c** was synthesized by applying the same conditions as for the (4,4'-dichlorobiphenyl-2,2'-diyl)-dimethanol **S12b** (67%).

MF C₁₄H₁₂Br₂O₂, **MW** 372.05 g/mol

M.p. 133-134 °C

TLC *R_f* 0.40 (hexane/ethyl acetate, 1:1)

¹H NMR (400 MHz, DMSO-d₆, δ/ppm) 4.05 (dd, 4H, ²J = 14.1, ³J = 5.5),

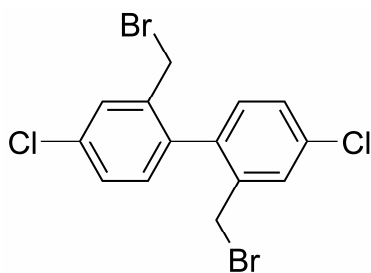
4.15 (dd, 2H, ²J = 14.1, ³J = 5.4), 5.23 (dd, 2H, ³J₁ = 5.5, ³J₂ = 5.5),

7.01 (d, 2H, ³J₁ = 8.1), 7.47 (dd, 2H, ³J = 8.0, ⁴J = 1.9), 7.69 (d, 2H, ⁴J = 1.9)

¹³C NMR (100 MHz, DMSO-d₆, δ/ppm) 61.0, 122.0, 130.1, 130.4, 131.9, 136.8, 143.4

FAB-MS *m/z* (%) = 372.9 [M+H]⁺

EA Analysis calcd for C₁₄H₁₂Br₂O₂: C 45.20, H 3.25; found: C 44.63, H 3.43

2,2'-Bis(bromomethyl)-4,4'-dichlorobiphenyl (S14b)

(4,4'-Dichloro-biphenyl-2,2'-diyl)-dimethanol **S12b**

(16.40 g, assuming 54.96 mmol) was dissolved in dry CH_2Cl_2 (100 mL). The brown solution was cooled to 5 °C and PBr_3 (12.9 mL, 0.136 mol, 2.5 equiv) was slowly dropped to the reaction mixture. After stirring at 0-25 °C (30 h), water (40 mL) was carefully added to quench the

reaction. The water phase was separated and extracted with CH_2Cl_2 (40 mL), the combined organic phases were filtered through a silica pad. After evaporation of the solvents and purification by flash chromatography (silica, CH_2Cl_2 in hexane, 10-80%), 2,2'-bis(bromomethyl)-4,4'-dichlorobiphenyl **S14b** was obtained as yellow crystals (10.70 g, 26.17 mmol, 48% over two steps).

MF $\text{C}_{14}\text{H}_{10}\text{Br}_2\text{Cl}_2$, **MW** 408.94 g/mol

M.p. 120-121 °C

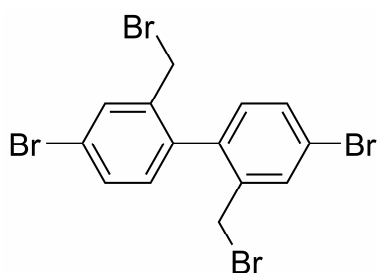
TLC R_f 0.44 (hexane/ CH_2Cl_2 , 95:5)

$^1\text{H NMR}$ (400 MHz, CDCl_3 , δ /ppm) 4.10 (d, 2H, $^2J = 10.3$), 4.25 (d, 2H, $^2J = 10.3$), 7.19 (d, 2H, $^3J = 8.2$), 7.36 (dd, 2H, $^3J = 8.2$, $^4J = 2.2$), 7.54 (d, 2H, $^4J = 2.2$)

$^{13}\text{C NMR}$ (100 MHz, CDCl_3 , δ /ppm) 30.6, 128.8, 130.8, 131.5, 134.7, 136.6, 137.9

EI-MS m/z (%) = 405.9, 407.9, 409.9, 411.9 [M^+]

EA Analysis calcd for $\text{C}_{14}\text{H}_{10}\text{Br}_2\text{Cl}_2$: C 41.12, H 2.46; found: C 40.98, H 2.48

2,2'-Bis(bromomethyl)-4,4'-dibromobiphenyl (S15c)

By applying the same procedure as for the dichloro-compound **S14b** described above, 4,4'-dibromo-biphenyl-2,2'-diyl)-dimethanol **S13c** was converted into 2,2'-bis(bromomethyl)-4,4'-dibromobiphenyl **S15c** (63%).

MF C₁₄H₁₀Br₄, **MW** 497.85 g/mol

M.p. 147 °C

TLC *R_f* 0.27 (hexane/*t*-BME, 1:1)

¹H NMR (400 MHz, CDCl₃, δ/ppm) 4.09 (d, 2H, ²J = 10.3), 4.26 (d, 2H, ²J = 10.3), 7.12 (d, 2H, ³J = 8.2), 7.50 (dd, 2H, ³J = 8.2, ⁴J = 2.0), 7.69 (d, ⁴J = 2.0, 2H)

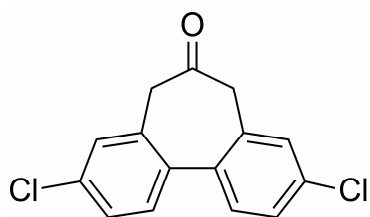
¹³C NMR (100 MHz, CDCl₃, δ/ppm) 30.7, 123.1, 131.98, 132.00, 134.0, 137.5, 138.4

EI-MS *m/z* (%) = 493.7, 495.7, 497.7, 499.7, [M⁺]

EA Analysis calcd for C₁₄H₁₀Br₄: C 33.78, H 2.02; found: C 33.67, H 2.01

3,9-Dichloro-5,7-dihydrodibenzo[a,c]cyclohepten-6-one (S16b)

NaOH (430 mg, 10.80 mmol, 5.1 equiv) was dissolved in H₂O (5 mL) and added to a solution of 2,2'-bis(bromomethyl)-4,4'-dichlorobiphenyl **S14b** (866 mg, 2.12 mmol), toluenesulfonyl-methyl isocyanide (462 mg, 2.37 mmol, 1.1 equiv) and tetrabutylammonium bromide (161 mg, 0.50 mmol, 24.0 mol%) in CH₂Cl₂ (20 mL) at 0 °C. The two phase mixture was stirred vigorously at room temperature overnight. The phases were separated and the water phase was extracted with CH₂Cl₂ (6 mL). *t*-BME (15 mL) and HCl (6 mL, 37 %) was added to the organic mixture which was then stirred vigorously for 3 h. The phases were separated and the organic layer was washed with water (5 mL), sat NaHCO₃ (8 mL), dried over Na₂SO₄ and the solvent was evaporated. The crude product was purified by flash chromatography (silica gel, 20-80%, CH₂Cl₂ in hexane) to afford 3,9-dichloro-5,7-dihydrodibenzo[a,c]cyclohepten-6-one **S16b** as a white solid (454 mg, 1.64 mmol, 77%).



MF C₁₅H₁₀Cl₂O, **MW** 277.15 g/mol

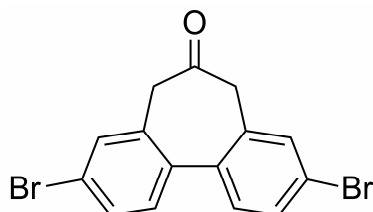
M.p. 223-224 °C.

TLC *R_f* = 0.24 (hexane/CH₂Cl₂, 6:4)

¹H NMR (400 MHz, CDCl₃, δ/ppm) 3.53 (d, 2H, ²J = 13.0), 3.56 (d, 2H, ²J = 13.0), 7.27-7.30 (m, 2H), 7.38-7.43 (m, 2H), 7.44-7.49 (m, 2H)

¹³C NMR (100 MHz, CDCl₃, δ/ppm) 49.2, 128.4, 129.8, 130.9, 134.6, 134.8, 137.1, 208.5. **EI-MS** *m/z* (%) = 276.0 (89) [M⁺], 248.0 (33) [M⁺ - CO], 213.1 (84) [M⁺ - CO, - Cl], 178.1 (100) [M⁺ - CO, - 2 Cl], 151.1 (9), 106.0 (18), 88.0 (36).

EA Analysis calcd for C₁₅H₁₀Cl₂O: C 65.01, H 3.64; found: C 64.71, H 3.74.

3,9-Dibromo-5,7-dihydrodibenzo[a,c]cyclohepten-6-one (S17c)

According to the synthesis of 3,9-dichloro-5,7-dihydrodibenzo[a,c]cyclohepten-6-one **S16b**, the dibromo-derivate **S17b** was isolated as a white solid (44%).

MF C₁₅H₁₀Br₂O, **MW** 366.05 g/mol

M.p. 242-244 °C

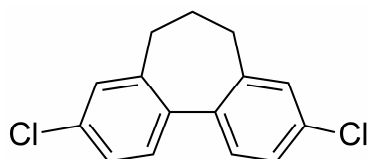
TLC R_f 0.13 (hexane/CH₂Cl₂, 1:1)

¹H NMR (400 MHz, CDCl₃, δ/ppm) 3.48 (d, 2H, ²J = 14.0), 3.54 (d, 2H, ²J = 14.0), 7.38-7.43 (m, 4H), 7.54-7.58 (m, 2H)

¹³C NMR (100 MHz, CDCl₃, δ/ppm) 49.1, 122.8, 131.0, 131.4, 132.8, 135.0, 137.6, 208.5.

EI-MS *m/z* (%) = 363.9, 365.9, 367.9 [M⁺]

EA Analysis calcd for C₁₅H₁₀Br₂O₁: C 49.22, H 2.75; found: C 49.21, H 2.70

3,9-Dichloro-6,7-dihydro-5H-dibenzo[a,c]cycloheptene (S3b)

To a solution of 3,9-dichloro-5,7-dihydrodibenzo[a,c]cyclohepten-6-one **S16b** (1.44 g, 5.20 mmol) in CH₂Cl₂ (40 mL) was added tris(pentafluorophenyl)borane (55.0 mg, 0.11 mmol, 2.0 mol%). While maintaining the reaction temperature at room temperature, polymethylhydrosiloxane (6.0 mL) was slowly added. After 20 min another portion of catalyst (80.0 mg, 0.16 mmol, 3.0 mol%) was added (foaming!). After the TLC showed full conversion of the starting material, the solvent was evaporated. The resulted gel was extracted with hexane (4 x 80 mL) and filtered through a silica pad. The concentrated extract was recrystallized from MeOH/H₂O (15 mL and 0.3 mL) to obtain 3,9-dichloro-6,7-dihydro-5H-dibenzo[a,c]cycloheptene **S3b** as white long needles (835 mg, 3.17 mmol, 61%).

MF C₁₅H₁₂Cl₂, **MW** 263.16 g/mol

M.p. 87-88 °C

TLC *R_f* 0.74 (hexane/CH₂Cl₂, 6:4)

¹H NMR (400 MHz, CDCl₃, δ/ppm) 2.21 (m, 2H), 2.49 (m, 4H), 7.24-7.37 (m, 6H)

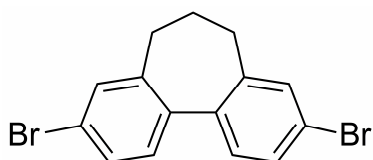
¹³C NMR (100 MHz, CDCl₃, δ/ppm) 31.6, 33.3, 127.2, 129.0, 129.8, 133.7, 138.8, 141.6

EI-MS *m/z* (%) = 262.0 (100) [M⁺], 227.1 (25) [M⁺ - Cl], 212.1 (32),

192.1 (58) [M⁺ - 2 Cl], 176.1 (11), 94.5 (16).

EA Analysis calcd for C₁₅H₁₂Cl₂: C 68.46, H 4.60; found: C 68.39, H 4.67

3,9-Dibromo-6,7-dihydro-5*H*-dibenzo[*a,c*]cycloheptene (**S3c**)



Tris(pentafluorophenyl)borane (18.2 mg, 35.5 μmol, 5.3 mol%,) was added to a solution of (260 mg, 0.71 mmol) 3,9-dibromo-5,7-dihydrodibenzo[*a,c*]cyclohepten-6-one **S17c** in CH₂Cl₂ (13 mL).

While maintaining the temperature at 25 °C, polymethylhydrosiloxane (0.85 mL) was slowly added. After 5 min the solvent was evaporated. The resulting gel was extracted with hexane (7 x 30 mL). The combined organic layers were concentrated *in vacuo* and purified by column chromatography (silica, hexane/CH₂Cl₂, 6:4). The obtained oil was then recrystallized from methanol/water (100:1) to afford 3,9-dibromo-6,7-dihydro-5*H*-dibenzo[*a,c*]-cycloheptene **S3c** (195 mg, 4.60 mmol, 78%) as a colorless powder.

MF C₁₅H₁₂Br₂, **MW** 352.06 g/mol

M.p. 114–115 °C

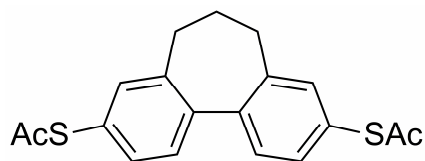
TLC *R_f* 0.61 (silica, hexane/CH₂Cl₂, 6:4)

¹H-NMR (400 MHz, CDCl₃, δ/ppm) 2.14-2.47 (m, 2H), 2.43-2.47 (m, 4H),

7.19 (d, 2H, ³J = 8.1), 7.39 (d, 2H, ⁴J = 2.0), 7.46 (dd, 2H, ³J = 8.1 Hz, ⁴J = 2.0 Hz)

¹³C-NMR (100 MHz, CDCl₃, δ/ppm) 31.0, 32.9, 121.5, 129.6, 129.7, 131.4, 138.9

141.5. **HRMS** (ESI) calcd for C₁₅H₁₃Br₂ [M+H]⁺: 350.9383; found: 350.9385

3,9-Bis(acetylsulfanyl)-6,7-dihydro-5H-dibenzo[a,c]cycloheptene (S3a)

Under inert atmosphere 3,9-dichloro-6,7-dihydro-5H-dibenzo-[a,c]cycloheptene **S3b** (383 mg, 1.46 mmol) was dissolved in dry and degassed DMI. Sodium methanethiolate (2.00 g, 28.53 mmol, 19.5 equiv) was added at once and the reaction mixture was stirred at 110 °C over night. After cooling to room temperature, AcCl (9 mL) was carefully added and stirring was continued over night at room temperature. The reaction was poured onto ice, the phases were separated and extracted with toluene (4 x 40 mL). The organic phase was washed with brine/water 1:1 (4 x 10 mL), brine (1 x 10 mL), filtered over wool and the solvent was evaporated. The crude product was separated on a flash column (silica gel, hexane/*t*-BME, 8:2) to afford the pure 3,9-bis(acetylsulfanyl)-6,7-dihydro-5H-dibenzo[a,c]-cycloheptene **S3a** (242 mg, 0.71 mmol, 49%). Crystallization using cyclohexane yielded beautiful single crystals for the X-Ray analysis.

MF C₁₉H₁₈O₂S₂, **MW** 342.48 g/mol

M.p. 134 °C

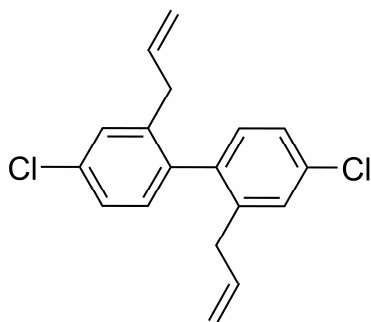
TLC *R_f* 0.27 (hexane/*t*-BME, 8:2)

¹H NMR (400 MHz, CDCl₃, δ/ppm) 2.20 (m, 2H), 2.45 (s, 6H), 2.50 (m, 4H), 7.29-7.31 (m, 2H), 7.38-7.44 (m, 4H)

¹³C NMR (100 MHz, CDCl₃, δ/ppm) 30.7, 31.6, 33.5, 127.5, 129.6, 133.1, 134.7, 141.0, 141.8, 194.7

EI-MS *m/z* (%) = 342.0 (28) [M⁺], 300.0 (26) [M⁺ - CH₃CO], 258.0 (100) [M⁺ - 2 CH₃CO], 192.1 (10), 165.1 (7)

EA Analysis calcd for C₁₉H₁₈O₂S₂: C 66.63, H 5.30; found: C 66.32, H 5.32

2,2'-Diallyl-4,4'-dichlorobiphenyl (S18b)

Under argon 2,2'-bis-(bromomethyl)-4,4'-dichlorobiphenyl **S14b** (673 mg, 1.65 mmol) was dissolved in CH₂Cl₂ (15 mL). CuI (313 mg, 1.64 mmol, 1.0 equiv) was added at once and the reaction mixture was cooled to -70 °C. In absence of light vinyl magnesium bromide (9.4 mL, 6.58 mmol, 4.0 equiv, 0.7 M) in dry THF was slowly dropped to the reaction mixture and stirring was continued at -70 °C for 1 h. After stirring overnight (0-25°C), the reaction was quenched with sat. NH₄Cl (50 mL) and brine (50 mL). The mixture was extracted with *t*-BME (3 x 50 mL), separated and the combined organic phases were dried over MgSO₄. The crude product was purified by flash chromatography to afford 2,2'-diallyl-4,4'-dichlorobiphenyl **S18b** as a smelly and colorless oil (290 mg, 0.96 mmol, 58%).

MF C₁₈H₁₆Cl₂, **MW** 303.23 g/mol

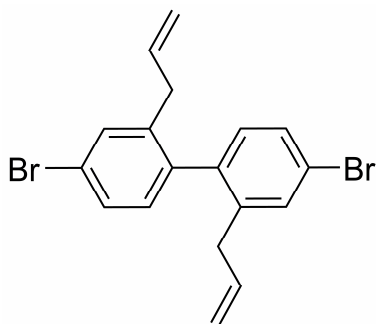
TLC *R_f* 0.76 (hexane/CH₂Cl₂, 95:5)

¹H NMR (400 MHz, CDCl₃, δ/ppm) 3.02 (dddd, 2H, ²J = 15.5, ³J = 6.6, ⁴J₁ = 1.5, ⁴J₂ = 1.5), 3.08 (dddd, 2H, ²J = 15.5, ³J = 6.7, ⁴J₁ = 1.5, ⁴J₂ = 1.5), 4.87 (dddd, 2H, ²J₁ = 1.7, ³J_Z = 17.0, ⁴J₁ = 1.5, ⁴J₂ = 1.5), 5.00 (dddd, 2H, ²J = 1.7, ³J_E = 10.0, ⁴J₁ = 1.5, ⁴J₂ = 1.5), 5.74 (dddd, 2H, ³J₁ = 17.0, ³J₂ = 10.0, ³J₃ = 6.7, ³J₃ = 6.6), 7.01 (d, 2H, ³J = 8.0), 7.19 (dd, 2H, ³J = 7.8, ⁴J = 2.2), 7.36 (d, 2H, ⁴J = 2.2)

¹³C NMR (100 MHz, CDCl₃, δ/ppm) 37.9, 117.2, 126.6, 129.7, 131.6, 134.0, 136.4, 138.4, 140.3

EI-MS *m/z* (%) = 302.1 (35) [M⁺], 267.1 (98) [M⁺ - Cl], 238.0 (62), 226.1 (100) [M⁺ - Cl, - C₃H₅ (allyl)], 203.1 (66), 191.1 (61), 101.0 (20)

EA Analysis calcd for C₁₈H₁₆Cl₂: C 71.30, H 5.32; found: C 71.07, H 5.30

2,2'-Diallyl-4,4'-dibromobiphenyl (S19c)

According to the synthesis of 2,2'-diallyl-4,4'-dichlorobiphenyl **S18b**, the bromo-derivate **S19c** (79%) was obtained as a colorless oil.

MF C₁₈H₁₆Br₂, **MW** 392.13 g/mol

TLC *R_f* 0.46 (hexane/CH₂Cl₂, 95:5)

¹H NMR (400 MHz, CDCl₃, δ/ppm) 3.13- 2.97 (m, 4H),

4.87 (dd, 2H, ²J = 1.6, ³J = 17.0), 5.01 (dd, 2H, ²J = 1.6, ³J = 10.1),

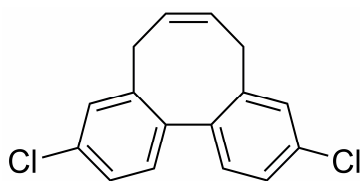
5.80-5.67 (m, 2H), 6.95 (d, 2H, ³J = 8.1), 7.37 (dd, 2H, ³J = 8.4, ⁴J = 2.1),

7.43 (2H, ⁴J = 2.4)

¹³C NMR (100 MHz, CDCl₃, δ/ppm) 37.3, 116.8, 121.8, 129.1, 131.3, 132.2, 135.9, 138.4, 140.1.

EI-MS *m/z* (%) = 390.0, 392.0, 394.0 [M⁺]

EA Analysis calcd for C₁₈H₁₆Br₂: C 55.13, H 4.11; found: C 55.24, H 4.19

3,10-Dichloro-5,8-dihydrodibenzo[a,c]cyclooctene (S20b)

2,2'-Diallyl-4,4'-dichlorobiphenyl **S18b** (121 mg, 0.40 mmol) and *Grubbs'* catalyst (2nd generation, 20.4 mg, 24 μ mol, 6.0 mol%) was refluxed in CH₂Cl₂ (30 mL). After 3 h the solvent was evaporated and the crude product was purified by flash chromatography (silica gel, 0-5% CH₂Cl₂ in hexane) to yield 3,10-dichloro-5,8-dihydrodibenzo[a,c]cyclooctene **S20b** as a off-white solid (97 mg, 0.35 mmol, 88%).

MF C₁₆H₁₂Cl₂, **MW** 275.17 g/mol

M.p. 129-130 °C

TLC *R_f* 0.51 (hexane/CH₂Cl₂, 98:2, δ /ppm)

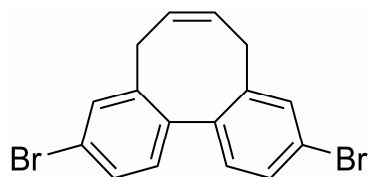
¹H NMR (400 MHz, CDCl₃, δ /ppm) 2.82-3.13 (m, 4H), 5.81-5.85 (m, 2H),

7.14-7.21 (m, 4H), 7.23-7.27 (m, 2H)

¹³C NMR (100 MHz, CDCl₃, δ /ppm) 33.4, 126.8, 129.1, 129.3, 129.4, 129.6, 134.5, 139.0, 139.7

EI-MS *m/z* (%) = 274.0 (80) [M⁺], 239.1 (82) [M⁺ - Cl], 204.1 (100) [M⁺ - 2 Cl], 176.1 (21), 101.0 (33)

EA Analysis calcd for C₁₆H₁₂Cl₂: C 69.84, H 4.40; found: C 69.35, H 4.50

3,10-Dibromo-5,8-dihydrodibenzo[a,c]cyclooctene (S21c)

According to the protocol described for 3,10-dichloro-5,8-dihydrodibenzo[a,c]cyclooctene **S20b**, the dibromo-derivate **S21c** was obtained as a white solid (94%).

MF C₁₆H₁₂Br₂, **MW** 364.07 g/mol

M.p. 147 °C

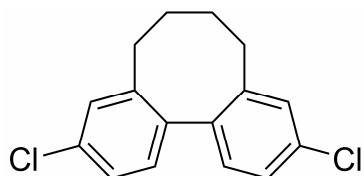
TLC *R_f* 0.61 (hexane/CH₂Cl₂, 95:5)

¹H NMR (400 MHz, CDCl₃, δ/ppm) 2.91 (d, 2H, ²J = 14.7), 3.02-3.13 (m, 2H), 5.79-5.87 (m, 2H), 7.11 (d, 2H, ³J = 8.1), 7.37 (d, 2H, ⁴J = 2.0), 7.42 (dd, 2H, ³J = 8.1, ⁴J = 2.0)

¹³C NMR (100 MHz, CDCl₃, δ/ppm) 32.9, 122.3, 128.7, 129.2, 129.3, 132.1, 138.8, 139.7

EI-MS *m/z* (%) = 361.9, 363.9, 365.9 [M⁺]

EA Analysis calcd for C₁₆H₁₂Br₂: C 52.78, H 3.32; found: C 52.66, H 3.35

3,10-Dichloro-5,6,7,8-tetrahydrodibenzo[a,c]cyclooctene (S4b)

3,10-Dichloro-5,8-dihydrodibenzo[a,c]cyclooctene **S20b** (102 mg, 0.37 mmol) was dissolved in ethyl acetate (6 mL) and Pd/C (10% Pd, 10.0 mg, 2.5 mol%) was added. The mixture was stirred under a hydrogen atmosphere (1 atm) for 3 h. Then filtered through a silica pad, washed with ethyl acetate and the solvent was evaporated. 3,10-Dichloro-5,6,7,8-tetrahydrodibenzo[a,c]cyclooctene **S4b** was collected as a white solid (98 mg, 0.36 mmol, 95%).

MF C₁₆H₁₄Cl₂, **MW** 277.19 g/mol

M.p. 163-164 °C

TLC *R_f* 0.51 (hexane/CH₂Cl₂, 98:2)

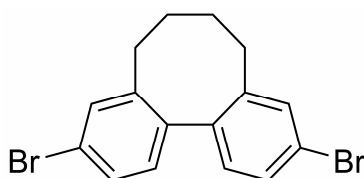
¹H NMR (400 MHz, CDCl₃, δ/ppm) 1.42-1.56 (m, 2H), 2.04-2.14 (m, 4H),
2.63-2.76 (m, 2H), 7.12-7.17 (m, 2H), 7.19-7.31 (m, 4H)

¹³C NMR (100 MHz, CDCl₃, δ/ppm) 29.6, 32.9, 126.3, 129.7, 129.9, 130.6, 134.1,
138.3, 144.9

EI-MS *m/z* (%) = 276.0 (100) [M⁺], 241 (24) [M⁺, - Cl], 212.0 (32),
178.1 (35),
88.0 (13)

EA Analysis calcd for C₁₆H₁₄Cl₂: C 69.33, H 5.09; found: C 69.88, H 5.40

3,10-Dibromo-5,6,7,8-tetrahydridibenzo[a,c]cyclooctene (**S4c**)



By applying the same reaction conditions as for the conversion of the dichloro-compound **S20b** to **S4b**, the dibromo-compound **S4c** was obtained from **S21c** as a white solid (98%).

MF C₁₆H₁₄Br₂, **MW** 366.09 g/mol

M.p. 168-170 °C

TLC *R_f* 0.75 (hexane/CH₂Cl₂, 95:5)

¹H NMR (400 MHz, CDCl₃, δ/ppm) 1.45-1.53 (m, 2H), 2.03-2.14 (m, 4H),
2.69 (dd, 2H, ²J = 13.4, ³J = 8.4), 7.07 (d, 2H, ³J = 8.1),
7.37 (dd, 2H, ³J = 8.1, ⁴J = 2.0), 7.43 (d, 2H, ⁴J = 2.0)

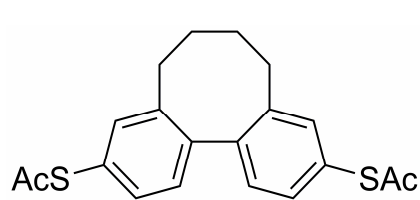
¹³C NMR (100 MHz, CDCl₃, δ/ppm) 29.3, 32.6, 122.1, 129.0, 130.6, 132.4,
138.5, 144.9

EI-MS *m/z* (%) = 363.9, 365.9, 367.9 [M⁺]

EA Analysis calcd for C₁₆H₁₄Br₂: C 52.49, H 3.85; found: C 52.45, H 3.81

3,10-Bis(acetylsulfanyl)-5,6,7,8-tetrahydrodibenzo[a,c]-cyclooctene (S4a)

Under inert atmosphere 3,10-dichloro-5,6,7,8-tetrahydrodibenzo[a,c]cyclooctene **S4b**



(175 mg, 0.63 mmol) was dissolved in dry and degassed DMI (10 mL) and sodium methanethiolate (620 mg, 8.85 mmol, 14.0 equiv) was added. The reaction was

kept at 110 °C overnight. To the cooled reaction mixture AcCl (7.0 mL) was carefully added and the milky mixture was stirred at room temperature overnight. The reaction was then quenched on ice and extracted with toluene (3 x 20 mL). The organic phase was washed with brine/water 1:1 (3 x 15 mL), brine (1 x 20 mL), filtered over wool and the solvent was evaporated. The crude product was separated on a flash column (silica gel, 10-20%, *t*-BME in hexane). 3,10-Bis(acetylsulfanyl)-5,6,7,8-tetrahydrodibenzo[a,c]cyclooctene **S4a** was obtained (72.0 mg, 0.20 mmol, 32%). Recrystallization from cyclohexane yielded beautiful single crystals for the X-Ray analysis.

MF C₂₀H₂₀O₂S₂, **MW** 356.50 g/mol

M.p. 144 °C

TLC *R_f* 0.23 (hexane/*t*-BME, 8:2)

¹H NMR (400 MHz, CDCl₃, δ/ppm) 1.51-1.59 (m, 2H), 2.07-2.19 (m, 4H), 2.48 (s, 6H), 2.74-2.78 (m, 2H), 7.29-7.36 (m, 6H)

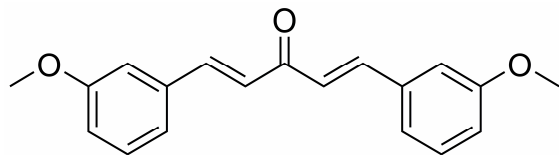
¹³C NMR (100 MHz, CDCl₃, δ/ppm) 29.6, 31.0, 33.2, 128.1, 130.5, 132.3, 135.9, 141.6, 144.4, 194.9

EI-MS *m/z* (%) = 356.2 (26) [M⁺], 314.1 (31) [M⁺ - CH₃CO], 272.1 (100) [M⁺ - 2 CH₃CO].

EA Analysis calcd for C₂₀H₂₀O₂S₂: C 67.38, H 5.65; found: C 67.39, H 5.91 found: C 67.39, H 5.91

1,5-Bis(3-methoxyphenyl)-1,4-pentadien-3-one (precursor of S22)

To a solution of NaOH (15.0 g, 0.375 mol, 5.1 equiv) in EtOH (125 mL) and water (125 mL) was dropped a solution of *m*-anisaldehyde (20.0 g, 0.147 mol,



2.0 equiv), acetone (5.4 mL, 0.073 mol, 1.0 equiv) in EtOH (30 mL) while maintaining the reaction temperature at 20 °C with a water bath. After stirring the

mixture at room temperature for 2 h, CH₂Cl₂ (100 mL) was added and the phases were separated. The organic layer was washed with brine/water (80 mL, 1:1) and dried over MgSO₄. After evaporation of the solvent, a thick oil (22.50 g) was obtained which was used without further purification for the next step. For analytical purposes a sample was recrystallized from EtOH/water.

MF C₁₉H₁₈O₃, **MW** 294.34 g/mol

M.p. 109 °C.

TLC *R_f* 0.55 (hexane/ethyl acetate, 2:1).

¹H NMR (400 MHz, CDCl₃, δ/ppm) 3.85 (s, 6H), 6.93-6.98 (m, 2H),

7.06 (d, 2H, ³J = 15.9), 7.12-7.14 (m, 2H), 7.19-7.23 (m, 2H), 7.33 (m, 2H),

7.70 (d, 2H, ³J = 15.9)

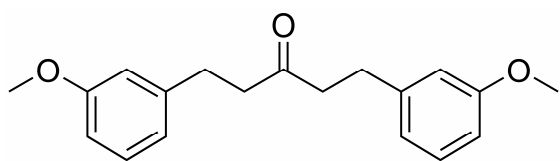
¹³C NMR (100 MHz, CDCl₃, δ/ppm) 55.8, 113.7, 116.8, 121.1, 126.1, 130.4, 136.6, 143.6, 160.4, 189.3.

EI-MS *m/z* (%) = 294.1 (100) [M⁺], 263.1 (32) [M⁺ - CH₃O], 161.1 (23), 121.1 (23).

EA Analysis calcd for C₁₉H₁₈O₃: C 77.53, H 6.16; found: C 77.39, H 6.27.

1,5-Bis(3-methoxyphenyl)-3-pentanone (S22)

The crude 1,5-Bis(3-methoxyphenyl)-1,4-pentadien-3-one (assuming 73.45 mmol)



was dissolved in ethyl acetate (200 mL) and Pd/C (0.50 g, 10% Pd) was added under an inert atmosphere. The suspension was saturated with hydrogen

gas and then vigorously stirred until the required volume of hydrogen (3.3 L, 147 mmol, 2.0 equiv) was consumed. The suspension was degassed and filtered through a short silica pad. After evaporation of the solvent a flash chromatography (silica gel, ethyl acetate in hexane, 30-60%) was performed to obtain 1,5-bis(3-methoxyphenyl)-3-pentanone **S22** (10.10 g, 33.85 mmol, 46% over two steps) as an oil.

MF C₁₉H₂₂O₃, **MW** 298.38 g/mol

TLC *R_f* 0.43 (CH₂Cl₂).

¹H NMR (400 MHz, CDCl₃, δ/ppm) 2.71 (t, 4H, ³J = 8.0), 2.85 (t, 4H, ³J = 8.0), 3.79 (s, 6H), 6.73 (m, 6H), 7.16-7.22 (m, 2H).

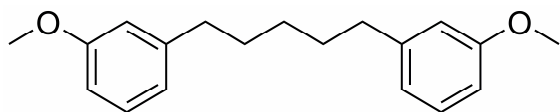
¹³C NMR (100 MHz, CDCl₃, δ/ppm) 30.2, 44.8, 55.6, 111.8, 114.5, 121.1, 129.9, 143.1, 160.1, 209.4.

EI-MS *m/z* (%) = 298.2 (34) [M⁺], 163.1 (22), 135.1 (100), 121.1 (40), 91.1 (14).

EA Analysis calcd for C₁₉H₂₂O₃: C 76.48, H 7.43; found: C 75.55, H 7.43.

1,5-Bis(3-methoxyphenyl)pentane (S23)

To a suspension of 1,5-bis(3-methoxyphenyl)-3-pentanone **S22** (3.83 g, 12.84 mmol)



and powdered KOH (2.88 g, 51.33 mmol, 4.0 equiv) in triethylenglycole (13 mL) was added hydrazine hydrate (2.3 mL,

39.00 mmol, 3.0 equiv, 85%) under cooling. The mixture was heated up to reflux for 2 h. The water and excess of hydrazine was distilled off at an oil bath temperature of 190 °C. After 4 h at this reaction temperature the reaction was stopped. Water was added to the cooled reaction mixture and the mixture was extracted with hexane/ethyl acetate, 4:1 (3 x 60 mL). The combined organic layers were washed with water (3 x 15 mL) and brine (50 mL) and dried over MgSO₄. After evaporation of the solvent and purification by flash chromatography (silica gel, hexane/ethyl acetate, 6:1) 1,5-bis(3-methoxy-phenyl)pentane **S23** (2.64 g, 9.30 mmol, 72%) was obtained as a colorless oil.

MF C₁₉H₂₄O₂, **MW** 284.39 g/mol

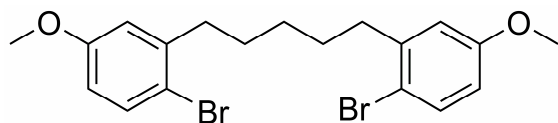
TLC *R_f* 0.53 (hexane/ethyl acetate, 5:1).

¹H NMR (400 MHz, CDCl₃, δ/ppm) 1.41 (m, 2H), 1.65 (m, 4H), 2.59 (t, 4H, ³J = 8.0), 3.82 (s, 6H), 6.72-6.78 (m, 6H), 7.18-7.22 (m, 2H).

¹³C NMR (100 MHz, CDCl₃, δ/ppm) 29.4, 31.7, 36.4, 55.5, 111.3, 114.6, 121.3, 129.6, 144.9, 159.9.

EI-MS *m/z* (%) = 284.2 (54) [M⁺], 163.1 (8), 135.1(23), 122.1 (100), 91.1 (15).

EA Analysis calcd for C₁₉H₂₄O₂: C 80.24, H 8.51; found: C 80.36, H 8.62.

1,5-Bis(2-bromo-5-methoxyphenyl)pentane (S24)

To a solution of 1,5-bis(3-methoxyphenyl)pentane **S23** (4.10 g, 14.42 mmol) and dry pyridine (4.0 mL, 49.65 mmol, 3.5 equiv) in CH₂Cl₂ (40 mL) was dropped a solution of bromine (5.30 g, 33.16 mmol, 2.3 equiv) in CH₂Cl₂ (20 mL) at -10 °C over 30 min. After stirring another 2 h at room temperature, the reaction mixture was washed with sat. NaHCO₃ and dried over MgSO₄. After evaporation of the solvent, a short flash chromatography (silica gel, CH₂Cl₂/hexane, 1:1) was performed to obtain 6.3 g of the crude product. The chromatographically inseparable impurities could be removed by a recrystallization from pentane (60 mL) at +4 °C. The pure 1,5-bis(2-bromo-5-methoxyphenyl)pentane **S24** (2.65 g, 5.99 mmol, 42%) was collected as fine white crystals.

MF C₁₉H₂₂Br₂O₂, **MW** 442.18 g/mol

M.p. 44-45 °C.

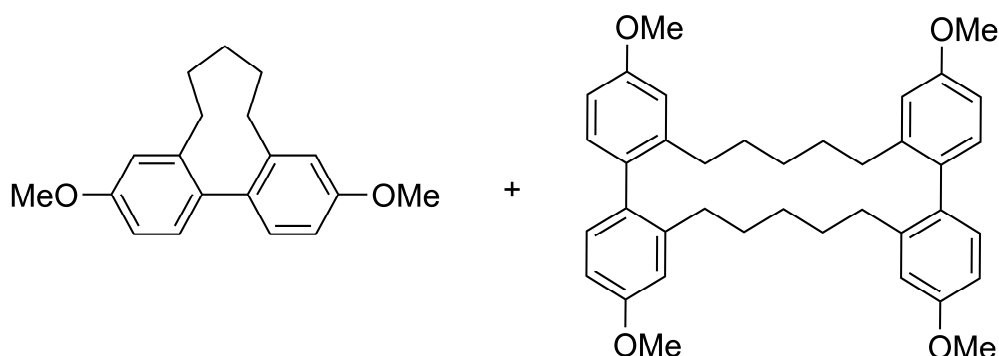
TLC *R_f* 0.53 (hexane/ethyl acetate, 5:1).

¹H NMR (400 MHz, CDCl₃, δ/ppm) 1.43-1.51 (m, 2H), 1.62-1.72 (m, 4H), 2.70 (t, 4H, ³J = 8.0), 3.78 (s, 6H), 6.62 (dd, 2H, ⁴J = 3.0, ³J = 8.7), 6.78 (d, 2H, ⁴J = 3.0), 7.41 (d, 2H, ³J = 8.7).

¹³C NMR (100 MHz, CDCl₃, δ/ppm) 29.5, 30.1, 36.7, 55.8, 113.4, 115.3, 116.4, 133.6, 143.4, 159.3.

EI-MS *m/z* (%) = 440.0, 442.0, 444.0 [M⁺].

EA Analysis calcd for C₁₉H₂₂Br₂O₂: C 51.61, H 5.01; found: C 51.63, H 5.03.

3,11-Dimethoxy-6,7,8,9-tetrahydro-5H-dibenzo[a,c]cyclononene (S26) and dimer (S25)

Under inert atmosphere 1,5-bis(2-bromo-5-methoxyphenyl)-pentane **S24** (2.00 g, 4.50 mmol) was dissolved in dry *Me*THF (170 mL). The solution was cooled to -50°C in a dry ice/acetone bath and *t*-BuLi (11.1 mL, 18.0 mmol, 4.0 equiv) was added drop wise. After the addition was completed the yellow solution was stirred at this temperature for another 15 min. A fresh solution of anhydrous LiBr (825 mg, 9.50 mmol, 2.1 equiv) and CuCN (425 mg, 4.75 mmol, 1.1 equiv) in *Me*THF (10 mL) was prepared. This almost clear green copper solution was transferred to the reaction mixture over 10 min while keeping the reaction temperature below -50°C . The cloudy reaction mixture was then stirred for another hour at -20°C and then cooled again to -40°C . 1,3-Dinitrobenzene (3.00 g, 18.0 mmol, 4.0 equiv) was added at once and the cooling was removed. After stirring at room temperature overnight, the black reaction mixture was quenched with a mixture of NH_4Cl (40 mL, 10%) and NH_4OH (40 mL, 25%). The layers were separated and the water phase was extracted with *t*-BME (2 x 80 mL). The combined organic layers were washed with brine and dried over MgSO_4 . After evaporation of the solvent a flash chromatography (silica, *t*-BME in hexane, 0-20%) was performed to obtain the monomer-fraction **S26** (568 mg) and a fraction containing the dimer **S25** according to the MS (343 mg, 0.61 mmol, 27%). A recrystallization of the monomer-fraction from hexane (10 mL) afforded the pure monomer **S26** (292 mg, 1.03 mmol, 23%) as colorless crystals.

S26 (monomer):

MF C₁₉H₂₂O₂, **MW** 282.38 g/mol

M.p. 112-113 °C

TLC *R_f* 0.53 (hexane/t-BME, 5:1)

¹H NMR (400 MHz, CDCl₃, δ/ppm) 1.37-1.43 (m, 2H), 1.48-1.56 (m, 2H),
1.71-1.77 (m, 2H), 2.06-2.13 (m, 2H), 2.57-2.64 (m, 2H), 3.80 (s, 6H),
6.76-6.78 (m, 4H), 7.03-7.06 (m, 2H)

¹³C NMR (100 MHz, CDCl₃, δ/ppm) 28.6, 29.5, 33.9, 55.6, 111.2, 114.5, 130.5, 134.7,
144.1, 159.3

EI-MS *m/z* (%) = 282.2 (100) [M⁺], 267.2 (6) [M⁺ - CH₃], 239.1 (10), 225.1 (9),
211.1 (7), 165.1 (6), 122.1 (6)

EA Analysis calcd for C₁₉H₂₂O₂: C 80.82, H 7.85; found: C 80.47, H 7.93

S25 (dimer): Colorless oil

MF C₃₈H₄₄O₄, **MW** 564.75 g/mol

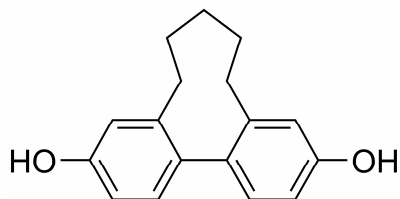
¹H NMR (400 MHz, CDCl₃, δ/ppm) 1.00-1.13 (m, 4H), 1.30-1.52 (m, 8H),
2.33 (t, 8H, ³J = 7.3), 3.84 (s, 12H), 6.70 (dd, 4H, ³J = 8.3, ⁴J = 2.6),
6.80 (d, 4H, ⁴J = 2.6), 6.92 (d, ³J = 8.3, 2H)

¹³C NMR (100 MHz, CDCl₃, δ/ppm) 29.3, 29.6, 33.6, 55.5, 110.7, 113.7, 131.7, 133.5,
141.9, 158.9

EI-MS *m/z* (%) = 564.3 (100) [M⁺], 282.2 (8), 239.1 (10), 121.1 (11)

3,11-Dihydroxy-6,7,8,9-tetrahydro-5H-dibenzo[a,c]cyclononene (S27)

To a solution of **S26** (288 mg, 1.02 mmol) in dry CH₂Cl₂ (20 mL) was slowly dropped a solution of BBr₃ (4.1 mL, 4.10 mmol, 4.0 equiv, 1.0 M) in CH₂Cl₂ at 0 °C. Then stirring was continued at room temperature until TLC showed full conversion of the starting material (1.5 h). The reaction was quenched with MeOH under ice cooling. The reaction mixture was then washed with water (10 mL), dried over MgSO₄ and the solvents was evaporated. The crude 3,11-dihydroxy-6,7,8,9-tetrahydro-5H-dibenzo[a,c]cyclononene **S27** as a white powder was obtained which was pure enough to use for the next step.



MF C₁₇H₁₈O₂, **MW** 254.32 g/mol

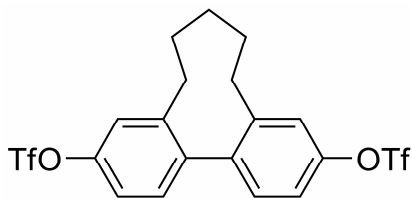
TLC R_f 0.40 (hexane/*t*-BME, 1:2)

¹H NMR (400 MHz, CDCl₃, δ/ppm) 1.31-1.37 (m, 2H), 1.41-1.52 (m, 2H), 1.65-1.76 (m, 2H), 2.00-2.09 (m, 2H), 2.47-2.56 (m, 2H), 6.64-6.70 (m, 4H), 6.93 (d, 2H, ³J = 8.0)

¹³C NMR (100 MHz, CDCl₃, δ/ppm) 28.1, 29.0, 33.2, 112.4, 115.3, 130.1, 133.8, 143.7, 155.4

EI-MS *m/z* (%) = 254.1 (100) [M⁺], 211.1 (25), 198.1 (15), 108.1 (16)

3,11-Bis(trifluoromethanesulfonyloxy)-6,7,8,9-tetrahydro-5H-dibenzo[a,c]cyclononene (S5e)



The crude 3,11-dihydroxy-6,7,8,9-tetrahydro-5H-dibenzo[a,c]cyclononene **S27** (assuming 1.02 mmol) from the previous step was dissolved in dry pyridine (8mL). Then triflic anhydride (677 μ L, 4.02 mmol, 4.0 equiv) was slowly dropped to the solution. Stirring was continued at rt (30 min) and the beige solution was quenched with a cold NaHCO₃ solution. The product was extracted with CH₂Cl₂ (3 x 30 mL) and the combined organic phases were dried over MgSO₄. After evaporation of the solvent a flash chromatography (silica, hexane/CH₂Cl₂, 7:3) was performed to afford 3,11-bis(trifluoromethanesulfonyloxy)-6,7,8,9-tetrahydro-5H-dibenzo[a,c]cyclononene **S5e** (620 mg) as a colorless oil which contained some inseparable material which did not disturb in the next step. Upon standing at room temperature a sample of the triflate solidified after a few weeks.

MF C₁₉H₁₆F₆O₆S₂, **MW** 518.45 g/mol

TLC *R_f* 0.73 (hexane/*t*-BME, 1:2)

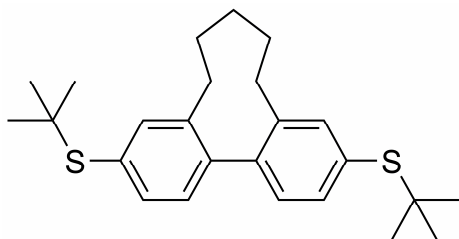
¹H NMR (400 MHz, CDCl₃, δ /ppm) 1.34-1.39 (m, 2H), 1.47-1.56 (m, 2H), 1.76-1.87 (m, 2H), 1.99-2.06 (m, 2H), 2.67-2.73 (m, 2H), 7.15-7.22 (m, 6H)

¹³C NMR (100 MHz, CDCl₃, δ /ppm) 28.3, 29.1, 33.7, 119.1, 119.2 (q, J = 321), 122.1, 130.9, 140.8, 145.2, 149.7

EI-MS *m/z* (%) = 518.0 [M⁺], 385.1 (17) [M⁺ - SOCF₃], 252.1 (34) [M⁺ - 2 SOCF₃], 235.1 (44), 107 (23)

EA Analysis calcd for C₁₉H₁₆F₆O₆S₂: C 44.02, H 3.11; found: C 44.15, H 3.04

3,11-Bis(*tert.*-butylsulfanyl)-6,7,8,9-tetrahydro-5*H*-dibenzo[*a,c*]-cyclononene (S28)



Under an inert atmosphere **S5e** (336 mg, assuming 0.55 mmol) was dissolved in degassed *p*-xylene (10 mL). Then Pd₂(dba)₃·CHCl₃ (78.0 mg, 75.4 μmol, 11.6 mol%), xantphos (52.0 mg, 89.9 μmol, 13.8 mol%) and sodium *t*-thiobutanolate (290 mg, 2.58 mmol, 4.0 equiv) were added. The reaction mixture was stirred at 140 °C for 6 h. Then toluene (20 mL) was added and the mixture was washed with brine (2 mL). The water phase was extracted with toluene (2 x 20 mL) and the combined organic phases were dried over MgSO₄. After evaporation of the solvent a flash chromatography (silica, *t*-BME in hexane, 1-5%) was performed to afford (134 mg, 0.34 mmol, 62% over 3 steps) of 3,11-bis(*tert.*-butylsulfanyl)-6,7,8,9-tetrahydro-5*H*-dibenzo[*a,c*]cyclononene **S28** as a bright yellow solid.

MF C₂₅H₃₄S₂, **MW** 398.67 g/mol

M.p. 108-110 °C

TLC *R_f* 0.58 (hexane/*t*-BME, 97:3)

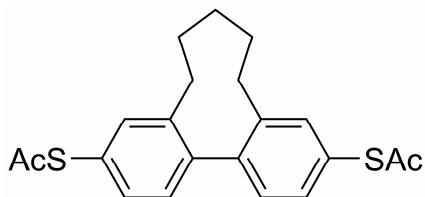
¹H NMR (400 MHz, CDCl₃, δ/ppm) 1.31-1.41 (m, 20H), 1.48-1.56 (m, 2H), 1.72-1.83 (m, 2H), 1.99-2.06 (m, 2H), 2.62-2.68 (m, 2H), 7.09 (d, 2H, ³J = 8.0), 7.37-7.43 (m, 4H)

¹³C NMR (100 MHz, CDCl₃, δ/ppm) 28.5, 29.5, 31.4, 33.5, 46.2, 129.1, 132.0, 134.9, 138.4, 142.3, 142.4

EI-MS *m/z* (%) = 398.2 (24) [M⁺], 342.1 (7) [M⁺ - C₄H₈], 286.1 (100) [M⁺ - 2 C₄H₈]

HRMS (ESI) calcd for C₂₅H₃₅S₂ [M+H]⁺: 399.2180; found: 399.2185

3,11-Bis(acetylsulfanyl)-6,7,8,9-tetrahydro-5H-dibenzo[a,c]cyclo-nonene (S5a)



To a solution of **S28** (124 mg, 0.31 mmol) in AcCl (13 mL) and dry toluene (30 mL) was slowly dropped BBr_3 (0.93 mL, 0.93 mmol, 3.0 equiv, 1.0 M in CH_2Cl_2) at 0 °C. Then stirring was continued at room temperature. After TLC showed full conversion (1 h) of the starting material, the reaction mixture was quenched with ice and the organic phase was separated. The water phase was extracted with toluene (2 x 30 mL). The combined organic layers were dried over MgSO_4 and evaporated in *vacuo*. The crude product was purified by flash chromatography (silica, *t*-BME/hexane 1:1) followed by a recrystallization from pentane (+4 °C) to afford 3,11-bis(acetylsulfanyl)-6,7,8,9-tetrahydro-5H-dibenzo[a,c]cyclo-nonene **S5a** (70.0 mg, 0.19 mmol, 61 %) as colorless crystals.

MF $\text{C}_{21}\text{H}_{22}\text{O}_2\text{S}_2$, **MW** 370.53 g/mol

M.p. 151 °C

TLC R_f 0.53 (hexane/*t*-BME, 5:1)

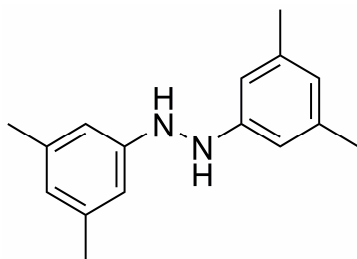
^1H NMR (400 MHz, CDCl_3 , δ /ppm) 1.38-1.42 (m, 2H), 1.44-1.55 (m, 2H), 1.63-1.82 (m, 2H), 2.04-2.11 (m, 2H), 2.45 (s, 6H), 2.63-2.70 (m, 2H), 7.18-7.20 (m, 2H), 7.28-7.30 (m, 4H)

^{13}C NMR (100 MHz, CDCl_3 , δ /ppm) 28.5, 29.3, 30.7, 33.5, 127.5, 129.9, 132.0, 135.3, 142.7, 143.3, 194.7

EI-MS m/z (%) = 370.1 (28) [M^+], 328.1 (39) [$\text{M}^+ - \text{CH}_3\text{CO}$], 286.1(100) [$\text{M}^+ - 2 \text{CH}_3\text{CO}$]. Analysis calcd for $\text{C}_{21}\text{H}_{22}\text{O}_2\text{S}_2$: C 68.07, H 5.98; found: C 68.03, H 6.04

1,2-Bis(3,5-dimethylphenyl)hydrazine (precursor of S29)

A suspension of 3,5-dimethyl-nitrobenzene (10.00 g, 66.20 mmol) and zinc powder (25.00 g, 0.382 mol, 5.8 equiv) in EtOH (40 mL) was heated up to reflux under an inert atmosphere. Then the heating was removed and a solution of NaOH (15.00 g, 0.375 mol, 5.7 equiv) in water (50 mL) was dropped to the reaction mixture at such a rate that the solution boiled vigorously. After addition of about a third of the base, heating needed to be continued to maintain steady refluxing. After all of the base was added, refluxing was continued for 4 h while more zinc powder (10.0 g, 0.153 mol, 2.3 equiv) was added in portions over this period of time. The hot suspension was filtered over celite and washed with hot EtOH (60 mL) into a mixture of AcOH (150 mL, 30%) and sodium bisulfite (1.0 g, 9.6 mmol, 0.15 equiv). The slurry was cooled down to 10 °C and the solid was filtered off. Recrystallization from hot heptane (80 mL) afforded 1,2-bis(3,5-dimethyl-phenyl)hydrazine (3.96 g, 16.48 mmol, 50%) as white long needles.

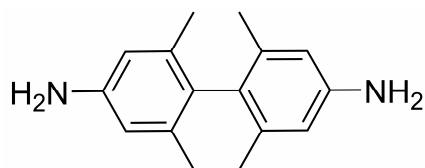


MF C₁₆H₂₀N₂, **MW** 240.34 g/mol

M.p. 119-123 °C

TLC R_f 0.77 (ethyl acetate/hexane, 2:1)

¹H NMR (400 MHz, CDCl₃, δ/ppm) 2.24(s, 12H), 5.46 (s, 2H), 6.52 (s, 6H).

2,2',6,6'-Tetramethylbenzidine (S29)

Diluted HCl (175 mL, 10%) was degassed with nitrogen for 30 min. Then 1,2-bis(3,5-dimethylphenyl)hydrazine (3.70 g, 15.4 mmol) was added and the reaction mixture was refluxed. After

2 h, TLC showed full conversion of the starting material. The solution was cooled to room temperature and basified with NaOH to pH = 10. The product was extracted with *t*-BME (3 x 60 mL) and the combined organic phases were washed with brine and dried over MgSO₄. After evaporation of the solvent, the residue was recrystallized from benzene/hexane to obtain 2,2',6,6'-tetramethylbenzidine **S29** (2.87 g, 11.90 mmol, 77%) as a pink powder. For a further purification the free base was recrystallized several times from EtOH/water. A trace of the isomeric side-product remained in the sample.

MF C₁₆H₂₀N₂, **MW** 240.34 g/mol

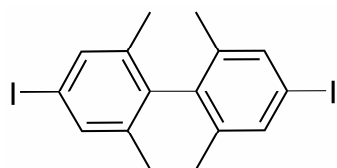
M.p. 163-165 °C

TLC R_f 0.47 (ethyl acetate/hexane, 2:1)

¹H NMR (400 MHz, CDCl₃, δ/ppm) 1.82 (s, 12H), 3.52 (br s, 4H), 6.48 (s, 4H)

¹³C NMR (100 MHz, CDCl₃, δ/ppm) 20.4, 114.7, 131.1, 137.7, 145.0

EI-MS m/z (%) = 240.2 (100) [M⁺], 225.1 (14) [M⁺ - CH₃], 210.1 (30) [M⁺ - 2 CH₃], 105.1 (11).

4,4'-Diiodo-2,2',6,6'-tetramethylbiphenyl (S8d)

To a suspension of 2,2',6,6'-tetramethylbenzidine **S29** (0.93 g, 3.87 mmol) in water (15 mL) and H₂SO₄ (8 mL, 0.142 mol, 36.4 equiv, 95%) a solution of NaNO₂ (600 mg, 8.70 mmol, 2.2 equiv) in water (2.0 mL) was added at 4 °C. After stirring another 30 min at this temperature all starting material was dissolved and the reaction mixture was transferred to a cold solution of I₂ (2.70 g, 10.64 mmol, 2.8 equiv) and NaI (2.70 g, 18.00 mmol, 4.7 equiv) in water (5 mL). After 20, min more water (20 mL) and CH₂Cl₂ (50 mL) was added to bring the reaction components in solution again. After stirring at room temperature overnight, sodium thiosulfate (2.00 g, 12.7 mmol, 3.3 equiv) was added and the reaction mixture was stirred for 10 min. The black precipitate was filtered off and the phases were separated. The water phase was extracted with CHCl₃ (2 x 30 mL) and the combined organic layers were washed again with a thiosulfate solution (25 mL, 10%) and brine. After drying over MgSO₄ and evaporation of the solvent, a flash chromatography was performed to obtain 4,4'-diiodo-2,2',6,6'-tetramethylbiphenyl **S8d** (908 mg, 1.97 mmol, 51%) as bright yellow crystals.

MF C₁₆H₁₆I₂, **MW** 462.11 g/mol

M.p. 196 °C

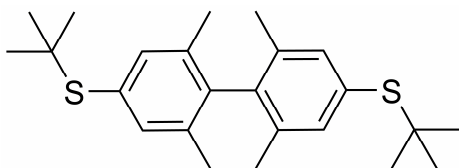
TLC R_f 0.52 (hexane)

¹H NMR (400 MHz, CDCl₃, δ/ppm) 1.83 (s, 12H), 7.48 (s, 4H)

¹³C NMR (100 MHz, CDCl₃, δ/ppm) 19.8, 93.3, 136.9, 138.2, 138.9

EI-MS m/z (%) = 461.9 (20) [M⁺], 336.0 (100) [M⁺ - iodine], 209.1 (13) [M⁺ - 2 iodine], 194.1 (76), 179.1 (36)

EA Analysis calcd for C₁₆H₁₆I₂: C 41.59, H 3.49; found: C 42.53, H 3.52

4,4'-Bis-(*tert.*-butylsulfanyl)-2,2',6,6'-tetramethylbiphenyl (S30)

Under an inert atmosphere 4,4'-diiodo-2,2',6,6'-tetramethylbiphenyl **S8d** (690 mg, 1.49 mmol) was dissolved in degassed *p*-xylene (15 mL). Then Pd₂(dba)₃·CHCl₃ (155 mg, 150 μmol, 10.0 mol%), xantphos (104 mg, 180 μmol, 12.1 mol%) and sodium *t*-thiobutanolate (503 mg, 4.48 mmol, 3.0 equiv) were added. The reaction mixture was stirred at 140 °C for 16 h. Then toluene (20 mL) and brine (20 mL) was added and the phases were separated. The water phase was extracted with *t*-BME (2 x 30 mL) and the combined organic phases were dried over MgSO₄. After evaporation of the solvent a flash chromatography (silica, Et₂O in hexane, 3%) was performed to afford 4,4'-bis-(*tert.*-butylsulfanyl)-2,2',6,6'-tetramethylbiphenyl **S30** (289 mg, 0.75 mmol, 74%) as a yellow oil.

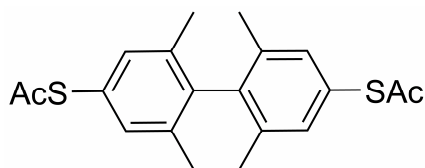
MF C₂₄H₃₄S₂, **MW** 386.66 g/mol

TLC R_f 0.52 (hexane)

¹H NMR (400 MHz, CDCl₃, δ/ppm) 1.32 (s, 18H), 1.88 (s, 12H), 7.30 (s, 4H)

¹³C NMR (100 MHz, CDCl₃, δ/ppm) 20.0, 31.5, 46.0, 131.2, 136.0, 136.8, 140.5

EI-MS m/z (%) = 386 (33) [M⁺], 330 (7) [M⁺ - C₄H₈], 274 (100) [M⁺ - 2 C₄H₈]

4,4'-Bis-(acetylsulfanyl)-2,2',6,6'-tetramethyl-biphenyl (S8a)

To a solution of 4,4'-bis-(*tert.*-butylsulfanyl)-2,2',6,6'-tetramethylbiphenyl **S30** (130 mg, 0.34 mmol) in AcCl (13 mL) and dry toluene (35 mL) was slowly dropped BBr₃ (1.0 mL, 1.00 mmol, 2.9 equiv, 1.0 M in CH₂Cl₂) at 0 °C. Then stirring was continued at room temperature. After TLC showed full conversion (45 min) of the starting material, the reaction mixture was quenched with ice and the organic phase was separated. The water phase was extracted with toluene (2 x 30 mL). The combined organic layers were dried over MgSO₄ and evaporated in *vacuo*. The crude product was purified by flash chromatography (silica, *t*-BME/hexane 1:1) followed by a recrystallization from a mixture of hexane (2 mL) and cyclohexane (4 mL) to afford 4,4'-bis-(acetylsulfanyl)-2,2',6,6'-tetramethyl-biphenyl **S8a** (101 mg, 0.28 mmol, 84%) as beautiful crystals.

MF C₂₀H₂₂O₂S₂, **MW** 358.52 g/mol

M.p. 141 °C

TLC *R_f* 0.52 (hexane/*t*-BME, 4:1)

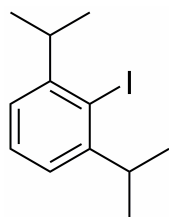
¹H NMR (400 MHz, CDCl₃, δ/ppm) 1.91 (s, 12H), 2.43 (s, 6H), 7.20 (s, 4H)

¹³C NMR (100 MHz, CDCl₃, δ/ppm) 20.2, 30.6, 126.7, 133.8, 137.0, 140.9, 193.8

EI-MS *m/z* (%) = 358.1 (20) [M⁺], 316.1 (27) [M⁺ - CH₃CO],

274.1 (100) [M⁺ - 2 CH₃CO]

EA Analysis calcd for C₂₀H₂₂O₂S₂: C 67.00, H 6.10; found: C 67.10, H 6.16

2,6-Diisopropyl-iodobenzene (S31)

2,6-Diisopropylaniline (10.64 g, 60.00 mmol) and *p*-TSA·H₂O (34.40 g, 0.181 mol, 3.0 equiv) was dissolved in *t*-BuOH (120 mL). The reaction mixture was cooled to 0-5 °C and a solution of sodium nitrite (8.30 g, 0.120 mol, 2.0 equiv) and potassium iodide (25.00 g, 0.151 mol, 2.5 equiv) in H₂O (36 mL) was slowly added. After stirring 30 min at 5-10 °C, H₂O (100 mL) was added. The reaction mixture was extracted with hexane. After evaporation of the solvent, the crude product was purified by flash chromatography (silica, hexane). 2,6-Diisopropyl-4-iodobenzene **S31** was obtained as clear oil (6.85 g, 23.77 mmol, 40%).

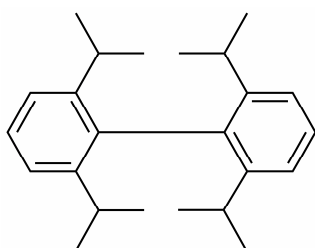
MF C₁₂H₁₇I, **MW** 288.17 g/mol

TLC *R_f* 0.47 (hexane)

¹H NMR (400 MHz, CDCl₃, δ/ppm) 1.24 (d, 12H, ³J = 6.8,), 3.37-3.45 (m, 2H), 7.06-7.11 (m, 2H), 7.21-7.29 (m, 1H)

¹³C NMR (100 MHz, CDCl₃, δ/ppm) 23.8, 39.8, 109.6, 124.2, 128.7, 151.6

EI-MS *m/z* (%) = 288 (69) [M⁺], 273 (100) [M⁺ - CH₃], 131 (21), 91 (23)

2,2',6,6'-Tetraisopropylbiphenyl (S9)

Under inert atmosphere 2,6-diisopropyl-iodobenzene **S31** (2.88 g, 10.00 mmol) was dissolved in dry *Me*THF (40.00 mL). The solution was cooled to -50°C in a dry ice/acetone bath and *t*-BuLi (12.00 mL, 20.04 mmol 2.0 equiv) was added drop wise. After the addition was completed the yellow solution was stirred at this temperature for another 15 min. A fresh solution of LiBr (2.00 g, 23.00 mmol, 2.23 equiv) and CuCN (1.03 g, 11.50 mmol, 1.15 equiv) in *Me*THF (8 mL) was prepared. The almost clear green copper solution was transferred to the reaction mixture over 10 min while keeping the reaction temperature below -60°C . The cloudy reaction mixture was then stirred for another hour at -20°C and then cooled again to -40°C . 1,3-Dinitrobenzene (5.04 g, 30.00 mmol, 3.0 equiv) was added at once and the cooling was removed. After stirring overnight, the black reaction mixture was quenched with a mixture of NH_4Cl (30 mL, 10%) and NH_4OH (30 mL, 25%). The layers were separated and the water phase was extracted with *t*-BME (2 x 80 mL). The combined organic layers were washed with brine and dried over MgSO_4 . After evaporation of the solvent a flash chromatography (silica, *t*-BME in hexane, 0-10%) was performed to obtain a fraction containing 2,2',6,6'-tetraisopropylbiphenyl **S9**. A recrystallization from hexane (10 mL) afforded the pure **S9** (320 mg, 20%) as colorless crystals.

MF $\text{C}_{24}\text{H}_{34}$, **MW** 322.53 g/mol

M.p. 224-225 $^{\circ}\text{C}$

TLC R_f 0.69 (hexane/*t*-BME, 95:5)

^1H NMR (400 MHz, CDCl_3 , δ/ppm) 1.11 (d, 24H, $^3J = 6.75$), 2.41-2.53 (m, 4H), 7.21-7.27 (m, 4H), 7.34-7.40 (m, 2H)

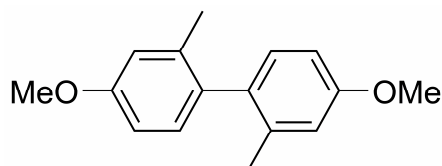
^{13}C NMR (100 MHz, CDCl_3 , δ/ppm) 25.6, 30.00, 123.4, 127.9, 136.0, 148.3

EI-MS 322.3 (67) [M^+]

EA Analysis calcd for $\text{C}_{24}\text{H}_{34}$; C 89.38; H 10.62; found: C 89.21, H 10.48

5.2.2 Chapter 3: Exploring π -Electron-Delocalization in the Structure's LUMO: Dicyano-Biphenyls (CN)

4,4'-Dimethoxy-2,2'-dimethylbiphenyl (CN 7)



Under an inert atmosphere 1-bromo-4-methoxy-2-methylbenzene (34.90 g, 0.174 mol) was dropped to a suspension of magnesium (6.10 g, 0.251 mol, 1.4 equiv) in dry *Me*THF (150 mL) at such a rate that the conversion of the halogenide maintained moderately. Then the reaction mixture was refluxed for 30 min and cooled to room temperature. The Grignard reagent was slowly transferred to a refluxing solution of 1,2-dichloroethane (23 mL, 0.292 mol, 1.7 equiv) and anhydrous FeCl_3 (2.00 g, 12.33 mmol, 7.1 mol%) in dry diethyl ether (250 mL). The reaction was refluxed for 70 min, cooled to room temperature and poured onto ice. Then, HCl (20 mL, 37%) was added, the organic layer was separated and the aqueous phase was extracted with *t*-BME (3 x 50 mL). The combined extracts were washed with NaOH (2 x 50 mL, 1.0 M) and filtered through a silica pad. The colorless oil was dried *in vacuo* to afford **CN 7** (19.40 g, 80.06 mmol, 92%) which was pure enough to use in the next step without further purification. For analytical purposes a flash chromatography was performed (silica, CH_2Cl_2 in hexane, 20-100%).

MF $\text{C}_{16}\text{H}_{18}\text{O}_2$, **MW** 242.31 g/mol

M.p. 54 °C.

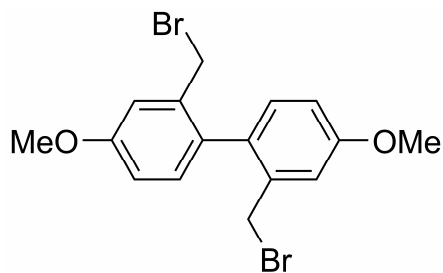
TLC R_f 0.32 (CH_2Cl_2 /hexane, 2:3)

^1H NMR (400 MHz, CDCl_3 , δ /ppm) 2.06 (s, 6H), 3.85 (s, 6H), 6.78 (dd, 2H, $^3J = 8.3$, $^4J = 2.5$), 6.84 (d, 2H, $^4J = 2.5$), 7.03 (d, 2H, $^3J = 8.3$).

^{13}C NMR (100 MHz, CDCl_3 , δ /ppm) 20.6, 55.6, 111.2, 115.6, 131.1, 134.2, 138.1, 159.0.

EI-MS m/z (%) = 242.1 (100) [M^+], 227.1 (27) [$\text{M}^+ - \text{CH}_3$]

EA Analysis calcd for $\text{C}_{16}\text{H}_{18}\text{O}_2$: C 79.31, H 7.49; found: C 78.14, H 7.26

2,2'-Bis(bromomethyl)-4,4'-dimethoxybiphenyl (CN 8)

To a solution of **CN 7** (2.00 g, 8.25 mmol) in CCl_4 (60 mL), NBS (3.10 g, 17.41 mmol, 2.1 equiv) and benzoyl peroxide (0.20 g, 0.62 mmol, 7.5 mol%, 75%) was added. The reaction was kept at reflux until all starting material was converted (GC-MS, 2 h). The cooled reaction mixture was filtered

through a silica pad and the solvent was evaporated. A flash chromatography was performed (silica, CH_2Cl_2 in hexane, 30-90%) to afford pure 2,2'-bis(bromomethyl)-4,4'-dimethoxy-biphenyl **CN 8** (2.23 g, 5.57 mmol, 68%) as a thick colorless oil which solidified upon standing.

MF $\text{C}_{16}\text{H}_{16}\text{Br}_2\text{O}_2$, **MW** 400.11 g/mol

M.p. 75 °C.

TLC R_f 0.23 (CH_2Cl_2 /hexane, 2:3)

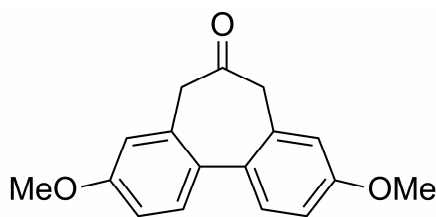
^1H NMR (250 MHz, CDCl_3 , δ /ppm) 3.87 (s, 6H), 4.17 (d, 2H, $^2J = 9.9$), 4.31 (d, 2H, $^2J = 9.9$), 6.91 (dd, 2H, $^3J = 8.4$, $^4J = 2.7$), 7.06 (d, 2H, 7.18, $^4J = 2.7$), 7.18 (d, 2H, $^3J = 8.4$)

^{13}C NMR (100 MHz, CDCl_3 , δ /ppm) 32.6, 55.8, 114.7, 115.8, 131.9, 132.1, 137.9, 159.8

EI-MS m/z (%) = 398.0 (50), 400.0 (100), 402.0 (49) [M^+]

HRMS (ESI) calcd for $\text{C}_{16}\text{H}_{16}\text{O}_2\text{Br}_2$ [$\text{M}+\text{Na}$] $^+$: 420.9416; found: 420.9414

EA Analysis calcd for $\text{C}_{16}\text{H}_{16}\text{Br}_2\text{O}_2$: C 48.03, H 4.03; found: C 47.94, H 3.91

3,9-Dimethoxy-5,7-dihydrodibenzo[a,c]cyclohepten-6-one (CN 9)

Under ice cooling NaOH (294 mg, 7.35 mmol, 5.0 equiv) was dissolved in H₂O (4 mL) and added to a suspension of **CN 8** (589 mg, 1.47 mmol), toluenesulfonylmethyl-isocyanide (287 mg, 1.47 mmol, 1.0 equiv) and TBAB (30 mg, 93 μmol, 6.3 mol%) in CH₂Cl₂ (10 mL). The two phase mixture was stirred vigorously at room temperature overnight. *t*-BME (16 mL) and HCl (8 mL, 37 %) was added and the mixture was stirred for 3 h. The phases were separated and the organic layer was washed with sat. NaHCO₃, dried over MgSO₄ and the solvent was evaporated. The crude product was purified by flash chromatography (silica, CH₂Cl₂) to afford **CN 9** as a white solid (326 mg, 1.22 mmol, 83%).

MF C₁₇H₁₆O₃, **MW** 268.31 g/mol

M.p. 126 °C

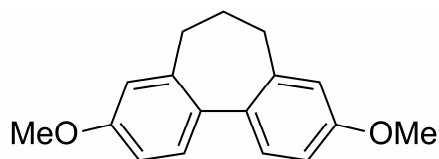
TLC *R_f* 0.17 (CH₂Cl₂/hexane, 2:1)

¹H NMR (250 MHz, CDCl₃, δ/ppm) 3.45 (d, ²J = 13.0, 2H), 3.59 (d, 2H, ²J = 13.0), 6.79 (d, 2H, ⁴J = 2.6), 6.94 (dd, 2H, ³J = 8.5, ⁴J = 2.6), 7.44 (d, 2H, ³J = 8.5)

¹³C NMR (100 MHz, CDCl₃, δ/ppm) 50.0, 55.8, 113.7, 114.9, 130.6, 132.1, 134.3, 159.4, 210.5

EI-MS *m/z* (%) = 268.1 (100) [M⁺], 225.1 (67), 165.1 (15), 153.1 (11)

HRMS (ESI) calcd for C₁₇H₁₆O₃ [M+Na]⁺: 291.0997; found: 291.0993

3,9-Dimethoxy-6,7-dihydro-5H-dibenzo[a,c]cycloheptene (CN 10)

To a suspension of **CN 9** (854 mg, 3.18 mmol), powdered KOH (750 mg, 13.37 mmol, 4.2 equiv) in diethylene glycol (10 mL) was added hydrazine monohydrate (0.35 mL, 7.21 mmol, 2.3 equiv) under ice cooling. The mixture was heated up to reflux for 2h. The water and excess of hydrazine was distilled off at an oil bath temperature of 190 °C. After a total reaction time of 3 h and a maximum oil bath temperature of 195 °C, the reaction was stopped. Water was added (40 mL) to the cooled reaction mixture and an extraction followed with *t*-BME (4 x 20 mL). The combined organic layers were washed with HCl (1 x 20 mL, 1.0 M), water (3 x 10 mL) and brine (1 x 30 mL), dried over MgSO₄ and filtered through a short silica pad. After evaporation of the solvent **CN 10** (700 mg, 2.75 mmol, 86%) was obtained as a white oil which solidified upon standing.

MF C₁₇H₁₈O₂, **MW** 254.32 g/mol

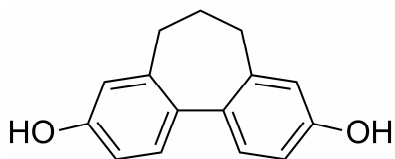
M.p. 110 °C

TLC *R_f* 0.38 (hexane/ethyl acetate, 5:1)

¹H NMR (250 MHz, CDCl₃, δ/ppm) 2.16 (m, 2H), 2.47 (m, 4H), 7.19 (d, 2H, ⁴J = 2.4), 7.27 (dd, 2H, ³J = 8.4, ⁴J = 2.6) 7.41 (d, 2H, ³J = 8.4)

¹³C NMR (100 MHz, CDCl₃, δ/ppm)

HRMS (ESI) calcd for C₁₇H₁₉O₂ [M+Na]⁺: 255.1385; found: 255.1385

3,9-Dihydroxy-6,7-dihydro-5H-dibenzo[a,c]cycloheptene (CN 11)

The dimethoxy-compound **CN 10** was deprotected with BBr_3 according to the protocol to afford **CN 16**. The crude diol **CN 11** was obtained as a white powder which was used without further purification for the next step.

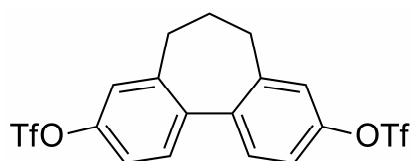
MF $\text{C}_{15}\text{H}_{14}\text{O}_2$, **MW** 226.27 g/mol

TLC R_f 0.27 (hexane/ *t*-BME, 1:1)

^1H NMR (250 MHz, CDCl_3 , δ /ppm) 2.14 (m, 2H), 2.44 (m, 4H), 4.66 (br s, 2H), 6.72 (d, 2H, $^4J = 2.4$), 6.78 (dd, 2H, $^3J = 8.0$, $^4J = 2.4$), 7.19 (d, 2H, $^3J = 8.0$)

^{13}C NMR (100 MHz, CDCl_3 , δ /ppm) 31.5, 32.7, 113.0, 115.2, 128.9, 132.6, 140.7, 155.4

MALD-TOF MS (without matrix) $m/z = 226.4$ $[\text{M}]^+$

3,9-Bis-(trifluoromethanesulfonyloxy)-6,7-dihydro-5H-dibenzo[a,c]cycloheptene (CN 12)

The crude diol **CN 11** was esterified with triflic anhydride and pyridine as the base according to the protocol to afford **CN 17**. **CN 12** was obtained as a colorless oil. The yield over two steps was 84%.

MF C₁₇H₁₂F₆O₆S₂, **MW** 490.39 g/mol

TLC *R_f* 0.66 (hexane/*t*-BME, 2:1)

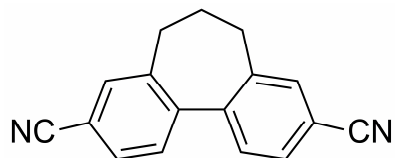
¹H NMR (250 MHz, CDCl₃, δ/ppm) 2.24 (m, 2H), 2.52 (m, 4H), 7.19 (d, 2H, ⁴J = 2.5), 7.27 (dd, 2H, ³J = 8.4, ⁴J = 2.5), 7.41 (d, 2H, ³J = 8.4)

¹³C NMR (100 MHz, CDCl₃, δ/ppm) 31.2, 32.6, 119.6, 121.4, 130.0, 139.6, 142.1, 149.0

¹⁹F NMR (376 MHz, CDCl₃, δ/ppm) -74.0

EI-MS *m/z* (%) = 490.0 (37) [M⁺], 357.1 (100) [M⁺ - SOCF₃], 224.1 (13) [M⁺ - 2 SOCF₃]

EA Analysis calcd for C₁₇H₁₂F₆O₆S₂: C 41.64, H 2.47; found: C 41.72, H 2.48

Representative example for cyanation *method A*:**3,9-Dicyano-6,7-dihydro-5H-dibenzo[*a,c*]cycloheptene (CN 3)**

To a solution of **CN 12** (251 mg, 0.51 mmol) in dry and degassed acetonitrile (5 mL) was added potassium cyanide (100 mg, 1.54 mmol, 3.0 equiv), Pd₂(dba)₃·CHCl₃ (53 mg, 51 μmol, 10.0 mol%), xantphos (30 mg, 51 μmol, 10.0 mol%). Tributyltin chloride (3.9 μL, 14.4 μmol, 2.8 mol%) was added and the reaction mixture was refluxed for 16 h, cooled to room temperature, the solvent was evaporated and the dicyano compound **CN 3** was purified by flash chromatography (silica, CH₂Cl₂) to obtain a white solid. Recrystallization from a mixture of hot dioxane and cyclohexane using the slow evaporation technique gave single crystals suitable for the X-ray analysis (102 mg, 0.418 mmol, 82%).

MF C₁₇H₁₂N₂, **MW** 244.29 g/mol

M.p. 246-248 °C

TLC R_f 0.57 (CH₂Cl₂)

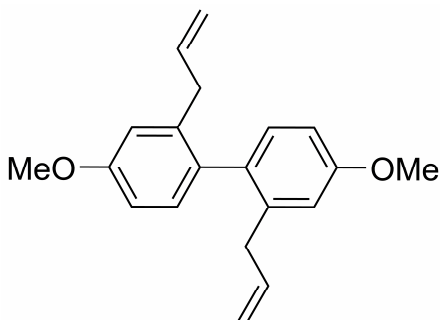
¹H NMR (400 MHz, CDCl₃-d₃, δ/ppm) 2.21-2.29 (m, 2H), 2.52 (br s, 4H),

7.45 (d, 2H, ³J = 7.9), 7.57 (d, 2H, ⁴J = 1.6), 7.67 (dd, 2H, ³J = 8.1, ⁴J = 1.6)

¹³C NMR (100 MHz, CDCl₃, δ/ppm) 31.2, 33.1, 112.7, 119.1, 129.4, 131.2, 132.6, 141.1, 144.3

EI-MS *m/z* (%) = 244.1 (100) [M⁺], 229.1 (74), 216.1 (26), 202.1 (11)

EA Analysis calcd for C₁₇H₁₂N₂: C 83.58, H 4.95, N 11.47; found: C 83.45, H 5.14, N 11.39

2,2'-Diallyl-4,4'-dimethoxybiphenyl (CN 13)

CN 8 (4.00 g, 10.00 mmol) was dissolved in dry CH_2Cl_2 (15 mL) and added at $-50\text{ }^\circ\text{C}$ to a vinyl magnesium bromide solution in dry THF (86 mL, 60.20 mmol, 6.0 equiv, 0.7 M). Then CuI (1.90 g, 10.00 mmol, 1.0 equiv) was added at once and the reaction mixture was allowed to reach room temperature to overnight. The black suspension

was poured onto a cold NH_4Cl solution (300 mL). The organic layer was separated and the aqueous phase was extracted with *t*-BME (3 x 150 mL). The combined organic phases were washed with brine (150 mL), dried over MgSO_4 and filtered through celite. After evaporating the solvent a flash chromatography (silica, hexane/ CH_2Cl_2 , 1:1) was performed to obtain **CN 13** (2.27 g, 7.71 mmol, 77%) as a colorless smelly oil.

MF $\text{C}_{20}\text{H}_{22}\text{O}_2$, **MW** 294.39 g/mol

TLC R_f 0.6 (CH_2Cl_2 /hexane, 3:2)

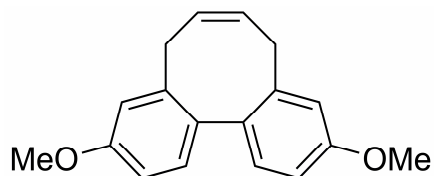
^1H NMR (400 MHz, CDCl_3 , δ /ppm) 3.03-3.14 (m, 4H), 3.84 (s, 6H), 4.87-4.98 (m, 4H), 5.74-5.84, (m, 2H), 6.79 (dd, 2H, $^3J = 8.3$, $^4J = 2.7$), 6.83 (d, 2H, $^4J = 2.7$), 7.03 (d, 2H, $^3J = 8.3$)

^{13}C NMR (100 MHz, CDCl_3 , δ /ppm) 38.3, 55.6, 111.5, 114.9, 116.3, 131.7, 133.4, 137.5, 140.1, 159.2

EI-MS m/z (%) = 294.2 (100) [M^+], 279.2 (23) [$\text{M}^+ - \text{CH}_3$], 253.1 (48) [$\text{M}^+ - \text{C}_3\text{H}_5$ (allyl)], 238.1 (42)

EA Analysis calcd for $\text{C}_{20}\text{H}_{22}\text{O}_2$: C 81.60, H 7.53; found: C 80.28, H 7.41.

HRMS (ESI) calcd for $\text{C}_{20}\text{H}_{22}\text{O}_2$ [$\text{M} + \text{Na}$] $^+$: 317.1517; found: 317.1512

3,10-Dimethoxy-5,8-dihydrodibenzo[a,c]cyclooctene (CN 14)

Compound **CN 13** (1.84 g, 6.25 mmol) was dissolved in CH_2Cl_2 (500 mL). After addition of the *Grubbs'* catalyst (1st generation, 0.26 g, 0.32 mmol, 5.0 mol%) the solution was refluxed for 16 h and the solvent was evaporated. The product was purified by flash chromatography (silica, hexane/ CH_2Cl_2 , 1:1) to give **CN 14** (1.32 g, 4.96 mmol, 79%) as a white solid.

MF $\text{C}_{18}\text{H}_{18}\text{O}_2$, **MW** 266.33 g/mol

M.p. 142°C

TLC R_f 0.27 (CH_2Cl_2 /hexane, 1:1)

^1H NMR (400 MHz, CDCl_3 , δ /ppm) 2.98-3.09 (m, 4H), 3.84 (s, 6H), 5.80-5.88 (m, 2H), 6.75 (d, 2H, $^4J = 2.7$), 6.83 (dd, 2H, $^3J = 8.3$, $^4J = 2.7$), 7.17 (d, 2H, $^3J = 8.3$).

^{13}C NMR (100 MHz, CDCl_3 , δ /ppm) 34.2, 55.7, 112.0, 114.8, 129.3, 129.4, 134.9, 138.7, 160.0.

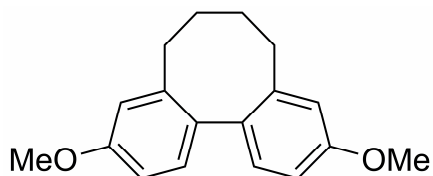
EI-MS m/z (%) = 266.1 (100) [M^+], 251.1 (27) [$\text{M}^+ - \text{CH}_3$], 235.1 (21) [$\text{M}^+ - \text{CH}_3\text{O}$]

EA Analysis calcd for $\text{C}_{18}\text{H}_{18}\text{O}_2$: C 81.17, H 6.81; found: C 80.72, H 6.84

HRMS (ESI) calcd for $\text{C}_{18}\text{H}_{18}\text{O}_2$ [$\text{M} + \text{Na}$] $^+$: 289.1204; found: 289.1210

3,10-Dimethoxy-5,6,7,8-tetrahydrodibenzo[a,c]cyclooctene (CN 15)

CN 14 (1.08 g, 4.06 mmol) was dissolved in ethyl acetate (70 mL) and Pd/C (120 mg, 10% Pd) was added. The mixture was stirred under a hydrogen atmosphere (1 atm) for 3 h. Then, the solution was filtered through a silica pad and the solvent was evaporated. **CN 15** was collected as a white solid (1.07 g, 3.99 mmol, 98%).



MF C₁₈H₂₀O₂, **MW** 268.35

TLC *R_f* 0.27 (CH₂Cl₂/hexane, 1:1)

M.p. 152°C

¹H NMR (400 MHz, CDCl₃, δ/ppm) 1.48-1.57 (m, 2H), 2.01-2.19 (m, 4H), 2.64-2.69 (m, 2H), 3.80 (s, 6H), 6.78-6.80 (m, 4H), 7.13-7.16 (m, 2H).

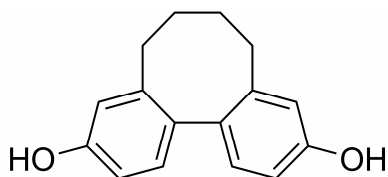
¹³C NMR (100 MHz, CDCl₃, δ/ppm) 30.1, 33.5, 55.7, 111.5, 114.8, 130.6, 133.5, 144.6, 159.5

EI-MS *m/z* (%) = 268.1 (100) [M⁺], 253.1 (12) [M⁺ -CH₃], 225.1 (12).

EA Analysis calcd for C₁₈H₂₀O₂: C 80.56, H 7.51; found: C 80.62, H 7.50.

3,10-Dihydroxy-5,6,7,8-tetrahydrodibenzo[a,c]cyclooctene (CN 16)

To a solution of **CN 15** (1.50 g, 5.59 mmol) in dry CH₂Cl₂ (80 mL) was slowly dropped BBr₃ (2.9 mL, 30.60 mmol, 5.5 equiv) at 0 °C. Then stirring was continued at room temperature until TLC showed full conversion of the starting material (1.5 h). The reaction was quenched with MeOH under ice cooling. The reaction mixture was washed with water (50 mL), dried over MgSO₄ and the solvent was evaporated. The crude **CN 16** (1.67 g) was obtained as a white powder which was pure enough to use for the next step. To obtain a sample for analytical purposes a flash chromatography was performed (silica, hexane/*t*-BME, 2:1).



MF C₁₆H₁₆O₂, **MW** 240.30 g/mol

M.p. 130-134°C

TLC *R_f* 0.26 (hexane/*t*-BME, 1:1)

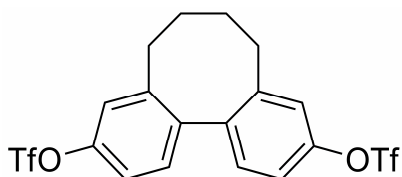
¹H NMR (400 MHz, DMSO-*d*₆, δ/ppm) 1.31-1.33 (m, 2H), 1.86-2.00 (m, 4H), 2.50-2.55 (m, 2H), 6.58-6.62 (m, 4H), 6.90 (d, 2H, ³*J* = 8.0), 9.23 (br s, 2H).

¹³C NMR (100 MHz, CDCl₃, δ/ppm) 30.4, 33.4, 113.7, 116.3, 130.6, 131.9, 144.1, 157.5

EI-MS *m/z* (%) = 240.1 (100) [M⁺], 211.1 (24), 197.1 (27), 165.1 (9)

HRMS (ESI) calcd for C₁₆H₁₆O₂ [M+Na]⁺: 263.1047; found: 263.1056

Bis-(trifluoromethanesulfonyloxy)-5,6,7,8-tetrahydrodibenzo[a,c]cyclo-octene (CN 17)



The crude diol **CN 16** from the previous step was dissolved in dry pyridine (40 mL). Then triflic anhydride (3.7 mL, 22.00 mmol, 3.9 equiv) was slowly dropped to the solution. Stirring was continued at room temperature (30 min) and the beige solution was quenched with a cold sat. NaHCO₃ solution. The product was extracted with CH₂Cl₂ (3 x 50 mL) and the combined organic phases were dried over MgSO₄. After evaporation of the solvent a flash chromatography (silica, hexane/CH₂Cl₂, 7:3) was performed to afford **CN 17** (2.33 g, 4.62 mmol, 83% over two steps) as a colorless oil which solidified upon standing.

MF C₁₈H₁₄F₆O₆S₂, **MW** 504.42 g/mol

M.p. 69-70 °C.

TLC *R_f* 0.66 (hexane/*t*-BME, 1:1)

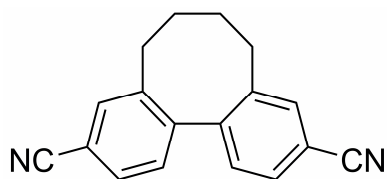
¹H NMR (400 MHz, CDCl₃, δ/ppm) 1.48-1.53 (m, 2H), 2.08-2.15 (m, 4H), 2.74-2.79 (m, 2H), 7.16-7.21 (m, 4H), 7.29 (d, 2H, ³J = 8.3)

¹³C NMR (100 MHz, CDCl₃, δ/ppm) 29.0, 32.6, 118.7, 119.2 (q, J = 319), 122.0, 130.6, 140.0 145.4, 149.5

¹⁹F NMR (376 MHz, CDCl₃, δ/ppm) -74.0

EI-MS *m/z* (%) = 504.0 [M⁺], 371.0 (85) [M⁺ - SO₂CF₃], 238.1 (24.8), 210.1 (22)

EA Analysis calcd for C₁₈H₁₄F₆O₂S₂: C 42.86, H 2.80; found: C 42.91, H 2.75

3,10-Dicyano-5,6,7,8-tetrahydrodibenzo[a,c]cyclooctene (CN 4)

The triflate **CN 17** was converted to the dicyanide **CN 4** according to *method A* (see synthetic protocol of **CN 3**). **CN 4** was purified by flash chromatography (silica, CH₂Cl₂/hexane, 8:2) to give a white solid.

Recrystallization from a mixture of hot dioxane and cyclohexane using the slow evaporation technique gave single crystals of **CN 4** suitable for the X-ray analysis (132 mg, 0.51 mmol, 86%).

MF C₁₈H₁₄N₂, **MW** 258.32 g/mol

M.p. 248-249 °C

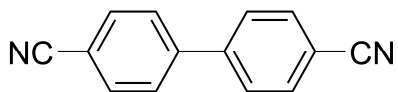
TLC *R_f* 0.31 (CH₂Cl₂/hexane, 8:2)

¹H NMR (400 MHz, CDCl₃-d₃, δ/ppm) 1.45-1.53 (m, 2H), 2.04-2.18 (m, 4H), 2.75-2.82 (m, 2H), 7.31 (d, 2H, ³J = 7.9), 7.57 (dd, 2H, ³J = 7.9, ⁴J = 1.6), 7.61 (d, 2H, ³J = 7.9)

¹³C NMR (100 MHz, CDCl₃, δ/ppm) 29.3, 32.6, 113.1, 119.1, 129.9, 130.0, 133.7, 143.8, 144.2

EI-MS *m/z* (%) = 258.1 [M⁺], 243.1 (18), 229.1 (67), 216.1 (35), 202.1 (15), 190.1 (14)

EA Analysis calcd for C₁₈H₁₄N₂: C 83.69, H 5.46, N 10.84; found: C 83.37, H 5.54, N 10.82

Representative example for cyanation *method B*:**4,4'-Dicyanobiphenyl (CN 5)**

Copper(I)cyanide (0.860 g, 9.62 mmol, 3.0 equiv) was dried under high vacuum. Then, the copper salt and 4,4'-dibromobiphenyl (1.00 g, 3.20 mmol) was suspended in dry DMF and the reaction mixture was stirred at 150-160 °C for 16h. The reaction mixture was cooled to room temperature, water (80 mL) and ethylenediamine (10 mL) was added, stirred at 70 °C for 10 min and cooled again to room temperature. The dark blue reaction mixture was extracted with CH₂Cl₂. The organic phase was washed with water, brine, dried over MgSO₄ and evaporated on rotary evaporator. The residue was taken up in hot EtOH/water, cooled to room temperature and powder was filtered off, and dried in vacuo. Compound **CN 5** was obtained as a beige powder (480 mg, 2.35 mmol, 73%). A chromatographic purification (silica, CH₂Cl₂) of **CN 5** was achieved by dissolving the compound in a large amount of chloroform and adsorbing it to the immobilized phase. This was followed by a recrystallization from a hot mixture of dioxane and cyclohexane using the slow evaporation technique affording single crystals suitable for the X-ray analysis.

MF C₁₄H₈N₂, **MW** 204.23

M.p. 227-239 °C

TLC *R_f* 0.18 (CH₂Cl₂/hexane, 4:1)

¹H NMR (250 MHz, DMSO-*d*₆, δ/ppm) 7.81-7.87 (m, 8H)

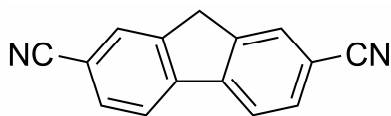
¹³C NMR (100 MHz, CDCl₃, δ/ppm) 112.9, 118.3, 119.4, 129.0, 133.9

EI-MS *m/z* (%) = 204.1 (100) [M⁺], 177.0 (10) [M⁺ - HCN]

EA Analysis calcd for C₁₄H₈N₂: C 82.34, H 3.95, N 13.72; found: C 82.07, H 4.17, N 13.75

HPLC-DAD (Reprosil 100 C18, 125x3 mm, CH₃CN, flow 0.2mL/min, T = 25 °C):

R_t = 3.53 min.

2,7-Dicyanofluorene (CN 1)

2,7-Dicyanofluorene **CN 1** was obtained from the commercially available 2,7-dibromofluorene according to *method B*. The reaction time was 6 h, 2.6 equivalent copper(I)cyanide was used and the product was extracted with several times ethyl acetate. The combined extracts were filtered through a silica pad and the solvent was evaporated on the rotary evaporator. The beige residue was repeatedly recrystallized from hot acetonitrile, ethanol and methoxyethanol. **CN 1** (540 mg, 2.49 mmol, 51%) was obtained as yellow fine crystals. To pass the elemental analysis a final chromatographic purification of **CN 1** was achieved by dissolving the compound in a large amount of chloroform and adsorbing it to silica (eluent: CH₂Cl₂). This was followed by a recrystallization from a hot mixture of dioxane and cyclohexane affording single crystalline material suitable for the X-ray analysis and passing all analytical tests.

MF C₁₅H₈N₂, **MW** 216.24 g/mol

M.p. 279-281 °C

TLC R_f 0.46 (CH₂Cl₂)

¹H NMR (400 MHz, CDCl₃-d₃, δ/ppm) 4.04 (s, 2H), 7.74 (dd, 2H, ³J = 8.0, ⁴J = 1.3), 7.89 (d, 2H, ³J = 8.0), 7.93 (dd, 2H, ³J = 8.0)

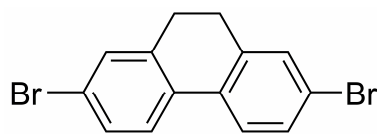
¹³C NMR (100 MHz, CDCl₃, δ/ppm) 37.1, 112.1, 119.4, 122.0, 129.4, 131.9, 144.5, 144.6

EI-MS *m/z* (%) = 216.1 (100) [M⁺], 189.1 (13) [M⁺ - HCN]

EA Analysis calcd for C₁₅H₈N₂: C 83.32, H 3.73, N 12.95; found: C 83.35, H 3.91, N 12.83.

HPLC-DAD (Reprosil 100 C18, 125x3 mm, CH₃CN, flow 0.2mL/min, T = 25 °C):

R_t = 3.7 min.

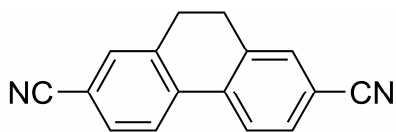
2,7-Dibromo-9,10-dihydrophenanthrene (CN 18)

In a 100 mL round bottom flask dihydrophenanthrene (5.00 g, 27.73 mmol) was dissolved in of trimethyl phosphate (30 mL). Bromine (9.50 g, 59.45 mmol, 2.1 equiv) was dissolved in 20 mL of trimethyl phosphate and the solution was slowly added to the reaction mixture and stirred at room temperature overnight. The reaction mixture was placed in the refrigerator for one day. Then, a first crop was formed and the crude material was filtered off and then washed with cold ethanol. After three days another 1.60 g product was collected and washed. A total amount of 4.41 g (13.05 mmol, 47%) 2,7-dibromo-dihydrophenanthrene **CN 18** was obtained as a white solid.

MF C₁₄H₁₀Br₂, **MW** 338.04 g/mol

¹H NMR (400 MHz, CDCl₃, δ/ppm) 2.83 (s, 4H), 7.37-7.43 (m, 4H), 7.55 (d, 2H, ³J = 8.3)

EI-MS *m/z* (%) = 336 (51%), 338 (100), 340 (49%) [M⁺]

2,7-Dicyano-9,10-dihydrophenanthrene (CN 2)

2,7-Dicyano-9,10-dihydrophenanthrene **CN 2** was obtained according to *method B* from dibromide **CN 18**.

The reaction time was 18 h. The obtained beige powder containing traces of DMF was recrystallized from hot toluene to give **CN 2** (360 mg, 1.56 mmol, 53%) as yellow fine crystals. Subsequent recrystallization from a boiling mixture of dioxane and cyclohexane gave the **CN 2** as colorless crystals suitable for the X-ray measurement.

MF C₁₆H₁₀N₂, **MW** 230.26 g/mol

M.p. 299-300 °C

TLC *R_f* 0.56 (CH₂Cl₂)

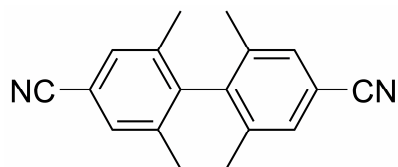
¹H NMR (400 MHz, CDCl₃-d₃, δ/ppm) 2.94 (s, 4H), 7.57 (d, 2H, ³J = 8.1),

7.64 (dd, 2H, ³J = 8.1, ⁴J = 1.4), 7.83 (d, 2H, ³J = 8.1)

¹³C NMR (100 MHz, CDCl₃, δ/ppm) 28.4, 112.5, 119.0, 125.4, 131.5, 132.3, 137.49, 139.10

EI-MS *m/z* (%) = 230.1 (100) [M⁺], 215.1 (16), 202.1 (14), 190.1 (26)

EA Analysis calcd for C₁₆H₁₀N₂: C 83.46, H 4.38, N 12.17; found: C 83.19, H 4.56, N 12.15.

4,4'-Dicyano-2,2',6,6'-tetramethylbiphenyl (CN 6)

CN 6 was obtained according to *method B* starting from 4,4'-diiodo-2,2',6,6'-tetramethylbiphenyl **S8d** (chapter 2). The reaction was completed within 8 h at 140 °C. The cyano compound **CN 6** was purified by flash chromatography (silica, CH₂Cl₂/hexane, 8:2) affording an off-white crystalline powder (344 mg, 1.32 mmol, 84%). A recrystallization using the slow evaporation technique (cyclohexane) gave single crystals suitable for the X-ray analysis.

MF C₁₈H₁₆N₂, **MW** 260.33 g/mol

M.p. 249-250 °C

TLC *R_f* 0.39 (CH₂Cl₂/hexane, 8:2)

¹H NMR (400 MHz, CDCl₃-d₃, δ/ppm) 1.91 (s, 12H), 7.46 (s, 4H)

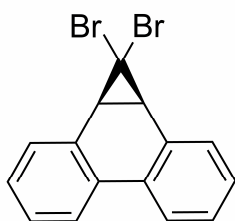
¹³C NMR (100 MHz, CDCl₃, δ/ppm) 19.9, 112.2, 119.2, 131.8, 137.0, 143.7

EI-MS 260.1 (62) [M⁺], 245.1 (100) [M⁺ - CH₃]

EA Analysis calcd for C₁₈H₁₆N₂: C 83.04, H 6.19, N 10.76; found: C 83.03, H 6.40, N 10.74

5.2.3 Chapter 4 - Complementation of the Series: Planar Biphenyl Model Structures

1,1-Dibromo-1a,9b-dihydrocyclopropa[*h*]phenanthrene (CP 12)

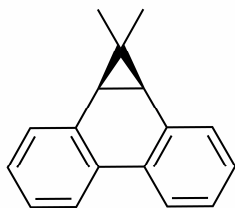


Phenanthrene (3.56 g, 19.97 mmol), benzyltriethylammonium chloride (50 mg, 0.22 mmol, 1.1 mol%), bromoform (4.0 mL, 0.46 mol, 23.0 equiv), CH₂Cl₂ (5 mL) and EtOH (0.1 mL) were mixed and stirred with a magnetic stir bar. To this mixture was added aqueous NaOH (8.0 mL, 50%) in small portions over 15 min. The flask was closed with a stopper with a small hole and stirring was continued at room temperature for 2 days. Then again, bromoform, NaOH and catalyst in equal amount were added and the mixture was stirred for two more days. To the resulting thick, dark brown mixture water and CH₂Cl₂ was added. The water phase was twice re-extracted with CH₂Cl₂. The combined organic phases were washed with diluted HCl, water and dried over MgSO₄. The brown residue was taken up in a small amount of a mixture of CH₂Cl₂ and toluene. The clear solution was dropwise added to pentane (250 mL) to precipitate 1,1-dibromo-1a,9b-dihydrocyclopropa[*h*]phenanthrene **CP 12** as a grey powder (3.17 g, 9.06 mmol, 45%).

MF C₁₅H₁₀Br₂, **MW** 350.05 g/mol

¹H NMR (250 MHz, CDCl₃, δ/ppm) 3.53 (s, 2H), 7.32-7.46 (m, 4H), 7.52 (dd, 2H, ³J = 7.7, ⁴J = 1.8), 8.01-8.06 (m, 2H).

1,1-Dimethyl-1a,9b-dihydrocyclopropa[*h*]phenanthrene (CP 13)



To a suspension of CuI (1.96 g, 10.29 mmol, 3.0 equiv) in diethylether (50 mL) was added a 1.60 M THF solution of MeLi (6.0 mL, 9.60 mmol, 2.8 equiv) at 0 °C. After being stirred for 15 min, a solution of 1,1-dibromo-1a,9b-dihydrocyclopropa[*h*]phenanthrene **CP 12** (1.20 g, 3.43 mmol) in benzene (10 mL) was added at -20 °C. After being stirred for 2-3 h at -20 °C, iodomethane (6.0 mL, 96.33 mmol, 28.0 equiv) was added. After being stirred over at room temperature over night, a saturated aqueous NH₄Cl solution was added. The mixture was separated, and the aqueous layer was extracted with *t*-BME. The combined organic layers were washed with brine and dried over MgSO₄. Concentration under reduced pressure followed by column chromatography (silica, hexane) afforded **CP 13** as a yellow oil which solidified upon standing. Recrystallization from ethanol gave pure **CP 13** as colorless crystals which were suitable for X-ray measurements (257 mg, 1.17 mmol, 34%).

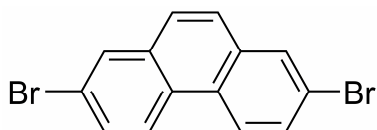
MF C₁₇H₁₆, **MW** 220.31 g/mol

¹H NMR (400 MHz, CDCl₃, δ/ppm) 0.50 (s, 3H), 1.38 (s, 3H), 2.35 (s, 2H), 7.23-7.27 (m, 4H), 7.32-7.36 (m, 2H), 7.93-7.98 (m, 2H)

¹³C NMR (100 MHz, CDCl₃, δ/ppm) 14.5, 14.6, 28.0, 32.0, 122.9, 126.4, 127.8, 130.6, 131.6, 134.2

EI-MS *m/z* (%) = 220.1 (40), 205.1 (100) [M⁺]

UV-VIS (hexane) λ_{max} (ε) = 310 (6300), 275 (16200), 220 (62100)

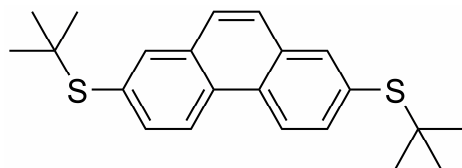
2,7-Dibromophenanthrene (CP 10)

2,7-Dibromodihydrophenanthrene **CN 18** (2.73 g, 8.08 mmol), NBS (12.7 g, 8.43 mmol, 1.05 equiv) were mixed with cyclohexane (80 mL). The mixture was stirred at 80-90 °C for 2 hours and cooled down. CH₂Cl₂ (80 mL) was added and the mixture was twice washed with water and dried over MgSO₄. The solvent was removed to obtain 2,7-dibromo-phenanthrene **CP 10** (2.41g, 7.17 mmol, 89%) as a off-white solid.

MF C₁₄H₈Br₂, **MW** 336.02 g/mol

¹H NMR (400 MHz, CDCl₃, δ/ppm) 7.66 (s, 2H), 7.74 (dd, 2H, ³J = 8.8, ⁴J = 2.1), 8.03 (d, 2H, ⁴J = 2.1), 8.47 (d, 2H, ³J = 8.8)

EI-MS *m/z* (%) = 334 (50%), 336 (100%), 338 (49%) [M⁺]

2,7-Bis-(*tert.*-butylsulfanyl)phenanthrene (CP 11)

Under an inert atmosphere 2,7-dibromo-phenanthrene **CP 10** (594 mg, 1.77 mmol) was dissolved in degassed *p*-xylene (15 mL). Then $\text{Pd}_2(\text{dba})_3 \cdot \text{CHCl}_3$ (183 mg, 0.18 mmol, 10.0 mol%), xantphos (123 mg, 0.21 mmol, 12.0 mol%) and sodium *t*-thiobutanolate (793 mg, 7.07 mmol, 4.0 equiv) were added. The reaction mixture was stirred at 140 °C for 20 h. Then toluene (20 mL) was added and the mixture was washed with brine and the organic phase was dried over MgSO_4 . After evaporation of the solvent a flash chromatography (silica, *t*-BME in hexane, 5%) was performed to afford (594 mg, 1.68 mmol, 95%) of 2,7-bis-(*tert.*-butylsulfanyl)phenanthrene **CP 11** as a yellow solid.

MF $\text{C}_{22}\text{H}_{26}\text{S}_2$, **MW** 354.57 g/mol

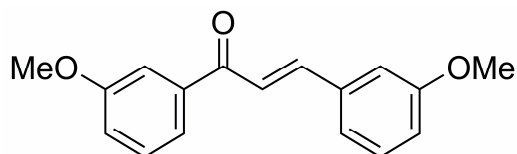
TLC R_f 0.43 (hexane)

$^1\text{H NMR}$ (400 MHz, CDCl_3 , δ/ppm) 1.35 (s, 18H), 7.26 (s, 2H),

7.79 (dd, 2H, $^3J = 8.6$, $^4J = 1.8$), 8.08 (d, 2H, $^4J = 1.8$), 8.61 (d, 2H, $^3J = 8.6$)

$^{13}\text{C NMR}$ (100 MHz, CDCl_3 , δ/ppm) 31.5, 46.9, 123.3, 127.6, 130.3, 131.9, 132.7, 135.7, 137.9

EI-MS m/z (%) = 354 (32) [M^+], 298 (9) [$\text{M}^+ - \text{C}_4\text{H}_8$], 242 (100) [$\text{M}^+ - 2 \text{C}_4\text{H}_8$]

3,3'-Dimethoxychalcone**(1,3-Bis(3-methoxyphenyl)-2-propen-1-one) (CP 2)**

In a 1000 mL round bottom flask *m*-acetylanisole (31.54 g, 0.210 mol, 1.0 equiv), *m*-anisaldehyde (28.60 g, 0.210 mol, 1.0 equiv), aqueous NaOH (33.30 g, 0.416 mol, 2.0 equiv, *w* = 0.5) and MeOH (500 mL) were mixed. The solution was closed with a balloon, filled with N₂, and stirred at room temperature for 16 h. Most of the solvent was evaporated and water (100 mL) was added. The biphasic mixture was extracted with *t*-BME and the organic phase was dried over MgSO₄ and evaporated on the rotary evaporator. The crude chalcone **CP 2** was obtained as yellow syrup (56.73 g, assuming 0.210 mol) which was used for the next step without further purification. An analytical sample was obtained by flash chromatography (silica, hexane/*t*-BME, 6:4).

MF C₁₇H₁₆O₃, **MW** 268.31 g/mol

TLC *R_f* = 0.29 (hexane/*t*-BME, 6:4)

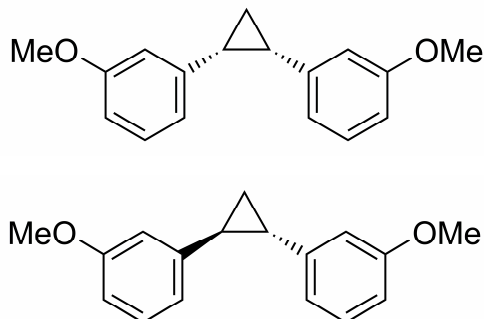
¹H-NMR (400 MHz, CDCl₃, δ/ppm) 3.86 (s, 3H), 3.89 (s, 3H), 6.95-7.80 (m, 10H)

¹³C-NMR (100 MHz, CDCl₃, δ/ppm) 55.8, 55.9, 113.3, 113.9, 116.7, 119.7, 121.4, 121.5, 122.8, 130.0, 130.4, 136.7, 140.0, 145.2, 160.3, 160.4, 190.6

EI-MS *m/z* (%) = 268.1 (100) [M⁺], 237.1 (63) [M⁺ - CH₃O], 161.1 (33)

***cis*-1,2-Bis(3-methoxyphenyl)cyclopropane (CP *cis*-4a) and
trans-1,2-bis-(3-methoxyphenyl)-cyclopropane (CP *trans*-4b)**

A solution of the crude 1,3-bis(3-methoxyphenyl)-2-propen-1-one (**CP 2**) (56.73g, assuming 0.210 mol) and hydrazine monohydrate (36 mL, 0.74 mmol, 3.5 equiv) in abs. EtOH (150 mL) was stirred at reflux (1 h). After cooling the reaction mixture down to room temperature, the solvent was evaporated under reduced pressure. Then, KOH (1.50 g, 26.73 mmol, 12.7 mol%) and diethylene glycol (100 mL) were added and the mixture was stirred at 190-210 °C. After 1 h the production of N₂ stopped and TLC showed full conversion of the starting material. The reaction mixture was cooled to room temperature, water (400 mL) was added and the product was extracted with *t*-BME/hexane (1:1, 3 x 120 mL). The combined organic phases were washed with water (3 x 50 mL), brine (1 x 200 mL) and dried over MgSO₄. After evaporating the solvent, the crude product was obtained as a yellow syrup which was purified by flash chromatography (silica, hexane/*t*-BME, 3:1) to afford a mixture of the *cis/trans*-isomers of 1,2-bis(3-methoxyphenyl)cyclopropane **CP *cis*-4a/*trans*-4b** (49.59 g, 0.195 mol, 93% over two steps) as a colorless oil. The ratio of the isomer-composition was determined by ¹H NMR spectroscopy: *cis/trans* = 44:56.



MF C₁₇H₁₈O₂, **MW** 254.32 g/mol

TLC R_f 0.52 (hexane/*t*-BME, 3:1)

¹H NMR (400 MHz, CDCl₃, δ/ppm) **CP *cis*-4a**: 1.34 (dt, 1H, ²J = 6.0, ³J = 6.4), 1.46 (pseudo q (dt), 1H, ²J = 6.0, ³J = 8.6), 2.46 (dd, 2H, ³J = 8.6, ³J = 6.4), 3.66 (s, 6H), 6.49-6.53 (m, 2H), 6.61-6.67 (m, 4H), 6.98-7.06 (m, 2H); **CP *trans*-4b**: 1.44 (m, 2H), 2.14 (m, 2H), 3.84 (s, 6H), 6.70-6.80 (m, 6H), 7.21-7.27 (m, 2H)

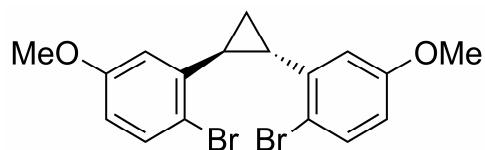
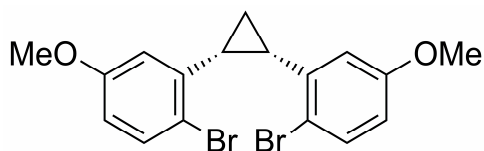
¹³C NMR (100 MHz, CDCl₃, δ/ppm) **CP *cis*-4a**: 12.3, 24.8, 55.4, 111.9, 114.8, 122.0, 140.6, 159.5; **CP *trans*-4b**: 18.6, 28.5, 55.6, 111.5, 112.1, 118.6, 129.0, 129.8, 144.6, 160.2

EI-MS *m/z* (%) = 254.1 (100) [M⁺], 239.1 (31) [M⁺ - CH₃], 223.1 (58) [M⁺ - CH₃O], 145.1 (24), 115.1 (23)

EA Analysis calcd for C₁₇H₁₈O₂: C 80.29, H 7.13; found: C 80.24, H 7.18

***cis*-1,2-Bis(2-bromo-5-methoxyphenyl)cyclopropane (CP *cis*-5a) and *trans*-bis(2-bromo-5-methoxyphenyl)cyclopropane (CP *trans*-5b)**

To a solution of *cis/trans*-1,2-bis(3-methoxy-phenyl)cyclopropane **CP *cis*-4a/*trans*-4b** (2.36 g, 9.28 mmol) and pyridine (3.0 mL, 37.24 mmol, 4.0 equiv) in CH₂Cl₂ was



added dropwise bromine at -10 °C. After the addition was completed, the reaction mixture was stirred at room temperature for another 2 h and then quenched with sat. NaHCO₃ solution. The phases were separated and the water phase was extracted with CH₂Cl₂. The combined organic phases were dried over MgSO₄ and the

solvent was evaporated on the rotary evaporator. The remaining pyridine was co-evaporated with toluene and the products were separated by flash column chromatography (silica, CHCl₃ in hexane, gradient: 15-100%). *trans*-Bis(2-bromo-5-methoxyphenyl)cyclopropane **CP *trans*-5b** (1.00 g, 2.43 mmol, 26%) was obtained as white solid material, which was recrystallized from hexane to obtain crystals. *cis*-1,2-Bis(2-bromo-5-methoxyphenyl)-cyclopropane **CP *cis*-5a** was obtained as a yellow oil (1.50 g, 3.64 mmol, 45%).

For further purification, the *cis*-isomer was dissolved in hot hexane, cooled down over night and the formed fine crystals were removed by filtration. After evaporation of the solvent, the *cis*-fraction remained as yellow oil which was sufficiently pure for the next step.

***trans*-Bis(2-bromo-5-methoxyphenyl)cyclopropane CP *trans*-5a:**

MF C₁₇H₁₆Br₂O₂, **MW** 412.12 g/mol

TLC *R_f* 0.08 (hexane/CHCl₃, 7:3)

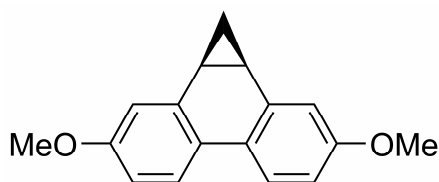
¹H NMR (400 MHz, CDCl₃, δ/ppm) 1.40 (m, 2H), 2.44 (m, 2H) 3.77 (s, 6H), 6.65 (dd, 2H, ³J = 8.7, ⁴J = 3.0), 6.75 (d, 2H, ⁴J = 3.0), 7.45 (d, 2H, ³J = 8.7)

¹³C NMR (100 MHz, CDCl₃, δ/ppm) 17.6, 27.5, 55.9, 113.3, 113.6, 116.7, 133.4, 142.3, 159.5

EI-MS *m/z* (%) = 409.9 (34), 411.9 (64), 413.9 (34) [M⁺]

EA Analysis calcd for C₁₇H₁₆Br₂O₂: C 49.54, H 3.91; found: C 49.63, H 3.96

cis*-1,2-Bis(2-bromo-5-methoxyphenyl)cyclopropane CP *cis*-5b:*MF** C₁₇H₁₆Br₂O₂, **MW** 412.12 g/mol**M.p.** 64-65 °C**TLC** *R_f* 0.12 (hexane/CHCl₃, 7:3)**¹H NMR** (400 MHz, CDCl₃, δ/ppm) 1.40 (dt, 1H, ²J = 6.0, ³J = 6.6), 1.63 (dt, 1H, ²J = 6.0, ³J = 8.6), 2.77 (dd, ³J = 8.6, ³J = 6.6, 2H), 3.55 (s, 6H), 6.30 (d, ⁴J = 3.0, 2H), 6.52 (dd, ³J = 8.7, ⁴J = 3.0, 2H), 7.32 (d, ³J = 8.7, 2H)**¹³C NMR** (100 MHz, CDCl₃, δ/ppm) 13.6, 26.3, 55.6, 114.0, 114.9, 117.9, 133.3, 138.8, 158.6**EI-MS** *m/z* (%) = 409.9 (34), 411.9 (63), 413.9 (33) [M⁺]**EA** Analysis calcd for C₁₇H₁₆Br₂O₂: C 49.54, H 3.91; found: C 49.49, H 3.80

3,8-Dimethoxy-1a,9b-dihydro-1H-cyclopropa[*l*]phenanthrene (CP 6)

Under inert atmosphere **CP cis-5a** (1.22 g, 2.96 mmol) was dissolved in dry *Me*THF (180 mL). The solution was cooled to -50 °C in a dry ice/acetone bath and *t*-BuLi (7.4 mL, 11.84 mmol,

4.0 equiv) was added dropwise. After the addition was completed the red solution was stirred at this temperature for another 30 min. A fresh solution of LiBr (538 mg, 6.20 mmol, 2.1 equiv) and CuCN (556 mg, 6.21 mmol, 2.1 equiv) in *Me*THF (10 mL) was prepared. The green solution was transferred to the reaction mixture over 5 min while keeping the reaction temperature below -50 °C. The cloudy reaction mixture was then stirred for another 20 min at -20 °C and then cooled again to -60 °C. 1,3-Dinitrobenzene (1.04 g, 6.19 mmol, 2.1 equiv) was added at once and the cooling was removed. After stirring overnight, the black reaction mixture was quenched with a mixture of NH₄Cl (50 mL, 10%) and NH₄OH (50 mL, 25%). The layers were separated and the water phase was extracted with *t*-BME (3 x 50 mL). The combined organic layers were washed with water, brine and dried over MgSO₄. After evaporation of the solvent a flash chromatography (silica, *t*-BME in hexane, 0-20%) was performed to obtain **CP 6** as a white solid (220 mg, 0.87 mmol, 29%). Recrystallization of an impure fraction from the chromatography afforded again **CP 6** (50 mg, 0.20 mmol, 7%) as fine crystals. Single crystals of the methoxy functionalized **CP 6** were grown from cyclohexane using the slow evaporation technique.

MF C₁₇H₁₆O₂, **MW** 252.31 g/mol

M.p. 138-139 °C

TLC *R*_f 0.42 (hexane/*t*-BME, 85:15)

¹H NMR (400 MHz, CDCl₃, δ/ppm) -0.01(m, 1H),

1.56 (td, 1H, ²J = 3.9, ³J = 8.9), 2.50 (dd, 2H, ³J₁ = 4.9, ³J₂ = 8.9), 3.85 (s, 6H),

6.82 (dd, 2H, ³J = 8.8, ⁴J = 2.8), 6.99 (d, 2H, ⁴J = 2.8), 7.81(d, 2H, ³J = 8.8)

¹³C NMR (100 MHz, CDCl₃, δ/ppm) 13.0, 20.2, 55.7, 112.5, 113.9, 122.8, 124.3,

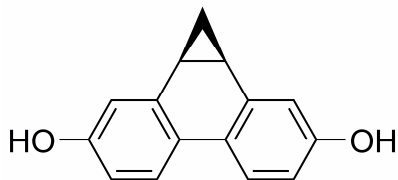
137.3, 159.0

EI-MS *m/z* (%) = 252.1(72) [M⁺], 237.1 (46), 219.2 (100), 191.1 (25), 165.1 (15)

EA Analysis calcd for C₁₇H₁₆O₂: C 80.93, H 6.39; found: C 80.71, H 6.69

3,8-Dihydroxy-1a,9b-dihydro-1*H*-cyclopropa[*l*]phenanthrene (CP 7)

Under inert atmosphere *n*-propanethiol (1.1 mL, 12.15 mmol, 10.2 equiv) was dissolved in dry DMF. Then NaH dispersion (171 mg, 4.3 mmol, 3.6 equiv, 60%) was carefully added and the reaction mixture was stirred until all of the hydride was dissolved. Then **CP 6** (300 mg, 1.19 mmol) was added and the reaction mixture was stirred at 140 °C for 14 h, cooled to room temperature and diluted with water (40 mL). The slurry was extracted with ethyl acetate (4 x 20 mL). The combined organic phases were washed with diluted brine (1 x 40 mL), filtered over glass wool and the solvent was removed on the rotary evaporator. The crude product was purified by flash chromatography (silica, ethyl acetate/hexane, gradient: 50-100%) which afforded 3,8-dihydroxy-1a,9b-dihydro-1*H*-cyclopropa[*l*]phenanthrene **CP 7** as a off-white solid (192 mg, 0.86 mmol, 72%).



MF C₁₅H₁₂O₂, **MW** 224.25 g/mol

M.p. 241 °C (decomp)

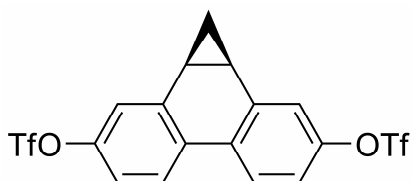
TLC *R_f* 0.46 (*t*-BME/hexane, 4:1)

¹H NMR (400 MHz, CD₃CN, δ/ppm) -0.06 (m, 1H), 1.64 (td, 1H, ²J = 3.6, ³J = 8.9), 2.59 (dd, 2H, ³J₁ = 4.9, ³J₂ = 8.9), 6.81 (dd, 2H, ³J = 8.8, ⁴J = 2.8), 7.00 (d, 2H, ⁴J = 2.8), 7.86 (d, 2H, ³J = 8.8)

¹³C NMR (100 MHz, CD₃CN, δ/ppm) 13.4, 20.4, 114.5, 116.2, 122.9, 125.2, 138.2, 157.1.

EI-MS *m/z* (%) = 224.1 (100) [M⁺], 207.1 (9) [M⁺ - OH], 165.1 (9)

**3,8-Di(trifluoromethanesulfonyloxy)-
1a,9b-dihydro-1H-cyclopropa[*l*]phenanthrene (CP 8)**



The diol **CP 7** (170 mg, 0.76 mmol) was dissolved in dry pyridine (8 mL). The solution was cooled to 0 °C and triflic anhydride (512 μ L, 3.04 mmol, 4.0 equiv) was slowly added dropwise to the solution. The reaction was stirred for another hour at room temperature and quenched with aqueous NaHCO₃. The slurry was extracted with *t*-BME and the combined organic phases were filtered through a short silica pad. The solvent was evaporated on the rotary evaporator which afforded the triflate **CP 8**, which crystallized upon standing at room temperature (368 mg, 0.75 mmol, 99%).

MF C₁₇H₁₀F₆O₆S₂, **MW** 488.38 g/mol

M.p. 103-105 °C

TLC *R_f* 0.60 (*t*-BME/hexane, 1:1)

¹H NMR (400 MHz, CDCl₃, δ /ppm) 0.02 (pseudo q, 1H, ³J = 4.4),

1.74 (dt, 1H, ²J = 4.4, ³J = 8.9), 2.56 (dd, 2H, ³J₁ = 5.0, ³J₂ = 8.9),

7.17 (dd, 2H, ³J = 8.9, ⁴J = 2.7), 7.36 (d, 2H, ⁴J = 2.7), 7.94 (d, 2H, ³J = 8.9)

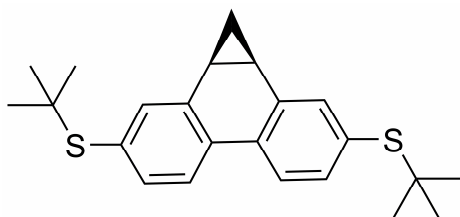
¹³C NMR (100 MHz, CDCl₃, δ /ppm) 13.5, 20.4, 119.2 (q, J = 359), 119.4, 122.1,

125.9, 128.6, 139.4, 149.6

¹⁹F NMR (376 MHz, CDCl₃, δ /ppm) -73.06

EI-MS *m/z* (%) = 488.0 (35) [M⁺], 355.0 (100) [M⁺ - SOCF₃], 194.1 (23), 165.1 (22)

3,8-Di-(*tert.*-butylsulfanyl)-1a,9b-dihydro-1*H*-cyclopropa[*h*]phenanthrene (CP 9)



Under an inert atmosphere **CP 8** (225 mg, 0.46 mmol) was dissolved in degassed *p*-xylene (10 mL). Pd₂(dba)₃·CHCl₃ (48 mg, 46 μmol, 10.0 mol%), xantphos (32 mg, 55 μmol, 12.0 mol%) and sodium *tert.*-thiobutanolate (206 mg, 1.84 mmol, 4.0 equiv) were added. The reaction mixture was stirred at 140 °C for 16 h. The solvent was co-evaporated with toluene and the residue was applied to a flash column chromatography (silica, *t*-BME in hexane, gradient 0-5%) which afforded **CP 9** (115 mg, 0.31 mmol, 68%) as a yellow solid.

MF C₂₃H₂₈S₂, **MW** 368.60 g/mol

M.p. 108-109 °C

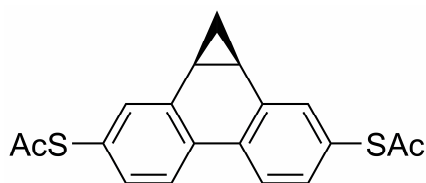
TLC *R_f* 0.56 (hexane/*t*-BME, 95:5)

¹H NMR (400 MHz, CDCl₃, δ/ppm) -0.06 (pseudo q, 1H, ³J = 3.6), 1.33 (s, 16H), 1.62 (dt, 1H, ²J = 3.6, ³J = 8.9), 2.56 (dd, 2H, ³J₁ = 4.9, ³J₂ = 8.9), 7.40 (dd, 2H, ³J = 8.9, ⁴J = 2.7), 7.60 (d, 2H, ⁴J = 2.7), 7.89 (d, 2H, ³J = 8.9)

¹³C NMR (100 MHz, CDCl₃, δ/ppm) 13.4, 20.0, 31.5, 46.6, 123.8, 129.6, 132.8, 135.3, 137.1, 138.3

EI-MS *m/z* (%) = 368.2 (39) [M⁺], 312.1 (10) [M⁺ - C₄H₈], 256.0 (100) [M⁺ - 2 C₄H₈], 223.1 (25) [M⁺ - 2 C₄H₈, - SH]

**3,8-Di-(acetylsulfanyl)-
1a,9b-dihydro-1H-cyclopropa[*l*]phenanthrene (CP 10)**



To a solution of **CP 9** (105 mg, 0.29 mmol) in dry toluene (25.0 mL) and acetyl chloride (10.0 mL, 0.141 mol) was added dropwise a solution of BBr_3 (67 μL , 0.71 mmol, 2.4 equiv) at 0 °C. After the addition was completed the cooling was removed and the reaction mixture was stirred another 30 min at room temperature until all starting material was gone (monitored by TLC). Then, anhydrous sodium acetate (800 mg, 9.75 mmol, 33.6 equiv) was added and the solvent was evaporated under reduced pressure. The residue was taken up in a mixture of CH_2Cl_2 (5.0 mL) and acetyl chloride (15.0 mL, 0.210 mol). Then silica (2.00 g) was added and the solvent was evaporated. The remaining material was immediately applied on a flash column (silica, *t*-BME in hexane, gradient 30-60%). The acetyl protected **CP 1** was afforded as yellow powder (56 mg, 0.16 mmol, 58%).

MF $\text{C}_{19}\text{H}_{16}\text{O}_2\text{S}_2$, **MW** 340.46 g/mol

M.p. 142-144 °C

TLC R_f 0.23 (hexane/*t*-BME, 2:1)

$^1\text{H NMR}$ (250 MHz, CDCl_3 , δ/ppm) -0.02 (pseudo q, 1H, $^3J = 5.0$),

1.62 (dt, 1H, $^2J = 4.1$, $^3J = 8.9$), 2.45 (s, 6H), 2.56 (dd, 2H, $^3J_1 = 5.0$, $^3J_2 = 8.9$),

7.30 (dd, 2H, $^3J = 8.4$, $^4J = 1.9$), 7.50 (d, 2H, $^4J = 1.9$), 7.98 (d, $^3J = 8.4$, 2H)

$^{13}\text{C NMR}$ (100 MHz, CDCl_3 , δ/ppm) 13.3, 20.1, 30.7, 124.7, 127.9, 130.2, 132.3, 135.2, 138.0, 194.5

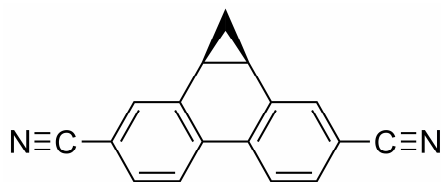
EI-MS m/z (%) = 340.1 (39) [M^+], 298.1 (34) [$\text{M}^+ - \text{CH}_3\text{CO}$], 256.1 (100)

[$\text{M}^+ - 2 \text{CH}_3\text{CO}$], 223.1 (30) [$\text{M}^+ - 2 \text{CH}_3\text{CO}, -\text{SH}$]

EA Analysis calcd for $\text{C}_{19}\text{H}_{16}\text{O}_2\text{S}_2$: C 67.03, H 4.74; found: C 67.08, H 4.80

UV/Vis (1×10^{-5} *n*-hexane) λ_{max} (ϵ) = 220 (32900), 302 (22500), 322 (17200), 334 (16200) nm

3,8-Dicyano-1a,9b-dihydro-1H-cyclopropa[*l*]phenanthrene (CP 14)



The triflate **CP 8** was converted to **CP 14** according to cyanation *method A* (see synthetic protocol for **CN 3**). The reaction was kept at 80°C for 90 min to convert all starting material. **CP 14** was purified by flash column chromatography (silica, *t*-BME/hexane, 1:1) to give a white solid. Recrystallization from a mixture of dioxane and cyclohexane using the slow evaporation technique gave single crystals suitable for X-ray analysis (yield: 15%).

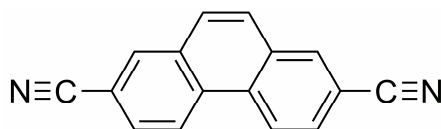
MF C₁₇H₁₀N₂, **MW** 242.27 g/mol

¹H NMR (400 MHz, CDCl₃, δ/ppm) -0.05 (pseudo q, 1H, ³J = 4.7), 1.79 (dt, 1H, ²J = 4.4, ³J = 8.9), 2.64 (dd, 2H, ³J₁ = 5.0, ³J₂ = 8.9), 7.57 (dd, 2H, ³J = 8.3, ⁴J = 1.7), 7.50 (d, 2H, ⁴J = 1.7), 8.03 (d, ³J = 8.4, 2H)

¹³C NMR (100 MHz, CDCl₃, δ/ppm) 13.7, 20.0, 112.9, 118.9, 125.1, 130.1, 132.3, 133.4, 138.5

EI-MS *m/z* (%) = 242.1 (100) [M⁺]

2,7-Dicyano-phenanthrene (CP 16)

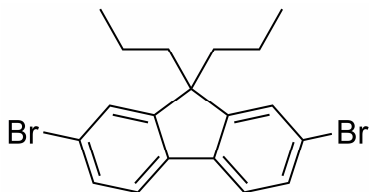


2,7-Dibromo-phenanthrene (**CP 10**) was converted to **CP 16** by applying cyanation *method B* yielding 2,7-dicyano-phenanthrene **CP 16** in 27% yield after column chromatography (silica, CH₂Cl₂/ethyl acetate 9:1).

MF C₁₆H₈N₂, **MW** 228.07 g/mol

¹H NMR (400 MHz, CDCl₃, δ/ppm) 7.88 (s, 2H), 7.92 (dd, 2H, ³J = 8.6, ⁴J = 1.4), 8.30 (d, 2H, ⁴J = 1.4), 8.77 (d, 2H, ³J = 8.6)

EI-MS *m/z* (%) = 228.1 (100) [M⁺]

2,7-Dibromo-9,9-di-(*n*-propyl)-fluorene (CP 17)

Under an inert atmosphere 2,7-dibromofluorene (3.00 g, 9.26 mmol) and *n*-propylbromide (3.4 mL, 37.40 mmol, 4.0 equiv) was dissolved in dry THF (20 mL). The mixture was cooled to 0-5 °C and a solution of *t*-BuOK (2.34g, 20.84 mmol, 2.3 equiv) in dry THF (20 mL) was

added drop wise while vigorous stirring. The yellow reaction mixture was stirred at 5 °C for another 30 min, filtered through a short silica pad and the remained precipitate was washed with *t*-BME. The filtrate was evaporated and the residue was recrystallized from abs. EtOH (70 mL). 2,7-Dibromo-9,9-di-(*n*-propyl)-fluorene **CP 17** was obtained as fine off-white needles (2.45 g, 6.00 mmol, 65%).

MF C₁₉H₂₀Br₂, **MW** 408.17 g/mol

M.p. 138-139 °C

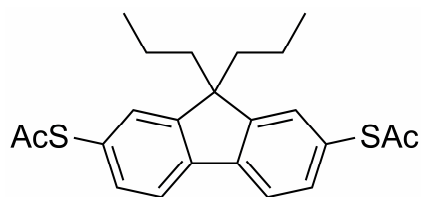
TLC *R_f* 0.58 (hexane)

¹H NMR (400 MHz, CDCl₃, δ/ppm) 0.61-0.72 (m, 10H), 1.89-1.93 (m, 4H), 7.44-7.53 (m, 4H), 7.51 (d, 2H, ³J = 8.5)

¹³C NMR (100 MHz, CDCl₃, δ/ppm) 14.7, 17.5, 42.9, 56.3, 121.5, 121.9, 126.6, 130.6, 139.5, 153.0

EI-MS *m/z* (%) = 405.9 (46), 408.0 (91), 409.9 (45) [M⁺]

EA Analysis calcd for C₁₉H₂₀Br₂: C 55.91, H 4.94; found: C 55.82, H 4.90

2,7-Bis-(acetylsulfanyl)-9,9-di-(*n*-propyl)-fluorene (CP 18)

2,7-Dibromo-9,9-di-(*n*-propyl)-fluorene **CP 17** (0.80 g, 1.96 mmol) and sodium methanethiolate (1.50 g, 21.43 mmol, 10.9 equiv) was suspended in dry and degassed DMI. The reaction mixture was stirred at 140 °C under N₂ atmosphere for 15 h. After addition of acetyl chloride at 0 °C (3.0 mL, 42.19 mmol, 21.5 equiv) the solution was stirred at room temperature for 1.5 h and then poured on ice. The aqueous phase was extracted with toluene, the organic extracts were dried over MgSO₄ and the solvent was removed. The product was purified by flash chromatography (silica gel, hexane/*t*-BME, 4:1). The product was further purified by recrystallization from hot hexane. 2,7-Bis-(acetylsulfanyl)-9,9-di-(*n*-propyl)-fluorene **CP 18** (174 mg, 0.44 mmol, 22%) was obtained as yellow crystals.

MF C₂₃H₂₆O₂S₂, MW: 398.58.

M.p. 100-101 °C.

TLC *R_f* 0.58 (hexane/*t*-BME, 4:1).

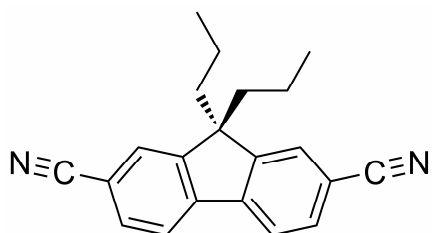
¹H NMR (400 MHz, CDCl₃, δ/ppm) 0.61-0.72 (m, 10H), 1.92-1.97 (m, 4H), 2.44 (s, 6H), 7.37-7.40 (m, 4H), 7.71-7.74 (m, 2H)

¹³C NMR (100 MHz, CDCl₃, δ/ppm) 14.9, 17.6, 30.6, 42.8, 56.1, 121.1, 127.5, 129.5, 133.6, 141.7, 152.3, 194.6

EI-MS *m/z* (%) = 398.1 (60) [M⁺], 356.1 (53), 314.1 (100), 271.0 (17), 238.0 (29).

EA Analysis calcd for C₂₃H₂₆O₂S₂: C 69.31, H 6.57; found: C 69.08, H 6.58.

UV/Vis (1 × 10⁻⁵ *n*-hexane) λ_{max} (ε) = 214 (36200), 293 (24700), 317 (28800) nm

2,7-Dicyano-9,9-di(*n*-propyl)-fluorene (CP 19)

CP 19 was obtained from 2,7-dibromo-9,9-di(*n*-propyl)-fluorene **CP 17** according to cyanation *method B* in 67% yield after recrystallization from a hot mixture of ethanol and water. These crystals were suitable for X-ray measurement.

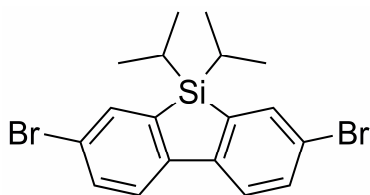
MF C₂₁H₂₀N₂, **MW** 300.40 g/mol

¹H NMR (400 MHz, CD₃CN, δ/ppm) 0.45-0.66 (m, 10 H), 2.03-2.07 (m, 4H), 7.75-7.77 (m, 2H), 7.84-7.85 (m, 2H), 7.97-7.99 (m, 2H)

¹³C NMR (100 MHz, CD₃CN, δ/ppm) 13.8, 17.2, 41.9, 56.6, 111.9, 119.6, 122.1, 127.7, 132.1, 144.0, 152.4

EI-MS *m/z* (%) = 300.2 (40) [M⁺]

EA Analysis calcd for C₂₁H₂₀N₂: C 83.96, H 6.71, N 9.33; found: C 83.10, H 7.05, N 9.14

3,7-Dibromo-5,5-diisopropyl-5H-dibenzosilole (CP 23)

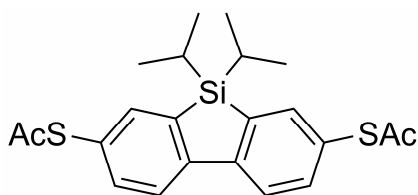
t-Butyllithium (13.30 mL, 21.28 mmol, 4.0 equiv) was added over 30 min to a stirring solution of **CP 20**³¹⁹ (3.0 g, 5.32 mmol) in dry THF (80 mL) at -60 °C, under a nitrogen atmosphere. The mixture was stirred for additional 30 min at -60 °C. Then, dichloro-diisopropylsilane (1.182 g, 6.39 mmol, 1.2 equiv) was added over a period of 5 min. Stirring was continued for 10 min at -60 °C and then 1.5h at room temperature. The reaction mixture was then quenched with sat. NaHCO₃ (100.0 mL) and the phases were separated (re-extracted with *t*-BME). The combined organic layers were washed with brine, dried over anhydrous Na₂SO₄, filtered, and concentrated in vacuo giving the crude product as a brownish oil. Recrystallization from hot hexane gave the dibromide **CP 23** in a yield of 56%. Long needles suitable for X-ray analysis were grown from hexane using the slow evaporation technique.

MF C₁₈H₂₀Br₂Si, **MW** 424.24 g/mol

¹H NMR (400 MHz, CDCl₃, δ/ppm) 1.02 (d, 12H, ³J = 7.4), 1.37 (m, 2H), 7.53 (dd, 2H, ³J = 8.3, ⁴J = 2.0), 7.63 (d, 2H, ³J = 8.3), 7.67 (d, 2H, ⁴J = 2.0)

EI-MS *m/z* (%) = 422.0 (20), 224.0 (41), 426.0 (21) [M⁺]

EA Analysis calcd for C₁₈H₂₀Br₂Si: C 50.96, H 4.75; found: C 50.97 H 4.74

3,7-Di-(acetylsulfanyl)-5,5-diisopropyl-5H-dibenzosilole (CP 24)

CP 23 (200 mg, 0.47 mmol), potassium thioacetate (164 mg, 1.41 mmol, 3.0 equiv), $\text{Pd}_2(\text{dba})_3 \cdot \text{CHCl}_3$ (24 mg, 24 μmol , 5 mol%) and xantphos (27 mg, 47 μmol , 10 mol%) were placed in a microwave tube capped with a rubber septum. The tube was evacuated under vacuum and refilled with nitrogen. Then, dry and degassed 1,4-dioxane (8 mL) and *Hünig's* base (164 μL , 0.94 mmol, 2.0 equiv) were added to the tube and the rubber septum was quickly replaced with a microwave tube cap. The reaction mixture was heated in a microwave at 160 °C for 25 min. Then, anhydrous MgSO_4 (0.50 g) was added and the reaction mixture was concentrated in vacuo. The crude material was purified by repetitive flash chromatography on silica gel: 1.) hexane, *t*-BME, CH_2Cl_2 (75:20:5), 2.) hexane, *t*-BME, CH_2Cl_2 (89:10:1), 3.) hexane, CHCl_3 (60-100% CHCl_3) to give 3,7-di-(acetylsulfanyl)-5,5-diisopropyl-5H-dibenzosilole **CP 24** as an oily solid (42 mg, 22%). Almost colorless crystals were obtained by recrystallization from methyl-cyclohexane. Unfortunately these crystals were not suitable for the X-ray measurement.

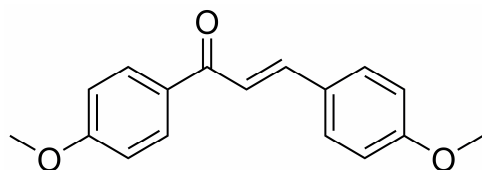
MF $\text{C}_{22}\text{H}_{26}\text{O}_2\text{S}_2\text{Si}$, **MW** 414.66g/mol

$^1\text{H NMR}$ (400 MHz, CDCl_3 , δ/ppm) 1.04 (d, 12H, $^3\text{J} = 7.4$), 1.40 (m, 2H), 2.44 (s, 6H), 7.48 (dd, 2H, $^3\text{J} = 8.1$, $^4\text{J} = 1.7$), 7.62 (d, 2H, $^4\text{J} = 1.7$), 7.85 (d, 2H, $^3\text{J} = 8.1$)

$^{13}\text{C NMR}$ (100 MHz, CDCl_3 , δ/ppm) 11.4, 18.5, 30.7, 122.4, 127.6, 136.4, 138.2, 139.7, 149.4, 194.5

EI-MS m/z (%) = 414.1(100) [M^+]

EA Analysis calcd for $\text{C}_{22}\text{H}_{26}\text{O}_2\text{S}_2\text{Si}$: C 63.73, H 6.32; found: C 64.08 H 6.52

4,4'-Dimethoxychalcone**(1,3-Bis(4-methoxyphenyl)prop-2-en-1-one) (CP 25)**

Under ice cooling a solution of NaOH (14.0 mL, 0.268 mol, 2.0 equiv, 50%) was slowly added to a mixture of *p*-acetylanisole (20.00 g, 0.133 mol) and *p*-anisaldehyde (18.30 g, 0.134 mol) in EtOH (250 mL). The reaction mixture stirred at room temperature over night. After cooling the mixture in the fridge, the precipitated solid was filtered off, washed with cold EtOH and dried *in vacuo* yielding 4,4'-dimethoxychalcone (**CP 25**) (26.80 g, 99.88 mmol, 75%) as a yellow solid.

MF C₁₇H₁₆O₃, **MW** 268.31 g/mol

M.p. 104–106 °C

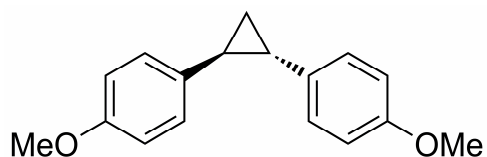
TLC *R_f* = 0.38 (silica, hexane/ethyl acetate, 1:1)

¹H NMR (250 MHz, CDCl₃, δ/ppm) 3.86 (s, 3H), 3.89 (s, 3H), 6.91-7.01 (m, 4H), 7.43 (d, 1H, ³J = 15.6), 7.57-7.63 (m, 2H), 7.78 (d, 1H, ³J = 15.6), 8.01-8.06 (m, 2H)

¹³C NMR (100 MHz, CDCl₃, δ/ppm) 55.57, 55.64, 113.9, 114.5, 119.7, 128.0, 130.3, 130.9, 131.5, 144.0, 161.7, 163.4, 188.9

EI-MS *m/z* (%) = 368.1 (100) [M⁺], 253.1 (31) [M⁺ -CH₃], 237.1 (16) [M⁺ -CH₃O], 225.1 (15), 161.1 (15), 135.0 (25)

EA Analysis calculated for C₁₇H₁₆O₃: C 76.10, H 6.01; found: C 76.04, H 6.07

***trans*-1,2-Bis(4-methoxyphenyl)cyclopropane (CP 26)**

A solution of 4,4'-dimethoxychalcone **CP 25** (20.00 g, 74.45 mmol) and hydrazine monohydrate (12.0 mL, 0.247 mol, 3.3 equiv) in EtOH (60 mL) was stirred at reflux for 2 hours.

The reaction mixture was cooled to room temperature and the solvent was evaporated under reduced pressure. Then, powdered KOH (0.63 g, 11.22 mmol, 15.1 mol%) and diethylene glycol (50 mL) was added and the mixture was stirred at 190-210 °C. After 45 min the reaction was completed (monitored by TLC) and the reaction mixture was cooled to room temperature. Water (100 mL) was added to the mixture and the product was extracted with hexane/*t*-BME 1:1 (3 x 30 mL). The combined organic phases were washed with water (3 x 20 mL), brine (1 x 80 mL) and dried over MgSO₄. After evaporating the solvent, the remaining crude product was recrystallized from hot cyclohexane to afford pure *trans*-1,2-bis(4-methoxyphenyl)cyclopropane (**CP 26**) (5.69 g, 22.37 mmol, 30%) as bright yellow crystals.

MF C₁₇H₁₈O₂, **MW** 254.32 g/mol

M.p. 70-75 °C

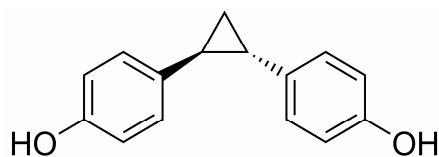
TLC (silica, Hexane/*t*-BME 3:2) *R_f* = 0.58

¹H-NMR (250 MHz, CDCl₃, δ/ppm) 1.31-1.38 (m, 2H), 2.03-2.11 (m, 2H), 3.81 (s, 6H), 6.83-6.90 (m, 4H), 7.06-7.13 (m, 4H)

¹³C NMR (101 MHz, CDCl₃, δ/ppm) 17.6, 27.0, 55.5, 114.0, 127.0, 134.9, 158.0

EI-MS *m/z* (%) = 254.1 (100) [M⁺], 239.1 (48) [M⁺ -CH₃], 223.1 (48) [M⁺ -CH₃O], 145.1 (23)

EA Analysis calculated for C₁₇H₁₈O₂: C 80.29, H 7.13; found: C 79.92, H 7.11

***trans*-1,2-Bis(4-hydroxyphenyl)cyclopropane (CP 27)**

Under an inert atmosphere, NaH dispersion (1.69 g, 42.25 mmol, 3.6 equiv, 60%) was added in portions to a solution of *n*-propanethiol (10.7 mL, 0.118 mol, 10.0 equiv) in dry DMF (150 mL) maintaining the temperature below 20 °C. The reaction mixture was stirred for another 15 min until a clear solution was obtained. Then, *trans*-1,2-bis(4-methoxyphenyl)cyclopropane **CP 26** (3.00 g, 11.80 mmol) was added and the reaction mixture was stirred at 140 °C over night. After cooling to room temperature, the reaction mixture was diluted with water (200 mL) and extracted with EtOAc (5 x 30 mL). The combined organic phases were washed with brine/water 2:1 and dried over MgSO₄. After evaporation of the solvent a short flash chromatography (silica, hexane/EtOAc, 65:35) was performed to afford *trans*-1,2-bis(4-hydroxyphenyl)cyclopropane (**CP 27**) (1.65 g) as a yellow solid. The product containing traces of inseparable impurities was used directly for the next step without further purification.

MF C₁₅H₁₄O₂, MW 226.27 g/mol

TLC (silica, hexane/EtOAc, 65:35) *R_f* = 0.61

M.p. 147-150 °C

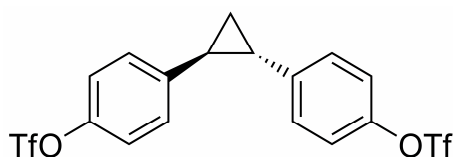
¹H-NMR (250 MHz, DMSO-d₆, δ/ppm) 1.18-1.28 (m, 2H), 1.90-1.98 (m, 2H), 6.63-6.70 (m, 4H), 6.91-6.98 (m, 4H), 9.14 (s, 2H)

¹³C NMR (100 MHz, DMSO-d₆, δ/ppm) 17.6, 26.5, 115.1, 126.4, 132.6, 155.2

EI-MS *m/z* (%) = 226.1 (100) [M⁺], 209.1 (19) [M⁺ -OH], 131.1 (37), 107.1 (28)

EA Analysis calculated for C₁₅H₁₄O₂: C 79.62, H 6.24; found: C 78.61, H 7.44

***trans*-1,2-Bis(4-trifluoromethanesulfonyloxyphenyl)-
cyclopropane (CP 28)**



In a dry flask and under an inert atmosphere was dissolved *trans*-1,2-bis(4-hydroxyphenyl)cyclopropane **CP 27** (700 mg, assuming 5.00 mmol) from the previous step in dry pyridine (30 mL).

Then triflic anhydride (2.1 mL 12.40 mmol, 4.00 equiv) was slowly dropped to the solution at 0 °C. After stirring at room temperature for another hour, the solution was quenched with sat NaHCO₃ solution. The slurry was extracted with CH₂Cl₂ (3 x 50 mL) and the combined organic phases were dried over MgSO₄. After evaporation of the solvent under reduced pressure a flash chromatography (silica, hexane/CH₂Cl₂, 7:3) was performed to afford *trans*-1,2-bis(4-trifluoromethanesulfonyloxyphenyl)cyclopropane (**CP 28**) (0.75 g, 1.53 mmol, 31% over two steps) as a colorless solid.

MF C₁₇H₁₂F₆O₆S₂, **MW** 490.39 g/mol

M.p. 56-60 °C

TLC (SiO₂, hexane/CH₂Cl₂ 7:3) *R_f* = 0.37

¹H NMR (250 MHz, DMSO-d₆, δ/ppm) 1.54-1.52 (m, 2H), 2.34-2.41 (m, 2H), 7.35-7.43 (m, 8H)

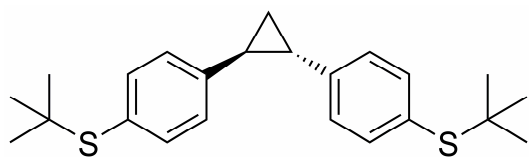
¹³C NMR (100 MHz, DMSO-d₆, δ/ppm) 19.3, 27.5, 118.2 (q, J = 319), 121.3, 127.6, 143.2, 147.3

EI-MS *m/z* (%) = 490.0 (98) [M⁺], 357.1 (100) [M⁺ - SO₂CF₃], 224.1 (54)

EA Analysis calculated for C₁₇H₁₂F₆O₆S₂: C 41.64, H 2.47; found: C 41.71, H 2.52

***trans*-1,2-Bis(4-*tert*-butylsulfanylphenyl)cyclopropane (CP 29)**

Under an inert atmosphere **CP 28** (220 mg, 0.45 mmol) was dissolved in dry *p*-xylene (15 mL) and the solution was degassed with N₂ for 10 min. Then Pd₂(dba)₃·CHCl₃ (100 mg, 97 μmol, 21.5 mol%), xantphos (50.0 mg, 86 μmol, 19.2 mol%) and sodium *t*-thiobutanolate (211 mg, 1.88 mmol, 4.2 equiv) was added. The mixture was stirred at 140°C over night. After cooling to room temperature, toluene (20 mL) was added and the solution was washed with brine. The aqueous phase was extracted with toluene (2 x 20 mL) and the combined organic phases were dried over MgSO₄. After evaporating the solvent a flash chromatography (silica, *t*-BME in hexane, 2%) was performed to afford *trans*-1,2-bis(4-*tert*-butylsulfanylphenyl)cyclopropane (**CP 29**) (98 mg, 0.26 mmol, 59 %) as colorless solid.



MF C₂₃H₃₀S₂, **MW** 370.61 g/mol

M.p. 108-109 °C

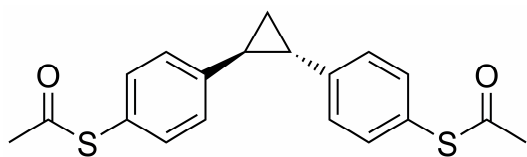
TLC (silica, *t*-BME in hexane, 2%) *R_f* = 0.32

¹H NMR (250 MHz, CDCl₃, δ/ppm) 1.28 (s, 18 H), 1.46-1.54 (m, 2H), 2.14-2.22 (m, 2H), 7.10 (pseudo d, 4H, ³J = 8.0), 7.45 (pseudo d, 2H, ³J = 8.0)

¹³C NMR (101 MHz, CDCl₃, δ/ppm) 19.1, 28.4, 31.1, 46.0, 126.0, 129.9, 137.8, 143.3.

HRMS (ESI) calcd for C₂₃H₃₀S₂ [M+H]⁺: 371.1867; found: 371.1876

***trans*-1,2-Bis(4-acetylsulfanylphenyl)cyclopropane**
(CP 30, “*trans*-OPCP”)



CP 29 (45 mg 0.12 mmol) and AcCl (5 mL) was dissolved in dry toluene (11 mL). Then, the solution was cooled to 0 °C and a solution of BBr₃ in CH₂Cl₂ (0.3 mL, 0.30 mmol, 2.5 equiv, 1.0 M) was slowly dropped to the solution. The stirring was continued at room temperature until the TLC showed full conversion of the starting material (30 min). A spatula of anhydrous sodium acetate was added to the reaction mixture and the solvent was evaporated under reduced pressure. The residue was taken up in CH₂Cl₂, then acetic anhydride (0.3 mL) and silica (2.00 g) was added. The solvent was evaporated under reduced pressure and the remained powder was directly applied on a flash column. After the chromatographic purification (silica, hexane/*t*-BME, 2:1) and a recrystallization from hot cyclohexane, *trans*-1,2-bis(4-acetylsulfanyl-phenyl)cyclopropane (**CP 30**) (28 mg, 82 μmol, 68%) was obtained as colorless fine plates.

MF C₁₉H₁₈O₂S₂, **MW** 342.48 g/mol

M.p. 107-108 °C

TLC (SiO₂, hexane/*t*-BME, 2:1) *R*_f = 0.39

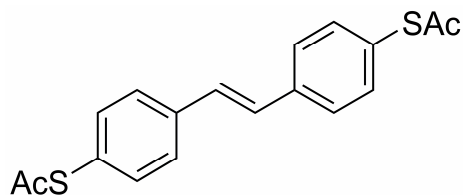
¹H NMR (250 MHz, CDCl₃, δ/ppm) 1.48-1.56 (m, 2H), 2.15-2.23 (m, 2H), 2.41 (s, 6H), 7.14-7.19 (m, 4H), 7.28-7.35 (m, 4H)

¹³C NMR (100 MHz, CDCl₃, δ/ppm) 18.9, 28.6, 30.4, 125.1, 126.8, 134.8, 144.1, 194.7

EI-MS *m/z* (%) = 342.1 [M⁺], 300.1 (76) [M⁺ - CH₃CO], 267.1 (36), 258.1 (100) [M⁺ - 2 CH₃CO], 225.1 (66), 192.1 (27)

EA Analysis calculated for C₁₉H₂₀O₂S₂: C 66.25, H 5.85; found: C 66.37, H 5.48

UV/Vis (1 × 10⁻⁵ *n*-hexane) λ_{max} (ε) = 203 (55400), 255 (29700) nm

4,4'-Diacetylsulfanyl-*trans*-stilbene (CP 31, "OPV" , via S_NAr)

Under an inert atmosphere 4,4'-dibromo-*trans*-stilbene (600 mg, 1.77 mmol) and sodium thiomethanolate (1.50 g, 21.40 mmol, 12.0 equiv) was suspended in dry DMI. The reaction mixture was stirred at 120 °C for 2 days. The reaction mixture was cooled to room temperature and poured into a solution of NH₄Cl (5%). The solid was filtered off, washed well with water. The residue was taken up in CH₂Cl₂, dried over Na₂SO₄ and the solvent was removed under reduced pressure. A recrystallization from *n*-heptane afforded **CP 31** as shiny crystals (396 mg, 1.21 mmol, 68%).

MF C₁₈H₁₆O₂S₂, **MW** 328.45 g/mol

M.p. 167-138 °C

TLC *R_f* 0.48 (CH₂Cl₂)

¹H NMR (400 MHz, CDCl₃, δ/ppm) 2.44 (s, 6 H), 7.14 (s, 2H),

7.41 (pseudo d, 4H, ³J = 8.1), 7.55 (pseudo d, 4H, ³J = 8.1)

¹³C NMR (100 MHz, CDCl₃, δ/ppm) 30.7, 127.7, 127.7, 129.6, 135.1, 138.6, 194.4

EI-MS *m/z* (%) = 328.1 (37), 286.0 (39) [M⁺ - CH₃CO], 244.0 (100) [M⁺ - 2 CH₃CO]

EA Analysis calcd for C₁₈H₁₆O₂ S₂: C 65.83, H 4.91; found: C 65.57, H 4.91

UV/Vis (1×10⁻⁵ *n*-hexane) λ_{max} (ε) = 199 (37400), 227 (20600), 326 (51800) nm

6 Abbreviations

Ac	acetyl
Ar	aryl
BPDT	biphenyldithiol
Bu	butyl
CN	cyano
cos	cosine
CP	cyclopropyl
DMF	<i>N,N</i> -dimethylformamide
DMSO	dimethylsulfoxide
EA	elemental analysis
EI	electron impact
equiv	equivalent
ESI	electron spray ionization
Et	ethyl
EtOAc	ethyl acetate
FAB	fast atom bombardment
GC	gas chromatography
HOMO	highest occupied molecular orbital
LUMO	lowest unoccupied molecular orbital
M.p.	melting point
<i>m/z</i>	mass per charge
MALDI	matrix-assisted laser desorption/ionization
MCBJ	mechanically controlled break junctions
Me	methyl
MF	molecular formula
MS	mass spectrometry
MW	molecular weight
NBS	<i>N</i> -bromosuccinimide
NC	isocyano

NMR	nuclear magnetic resonance
OPE	oligo-phenylene-ethynylene
OPV	oligo-phenylene-vinylene
Pd ₂ (dba) ₃	tris(dibenzylideneacetone)dipalladium
Ph	phenyl
PMHS	polymethylhydrosiloxane
ppm	parts per million
Pr	propyl
<i>p</i> -TSA	<i>p</i> -toluenesulfonic acid
<i>R_f</i>	retention factor
SOMO	singly occupied molecular orbital
STM	scanning tunneling microscopy
STM-BJ	break junctions based on scanning tunneling microscopy
TBAB	tetra- <i>n</i> -butylammonium bromide
TBAPF ₆	tetrabutylammonium hexafluorophosphate
<i>t</i> -BME	<i>t</i> -butyl methyl ether
TEAPF ₆	tetraethylammonium hexafluorophosphate
Tf	trifluoromethane sulfonyl
THF	tetrahydrofuran
TLC	thin layer chromatography
TosMic	<i>p</i> -toluenesulfonylmethyl isocyanide
UV/VIS	ultraviolet/ visible
xantphos	4,5-bis(diphenylphosphino)-9,9-dimethylxanthene
X-ray	X-ray spectrometry

7 Bibliography

1. G. E. Moore, *Electronics*, **1965**, 38.
2. G. Maruccio, R. Cingolani and R. Rinaldi, *J. Mater. Chem.*, **2004**, 14, 542-554.
3. *The international Technology Roadmap for Semiconductors (ITRS)*, 2009.
4. A. Hand, *Semiconductor Int.*, **2001**, 24, 62.
5. V. Ferri, M. Elbing, G. Pace, Michael D. Dickey, M. Zharnikov, P. Samorì, M. Mayor and Maria A. Rampi, *Angew. Chem. Int. Ed.*, **2008**, 47, 3407-3409.
6. M. A. Reed, *Sci. Am.*, **2000**, 292, 86.
7. G. E. Moore, Solid-State Circuits Conference, Digest of Technical Papers, IEEE International, 2003.
8. R. Compano, *Technology Roadmap for Nanoelectronics*, Information Society Technologies, Luxembourg, 2000.
9. H. Kuhn and D. Möbius, *Angew. Chem.*, **1971**, 83, 672-690.
10. A. Aviram and M. A. Ratner, *Chem. Phys. Lett.*, **1974**, 29, 277-283.
11. R. M. Metzger, *Acc. Chem. Res.*, **1999**, 32, 950-957.
12. M.-K. Ng and L. Yu, *Angew. Chem. Int. Ed.*, **2002**, 41, 3598-3601.
13. J. G. Kushmerick, D. B. Holt, J. C. Yang, J. Naciri, M. H. Moore and R. Shashidhar, *Phys. Rev. Lett.*, **2002**, 89, 086802.
14. R. E. Holmlin, R. F. Ismagilov, R. Haag, V. Mujica, M. A. Ratner, M. A. Rampi and G. M. Whitesides, *Angew. Chem.*, **2001**, 113, 2378-2382.
15. J. M. Mativetsky, G. Pace, M. Elbing, M. A. Rampi, M. Mayor and P. Samorì, *J. Am. Chem. Soc.*, **2008**, 130, 9192-9193.
16. G. Pace, V. Ferri, C. Grave, M. Elbing, C. von Hänisch, M. Zharnikov, M. Mayor, M. A. Rampi and P. Samorì, *Proc. Natl. Acad. Sci.*, **2007**, 104, 9937-9942.
17. J. Chen, M. A. Reed, A. M. Rawlett and J. M. Tour, *Science*, **1999**, 286, 1550-1552.
18. A. Mishchenko, D. Vonlanthen, V. Meded, M. Bürkle, C. Li, I. V. Pobelov, A. Bagrets, J. K. Viljas, F. Pauly, F. Evers, M. Mayor and T. Wandlowski, *Nano Lett.*, **2010**, 10, 156-163.
19. D. Vonlanthen, A. Mishchenko, M. Elbing, M. Neuburger, T. Wandlowski and M. Mayor, *Angew. Chem. Int. Ed.*, **2009**, 48, 8886-8890.
20. B. Xu and N. J. Tao, *Science*, **2003**, 301, 1221-1223.
21. Xiao, Xu and N. J. Tao, *Nano Lett.*, **2004**, 4, 267-271.
22. L. A. Bumm, J. J. Arnold, M. T. Cygan, T. D. Dunbar, T. P. Burgin, L. Jones, II, D. L. Allara, J. M. Tour and P. S. Weiss, *Science*, **1996**, 271, 1705-1707.
23. E. Lörtscher, Jacob W. Ciszek, J. Tour and H. Riel, *Small*, **2006**, 2, 973-977.
24. C. J. Muller, J. M. van Ruitenbeek and L. J. de Jongh, *Phys. C*, **1992**, 191, 485-504.

25. J. M. v. Ruitenbeek, A. Alvarez, I. Pineyro, C. Grahmann, P. Joyez, M. H. Devoret, D. Esteve and C. Urbina, *Rev. Sci. Instrum.*, **1996**, 67, 108-111.
26. R. H. M. Smit, Y. Noat, C. Untiedt, N. D. Lang, M. C. van Hemert and J. M. van Ruitenbeek, *Nature*, **2002**, 419, 906-909.
27. M. A. Reed, C. Zhou, C. J. Muller, T. P. Burgin and J. M. Tour, *Science*, **1997**, 278, 252-254.
28. J. Reichert, R. Ochs, D. Beckmann, H. B. Weber, M. Mayor and H. v. Löhneysen, *Phys. Rev. Lett.*, **2002**, 88, 176804.
29. R. Huber, M. T. González, S. Wu, M. Langer, S. Grunder, V. Horhoiu, M. Mayor, M. R. Bryce, C. Wang, R. Jitchati, C. Schönenberger and M. Calame, *J. Am. Chem. Soc.*, **2007**, 130, 1080-1084.
30. S. Wu, M. T. Gonzalez, R. Huber, S. Grunder, M. Mayor, C. Schönenberger and M. Calame, *Nat. Nanotechnol.*, **2008**, 3, 569-574.
31. C. K. Chiang, M. A. Druy, S. C. Gau, A. J. Heeger, E. J. Louis, A. G. MacDiarmid, Y. W. Park and H. Shirakawa, *J. Am. Chem. Soc.*, **1978**, 100, 1013-1015.
32. F. Cicoira and C. Santato, *Adv. Funct. Mater.*, **2007**, 17, 3421-3434.
33. R. H. Friend, R. W. Gymer, A. B. Holmes, J. H. Burroughes, R. N. Marks, C. Taliani, D. D. C. Bradley, D. A. D. Santos, J. L. Bredas, M. Logdl and W. R. Salaneck, *Nature*, **1999**, 397, 121-128.
34. D. Demus, J. Goodby, G. W. Gray, H. W. Spiess and V. Vill, *Handbook of Liquid Crystals Set*, Wiley-VCH, Weinheim, Germany, 2008.
35. A. Ulman, *An Introduction to Ultrathin Organic Films: From Langmuir-Blodgett to Self-Assembly*, Academic Press, Boston, 1991.
36. A. Ulman, *Chem. Rev.*, **1996**, 96, 1533-1554.
37. R. F. Bunshah, *Handbook of deposition technologies for films and coatings*, William Andrew Publishing/Noyes, 1994.
38. M. Mayor, H. B. Weber and R. Waser, *Nanoelectronics and Information Technology*, Wiley-VCH, Berlin, 2005.
39. J. Zasadzinski, R. Viswanathan, L. Madsen, J. Garnaes and D. Schwartz, *Science*, **1994**, 263, 1726-1733.
40. C. Vericat, M. E. Vela, G. Benitez, P. Carro and R. C. Salvarezza, *Chem. Soc. Rev.*, **2010**, 39, 1805-1834.
41. A. Ulman, *Chem. Rev.*, **1996**, 96, 1533-1554.
42. J. C. Love, L. A. Estroff, J. K. Kriebel, R. G. Nuzzo and G. M. Whitesides, *Chem. Rev.*, **2005**, 105, 1103-1170.
43. G. Whitesides, J. Mathias and C. Seto, *Science*, **1991**, 254, 1312-1319.
44. R. E. Holmlin, R. Haag, M. L. Chabinyc, R. F. Ismagilov, A. E. Cohen, A. Terfort, M. A. Rampi and G. M. Whitesides, *J. Am. Chem. Soc.*, **2001**, 123, 5075-5085.
45. F. C. Simeone and M. A. Rampi, *Chimia*, **2010**, 64, 362-369.
46. M. A. Rampi, O. J. A. Schueller and G. M. Whitesides, *Appl. Phys. Lett.*, **1998**, 72, 1781-1783.

47. M. Elbing, A. B. Istrok, aszczyk, C. v. Hänisch, M. Mayor, V. Ferri, C. Grave, M. A. Rampi, G. Pace, P. Samorì, A. Shaporenko and M. Zharnikov, *Adv. Funct. Mater.*, **2008**, 18, 2972-2983.
48. J. G. Kushmerick, A. S. Blum and D. P. Long, *Anal. Chim. Acta*, **2006**, 568, 20-27.
49. D. S. Seferos, S. A. Trammell, G. C. Bazan and J. G. Kushmerick, *Proc. Natl. Acad. Sci.*, **2005**, 102, 8821-8825.
50. J. R. Lloyd, *Semiconductor Science and Technology*, **1997**, 12, 1177.
51. H. Park, J. Park, A. K. L. Lim, E. H. Anderson, A. P. Alivisatos and P. L. McEuen, *Nature*, **2000**, 407, 57-60.
52. W. Liang, M. P. Shores, M. Bockrath, J. R. Long and H. Park, *Nature*, **2002**, 417, 725-729.
53. D. R. Ward and et al., *J. Phys.: Condens. Matter*, **2008**, 20, 374118.
54. H. S. J. v. d. Zant, E. A. Osorio, M. Poot and K. O'Neill, *Phys. Status Solidi B*, **2006**, 243, 3408-3412.
55. Z. W. Hawellek, University of Basel, 2008.
56. R. Sordan, K. Balasubramanian, M. Burghard and K. Kern, *Appl. Phys. Lett.*, **2005**, 87, 013106.
57. J. E. Green, J. Wook Choi, A. Boukai, Y. Bunimovich, E. Johnston-Halperin, E. Delonno, Y. Luo, B. A. Sheriff, K. Xu, Y. Shik Shin, H.-R. Tseng, J. F. Stoddart and J. R. Heath, *Nature*, **2007**, 445, 414-417.
58. W. G. Kuhr, *Electrochem. Soc. Interface*, **2004**, 13, 34-39.
59. P. Naulleau, *Pushing EUV lithography development beyond 22-nm half pitch* 2010.
60. G. Binnig, H. Rohrer, C. Gerber and E. Weibel, *Phys. Rev. Lett.*, **1983**, 50, 120.
61. J. Moreland and J. W. Ekin, *J. Appl. Phys.*, **1985**, 58, 3888-3895.
62. A. Nitzan and M. A. Ratner, *Science*, **2003**, 300, 1384-1389.
63. R. M. Metzger, *Chem. Rev.*, **2003**, 103, 3803-3834.
64. C. Joachim and M. A. Ratner, *Proc. Natl. Acad. Sci.*, **2005**, 102, 8800-8800.
65. N. J. Tao, *Nat. Nanotechnol.*, **2006**, 1, 173-181.
66. A. Salomon, D. Cahen, S. Lindsay, T. Tomfohr, V. B. Engelkes and C. D. Frisbie, *Adv. Mater.*, **2003**, 15, 1881-1890.
67. F. Chen, X. Li, J. Hihath, Z. Huang and N. Tao, *J. Am. Chem. Soc.*, **2006**, 128, 15874-15881.
68. L. Venkataraman, *Physics*, **2008**, 1, 5.
69. R. L. McCreery and A. J. Bergren, *Adv. Mater.*, **2009**, 21, 4303-4322.
70. J. M. Seminario, A. G. Zacarias and J. M. Tour, *J. Am. Chem. Soc.*, **1998**, 121, 411-416.
71. J. M. Seminario, C. E. De La Cruz and P. A. Derosa, *J. Am. Chem. Soc.*, **2001**, 123, 5616-5617.
72. R. M. Tovar, K. P. Johnson, K. Ashline and J. M. Seminario, *Int. J. Quantum Chem.*, **2008**, 108, 1546-1554.
73. M. Kiguchi, S. Miura, K. Hara, M. Sawamura and K. Murakoshi, *Appl. Phys. Lett.*, **2006**, 89, 213104-213103.

-
74. G. S. Tulevski, M. B. Myers, M. S. Hybertsen, M. L. Steigerwald and C. Nuckolls, *Science*, **2005**, 309, 591-594.
 75. L. Venkataraman, J. E. Klare, C. Nuckolls, M. S. Hybertsen and M. L. Steigerwald, *Nature*, **2006**, 442, 904-907.
 76. S. Y. Quek, L. Venkataraman, H. J. Choi, S. G. Louie, M. S. Hybertsen and J. B. Neaton, *Nano Lett.*, **2007**, 7, 3477-3482.
 77. M. Kiguchi and K. Murakoshi, *Thin Solid Films*, **2009**, 518, 466-469.
 78. J. R. Quinn, F. W. Foss, L. Venkataraman, M. S. Hybertsen and R. Breslow, *J. Am. Chem. Soc.*, **2007**, 129, 6714-6715.
 79. S. Y. Quek, M. Kamenetska, M. L. Steigerwald, H. J. Choi, S. G. Louie, M. S. Hybertsen, J. B. Neaton and L. Venkataraman, *Nat. Nanotechnol.*, **2009**, 4, 230-234.
 80. B. Xu, X. Xiao and N. J. Tao, *J. Am. Chem. Soc.*, **2003**, 125, 16164-16165.
 81. Y. S. Park, A. C. Whalley, M. Kamenetska, M. L. Steigerwald, M. S. Hybertsen, C. Nuckolls and L. Venkataraman, *J. Am. Chem. Soc.*, **2007**, 129, 15768-15769.
 82. Y. S. Park, J. R. Widawsky, M. Kamenetska, M. L. Steigerwald, M. S. Hybertsen, C. Nuckolls and L. Venkataraman, *J. Am. Chem. Soc.*, **2009**, 131, 10820-10821.
 83. F. von Wrochem, D. Gao, F. Scholz, H.-G. Nothofer, G. Nelles and J. M. Wessels, *Nat. Nano*, **2010**, 5, 618-624.
 84. C. A. Martin, D. Ding, J. K. Sørensen, T. Bjørnholm, J. M. van Ruitenbeek and H. S. J. van der Zant, *J. Am. Chem. Soc.*, **2008**, 130, 13198-13199.
 85. T. Morita and S. Lindsay, *J. Phys. Chem. B* **2008**, 112, 10563-10572.
 86. M. Kiguchi, O. Tal, S. Wohlthat, F. Pauly, M. Krieger, D. Djukic, J. C. Cuevas and J. M. van Ruitenbeek, *Phys. Rev. Lett.*, **2008**, 101, 046801.
 87. J. A. M. Simoes and J. L. Beauchamp, *Chem. Rev.*, **1990**, 90, 629-688.
 88. F. Tournus, S. Latil, M. I. Heggie and J. C. Charlier, *Phys. Rev. B*, **2005**, 72, 075431.
 89. Y. Lee, B. Carsten and L. Yu, *Langmuir*, **2008**, 25, 1495-1499.
 90. H. Basch, R. Cohen and M. A. Ratner, *Nano Lett.*, **2005**, 5, 1668-1675.
 91. M. Bürkle, J. K. Viljas, V. Meded, A. Bagrets, A. Mishenko, D. Vonlanthen, C. Li, V. Pobelov, G. Schön, M. Mayor, T. Wandlowski and F. Pauly, *in preparation*.
 92. A.P.Zaraiskii, *Russ. Chem. Rev.*, **1978**, 47, 440.
 93. M. J. S. Dewar, *J. Am. Chem. Soc.*, **1952**, 74, 3345-3350.
 94. H. Suzuki, *Bull. Chem. Soc. Jpn.*, **1959**, 32, 1340-1350.
 95. H. Suzuki, *Bull. Chem. Soc. Jpn.*, **1959**, 32, 1350-1356.
 96. H. Suzuki, *Bull. Chem. Soc. Jpn.*, **1959**, 32, 1357-1361.
 97. A. C. Benniston, A. Harriman, P. V. Patel and C. A. Sams, *Eur. J. Org. Chem.*, **2005**, 2005, 4680-4686.
 98. A. C. Benniston and A. Harriman, *Coord. Chem. Rev.*, **2008**, 252, 2528-2539.

99. A. Helms, D. Heiler and G. McLendon, *J. Am. Chem. Soc.*, **1991**, 113, 4325-4327.
100. A. Shaporenko, M. Elbing, A. Blaszczyk, C. von Hänisch, M. Mayor and M. Zharnikov, *J. Phys. Chem. B*, **2006**, 110, 4307-4317.
101. E. Lörtscher, M. Elbing, M. Tschudy, C. von Hänisch, H. B. Weber, M. Mayor and H. Riel, *ChemPhysChem*, **2008**, 9, 2252-2258.
102. N. I. Nijegorodov, W. S. Downey and M. B. Danailov, *Spectrochim. Acta, Part A*, **2000**, 56, 783-795.
103. L. Venkataraman, J. E. Klare, I. W. Tam, C. Nuckolls, M. S. Hybertsen and M. L. Steigerwald, *Nano Lett.*, **2006**, 6, 458-462.
104. L. Venkataraman, Y. S. Park, A. C. Whalley, C. Nuckolls, M. S. Hybertsen and M. L. Steigerwald, *Nano Lett.*, **2007**, 7, 502-506.
105. J. Wang, G. Cooper, D. Tulumello and A. P. Hitchcock, *J. Phys. Chem. A*, **2005**, 109, 10886-10896.
106. H.-S. Im and E. R. Bernstein, *J. Chem. Phys.*, **1988**, 88, 7337-7347.
107. Andrew C. Benniston, A. Harriman, P. Li, Pritesh V. Patel and Craig A. Sams, *Chem. Eur. J.*, **2008**, 14, 1710-1717.
108. F. Pauly, J. K. Viljas, J. C. Cuevas and G. Schön, *Phys. Rev. B*, **2008**, 77, 155312.
109. W. Haiss, C. Wang, R. Jitchati, I. Grace, M. Santiago, A. S. Batsanov, S. J. Higgins, M. R. Bryce, C. J. Lambert, P. S. Jensen and R. J. Nichols, *J. Phys.: Condens. Matter*, **2008**, 20, 374119.
110. H. Kondo, J. Nara, H. Kino and T. Ohno, *J. Chem. Phys.*, **2008**, 128, 064701-064707.
111. H. H. Jaffé and M. Orchin, *Theory and Applications of Ultraviolet Spectroscopy*, John Wiley, New York, 1963.
112. L. T. Cheng, W. Tam, S. R. Marder, A. E. Stiegman, G. Rikken and C. W. Spangler, *J. Phys. Chem.*, **2002**, 95, 10643-10652.
113. E. A. Braude and W. F. Forbes, *J. Chem. Soc.*, **1955**, 3776.
114. S. Woitellier, J. P. Launay and C. Joachim, *Chem. Phys.*, **1989**, 131, 481-488.
115. A. Nitzan, *J. Phys. Chem. A*, **2001**, 105, 2677-2679.
116. A. W. Ghosh, T. Rakshit and S. Datta, *Nano Lett.*, **2004**, 4, 565-568.
117. F. Pauly, J. K. Viljas and J. C. Cuevas, *Phys. Rev. B*, **2008**, 78, 035315.
118. J. Zhang, M. Nieuwenhuyzen, J. P. H. Charmant and S. L. James, *Chem. Commun.*, **2004**, 2808-2809.
119. D. V. Keith A. Hirsch, Scott R. Wilson, Jeffrey S. Moore and Stephen Lee, *J. Chem. Soc., Chem. Commun.*, **1995**, 2199 - 2200.
120. J. R. Farrell, C. A. Mirkin, L. M. Liable-Sands and A. L. Rheingold, *J. Am. Chem. Soc.*, **1998**, 120, 11834-11835.
121. N. Brigitte, Y. Yishan, L. Christophe and R. Régis, *Angew. Chem. Int. Ed.*, **2007**, 46, 8242-8245.
122. J. F. Kang, S. Liao, R. Jordan and A. Ulman, *J. Am. Chem. Soc.*, **1998**, 120, 9662-9667.
123. W. D. Xiao, Y. H. Jiang, K. Ait-Mansour, P. Ruffieux, H. J. Gao and R. Fasel, *J. Phys. Chem. C*, 114, 6646-6649.

124. C.-R. Lee, S. J. Bae, M.-S. Gong, K. Kim and S.-W. Joo, *J. Raman Spectrosc.*, **2002**, 33, 429-433.
125. S.-W. Joo, W.-J. Kim, W. S. Yoon and I. S. Choi, *J. Raman Spectrosc.*, **2003**, 34, 271-275.
126. K. H. Yu, J. M. Rhee, Y. Lee, K. Lee and S.-C. Yu, *Langmuir*, **2000**, 17, 52-55.
127. Y.-T. Tao, C.-C. Wu, J.-Y. Eu, W.-L. Lin, K.-C. Wu and C.-h. Chen, *Langmuir*, **1997**, 13, 4018-4023.
128. A. Mazzanti, L. Lunazzi, M. Minzoni and J. E. Anderson, *J. Org. Chem.*, **2006**, 71, 5474-5481.
129. F. Leroux, *ChemBioChem*, **2004**, 5, 644-649.
130. K. Müllen, W. H. Frank-Gerrit, K. W. R. Roth, I. Kindermann, O. Adamczak, M. Wette and J. Lex, *Chem. Ber.*, **1990**, 123, 2349-2371.
131. A. Mishchenko, L. Zotty, D. Vonlanthen, J. C. Cuevas, M. Bürkle, F. Pauly, M. Mayor and T. Wandlowski, *J. Am. Chem. Soc.* (submitted), **2010**.
132. Z. Huang, F. Chen, P. A. Bennett and N. Tao, *J. Am. Chem. Soc.*, **2007**, 129, 13225-13231.
133. C. Joachim, J. K. Gimzewski and A. Aviram, *Nature*, **2000**, 408, 541-548.
134. J. M. Seminario, *Nat. Mater.*, **2005**, 4, 111-113.
135. C. Joachim and M. A. Ratner, *Proc. Natl. Acad. Sci.*, **2005**, 102, 8801-8808.
136. S. Saha and J. F. Stoddart, *Chem. Soc. Rev.*, **2007**, 36, 77-92.
137. R. H. James and A. R. Mark, *Physics Today*, **2003**, 56, 43-49.
138. O. Hod, R. Baer and E. Rabani, *J. Phys.: Condens. Matter*, **2008**, 383201.
139. R. L. Carroll and C. B. Gorman, *Angew. Chem., Int. Ed.*, **2002**, 41, 4378-4400.
140. M. A. Reed, *Nat. Mater.*, **2004**, 3, 286-287.
141. N. Weibel, S. Grunder and M. Mayor, *Org. Biomol. Chem.*, **2007**, 5, 2343-2353.
142. F. Paul, J. Patt and J. F. Hartwig, *J. Am. Chem. Soc.*, **2002**, 116, 5969-5970.
143. D. S. Surry and S. L. Buchwald, *Angew. Chem., Int. Ed.*, **2008**, 47, 6338-6361.
144. J. F. Hartwig, *Angew. Chem., Int. Ed.*, **1998**, 37, 2046-2067.
145. R. F. Heck and J. P. Nolley, *J. Org. Chem.*, **1972**, 37, 2320-2322.
146. I. P. Beletskaya and A. V. Cheprakov, *Chem. Rev.*, **2000**, 100, 3009-3066.
147. N. Miyaura, K. Yamada and A. Suzuki, *Tetrahedron Lett.*, **1979**, 20, 3437-3440.
148. N. Miyaura and A. Suzuki, *Chem. Rev.*, **2002**, 95, 2457-2483.
149. J. K. Stille, *Angew. Chem., Int. Ed.*, **1986**, 25, 508-524.
150. K. Sonogashira, Y. Tohda and N. Hagihara, *Tetrahedron Lett.*, **1975**, 16, 4467-4470.
151. R. Chinchilla and C. Najera, *Chem. Rev.*, **2007**, 107, 874-922.

152. P. E. Fanta, *Synthesis*, **1974**, 1974, 9-21.
153. Y.-H. Lai, *Synthesis*, **1981**, 1981, 585-604.
154. D. Vonlanthen, J. Rotzler, M. Neuburger and M. Mayor, *Eur. J. Org. Chem.*, **2010**, 120-133.
155. B. Kiupel, C. Niederal, M. Nieger, S. Grimme and F. Vögtle, *Angew. Chem., Int. Ed.*, **1998**, 37, 3031-3034.
156. A. Helms, D. Heiler and G. McLendon, *J. Am. Chem. Soc.*, **1992**, 114, 6227-6238.
157. J. W. Ciszek and J. M. Tour, *Tetrahedron Lett.*, **2004**, 45, 2801-2803.
158. L. M. Tolbert and M. Z. Ali, *J. Org. Chem.*, **1982**, 47, 4793-4795.
159. W. Wenner, *J. Org. Chem.*, **1952**, 17, 523-528.
160. O. Possel and A. M. van Leusen, *Tetrahedron Lett.*, **1977**, 18, 4229-4231.
161. S. Chandrasekhar, C. R. Reddy and B. N. Babu, *J. Org. Chem.*, **2002**, 67, 9080-9082.
162. P. Cogolli, L. Testaferri, M. Tingoli and M. Tiecco, *J. Org. Chem.*, **1979**, 44, 2636-2642.
163. L. Testaferri, M. Tingoli and M. Tiecco, *J. Org. Chem.*, **1980**, 45, 4376-4380.
164. J. Clayden, *Organic Chemistry*, Oxford University Press, Oxford, 2001.
165. J. Rotzler, D. Vonlanthen, A. Barsella, A. Boeglin, A. Fort and M. Mayor, *Eur. J. Org. Chem.*, **2010**, 2010, 1096-1110.
166. T. Esumi, G. Makado, H. Zhai, Y. Shimizu, Y. Mitsumoto and Y. Fukuyama, *Bioorg. Med. Chem. Lett.*, **2004**, 14, 2621-2625.
167. T. A. Kirkland and R. H. Grubbs, *J. Org. Chem.*, **1997**, 62, 7310-7318.
168. A. Michaut and J. Rodriguez, *Angew. Chem., Int. Ed.*, **2006**, 45, 5740-5750.
169. A. Iuliano, P. Piccioli and D. Fabbri, *Org. Lett.*, **2004**, 6, 3711-3714.
170. W. M. Weber, L. A. Hunsaker, S. F. Abcouwer, L. M. Deck and D. L. Vander Jagt, *Bioorg. Med. Chem.*, **2005**, 13, 3811-3820.
171. W. M. Weber, L. A. Hunsaker, C. N. Roybal, E. V. Bobrovnikova-Marjon, S. F. Abcouwer, R. E. Royer, L. M. Deck and D. L. Vander Jagt, *Bioorg. Med. Chem.*, **2006**, 14, 2450-2461.
172. R. W. McDonald, W. Bunjobpon, T. Liu, S. Fessler, O. E. Pardo, I. Freer, M. Glaser, M. J. Seckl and J. Robins, *Anti Canc. Drug Des.*, **2001**, 16, 261-270.
173. V. B. Birman, A. L. Rheingold and K.-C. Lam, *Tetrahedron: Asymmetry*, **1999**, 10, 125-131.
174. F. Hewgill and M. Pass, *Aust. J. Chem.*, **1985**, 38, 537-554.
175. G. M. Whitesides, E. R. Stedronsky, C. P. Casey and J. San Filippo, *J. Am. Chem. Soc.*, **2002**, 92, 1426-1427.
176. B. H. Lipshutz, K. Siegmann, E. Garcia and F. Kayser, *J. Am. Chem. Soc.*, **1993**, 115, 9276-9282.
177. B. H. Lipshutz, F. Kayser and Z.-P. Liu, *Angew. Chem., Int. Ed.*, **1994**, 33, 1842-1844.
178. B. H. Lipshutz, Z.-P. Liu and F. Kayser, *Tetrahedron Lett.*, **1994**, 35, 5567-5570.

179. B. H. Lipshutz, F. Kayser and N. Maullin, *Tetrahedron Lett.*, **1994**, 35, 815-818.
180. D. R. Spring, S. Krishnan and S. L. Schreiber, *J. Am. Chem. Soc.*, **2000**, 122, 5656-5657.
181. J. F. W. McOmie, M. L. Watts and D. E. West, *Tetrahedron*, **1968**, 24, 2289-2292.
182. N. Zheng, J. C. McWilliams, F. J. Fleitz, J. D. Armstrong and R. P. Volante, *J. Org. Chem.*, **1998**, 63, 9606-9607.
183. C. Mispelaere-Canivet, J.-F. Spindler, S. Perrio and P. Beslin, *Tetrahedron*, **2005**, 61, 5253-5259.
184. N. Stuhr-Hansen, *Synth. Commun.*, **2003**, 33, 641 - 646.
185. S. Grunder, R. Huber, V. Horhoiu, M. T. Gonzalez, C. Schönenberger, M. Calame and M. Mayor, *J. Org. Chem.*, **2007**, 72, 8337-8344.
186. C. A. Hunter, P. S. Jones, P. M. N. Tiger and S. Tomas, *Chem. Commun.*, **2003**, 1642-1643.
187. E. B. Merkushev, N. D. Simakhina and G. M. Koveshnikova, *Synthesis*, **1980**, 1980, 486-487.
188. R. B. Carlin, *J. Am. Chem. Soc.*, **1945**, 67, 928-933.
189. Y. Nomura and Y. Takeuchi, *J. Chem. Soc. B*, **1970**, 956.
190. C. Lai and B. J. Backes, *Tetrahedron Lett.*, **2007**, 48, 3033-3037.
191. R. E. Gerkin, A. P. Lundstedt and W. J. Reppart, *Acta Crystallogr., Sect. C*, **1984**, 40, 1892-1894.
192. F. Grein, *J. Phys. Chem. A*, **2002**, 106, 3823-3827.
193. D. Schweitzer and M. Haenel, *Chem. Ber.*, **1985**, 118, 163-175.
194. A. Tajiri, H. Uchimura and M. Hatano, *Chem. Lett.*, **1975**, 4, 1021-1024.
195. H. Suzuki, *Electronic absorption spectra and geometry of organic molecules. An application of molecular orbital theory.*, Academic Press, New York, 1967.
196. A. C. Benniston and A. Harriman, *Chem. Soc. Rev.*, **2006**, 35, 169-179.
197. C. Li, I. Pobelov, T. Wandlowski, A. Bagrets, A. Arnold and F. Evers, *J. Am. Chem. Soc.*, **2008**, 130, 318-326.
198. G. B. Dutt, *ChemPhysChem*, **2005**, 6, 413-418.
199. J. Tomfohr and O. F. Sankey, *J. Chem. Phys.*, **2004**, 120, 1542-1554.
200. H. B. Mark and J. R. Jezorek, *J. Org. Chem.*, **1971**, 36, 666-670.
201. S. M. Bachrach, *J. Phys. Chem. A*, **2008**, 112, 7750-7754.
202. I. Novak, *J. Phys. Chem. A*, **2008**, 112, 2503-2506.
203. D. Vonlanthen, A. Rudnev, A. Mishchenko, A. Käslin, J. Rotzler, M. Neuburger, T. Wandlowski and M. Mayor, *Phys. Chem. Chem. Phys.*, (submitted).
204. A. Facchetti, *Mater. Today*, **2007**, 10, 28-37.
205. N. Blouin and M. Leclerc, *Acc. Chem. Res.*, **2008**, 41, 1110-1119.
206. M. He, J. Li, M. L. Sorensen, F. Zhang, R. R. Hancock, H. H. Fong, V. A. Pozdin, D.-M. Smilgies and G. G. Malliaras, *J. Am. Chem. Soc.*, **2009**, 131, 11930-11938.
207. C. R. Newman, C. D. Frisbie, D. A. da Silva Filho, J.-L. Brédas, P. C. Ewbank and K. R. Mann, *Chem. Mater.*, **2004**, 16, 4436-4451.

-
208. Y. Didane, P. Marsal, F. Fages, A. Kumagai, N. Yoshimoto, H. Brisset and C. Videlot-Ackermann, *Thin Solid Films*, In Press, Corrected Proof.
209. H. E. Katz, A. J. Lovinger, J. Johnson, C. Kloc, T. Siegrist, W. Li, Y. Y. Lin and A. Dodabalapur, *Nature*, **2000**, 404, 478-481.
210. H. E. Katz, J. Johnson, A. J. Lovinger and W. Li, *J. Am. Chem. Soc.*, **2000**, 122, 7787-7792.
211. Y. Didane, P. Marsal, F. Fages, A. Kumagai, N. Yoshimoto, H. Brisset and C. Videlot-Ackermann, *Thin Solid Films*, **In Press**.
212. J. Casanova, N. D. Werner and R. E. Schuster, *J. Org. Chem.*, **1966**, 31, 3473-3482.
213. M. Meier and C. Rüchardt, *Chem. Ber.*, **1987**, 120, 1-4.
214. J. Pakusch and C. Rüchardt, *Chem. Ber.*, **1989**, 122, 1593-1594.
215. W. Dianxun, Q. Ximei and Z. Qiyuan, *Chem. Phys. Lett.*, **1997**, 266, 560-567.
216. J. Sun, X. Qian, D. Chen, Y. Liu, D. Wang and Q. Chang, *J. Photochem. Photobiol., A* **1999**, 126, 23-26.
217. *DE Pat.*, 2004.
218. T. Nagano and T. Hayashi, *Org. Lett.*, **2005**, 7, 491-493.
219. G. Cahiez, C. Chaboche, F. Mahuteau-Betzer and M. Ahr, *Org. Lett.*, **2005**, 7, 1943-1946.
220. Z. Rappoport, *The chemistry of the cyano group*, Wiley, New York 1970.
221. S. Dixon and R. J. Whitby, *Tetrahedron Lett.*, **2006**, 47, 8147-8150.
222. J. Lindley, *Tetrahedron*, **1984**, 40, 1433-1456.
223. J. Spychala, *Monatsh. Chem.*, **2006**, 137, 1203-1210.
224. N. C. Yang, C. I. Lee, J. K. Kim and D. H. Suh, *J. Appl. Polym. Sci.*, **2004**, 92, 3112-3118.
225. C. E. Stephens, D. A. Patrick, H. Chen, R. R. Tidwell and D. W. Boykin, *J. Labelled Compd. Radiopharm.*, **2001**, 44, 197-208.
226. G. P. Ellis and T. M. Romney-Alexander, *Chem. Rev.*, **1987**, 87, 779-794.
227. F. Jin and P. N. Confalone, *Tetrahedron Lett.*, **2000**, 41, 3271-3273.
228. A. Zhang and J. L. Neumeyer, *Org. Lett.*, **2002**, 5, 201-203.
229. A. J. Allentoff, B. Markus, T. Duelfer, A. Wu, L. Jones, G. Ciszewska and T. Ray, *J. Labelled Compd. Radiopharm.*, **2000**, 43, 1075-1085.
230. C. Yang and J. M. Williams, *Org. Lett.*, **2004**, 6, 2837-2840.
231. L. S. Suwandi, G. E. Agoston, J. H. Shah, A. D. Hanson, X. H. Zhan, T. M. LaVallee and A. M. Treston, *Bioorg. Med. Chem. Lett.*, **2009**, 19, 6459-6462.
232. M. P. Wentland, R. Lou, Q. Lu, Y. Bu, M. A. VanAlstine, D. J. Cohen and J. M. Bidlack, *Bioorg. Med. Chem. Lett.*, **2009**, 19, 203-208.
233. S. E. Johnson and C. B. Knobler, *Organometallics*, **1992**, 11, 3684-3690.
234. W.-F. Jiang, H.-L. Wang, A.-G. Wang and Z.-Q. Li, *Synth. Commun.*, **2008**, 38, 1888 - 1895.
235. J. A. J. Vink, P. L. Verheijdt, J. Cornelisse and E. Havinga, *Tetrahedron*, **1972**, 28, 5081-5087.
236. M. Minabe and K. Suzuki, *Bull. Chem. Soc. Jpn.*, **1972**, 45, 3196-3201.

-
237. G. Kossmehl, K.-H. Hatscher and G. Manecke, *Makromol. Chem.*, **1975**, 176, 539-559.
 238. M. B. Andrew D. Abell, Mark A. Levy and Dennis A. Holt, *J. Chem. Soc., Perkin Trans. 1*, **1997**, 1663 - 1668.
 239. D. E. Pearson, M. G. Frazer, V. S. Frazer and L. C. Washburn, *Synthesis*, **1976**, 1976, 621-623.
 240. Johannes A. A. W. Elemans, S. Lei and S. De Feyter, *Angew. Chem. Int. Ed.*, **2009**, 48, 7298-7332.
 241. B. Moulton and M. J. Zaworotko, *Chem. Rev.*, **2001**, 101, 1629-1658.
 242. G. R. Desiraju, *Angew. Chem. Int. Ed.*, **1995**, 34, 2311-2327.
 243. K. Biradha, *CrystEngComm*, **2003**, 5, 374-384.
 244. Gautam R. Desiraju, *Angew. Chem. Int. Ed.*, **2007**, 46, 8342-8356.
 245. P. Metrangolo, G. Resnati, T. Pilati, R. Liantonio and F. Meyer, *J. Polym. Sci., Part A: Polym. Chem.*, **2007**, 45, 1-15.
 246. D. A. Dougherty, *Science*, **1996**, 271, 163-168.
 247. L. Sobczyk, S. J. Grabowski and T. M. Krygowski, *Chem. Rev.*, **2005**, 105, 3513-3560.
 248. J. K. Klosterman, Y. Yamauchi and M. Fujita, *Chem. Soc. Rev.*, **2009**, 38, 1714-1725.
 249. M. L. Bushey, T.-Q. Nguyen, W. Zhang, D. Horoszewski and C. Nuckolls, *Angew. Chem. Int. Ed.*, **2004**, 43, 5446-5453.
 250. C. Schmuck and W. Wienand, *Angew. Chem. Int. Ed.*, **2001**, 40, 4363-4369.
 251. H.-J. Schneider, *Angew. Chem. Int. Ed.*, **2009**, 48, 3924-3977.
 252. B. J. Holliday and C. A. Mirkin, *Angew. Chem. Int. Ed.*, **2001**, 40, 2022-2043.
 253. B. L. Schottel, H. T. Chifotides and K. R. Dunbar, *Chem. Soc. Rev.*, **2008**, 37, 68-83.
 254. G. Desiraju, *The weak hydrogen bond in structural chemistry and biology.*, Oxford University Press, Oxford, 1999.
 255. P. A. Wood, S. J. Borwick, D. J. Watkin, W. D. S. Motherwell and F. H. Allen, *Acta Crystallogr., Sect. B: Struct. Sci.*, **2008**, 64, 393-396.
 256. S. Lee, A. B. Mallik and D. C. Fredrickson, *Cryst. Growth Des.*, **2003**, 4, 279-290.
 257. G. R. Desiraju, *Chem. Commun.*, **2005**, 2995-3001.
 258. G. Jeffrey, *The weak hydrogen bond in structural chemistry and biology.*, Oxford University Press, Oxford, 1999.
 259. S. Kumar, K. Subramanian, R. Srinivasan, K. Rajagopalan and T. Steiner, *J. Mol. Struct.*, **1998**, 471, 251-255.
 260. T. Yokoyama, S. Yokoyama, T. Kamikado, Y. Okuno and S. Mashiko, *Nature*, **2001**, 413, 619-621.
 261. L. F. Pacios and L. Gómez, *Chem. Phys. Lett.*, **2006**, 432, 414-420.
 262. S. D. Chakarova and E. Schroder, *J. Chem. Phys.*, **2005**, 122, 054102.
 263. K. Nikki, *Magn. Reson. Chem.*, **1990**, 28, 385-388.
 264. F. H. A. Rummens and R. H. Krystynak, *J. Am. Chem. Soc.*, **1972**, 94, 6914-6921.
 265. H. Stamm and H. Jaeckel, *J. Am. Chem. Soc.*, **1989**, 111, 6544-6550.

-
266. G. M. Sanders, M. Van Dijk, A. Van Veldhuizen, H. C. Van der Plas, U. Hofstra and T. J. Schaafsma, *J. Org. Chem.*, **1988**, 53, 5272-5281.
267. J. A. N. F. Gomes and R. B. Mallion, *Chem. Rev.*, **2001**, 101, 1349-1384.
268. E. Steiner, P. W. Fowler and L. W. Jenneskens, *Angew. Chem.*, **2001**, 113, 375-379.
269. T. J. Seiders, K. K. Baldrige and J. S. Siegel, *J. Am. Chem. Soc.*, **1996**, 118, 2754-2755.
270. M. V. Arnim and R. Ahlrichs, *J. Comput. Chem.*, **1998**, 19, 1746-1757.
271. M. Häser and R. Ahlrichs, *J. Comput. Chem.*, **1989**, 10, 104-111.
272. R. Ahlrichs, M. Bär, M. Häser, H. Horn and C. Kölmel, *Chem. Phys. Lett.*, **1989**, 162, 165-169.
273. A. D. Becke, *J. Chem. Phys.*, **1993**, 98, 5648-5652.
274. C. Lee, W. Yang and R. G. Parr, *Phys. Rev. B*, **1988**, 37, 785.
275. A. D. Becke, *Phys. Rev. A*, **1988**, 38, 3098.
276. K. Eichkorn, F. Weigend, O. Treutler and R. Ahlrichs, *Theor. Chem. Acc.*, **1997**, 97, 119-124.
277. M. Sierka, A. Hogekamp and R. Ahlrichs, *J. Chem. Phys.*, **2003**, 118, 9136-9148.
278. K. Eichkorn, O. Treutler, H. Öhm, M. Häser and R. Ahlrichs, *Chem. Phys. Lett.*, **1995**, 242, 652-660.
279. A. Schafer, C. Huber and R. Ahlrichs, *J. Chem. Phys.*, **1994**, 100, 5829-5835.
280. *HOMO and LUMO levels of the dithiol-cyclophane counterparts were calculated for comparison using similar DFT methods as used for the dicyano-cyclophanes.*
281. A. Yassar, F. Demanze, A. Jaafari, M. E. Idrissi and C. Coupry, *Adv. Funct. Mater.*, **2002**, 12, 699-708.
282. N. R. Brinkmann, J. C. Rienstra-Kirakofe and H. F. Schaeffer, *Mol. Phys.*, **2001**, 99, 663 - 675.
283. U. Salzner, J. B. Lagowski, P. G. Pickup and R. A. Poirier, *J. Comput. Chem.*, **1997**, 18, 1943-1953.
284. M. Tanaka, *Bull. Chem. Soc. Jpn.*, **1976**, 49, 3382-3388.
285. T. Hoshi, H. Inoue, J. Shiraishi and Y. Tanizaki, *Bull. Chem. Soc. Jpn.*, **1971**, 44, 1743.
286. M. Baiwir and M. Lomba, *Bull. Soc. Roy. Sci. Liege*, **1972**, 41, 531-536.
287. J. Cornil, D. A. Dos Santos, D. Beljonne and J. L. Bredas, *J. Phys. Chem.*, **1995**, 99, 5604-5611.
288. A. Hargreaves and S. H. Rizvi, *Acta Crystallogr.*, **1962**, 15, 365-373.
289. T. Yoshinaga, H. Hiratsuka and Y. Tanizaki, *Bull. Chem. Soc. Jpn.*, **1978**, 51.
290. M. P. Johansson and J. Olsen, *J. Chem. Theory Comput.*, **2008**, 4, 1460-1471.
291. O. Bastiansen and S. Samdal, *J. Mol. Struct.*, **1985**, 128, 115-125.
292. P. H. Rieger, I. Bernal, W. H. Reinmuth and G. K. Fraenkel, *J. Am. Chem. Soc.*, **1963**, 85, 683-693.

-
293. A. Baranski and W. R. Fawcett, *J. Electroanal. Chem.*, **1979**, 100, 185-196.
294. W. R. Fawcett and J. S. Jaworski, *J. Phys. Chem.*, **1983**, 87, 2972-2976.
295. A. Gennaro, A. M. Romanin, M. G. Severin and E. Vianello, *J. Electroanal. Chem.*, **1984**, 169, 279-285.
296. A. Gennaro, F. Maran, A. Maye and E. Vianello, *J. Electroanal. Chem.*, **1985**, 185, 353-363.
297. M. Sertel, A. Yildiz and H. Baumgartel, *Electrochim. Acta*, **1986**, 31, 1625-1632.
298. M. Sertel, A. Yildiz, R. Gambert and H. Baumgartel, *Electrochim. Acta*, **1986**, 31, 1287-1292.
299. A. Yildiz, M. Sertel, R. Gambert and H. Baumgartel, *Electrochimica Acta*, **1988**, 33, 169-170.
300. A. J. Bard, *Electrochemical Methods: Fundamentals and Applications*, 2nd ed. edn., John Wiley, New York, 2000.
301. J. L. Town, F. MacLaren and H. D. Dewald, *J. Chem. Educ.*, **1991**, 68, 352.
302. J. Nikolic, E. Expósito, J. Iniesta, J. González-García and V. Montiel, *J. Chem. Educ.*, **2000**, 77, 1191.
303. P. Čárský and R. Zahradník, MO approach to electronic spectra of radicals in *Topics in Current Chemistry*, Springer Berlin / Heidelberg, 1973, vol. 43, pp. 1-55.
304. S. F. Nelsen, M. N. Weaver, J. I. Zink and J. P. Telo, *J. Am. Chem. Soc.*, **2005**, 127, 10611-10622.
305. H. B. Weber, J. Reichert, R. Ochs, D. Beckmann, M. Mayor and H. v. Löhneysen, *Physica E*, **2003**, 18, 231-232.
306. D. E. Richardson and H. Taube, *J. Am. Chem. Soc.*, **1983**, 105, 40-51.
307. S.-H. Ke, W. Yang and H. U. Baranger, *Nano Lett.*, **2008**, 8, 3257-3261.
308. D. M. Cardamone, C. A. Stafford and S. Mazumdar, *Nano Lett.*, **2006**, 6, 2422-2426.
309. G. C. Solomon, D. Q. Andrews, R. H. Goldsmith, T. Hansen, M. R. Wasielewski, R. P. Van Duyne and M. A. Ratner, *J. Am. Chem. Soc.*, **2008**, 130, 17301-17308.
310. M. Mayor, H. B. Weber, J. Reichert, M. Elbing, C. von Hänisch, D. Beckmann and M. Fischer, *Angew. Chem., Int. Ed.*, **2003**, 42, 5834-5838.
311. P. Sautet and C. Joachim, *Chem. Phys. Lett.*, **1988**, 153, 511-516.
312. K. Yoshizawa, T. Tada and A. Staykov, *J. Am. Chem. Soc.*, **2008**, 130, 9406-9413.
313. R. S. Mulliken, *J. Chem. Phys.*, **1939**, 7, 339-352.
314. J. R. Jezorek, A. Lagu, T. M. Seigel and H. B. Mark, *J. Org. Chem.*, **1973**, 38, 788-795.
315. L. Nyulászi and P. v. R. Schleyer, *J. Am. Chem. Soc.*, **1999**, 121, 6872-6875.
316. K. Tamao and S. Yamaguchi, *Pure Appl. Chem.*, **1996**, 68, 139-144.
317. M. Shimizu, H. Tatsumi, K. Mochida, K. Oda and T. Hiyama, *Chem. Asian J.*, **2008**, 3, 1238-1247.

318. X. Zhan, S. Barlow and S. R. Marder, *Chem. Commun.*, **2009**, 1948-1955.
319. G. Lu, H. Usta, C. Risko, L. Wang, A. Facchetti, M. A. Ratner and T. J. Marks, *J. Am. Chem. Soc.*, **2008**, 130, 7670-7685.
320. K.-D. Kim, J.-S. Park, H. K. Kim, T. B. Lee and K. T. No, *Macromolecules*, **1998**, 31, 7267-7272.
321. A. J. Boydston and B. L. Pagenkopf, *Angew. Chem. Int. Ed.*, **2004**, 43, 6336-6338.
322. K. Tamao, M. Uchida, T. Izumizawa, K. Furukawa and S. Yamaguchi, *J. Am. Chem. Soc.*, **1996**, 118, 11974-11975.
323. L. Li, J. Xiang and C. Xu, *Org. Lett.*, **2007**, 9, 4877-4879.
324. R. G. Pews and N. D. Ojha, *J. Am. Chem. Soc.*, **2002**, 91, 5769-5773.
325. J. C. Bourmanne, G. Leroy and J. Weiler, *Tetrahedron*, **1970**, 26, 2281-2289.
326. P. Rademacher, *Chem. Rev.*, **2003**, 103, 933-976.
327. R. S. Becker, L. Edwards, R. Bost, M. Elam and G. Griffin, *J. Am. Chem. Soc.*, **1972**, 94, 6584-6592.
328. G. Maier, *Angew. Chem. Int. Ed.*, **1967**, 6, 402-413.
329. A. A. Jarzeński, J. Gajewski and E. R. Davidson, *J. Am. Chem. Soc.*, **1999**, 121, 6928-6935.
330. E. Vogel, W. Wiedemann, H. D. Roth, J. Eimer and H. Günther, *Justus Liebigs Ann. Chem.*, **1972**, 759, 1-36.
331. J. M. Nguyen and D. M. Thamattoor, *Synthesis*, **2007**, 2007, 2093-2094.
332. B. R. Dent, *Austr. Journal of Chem.*, **1987**, 40, 925-936.
333. M. Robert, I. Likhovorik, M. S. Platz, S. C. Abbot and R. Johnson, *J. Phys. Chem. A*, **1998**, 102, 1507-1513.
334. R. T. Ruck and J. M. Jones, *Tetrahedron Lett.*, **1998**, 39, 4433-4436.
335. K. Kitatani, T. Hiyama and H. Nozaki, *J. Am. Chem. Soc.*, **1976**, 98, 2362-2364.
336. J. L. Castro, L. Castedo and R. Riguera, *J. Org. Chem.*, **1987**, 52, 3579-3584.
337. E. J. O'Connor, S. Brandt and P. Helquist, *J. Am. Chem. Soc.*, **1987**, 109, 3739-3747.
338. J.-E. Bäckvall, C. Löfström, S. K. Juntunen and M. Mattson, *Tetrahedron Lett.*, **1993**, 34, 2007-2010.
339. M. N. Mattson, J. P. Bays, J. Zakutansky, V. Stolarski and P. Helquist, *J. Org. Chem.*, **1989**, 54, 2467-2468.
340. *USA Pat.*, US 2006088728 A1, 2006.
341. C. Gao and A. S. Hay, *Synth. Commun.*, **1995**, 25, 1877 - 1883.
342. A. Lévai, *Chem. Heterocycl. Compd.*, **1997**, 33, 647-659.
343. S. G. Beech, J. H. Turnbull and W. Wilson, *J. Chem. Soc.*, **1952**, 4686 - 4690.
344. K. D. Belfield, K. J. Schafer, W. Mourad and B. A. Reinhardt, *J. Org. Chem.*, **2000**, 65, 4475-4481.
345. D. L. Pearson and J. M. Tour, *J. Org. Chem.*, **1997**, 62, 1376-1387.
346. J. Heurich, J. C. Cuevas, W. Wenzel and G. Schön, *Phys. Rev. Lett.*, **2002**, 88, 256803.

-
347. H. H. Jaffé, *Ber. Bunsenges. Phys. Chem.*, **1955**, 59, 823-827.
348. Q. Shen, C. Wells, M. Traetteberg, R. K. Bohn, A. Willis and J. Knee, *J. Org. Chem.*, **2001**, 66, 5840-5845.
349. R. E. Drumright, R. H. Mas, J. S. Merola and J. M. Tanko, *J. Org. Chem.*, **1990**, 55, 4098-4102.
350. R. Cohen, K. Stokbro, J. M. L. Martin and M. A. Ratner, *J. Phys. Chem. C*, **2007**, 111, 14893-14902.
351. H. Liu, W. Ni, J. Zhao, N. Wang, Y. Guo, T. Taketsugu, M. Kiguchi and K. Murakoshi, *J. Chem. Phys.*, **2009**, 130, 244501-244508.

8 Appendix

8.1 Contributions

All molecules in chapter 2 and 3 were synthesized, characterized and calculated (DFT) by David Vonlanthen. The synthesis of intermediate **CN 15** was conducted by Alex Käslin under the supervision of David Vonlanthen.

All STM-BJ measurements in section 2.5 and 3.4 were performed and analyzed by Artem Mishchenko in the group of Thomas Wandlowski at the University of Bern.

The spectroelectrochemical measurements in section 3.3.8 were conducted and analyzed by Dr. Alexander Rudnev in the group of Thomas Wandlowski. The concept, synthesis and characterization of all molecules in chapter 4 were developed and carried out by David Vonlanthen.

The synthesis of *trans*-**OPCP** in section 4.4.1 was conducted by Anna Senn under the supervision of David Vonlanthen. The reference compound **OPE** in section 4.4.1 was provided by Sergio Grunder, also from the Mayor group.

8.2 Complete Paper List

12. D. Vonlanthen, A. Rudnev, A. Mishchenko, A. Käslin, J. Rotzler, M. Neuburger, T. Wandlowski, M. Mayor, Conformationally-controlled electron delocalization in n-type rods: synthesis, structure, optical, electrochemical and spectro-electrochemical properties of dicyano-cyclophanes, *Phys. Chem. Chem. Phys.* **2010** (submitted)
11. A. Mishchenko, L. Zotty, D. Vonlanthen, J. C. Cuevas, F. Pauly, M. Mayor T. Wandlowski, Single molecule junctions based on nitrile-terminated biphenyls: A new promising anchoring group, *J. Am. Chem. Soc.* **2010** (accepted)
10. J. Rotzler, H. Gsellinger, M. Neuburger, D. Vonlanthen, D. Häussinger, M. Mayor, Racemisation Dynamics of Torsion Angle restricted Biphenyl Push-Pull Cyclophanes, *Org. Biomol. Chem.* **2010** (accepted)
9. M. Bürkle, J. K. Viljas, V. Meded, A. Bagrets, A. Mishchenko, D. Vonlanthen, C. Li, I. V. Pobelov, G. Schön, M. Mayor, T. Wandlowski, F. Pauly, Density-functional study of transmission eigenchannels in dithiolated biphenyl-derived single-molecule junctions, *Phys.Rev.B.* **2010** (in preparation)
8. D. Vonlanthen, J. Rotzler, M. Neuburger, M. Mayor; Synthesis of Rotationally Restricted and Modular Biphenyl Building Blocks, *Eur. J. Org. Chem.* **2010**, 120-133
7. A. Mishchenko, D. Vonlanthen, V. Meded, M. Bürkle, C. Li, I. V. Pobelov, A. Bagrets, J. K. Viljas, F. Pauly, F. Evers, M. Mayor, T. Wandlowski; Influence of Conformation on Conductance of Biphenyl-Dithiol Single-Molecule Contacts, *Nano Lett.* **2010**, 10, 156-163
6. J. Rotzler, D. Vonlanthen, A. Barsella, A. Boeglin, A. Fort, M. Mayor; Variation of the Backbone Conjugation in NLO Model Compounds: Torsion-Angle-Restricted Biphenyl-Based Push-Pull-Systems, *Eur. J. Org. Chem.* **2010**, 1096-1110

5. D. Vonlanthen, A. Mishchenko, M. Elbing, M. Neuburger, T. Wandlowski, M. Mayor; Chemically Controlled Conductivity: Torsion-Angle Dependence in a Single-Molecule Biphenyldithiol Junction, *Angew. Chem. Int. Ed.* **2009**, 48, 8886-8890;
Chemisch kontrollierte Leitfähigkeit: Torsionswinkel-abhängigkeit in Biphenyldithiol Einzelmolekül-bruchkontakten,
Angew. Chem. **2009**, 121, 9048-9052
4. D. Ittig, D. Renneberg, D. Vonlanthen, S. Luisier, Ch. Leumann, Oligonucleotide analogues: from supramolecular principles to biological properties,
Coll. Symp. Series (M. Hocek, Ed.), Academy of Sciences of the Czech Republic, Prague **2005**,
Vol 7, p. 21-26
3. D. Vonlanthen, C. Leumann, Hydroxycyclopentanone derivatives from D-mannose via ring closing metathesis: An improved synthesis of a key intermediate of tricyclo-DNA,
Synthesis **2003**, 7, 1087-1090
2. E. Gyr, R. Brenneisen, D. Bourquin, T. Lehmann, D. Vonlanthen, I. Hug, Pharmacodynamics and pharmacokinetics of intravenously, orally and rectally administered diacetylmorphine in opioid dependents, a two-patient pilot study within a heroin-assisted treatment program,
Int. J. Clin. Pharmacol. Therapeut. **2000**, 38(10), 486-91
1. H.J. Helmlin, K. Bracher, D. Bourquin, D. Vonlanthen, R. Brenneisen,
Analysis of 3,4-methylenedioxy-methamphetamine (MDMA) and its metabolites in plasma and urine by HPLC-DAD and GC-MS,
J. Anal. Toxicol. **1996**, 20 (6), 432-440

CURRICULUM VITAE

PERSONAL INFORMATION

Date/Place of birth 08.06.1974 in Schmitten/Cordast (Freiburg-CH)
Nationality Swiss
Email David.Vonlanthen@gmail.com

EDUCATION

- 2006-2010 **PhD work**
Department of Chemistry, University of Basel,
PhD thesis under the supervision of Prof. Dr. M. Mayor
- 2003-2006 **Master of Science** in Chemistry,
Department of Chemistry and Biochemistry, University of Bern
Master thesis under the supervision of Prof. Dr. C. Leumann
- 1998-2002 **Chemiker FH**, University of Applied Sciences, Burgdorf
Diploma thesis under the supervision of Dr. Franz Baumberger
- 1997-1998 **Professional Maturity**, High School for Vocational Education in
Trades and Industry, Bern
- 1996 **Appointment for Trainee**, Lipomed AG, Arlesheim
- 1995 **Visiting Scholar**, Department of Medicinal Chemistry and
Molecular Pharmacology, Purdue University, USA,
under the supervision of Prof. Dr. D. Nichols
- 1991-1994 **Apprenticeship** in Chemistry, Institute of Organic Chemistry,
University of Bern